Investigating the role of Quaking proteins in RNA metabolism in glial cells

by

Lama Darbelli

Department of Medicine

Division of Experimental Medicine

McGill University, Montreal

November 2018

A thesis submitted to McGill University in partial fulfillment of the requirements of the degree of Doctor of Philosophy

Table of Contents

Abstract ..... **iv**

Résumé ..... **vi**

Acknowledgements ..... **viii**

Preface ..... **ix**

Published manuscripts included in this thesis ..... **x**

Author contributions ..... **xi**

Other contributions by the candidate ..... **xii**

Contribution to original knowledge ..... **xiii**

Abbreviations list ..... **xiv**

List of figures ..... **xvii**

List of tables ..... **xix**

Introduction and thesis objectives **1**

Chapter 1: Literature review **2**

1.1 RNA binding proteins **2**
1.1.1 KH domain containing RNA binding proteins 2
1.1.2 STAR RNA binding proteins 3
1.1.2.1 Discovery of the STAR RNA binding proteins 3
1.2 QUAKING **6**
1.2.1 Discovery of the *Quaking* (*qkI*) gene and *Quaking Viable* mice 6
1.2.2 *qkI* null mice 7
1.2.3 Cloning of the *qkI* gene 9
1.2.4 QKI structure 10
1.2.5 Quaking response element 11
1.2.6 QKI expression 12
1.2.7 Regulation of *qkI* expression and activity 13
1.2.7.1 Transcriptional 13
1.2.7.2 Alternative splicing/ mRNA stability and translation 15
1.2.7.3 Post-translational modifications 15
1.2.7.4 microRNA 16
1.2.8 Functions of the QKI proteins 18
1.2.8.1 RNA trafficking 18
1.2.8.2 Translation 19

1.2.8.3 mRNA stability, turnover and decay 20
1.2.8.4 microRNA processing 22
1.2.8.5 circular RNA production 23
1.2.8.6 Cytoplasmic polyadenylation 24
1.2.9 Role of QKI in alternative splicing 27
1.2.9.1 General mechanism of RNA splicing 27
1.2.9.2 Regulation of pre-mRNA splicing by QKI proteins 30
1.2.10 Role of QKI in human diseases 33
1.2.10.1 Multiple Sclerosis 33
1.2.10.2 Schizophrenia 34
1.2.10.3 6q Terminal deletion 35
1.2.10.4 Cancer 36
1.2.10.5 Ataxia 38
1.3 Oligodendrocyte development and myelin formation 40
1.3.1 Myelin 40
1.3.2 Structure and Composition of myelin 41
1.3.2.1 Myelin lipids 43
1.3.2.2 Myelin proteins 44
1.3.3 Initiation of myelination and myelin compaction 46
1.3.4 Discovery of glial cells 47
1.3.5 Development of oligodendrocytes in the Central Nervous System 47
1.3.5.1 Oligodendrocyte morphology 47
1.3.5.2 Origin and specification of oligodendrocyte precursor cells (OPCs) 48
1.3.5.3 OPC proliferation and migration 50
1.3.5.4 OLs survival and differentiation 51
1.3.6 CNS myelination 54
1.3.7 QKI expression in the CNS 56
1.4 The Paranode 58
1.4.1 Structural domains along the axon 58
1.4.1.1 The Node 59
1.4.1.2 The Paranode 60
1.4.1.3 The juxtaparanode 61
1.4.2 The Paranode 61
1.4.2.1 Composition of the paranode 61
1.4.2.1 Function of the paranode and axoglial junctions 63
1.4.3 Neurofascin 64
1.4.3.1 Discovery of Neurofascin 64
1.4.3.2 Gene, alternative splicing, structure and expression of Neurofascin 64
1.4.3.3 Function of Neurofascin 67
1.4.3.4 Neurofascin and disease 69
Chapter 2 71
Quaking regulates Neurofascin 155 expression for myelin and axoglial junction maintenance 71
2.1 Preface 71

2.2 Title page **72**
2.3 Abstract **73**
2.4 Introduction **74**
2.5 Materials and methods **76**
2.6 Results **81**
2.6.1 Ablation of *qkI* in oligodendrocytes of mice leads to severe ataxia and death at the third post-natal week. 81
2.6.2 Hypomyelination in the CNS of $QKI^{FL/FL;Olig2\text{-}Cre}$ mice 85
2.6.3 Oligodendrocyte differentiation defects in $QKI^{FL/FL;Olig2\text{-}Cre}$ mice 87
2.6.4 Alternative splicing defects in $QKI^{FL/FL;Olig2\text{-}Cre}$ brains 90
2.6.5 QKI regulates alternative splicing of Neurofascin pre-mRNA 93
2.6.6 Loss of QKI in the CNS and PNS of adult mice leads to paralysis 96
2.6.7 QKI regulates Nfasc pre-mRNA alternative splicing in mature OLs 99
2.6.8 Paranodal defects in $QKI^{FL/FL;Olig2\text{-}Cre}$ and $QKI^{FL/FL;PLP\text{-}CreERT}$ mice 102
2.7 Discussion **107**
2.8 Acknowledgments **110**

Chapter 3 ..... **111**

Transcriptome profiling of mouse brains with *qkI*-deficient oligodendrocytes reveals major alternative splicing defects including self-splicing **111**

3.1 Preface **111**
3.2 Title page **112**
3.3 Abstract **113**
3.4 Introduction **114**
3.5 Materials and Methods **116**
3.6 Results **121**
3.6.1 QKI-depleted oligodendrocytes downregulate genes involved in myelination. 121
3.6.2 Alternative splicing changes observed in $QKI^{FL/FL;Olig2\text{-}Cre}$ mice 125
3.6.3 Quaking regulates the alternative splicing of its pre-mRNA 131
3.7 Supplementary figures and legends **137**
3.8 Discussion **143**
3.9 Acknowledgments **145**
3.10 Authors contribution **145**

Chapter 4 ..... **146**

General discussion: **146**

4.1 General summary **146**
4.2 The advantages of generating a *qkI* conditional allele **147**
4.3 Perspectives on regulation of *qkI* expression and function **150**
4.4 Concluding remarks **153**

References ..... **i**

Abstract

RNA-binding proteins (RBPs) are essential regulators of RNA metabolism in key cellular processes ranging from pre-mRNA splicing to mRNA translation. Quaking (QKI) is an RNA binding protein involved in post-transcriptional regulation of gene expression. The *Quaking* (qkI) gene was originally identified as the cause of hypomyelination in the central nervous system (CNS) in the mouse mutant *quaking viable* (qk^{v})). Since then, QKI has been implicated in a wide range of human diseases. The hypomyelination phenotype of this natural mutant has pointed, early on, to an essential role for the QKI proteins in myelination, specifically in oligodendrocytes (OLs), the myelinating cells of the CNS. The use of the spontaneously occurring qk^{v} mouse proved to be a valuable tool through the years to address some questions regarding the function of QKI proteins in the CNS. Yet, the qk^{v} mice display a mosaic expression pattern of QKI and the *qkI* null mice are embryonic lethal, precluding further investigations of the function of QKI proteins during development and in adulthood.

In the present study, we aimed to overcome embryonic lethality by generating a conditional allele of the *qkI* gene in order to allow for cell- and tissue-specific gene targeting. We deleted *qkI* expression using the *Olig2-Cre* driver that is specific to the OL lineage, as well as the inducible *PLP-CreERT* driver which is specific to the myelinating cells in the central and peripheral nervous system (PNS). The conditional knockout mice using *Olig2-Cre* displayed severe CNS hypomyelination with tremors starting around postnatal day 10 (P10) and death by the third postnatal week. A block in OLs differentiation was the cause of the extensive hypomyelination observed. Deleting QKI expression in myelinating cells in adults (*PLP-CreERT*) resulted in hindlimb paralysis, immobility and death by 30 days following QKI ablation. Analysis of alternative splicing defects in these mice have revealed significant changes. Moreover, we identified *Neurofascin-155* (*Nfasc-155*) as an alternatively spliced target of QKI and showed that its loss leads to an absence and deterioration of axoglial junctions during development and adulthood, respectively.

We next used RNA isolated from wild-type and conditional knockout brains (*Olig2-Cre*) to perform a transcriptomic analysis. Loss of QKI leads to major changes in global gene expression. More than 1800 transcripts displayed differential expression patterns with top categories being axon ensheathment and myelination, further supporting the function of QKI in OLs. Interestingly, the major downregulated genes belonged to myelin structural components.

Over 800 genes showed differential alterative splicing patterns. Surprisingly, *qkI* was identified as the top alternatively spliced event. We then confirmed that indeed the nuclear QKI-5 regulates the alternative splicing of *qkI-6* and *qkI-7* transcripts, therefore, providing the first evidence for a function for QKI protein in regulating its own pre-mRNA splicing.

Our data demonstrate an important role for QKI proteins in regulating RNA metabolism during OLs development and myelination as well as provide new mouse models that allow specific spatial and temporal targeting of QKI. This research provides a vital tool for studying the involvement of QKI proteins in other cellular processes as well as their contribution to human diseases.

Key words: Quaking, RNA-binding proteins, Oligodendrocytes, myelination, Neurofascin, alternative splicing.

Résumé

Les protéines liant l'ARN (RBP) sont des régulateurs essentiels du métabolisme de l'ARN dans les processus cellulaires clés allant de l'épissage de pré-ARN messager à la traduction de l'ARN messager. Quaking (QKI) est une protéine de liaison à l'ARN impliquée dans la régulation post-transcriptionnelle de l'expression génique. Il a été identifié à l'origine comme la cause de l'hypomyélinisation dans le système nerveux central (SNC) chez la souris mutante quaking viable (qk^{v})). Depuis lors, QKI a été impliqué dans un large éventail de maladies humaines. Le phénotype d'hypomyélinisation de ce mutant naturel a montré très tôt un rôle essentiel pour les protéines QKI dans la myélinisation, en particulier dans les oligodendrocytes (OL), les cellules myélinisantes du SNC. L'utilisation de la souris qk^{v} spontanée s'est révélée être un outil précieux au fil des ans pour répondre à certaines questions concernant la fonction des protéines QKI dans le SNC. Pourtant, les souris qk^{v} affichent un motif d'expression en mosaïque de QKI et les souris null *qkI* sont létales embryonnaires, ce qui empêche une étude plus approfondie de la fonction des protéines QKI au cours du développement et à l'âge adulte.

Dans la présente étude, nous avons cherché à surmonter cet obstacle en générant un allèle conditionnel du gène *qkI* afin de permettre le ciblage génique spécifique aux cellules et aux tissus. Nous avons supprimé l'expression de *qkI* en utilisant le driver *Olig2-Cre* spécifique à la lignée OL, ainsi que le driver *PLP-CreERT* inductible spécifique aux cellules myélinisantes du système nerveux central et périphérique (PNS). Les souris knock-out conditionnelles utilisant *Olig2-Cre* ont montré une hypomyélinisation sévère du SNC avec des tremblements débutant autour du jour 10 postnatal (P10) avec la mort à la troisième semaine postnatale. Un bloc dans la différenciation des OL était la cause de l'hypomyélinisation étendue observée. La suppression de l'expression de QKI dans les cellules myélinisantes chez les adultes (*PLP-CreERT*) a entraîné une paralysie des membres postérieurs, une immobilité et la mort de 30 jours après l'ablation de QKI. L'analyse des défauts d'épissage alternatifs chez ces souris a révélé des changements significatifs. De plus, nous avons identifié *Neurofascin-155* (*Nfasc-155*) comme une cible de QKI épissée alternativement et montré que sa perte entraîne une absence et une détérioration des jonctions axogliales au cours du développement et de l'âge adulte, respectivement.

Nous avons ensuite utilisé l'ARN isolé à partir de cerveaux knock-out de type sauvage et conditionnel (Olig2-Cre) pour effectuer une analyse transcriptomique. La perte de QKI entraîne des changements majeurs dans l'expression globale des gènes. Plus de 1800 transcrits affichaient

des modèles d'expression différentielle, les catégories supérieures étant l'empoisonnement axonal et la myélinisation, soutenant davantage la fonction de QKI dans les OLs. Fait intéressant, le principal gène sous-régulé appartenait aux composants structuraux de la myéline. Plus de 800 gènes ont montré des modèles d'épissage alternatif différentiel. Étonnamment, *qkI* a été identifié comme le meilleur événement alternativement épissé. Nous avons ensuite confirmé qu'en effet le QKI-5 nucléaire régule l'épissage alternatif des transcrits *qkI-6* et *qkI-7*, fournissant ainsi la première preuve d'une fonction de la protéine QKI dans la régulation de son propre épissage pré-ARNm.

Nos données démontrent un rôle important pour les protéines QKI dans la régulation du métabolisme de l'ARN au cours du développement des OL et de la myélinisation ainsi que de fournir de nouveaux modèles de souris qui permettent un ciblage spatial et temporel spécifique de QKI. Cette recherche fournit un outil essentiel pour étudier l'implication des protéines QKI dans d'autres processus cellulaires ainsi que leur contribution aux maladies humaines.

Mots-clés: Quaking, protéines liant l'ARN, Oligodendrocytes, Myélinisation, Neurofascin, épissage alternatif.

Acknowledgements

First and foremost, I would like to thank my supervisor, *Dr. Stéphane Richard* for his guidance and mentorship during the years I spent in his lab. Thank you for giving me the freedom and support I needed to carry out my research projects. The time I spent in your lab has helped me tremendously grow as a scientist as well as shape my personality. I am grateful for all the things I learned in your lab as it helped shape me into the person I am today.

Special thanks to the people who welcomed me in the lab 6 years ago. *Po Hien,* the extremely positive scientist, you were a ray of sunshine. *Gaya*, after so many memories, so many post-it messages and so many coffees, so many ups and downs, I am thankful to you for being there and for making me laugh so much. *Raja*, I am thankful for all the times you sat there listening to me complaining about my failed experiments and encouraged me to keep going. Thank you for all your support and help. *Mathieu*, thank you for your guidance and help and for being the goofy scientist everyone needs in a lab and for putting a smile on our faces. *Josephine*, the other ray of sunshine from across the hall, words cannot describe how grateful I am to you for encouraging me all those years, for your precious friendship and for always being there. I hope to maintain my friendship with all of you for the rest of my life.

Thank you to all the past and present members of the Richard lab for all the help and remarkable memories we shared every day. Special thanks to *Dr. Zhenbao Yu* and *Gillian Vogel*, for always providing help and guidance when needed.

Thank you to my mom and dad, *Hala* and *Hanna*, you are the most amazing parents anyone could ask for. You were always there supporting me and helping me move forward with my life. Thank you to my sister, *Leen*, and my brother, *Esber*, for your loving support and encouragement. Thank you to my best friend, *Gabra*, for always believing in me, listening to all my complaints and worries. I cannot ask for a better friend. You have been there through thick and thin and for that I am grateful.

Last but not least, my dear husband *Prateep*, none of this would have been accomplished without you. Your smile, wit and love made the impossible seem possible. You never gave up on me, even when I was about to give up on myself. Thank you for always being there for me, for believing in me and for providing the push I needed to keep going. You are my rock and my shelter. You lift me up when I fall. For that and a lot more, I thank you from the bottom of my heart.

Preface

As an original contribution to knowledge, this thesis describes the generation of a new conditional allele of the *Quaking* gene that was used to delete expression of QKI in glial cells in order to address its role in central nervous system development. **Chapter 1** is a general introduction and literature review that is an elaboration of a published review written in collaboration with Dr. Stéphane Richard. **Chapter 2** and **3** are the original research papers that have been published. These two chapters contain their own summary, introduction, materials and methods, results, discussion, supplementary information and acknowledgements sections. The authors contributions to each publication are stated below. A general discussion and conclusion are included in **Chapter 4**.

Published manuscripts included in this thesis

Chapter 1:

Darbelli, L., & Richard, S. (2016). Emerging functions of the Quaking RNA-binding proteins and link to human diseases. *Wiley Interdiscip Rev RNA, 7*(3), 399-412. doi:10.1002/wrna.1344

Chapter 2:

Darbelli, L., Vogel, G., Almazan, G., & Richard, S. (2016). Quaking Regulates *Neurofascin 155* Expression for Myelin and Axoglial Junction Maintenance. *J Neurosci, 36*(14), 4106-4120. doi:10.1523/*JNeurosci*.3529-15.2016

Chapter 3:

Darbelli, L*., Choquet, K*., Richard, S., & Kleinman, C. L. (2017). Transcriptome profiling of mouse brains with *qkI*-deficient oligodendrocytes reveals major alternative splicing defects including self-splicing. *Sci Rep, 7*(1), 7554. doi:10.1038/s41598-017-06211-1
(*Authors contributed equally)

Author contributions

Chapter 1:

LD wrote the review in collaboration with Dr. Stéphane Richard.

Chapter 2:

LD designed research, performed experiments, generated and analyzed data for the following figures in the manuscript: Figure 2.1A, 2.2A, 2.2C, Figure 2.3, Figure 2.4A, 2.4B, 2.4C, 2.4D, Figure 2.5, 2.6D, Figure 2.7, Figure 2.8, Figure 2.9 and Figure 2.10 and generated table 1. LD performed all statistical analyses.

GV performed experiments, generated data for the following figures. : Figure 2.1B, 2.1C, 2.1D, 2.1E, Figure 2.2B, Figure 2.4E, Figure 2.6A, 2.6B, 2.6C, 2.6E, 2.6F, 2.6G.

LD and SR wrote the manuscript. GA provided expertise on myelin and oligodendrocyte biology.

All authors read and approved the final version of the manuscript.

Chapter 3:

LD conceived the study, performed experiments, generated and analyzed data for the following figures: Figure 3.1C, Figure 3.4 the semi-quantitative PCR with relative band intensities, Figure 3.5B, Figure 3.6 and Figure 3.7. LD performed statistical analyses for these figures and wrote manuscript.

KC and CK performed all bioinformatics analysis, analyzed data and wrote manuscript. KC generated the following figures: Figure 3.1A, 3.1B, Figure 3.2, Figure 3.4 genomic reads, Figure 3.5A as well as table 3.1. KC performed statistical analyses for bioinformatics data.

SR conceived the study, analyzed data and wrote the manuscript.

All authors read and approved the final version of the manuscript.

Other contributions by the candidate

Collaborative manuscripts not included in this thesis:

Panganiban, C. H.*, J. L. Barth, J.L*., **Darbelli, L.***, Xing, Y., Zhang, J., Li, H., Noble, K. V., Liu, T., Brown, L. N., Schulte, B. A., Richard, S., and Lang, H. (2018). Noise-induced dysregulation of *Quaking* RNA binding proteins contributes to auditory nerve demyelination and hearing loss. *J Neurosci*. 38 (10) 2551-2568. Doi:10.1523/Jneurosci.2487-17.2018

*Authors contributed equally

Contribution: LD provided mouse model, performed perfusion of mice for tissue collection. Provided expertise on mouse colony maintenance, genotyping and immunostaining. Read the manuscript and provided insights.

Calabretta, S., Vogel, G.,Yu, Z., Choquet, K., **Darbelli, L**., Nicholson, T. B., Kleinman, C., & Richard, S. (2018). Loss of PRMT5 promotes PDGFRα degradation during oligodendrocyte differentiation and myelination. *Dev Cell*. (46) 1-15. Doi: 10.1016/j.devcel.2018.06.025

Contribution: LD performed sectioning of all brain tissues. Read the manuscript and provided insights.

Contribution to original knowledge

1. Generation and characterization of a conditional allele of the *Quaking* gene to overcome embryonic lethality.
2. Used this genetic mouse model to delete *Quaking* expression in oligodendrocytes during development and myelinating cells in adulthood.
3. Established a role for QKI in oligodendrocyte development and myelin maintenance.
4. Identified QKI as the long-sought regulator of *Neurofascin* alternative splicing in glial cells.
5. Identified genome-wide changes in gene expression and alternative splicing following loss of QKI expression in oligodendrocytes.
6. Provided the first evidence that the nuclear QKI-5 protein controls the alternative splicing of the *qkI* pre-mRNA.

Abbreviations list

3'SS	3'-splice site
5'SS	5'-splice site
AIP-1	Actin interacting protein-1
Ahr	Aryl hydrocarbon receptor
AIPD	Acute inflammatory demyelinating polyradiculoneuropathy
AIS	Axon initial segment
AMPA	α-amino-3-hydrocy-5-methyl-4-isoxazolepropionic acid
AR	Androgen receptor
ASD-2	Alternative Splicing Defective-2
ASE	Alternative splicing event
bFGF	Basic fibroblast growth factor
bHLH	Basic Helix-Loop-Helix
BDNF	Brain-derived neurotrophic factor
BMP	Bone morphogenic protein
Bp	Base pair
BPS	Branch point sequence
C/EBPα	CCAAT/enhancer-binding protein
Caspr	Contactin-associated protein
CCPD	Combined central and peripheral demyelination
ChIP	Chromatin immunoprecipitation
CIPD	Chronic inflammatory demyelinating polyradiculoneuropathy
CircRNA	Circular RNA
CNPase	2′,3′-cyclic nucleotide 3′-phosphodiesterase
CNS	Central nervous system
CNTF	Ciliary neurotrophic factor
CSF1R	Colony stimulating factor 1 receptor
CXCL1	Chemokine (C-X-C motif) ligand 1
DCC	Deleted in colorectal cancer
dsRBD	Double stranded RNA binding domain
EAE	Experimental autoimmune encephalomyelitis
EMSA	Electrophoretic mobility shift assay
EMT	Epithelial to mesenchymal transition
Emx1	Empty spiracles homeobox 1
ENU	N-ethyl-N-nitrosourea
ERK1/2	Extracellular signal-regulated kinases 1 and 2
FABP7	Fatty acid binding protein 7
FERM	4.1/ezrin/radixin/moesin domain
FEZ1	Fasciculation and elongation protein Zeta-1

FGF-2	Fibroblast growth factor-2
FMRP	Fragile X mental retardation protein
GalC	Galactocerebroside
GBM	Glioblastoma Multiforme
GFAP	Glial fibrillary acidic protein
Gld-1	Defective in Germ line development-1
Gli1/2	GLI-Kruppel family members 1 and 2
GPR17	G-protein coupled receptor 17
GRP17	Gagg-related protein 17
HOW	Held out wings
IgCAM	Immunoglobulin superfamily of cell adhesion
iPSC	Induced pluripotent stem cells
IGF-I	Insulin-growth factor I
KH	hnRNP K domain
KLF2	Krüppel-like factor 2
LINGO-1	Leucine-rich repeat and immunoglobulin domain containing 1
LISA	Layered and integrated system for splicing annotation
MAG	Myelin associated glycoprotein
Map1b	Microtubule associated protein 1B
MAPK	Mitogen activated protein kinase
Mash1/Ascl1	Achaete-scute family bHLH transcription factor 1
MGE	Medial ganglionic eminence
MBP	Myelin basic protein
MOG	Myelin oligodendrocyte glycoprotein
mRNA	Messenger RNA
MS	Multiple Sclerosis
mTOR	Mechanistic target of rapamycin kinase
Myrf	Myelin gene regulatory factor
Na_v	Voltage gated sodium channel
Nefl	Neurofilament light polypeptide
NeuN	Neuronal nuclei
Nfasc	Neurofascin
NK2.1	NK2 homeobox 1
NMDA	N-methyl-D-aspartate
NMR	Nuclear magnetic resonance
NPC	Neural precursor cells
NrCAM	Neural-glial-related cell adhesion molecule
NT-3	Neurotrophin-3

OL	Oligodendrocyte
OPC	Oligodendrocyte precursor cell
PDGF-A	platelet derived growth factor-A
PDGFR α	platelet derived growth factor α receptor
PLP	Proteolipid protein
pMN	Motor neuron precursors
PNS	Peripheral nervous sytem
Pre-OL	pre-oligodendrocyte
PRMT1	Protein Arginine Methyltransferase 1
PSA-NCAM	Poly-sialylated neural cell adhesion molecule
PTB	Polypyrimidine tract binding protein
QASE	QKI-5 alternative splicing element
QKI, *qkI, HqK*	Quaking
qk^v	Quaking viable
RBP	RNA-binding proteins
RG	Arginine/Glycine
RRM	RNA recognition motif
RT-qPCR	Reverse transcriptase- quantitative Polymerase Chain Reaction
Sam68	Src-associated in mitosis of 68kDa
SC	Spinal cord
SFK	Src family kinases
Shh	Sonic hedgehog
snRNPs	Small nuclear ribonucleoprotein particle
SR	Serine-arginine rich
STAR	Signal Transduction and Activator of RNA metabolism
SVZ	Subventricular zone
T3	Triiodothyronine/thyroid hormone 3
TAG-1	Transient axonal glycoprotein-1
TEM	Transmission electron microscopy
TGFβR2	Transforming growth factor β receptor-2
TLR4	Toll-like receptor 4
U2AF	U2 snRNP auxiliary factor
VEGFR-2	Vascular endothelial growth factor receptor 2
VSMC	Vascular smooth muscle cells
VZ	Ventricular zone
WAVE2	Verprolin-homologous protein 2

List of figures

Figure 1.1: STAR family of RNA binding proteins

Figure 1.2: Structure of the qkI gene.

Figure 1.3: Quaking response element.

Figure 1.4: The role of QKI in regulating several aspects of RNA metabolism.

Figure 1.5: A simplified schematics of the general mechanism of alternative splicing.

Figure 1.6: The role of QKI in human diseases.

Figure 1.7: Myelin structure.

Figure 1.8: Structural domains along the axon.

Figure 1.9: Molecular components of the structural domain along the axon.

Figure 1.10: Neurofascin gene.

Figure 2.1. *QKI*$^{FL/FL;Olig2\text{-}Cre}$ mice display tremors and die at the third post-natal week.

Figure 2.2. Recombination in *QKI*$^{FL/FL;Olig2\text{-}Cre}$ mice leads to loss of QKI proteins expression in OLs.

Figure 2.3 Ablation of QKI in oligodendrocytes leads to hypomyelination.

Figure 2.4. Ablation of QKI in oligodendrocytes leads to loss of mature oligodendrocytes.

Figure 2.5. QKI regulates alternative splicing of *Nfasc* pre-mRNA.

Figure 2.6. *QKI*$^{FL/FL;\ PLP\text{-}CreERT}$ mice display *Nfasc* pre-mRNA splicing defects.

Figure 2.7. Loss of QKI in differentiated primary mouse and rat oligodendrocytes leads to defects in *Nfasc* pre-mRNA splicing.

Figure 2.8. Ultrastructural paranodal defect in *QKI*$^{FL/FL;Olig2\text{-}Cre}$ mice.

Figure 2.9. QKI-deficient mice exhibit axoglial junction defects.

Figure 2.10. Ultrastructural paranodal defect in QKI-deficient mice.

Figure 3.1. Gene expression profiles comparing brains of *QKI*$^{FL/FL;Olig2\text{-}Cre}$ *and QKI*$^{FL/FL;-}$ mice.

Figure 3.2. Gene ontology analysis.

Figure 3.3. Brain alternative splicing patterns of mice with QKI-deficient oligodendrocytes.

Figure 3.4. Alternative splicing event in *Bcas1, Sema6a* and *Capzb* in *QKI*$^{FL/FL;Olig2\text{-}Cre}$ *and QKI*$^{FL/FL;-}$ mice.

Figure 3.5. Alterative splicing patterns of *qkI* in *QKI*$^{FL/FL;Olig2\text{-}Cre}$ *and QKI*$^{FL/FL;-}$ mice.

Figure 3.6. QKI proteins regulate self-splicing in mice.

Figure 3.7. QKI-5 regulates self-splicing *in vitro* in human cells.

Supplementary figures

Supplementary Figure 3.1. Global effects of loss of QKI in OLs on gene expression.

Supplementary Figure 3.2. Motif enrichment analysis for QKI activated and QKI repressed SE events.

Supplementary Figure 3.3. Alternative splicing of the 3'-UTR of the *qkI* gene.

Supplementary figure 3.4. Sashimi plots of alternative splicing events in *Bcas1, Sema6a, Capzb* and *qkI* in $QKI^{FL/FL;Olig2\text{-}Cre}$ *and* $QKI^{FL/FL;-}$ mice.

Supplementary Figure 3.5. Original PCR gels.

Supplementary Figure 3.6. Original PCR gels and western blots.

List of tables

Table 2.1. Top alternatively spliced events identified using LISA in $QKI^{FL/FL:Olig2\text{-}Cre}$ mice.

Table 3.1. Alternative splicing events in $QKI^{FL/FL;Olig2\text{-}Cre}$ mice identified by RNA-seq.

Introduction and thesis objectives

Ever since the discovery of the natural mouse mutant *quaking viable*, an interest in the Quaking proteins and their function in oligodendrocyte and myelination has developed. Several decades of research have focused on using *in vitro* systems as well as the *quaking viable* mouse both of which impose their own limitations. The main focus of my thesis was to investigate the role of Quaking proteins in oligodendrocytes during development and in adult myelinating cells. To overcome embryonic lethality of *qkI* null mice and provide a better model to study the functions of QKI, we generated a conditional allele of *qkI*. The objective of my thesis was to characterize the role of QKI proteins in regulating RNA metabolism in glial cells. To achieve this, we deleted the expression of *qkI* in oligodendrocytes during development using the *Olig2-Cre* driver and in adult myelinating cells using the *PLP-CreERT* driver. In chapter 2, we characterized our newly generated *qkI* conditional allele and evaluated the impact of ablating QKI expression on 1328 known alternative splice events in the mouse brain. In chapter 3, we used RNA-sequencing (RNA-seq) to identify global changes in gene expression and alternative splicing. Together, both studies have identified novel targets of QKI alternative splicing regulation and provided proof-of-principle that indeed the QKI proteins are essential players required for the proper development and maintenance of myelin through regulation of RNA metabolism.

Chapter 1: Literature review

1.1 RNA binding proteins

RNA binding proteins (RBPs) play pivotal roles in post-transcriptional regulation and maintaining cellular homeostasis by orchestrating the spatial, temporal and functional dynamics of transcripts. RBPs control gene expression by regulating pre-mRNA splicing, polyadenylation, mRNA trafficking, mRNA stability, translation, and decay. Target RNA recognition by RBPs typically occurs through RNA-binding domains or low complexity sequences that either bind single or double-stranded RNA, specific structural features or in a non-specific manner (Burd and Dreyfuss, 1994, Calabretta and Richard, 2015, Gerstberger et al., 2014). There are several RNA-binding domains that mediate protein-RNA recognition. These domains include but are not limited to: RNA recognition motifs (RRMs), double stranded RNA binding domains (dsRBDs), hnRNP K-homology (KH) domain, and DEAD-box helicase domain (reviewed in (Lukong et al., 2008)). In this thesis, only the KH domain containing RNA binding proteins will be discussed.

1.1.1 KH domain containing RNA binding proteins

The KH domain is named so due to its discovery in the human heterogeneous ribonucleoprotein K (hnRNP K) protein (Siomi et al., 1993a). This domain consists of about 70 amino acids that are found as either a single (Sam68 (Lukong and Richard, 2003)), double (Fragile X mental retardation or FMRP (Siomi et al., 1993b) or multiple copies (McKnight et al., 1992), suggesting that this domain may function cooperatively or independently (Burd and Dreyfuss 1994). The KH domain consists of three antiparallel β strands that are packed against three α helices with a minimal KH motif in the linear sequences (βααβ) (Grishin, 2001). An additional α and β element determine the type of the KH domain (either C-terminal in type I eukaryotes (βααββα), or N-terminal in type II prokaryotes (αββααβ)) (Grishin, 2001, Valverde et al., 2008). Within the KH domain, the RNA interacts with a highly conserved Gly-x-x-Gly loop; where x is a positively charged amino acid (Siomi et al., 1994 Nussbaum, & Dreyfuss, 1994, Lukong & Richard, 2003). The conserved loop functions to link the two helices of the minimal core (Musco et al., 1996, Grishin, 2001). KH domains are known to bind either single stranded DNA or RNA molecules. On one side, α1 and α2 helices that are linked by the GXXG loop along with the β-

sheet and a variable loop on the other side form the binding surface (Valverde et al., 2008). This allows the formation of a binding groove that accommodates four bases (Valverde et al., 2008). Due to the low affinity reported for the KH domain, RBPs have evolved two strategies to increase their affinity and specificity, which include: 1) extending the interaction surface with the KH domain, and 2) the inclusion of multiple KH domains within the RBP.

KH domain containing proteins play a role in a variety of cellular functions with several diseases being associated with the loss of the KH domain function. An example is the Fragile X syndrome where a single point mutation in the Fragile X mental retardation protein (FMRP) was shown to lead to the disease due to unfolding of the KH domain (De Boulle et al., 1993).

A subset of the KH domain containing proteins is a family of proteins that are involved in regulating RNA metabolism and are themselves regulated by signal transduction, allowing the coupling of cellular signalling to post-transcriptional regulation of gene expression (Vernet and Artzt, 1997). This family is known as the STAR family of proteins standing for **S**ignal **T**ransduction and **A**ctivation of **R**NA metabolism. The proteins in this family have a single KH domain flanked by conserved N-terminal and C-terminal sequences. Signalling pathways have been shown to regulate the function of these proteins due to the presence of proline rich regions bound by SH3 and WW domains; clusters of serine, threonine and tyrosines which are phosphorylated by kinases; arginines in RGG/RG motifs which are sites of methylation. In the following sections, the STAR proteins are discussed in detail.

1.1.2 STAR RNA binding proteins

1.1.2.1 Discovery of the STAR RNA binding proteins

The first member of the STAR family to be discovered was initially called p62 (Wong et al., 1992) . In 1994, it was renamed Sam68 (Src-associated in mitosis of 68kDa, also known as *KHDRBS1*) (Fumagalli et al., 1994, Taylor and Shalloway, 1994). Sam68 was also shown to function as an adapter protein for Src kinases (Richard et al., 1995, Weng et al., 1994). Later, in 1999, two mammalian orthologs of Sam68 were discovered, *Slm1* (known as *Khdrbs2*) and *Slm2/T-Star* (known as *Khdrbs3*) (Di Fruscio et al., 1999, Venables et al., 1999). Sam68 along with SLM1 and SLM2 make up one subfamily of STAR proteins. Another subfamily was identified shortly after the discovery of Sam68. It includes three genes that are evolutionarily conserved and share sequence homology to Sam68. These proteins include *Gld-1* (Defective in

Germ Line Development protein 1) in *C. elegans* (Jones and Schedl, 1995), *Quaking* in mouse (Ebersole et al., 1996a) and *How* (Held Out Wings) in *Drosophila* (Baehrecke, 1997, Zaffran et al., 1997). A new member was added to the family in 1996 which was the human Splicing Factor 1 (SF1) (Arning et al., 1996). In 2008, a final STAR family member was discovered in *C. elegans* and termed Alternative Splicing Defective-2 (*asd-2*) that phylogenetically belongs to the subfamily that includes *qkI*, *How* and *Gld-1* (Ohno et al., 2008). A phylogenetic representation of the STAR proteins is shown in Figure 1.1A.

In comparison to other members of the KH family of proteins, the STAR proteins differ in two aspects. While most KH containing proteins have multiple KH domains, the STAR proteins have only one maxi-KH domain comprising of two additional alpha helices and a variable loop (Maguire et al., 2005, Liu et al., 2001). Moreover, this unique KH domain is flanked by two domains, an N-terminal domain called QUA1 and a C-terminal domain called QUA2 (Figure 1.1B). The QUA1 has been shown to be necessary for homo- and/or heterodimerization that is thought to stabilize RNA binding (Chen and Richard, 1998, Wu et al., 1999). The QUA2 participates in RNA binding along with the KH domain (Liu et al., 2001). SF1 is the only exception to this domain organization due to the lack of QUA1 domain. The QUA1-KH-QUA2 domains make up approximately 200 amino acids and all together are known as the STAR domain (Vernet and Artzt, 1997). My thesis is focused entirely on Quaking and will be discussed in detail in the next section.

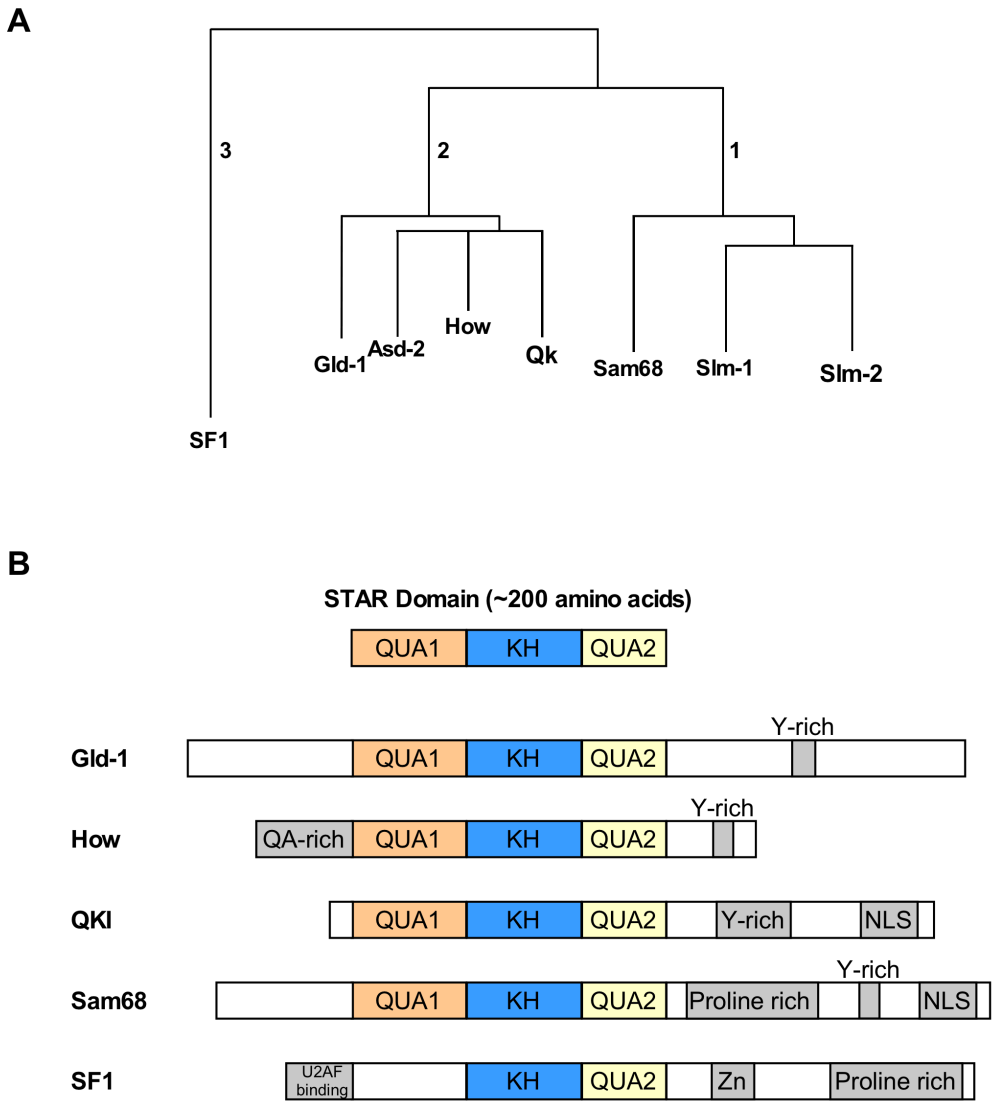

Figure 1.1: STAR family of RNA binding proteins. A. The tree of the STAR family of RNA binding proteins. B. Structural domains of the STAR domain for each of Gld-1, QKI, How, Sam68 and SF1. Other important domains are also shown. Permission to reprint is granted from Springer Nature (Figures are adapted from (Ryder and Massi, 2010, Artzt and Wu, 2010)).

1.2 QUAKING

1.2.1 Discovery of the Quaking (qkI) gene and Quaking Viable mice

The name "*quaking*" comes from the phenotype of the *quaking viable* (*qk*^{v}) mice that were discovered in 1961 in a female mouse of the DBA/2J strain (Sidman et al., 1964). Following a series of outcrossing and backcrossing with C3H/Fi strain, more *quaking* animals were recovered. *Quaking viable* is a spontaneous autosomal recessive mutant mouse with tremors in the hindquarters and severe myelination defects in the CNS (more so in the brain than spinal cord) albeit normal myelination occurs in the peripheral nerves (Sidman et al., 1964). The tremor is observed starting at post-natal days 10-12 and is accompanied by frequent seizures. Males and females are fertile, however, the males rarely sire litters due to arrested spermatid maturation (Bennett et al., 1971). Mild changes in lipid metabolism, myelin protein levels as well as levels of some neurotransmitters were reported (Hogan and Greenfield, 1984), yet these changes could be a result of the myelination defect.

The *qk*^{v} mice harbor a ~1 Mb deletion on chromosome 17 encompassing *parkin* and *parkin-co-regulated* (*parcg*) genes as well as the promoter/enhancer region of the *qkI* gene (Ebersole et al., 1996a). As a result, these mutants produce about 5 to 10% of normal myelin amounts in the brain and this myelin fails to compact leading to vigorous tremors starting at post-natal day 10 (Hardy, 1998a, Sidman et al., 1964). The dysmyelination phenotype is a consequence of the failure of oligodendrocytes to differentiate, resulting in reduced number of myelin lamellae and uncompacted myelin (Hardy, 1998a, Hogan and Greenfield, 1984). This leads to the severe tremor phenotype when myelin function becomes important around postnatal day 11-12 (Hardy, 1998a). Three distinct mRNAs are produced from the *qkI* gene: *qkI-5*, *qkI-6* and *qkI-7* (described in detail in section 1.2.3). QKI-6 and -7 isoforms are absent in oligodendrocytes of *qk*^{v} mice, yet in certain brain areas, the expression of all three isoforms is reduced, indicating a mosaic expression pattern due to loss of an oligodendrocyte-specific enhancer/element (Hardy et al., 1996). Specifically, the reduction in QKI-5 levels is only seen in severely affected areas of the brain (Hardy et al., 1996). Another example of the mosaic expression pattern in *qk*^{v} is the complete lack of QKI-6/QKI-7 in oligodendrocytes of the optic nerve whereas QKI-5 expression is normal (Hardy et al., 1996). Normal expression of QKI proteins is also seen in astrocytes and Bergmann glia in the cerebellum (Hardy et al., 1996). Similarly, in the PNS, the myelin forming Schwann cells lack QKI-6 and QKI-7 yet still show only mild dysmyelinating phenotype (Suzuki and Zagoren, 1977). The *qk*^{v}

mice also suffer from mild hydrocephalus (accumulation of cerebrospinal fluid in the brain leading to enlarged ventricles and increased intracranial pressure) due to loss of *parcg* gene. This leads to defects in ependymal cilia function resulting in a reduced cerebrospinal fluid movement and circulation (Wilson et al., 2010).

Parkin null mice do not display dysmyelination, tremors or seizures and therefore do not contribute to the phenotype of the qk^{v} mice (Itier et al., 2003). *Parkin-co-regulated* gene is abundantly expressed in testis and transgenic expression of *parcg* in qk^{v} testis restores male fertility, defining the lack of *parcg* as the gene responsible for the sterility of male qk^{v} mice (Lorenzetti et al., 2004, Wilson et al., 2010). Transgenic overexpression of QKI-6 in qk^{v} partially rescues the dysmyelination phenotype indicating a requirement for expression of all QKI isoforms in order for proper myelination to occur (Zhao et al., 2006b). Moreover, the ectopic expression of QKI-6 and QKI-7 *in vivo* in progenitors of the ventricular zone using brain injections can direct those cells to migrate to areas of high myelination such as the corpus callosum and become mature myelinating oligodendrocytes (Larocque et al., 2005).

1.2.2 qkI null mice

qkI null mice have provided insights into a function for QKI proteins that precedes their described roles in myelination in qk^{v} mice. Several N-ethyl-N-nitrosourea (ENU) induced mutant mice were generated within the *qkI* gene (Bode, 1984, Justice and Bode, 1988, Noveroske et al., 2005), including $Qk^{I\text{-}1}$, Qk^{kt1}, $Qk^{kt3/4}$, Qk^{k2} and Qk^{tm1abe} (Cox et al., 1999, Justice and Bode, 1988). These alleles when homozygous, are embryonic lethal at midgestation, between E9.5 and E13.5.

The $Qk^{I\text{-}1}$ abolishes the splice site necessary to produce the *qkI-5* transcript by an A to G transition and these homozygous null mice die of vascular insufficiency (Bohnsack et al., 2006). The Qk^{k2} is a T to A transversion which changes a valine to glutamic acid in the KH domain (Noveroske et al., 2005, Cox et al., 1999). The $Qk^{kt3/4}$ is an A to G transition and results in glutamic acid to glycine change in the QUA1 region which blocks dimerization leading to a null allele (Cox et al., 1999, Justice and Bode, 1988, Chen and Richard, 1998). The Qk^{kt1} mutation has yet to be identified but it is known to be outside of the coding sequence (Cox et al., 1999). The Qk^{tm1abe} is also embryonic lethal and the mutation includes a deletion of exon 1 that includes the translational start site (Cox et al., 1999, Justice and Bode, 1988). A viable ENU induced mutant has been identified as well, the *Qke5*, where the mutation is unknown but maps to 40 kb to 640 kb upstream

of the gene and results in extremely severe quaking and seizures (Noveroske et al., 2005). The postnatal OLs of *Qke5* lack QKI-6 and QKI-7 and have reduced levels of QKI-5, as well as Myelin Basic Proteins (MBP) (Larocque et al., 2002, Noveroske et al., 2005).

During embryogenesis, *de novo* differentiation of endothelial cells begins the vascular development. The visceral endoderm instructs mesodermal progenitors to differentiate into primitive endothelial cells (Flamme et al., 1997). Then vascular channels and a capillary plexus are formed and remodeled in a process known as angiogenesis (Flamme et al., 1997). By E9.5, the yolk sac in mouse has an established vascular system consisting of endothelial cell tubes that are stabilized by recruitment of vascular smooth muscle cells and pericytes (Flamme et al., 1997). Mice that are homozygous for Qk^{k2} or Qk^{I-1} alleles also have defects in the yolk sac and embryonic vascular remodeling prior to recruitment of smooth muscle cells resulting in vascular insufficiency and death by E10.5 (Bohnsack et al., 2006). QKI isoforms are known to be expressed in the visceral endoderm (Bohnsack et al., 2006), and Qk^{k2}/Qk^{k2} mice show increased endothelial cell proliferation and visceral endoderm apoptosis. One of the factors secreted by the visceral endoderm is retinoic acid (RA) which targets endothelial cells to allow cell growth control and migration (Bohnsack et al., 2004). In these two mutant mice, the expression of *ALdh1a2/Raldh2*, the enzyme required for RA synthesis, is downregulated (Bohnsack et al., 2006), possibly leading to lack of endothelial cell growth control and maturation and subsequent visceral endoderm apoptosis.

In 2003, a full body knockout mouse of *qkI* was generated, however, these mice were unable to progress beyond E10.5. The null mice were generated by deleting a 355 base pair (bp) region in the first coding sequence in exon 2, which deletes the initiation codon and the first 40 amino acids of the highly conserved QUA1 domain (Li et al., 2003). These mice lack the large vitelline vessels in the yolk sac, have kinky neural tubes, pericardial effusion, open neural tubes and incomplete embryonic turning (Li et al., 2003). Embryonic lethality was due to defective vascular remodeling and abnormally small vitelline vessels within the yolk sac that fail to connect and sustain the embryo at midgestation (Li et al., 2003). Moreover, the vitelline vessel itself was deficient in smooth muscle cells. *qkI* is expressed early in development in endothelial cells and smooth muscle cells and the abnormality in vitelline vessels was attributed to a lack of smooth muscle cells that are needed to stabilize the blood vessel structures and modulate their function (Li et al., 2003). Moreover, the authors of this study have shown a QKI-5 expression in epithelial cells

of the gut, myocardium, endocardium, notochord and neural tissues during embryogenesis. Taken together, this highlights a role for QKI in extraembryonic vascular as well as embryonic cardiovascular development.

1.2.3 Cloning of the qkI gene

The *qkI* gene is located on human and mouse chromosomes 6 and 17, respectively. The first positional cloning and expression analysis of *qkI* was done in 1996 by the Artzt group (Ebersole et al., 1996a) that identified the function of QKI as an RNA binding protein containing a KH domain. Shortly after, two homologs of *qkI* were cloned, the Xenopus *Xqua* (Zorn and Krieg, 1997) and the Drosophila *Held Out Wing* (*How*) (Zaffran et al., 1997). A detailed analysis of the genomic region of *qkI* was published in 1999 (Kondo et al., 1999), showing that the *qkI* locus spans ~65 kb of DNA with a single transcription start site.

The *qkI* pre-mRNA undergoes extensive alternative splicing at its 3' end to generate at least four transcripts producing isoforms termed QKI-5, QKI-6, QKI-7 and QKI-7b, which denote the mRNA length in kilobases (Kondo et al., 1999). These QKI isoforms are encoded by identical exons 1 to 6 but differ in their C-terminal 35 amino acids encoded by exons 7 and 8 (Figure 1.2). One isoform was identified to lack the KH domain and was proposed to be an antagonist to the other transcripts. This message contains only exons 1 to 4 (Kondo et al., 1999). Exons 2, 3, 4 and 5 encode the conserved QUA1, KH and QUA2 domains (Figure 1.2). Exon 7, however, is utilized in an unusual manner. It is made up of 529 6bp, based on sequences from the National Centre for Biotechnology Information. It represents the 3'-UTR for QKI-6 and QKI-7, yet parts of the UTR are used as coding sequences for other alternative transcripts (Figure 1.2). The first 44 bp are designated as exon 7a and is the 3' end of the coding sequence for QKI-7 with the rest representing the 3'-UTR. About 1.2 kb downstream of the start of exon 7, exon 7b is composed of 26 bp and is the 3'-end of the coding sequence for QKI-6, followed by ~4 kb of 3'-UTR that is part of exon 7. Exon 7c, which is 75 bp long, is about 2 kb downstream of exon 7a and is spliced into exon 8 that is part of QKI-5 coding sequence and contains the termination codon for QKI-5 (Kondo et al., 1999), which is immediately followed by the 3'-UTR (Kondo et al., 1999). Moreover, all the exons have proper slicing donor/acceptor sequences (i.e follow the GT-AG rule). It was also determined that the transcription start site was ~630 bp upstream of the 3' end of exon 1 with translation of the QKI proteins starting from the methionine found in the QUA1 domain (Kondo et al., 1999).

This research also identified that *qkI* transcripts with similar 3'-UTRs shared similar expression patterns (i.e. QKI-6 and QKI-7), whereas the transcript with a different 3'-UTR (i.e. QKI-5) showed a different expression pattern. The coding sequence and genomic organization of *qkI* are highly conserved in mammals (Kondo et al., 1999).

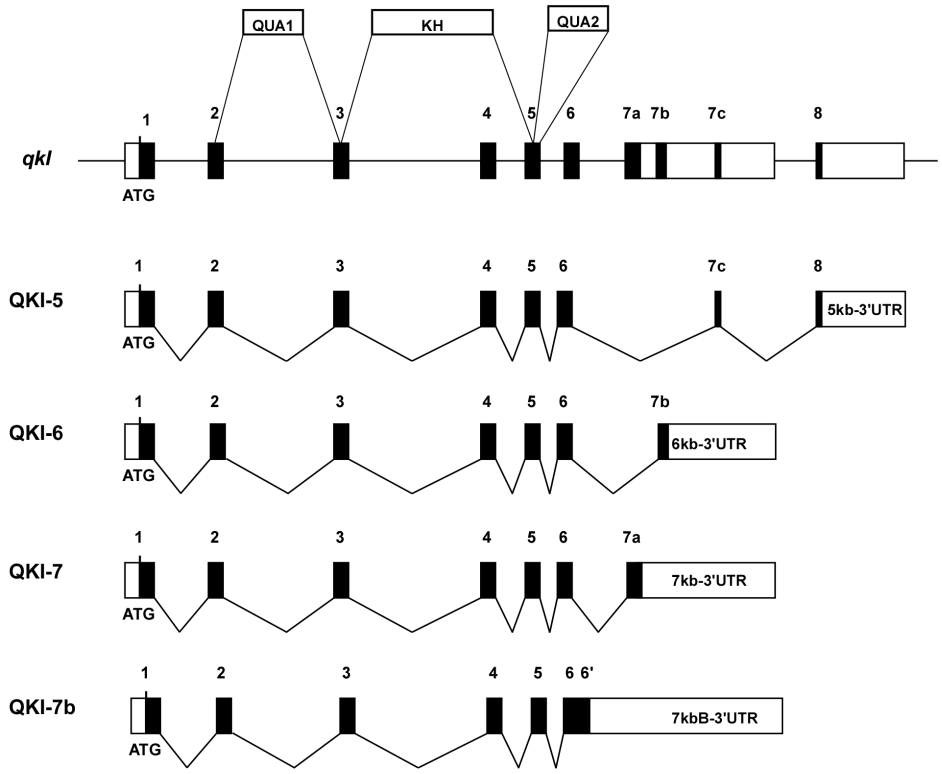

Figure 1.2: Structure of the *qkI* gene. A schematic showing the *qkI* locus with exons and introns. The alternative messages of *qkI* are shown. Name of distinct alternative transcripts are shown on the left. Permission to reprint is granted from John Wiley and Sons (Darbelli and Richard, 2016).

1.2.4 QKI structure

The QKI isoforms, QKI-5, QKI-6, and QKI-7, share an identical RNA binding domain. The RNA binding domain, termed the KH domain, is flanked by an N-terminal QUA1 region and a C-terminal QUA2 region (N- and C-terminal to the KH domain). The QUA1 region mediates homo- and heterodimerization that is required for RNA binding (Chen and Richard, 1998, Teplova et al., 2013, Beuck et al., 2012, Larocque et al., 2002). QKI proteins also contain several proline-

rich regions, and have five tyrosine residues preceding the alternative carboxy ends (Ebersole et al., 1996a).

A canonical KH domain can recognize up to four nucleotides with the addition of secondary structural domains (e.g. QUA2) to allow recognition of longer specific sequences (Wong et al., 2013a). The STAR domain is an example of an extended KH domain. The X-ray structure of the QKI STAR domain bound to RNA is solved (Teplova et al., 2013, Beuck et al., 2012). This KH domain along with the QUA2 region synergistically interact with bases and the sugar-phosphate backbone of the bound RNA recognition element. Homodimerization mediated by the QUA1 domain functions to produce a scaffold to allow simultaneous recognition of two RNA recognition elements and increases RNA binding affinity of the individual KH-QUA1 domains within the homodimer (Teplova et al., 2013). In the absence of RNA, the QUA2 helix is poorly ordered, (Daubner et al., 2014, Maguire et al., 2005) and upon RNA binding, the orientation and protein interaction surface is altered (Teplova et al., 2013, Daubner et al., 2014). The presence of the QUA2 region increases the specificity of recognition from 4 (a typical KH domain) to 6 nucleotides (Musunuru and Darnell, 2004, Teplova et al., 2013, Beuck et al., 2012).

1.2.5 Quaking response element

The QKI isoforms are sequence specific RNA binding proteins (Ryder and Williamson, 2004, Galarneau and Richard, 2005). Using *in vitro* SELEX (systemic evolution of ligands by exponential enrichment), the QKI binding site, also referred to as the QKI response element (QRE), was defined as a bipartite sequence with a core (ACUAAY) and a half site (UAAY) separated by 1 to 20 nucleotides (Figure 1.3) (Galarneau and Richard, 2005). SELEX is a technique of amplifying RNA aptamers from random sequences that preferentially bind QKI. Since all QKI isoforms have the same KH domain, QKI-5 was used in this study. The RNAs were transcribed using T7 RNA polymerase from a pool of 52-nucleotide DNAs with random sequences. Bioinformatic analysis identified the bipartite sequence and extrapolated it to ~1430 putative QKI RNA targets using the Refseq database. Electrophoretic mobility shift assays have demonstrated that while QKI-5 can bind to sequences containing only the core site (K_d~300nM), the presence of the half site allows it to bind with a higher affinity (K_d~100nM) (Galarneau and Richard, 2005). Moreover, QKI-5 binding to its QRE was abrogated when a hairpin structure was imposed on the QRE indicating that QKI binds to its unstructured QRE.

Immunoprecipitation assays using lysates from whole mouse embryos at E15.5 validated 23 mRNAs as novel targets of QKI (Galarneau and Richard, 2005). By annotating the RNA targets from the SELEX screen in the database for annotation, visualization and integrated discoveries (DAVID), it was found that the potential targets of QKI were mostly involved in development, cell adhesion, morphogenesis, organogenesis, transport and cell differentiation, cell growth and/or maintenance and cell communication (Galarneau and Richard, 2005). A later study further confirmed the QRE *in vivo* and found that it is frequently localized to intronic sequences using PAR-CLIP (Photoactivatable Ribonucleoside Enhanced Crosslinking and Immunoprecipitation), supporting a role for QKI in regulating alternative splicing (Hafner et al, 2010).

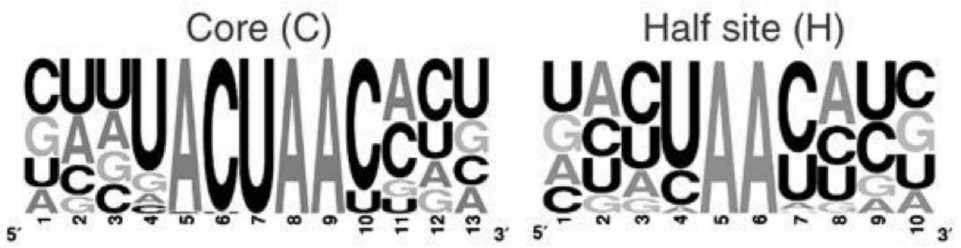

Figure 1.3: Quaking response element. Probability matrix (graphic logo) depicting the relative frequency of each residue at each position within the Quaking response element (QRE). Permission to reprint is granted from Springer Nature (Galarneau and Richard, 2005).

1.2.6 QKI expression

The cloning of the gene responsible for the dysmyelination of the *quaking viable* mice in 1996 revealed that the *qkI* gene encodes several RNA binding protein isoforms that contain a KH domain (Ebersole et al., 1996b). In mid 1990s, whole mount *in situ* hybridization of embryos first detected expression of QKI in the neuroepithelium of the head at E7.5. Then in the nascent brain and neural tube, expression was detected strongly between E8.5 and E9.5 and in the heart of E8.5 embryos (Ebersole et al., 1996a). Adult mice northern blots of total RNA from tissues detected the most abundant expression in the brain and lung (*qkI-6* and *qkI-7*), heart (*qkI-6*), and testis (*qkI-5*) with no expression detected in liver, kidney, ovaries and spleen (Ebersole et al., 1996a). We now know that the *qkI* isoforms are also expressed in muscle, prostate, colon and stomach, as well as cells of the myeloid lineage (Bian et al., 2012, Yang et al., 2010, de Bruin et al., 2016a).

The cellular localization of QKI-5 is predominantly nuclear under steady state, as this isoform contains a strong nuclear localization signal at its C-terminus (RVHPYQR), although it can shuttle between the nucleus and the cytoplasm (Wu et al., 1999). QKI-6 is distributed throughout the cell, while QKI-7 is mainly cytoplasmic at steady state (Pilotte et al., 2001). The localization of QKI-7b is cytoplasmic, however this isoform has not been extensively studied and its function remains relatively uncharacterized (Li et al., 2002). Moreover, the 14 C-terminal amino acids that are unique to QKI-7 have been shown to induce apoptosis in the cytoplasm independent of RNA-binding activity (Pilotte et al., 2001), whereas, coexpression of either QKI-5 or QKI-6 were sufficient to inhibit apoptosis by translocating QKI-7 to the nucleus (Pilotte et al., 2001). The nuclear and cytoplasmic QKI proteins play opposing roles in cell differentiation as the cytoplasmic QKI-6/QKI-7 promote cell cycle exit, whereas QKI-5 tends to keep cells in a proliferative state (Larocque et al., 2009, Larocque et al., 2005). Therefore, even though the QKI proteins share similar selectivity and affinity to target mRNAs (Galarneau and Richard, 2005), their cellular localization and temporal pattern of expression play a role in determining their influence on target RNAs.

1.2.7 Regulation of qkI expression and activity

QKI proteins are expressed in a defined spatial and temporal manner in different tissues and cell types. Therefore, an exquisite network of expression regulation must take place to ensure proper expression patterns. In the following sections, the regulation of *qkI* expression is discussed in detail.

1.2.7.1 Transcriptional

The expression of the QKI isoforms is tissue and cell type specific (Ebersole et al., 1996a), however, little is known about the transcriptional factors that regulate this selective expression. The first example of transcriptional regulation of the *qkI* gene is highlighted by the *quaking viable* mice that lack a 5' regulatory region upstream of the gene. The lack of QKI-6 and QKI-7 in myelinating cells indicates that specific regulatory regions control the expression of the QKI proteins in different cells. A later study looked at the genomic organization of the *qkI* gene in detail (Kondo et al., 1999). Following determination of the transcription start site, the authors of the study examined the genomic region immediately upstream of this site. This analysis failed to identify any TATA and CAAT boxes, but did identify a GC-rich element (74.8%) that is 472 bp

upstream of the transcription start site (Kondo et al., 1999). Several Sp1 (zinc transcription factor) potential binding sites were found in the GC-rich region as well as sites for v-Myb and AP2 (Kondo et al., 1999). Looking further upstream, possible binding sites for MyEF-2 (myelin gene expression factor-2) and Gtx (glial and testis specific homeobox gene) were found (Haas et al., 1995, Komuro et al., 1993).

Using hematopoietic progenitor cells, it was observed that an increase in *qkI* expression, specifically QKI-5, occurred during early stages of conversion of $CD34^+$ progenitor cells to monocytes, with monocyte-to-macrophage differentiation being associated with a striking decrease in QKI-5 expression (Fu et al., 2012). This increase in QKI-5 was due to transcriptional activation in early monocytic progenitors. Computational analysis identified multiple CCAAT/enhancer-binding protein (C/EBPα) binding sites within the promoter region of *qkI*, suggesting that this transcription factor induces *qkI* expression during the conversion of $CD34^+$ progenitor cells to monocytes. Indeed, chromatin immunoprecipitation (ChIP) analysis confirmed that C/EBPα occupies a distal C/EBPα-binding site and activates transcription of *qkI* (Fu et al., 2012). Blocking *qkI* induction using RNA interference leads to enhanced expression of endogenous colony stimulating factor 1 receptor (CSF1R) which facilitates macrophage differentiation.

Moreover, through examination of cancer genome data, QKI was identified as a potential downstream target of p53. A putative p53 binding site was found in the *qkI* promoter that was validated by ChIP assays to be bound by p53 and therefore, transcriptionally activated (Chen et al., 2012).

A recent study in endothelial cells has identified a novel transcription factor regulating *qkI* expression (de Bruin et al., 2016b). This study showed that QKI proteins are expressed in macro- and micro-vascular endothelial cells *in vivo*. Further, the endothelial cells increase QKI expression when cultured in laminar flow and the increase was due to transcriptional activation of the *qkI* promoter by Krüppel-like factor 2 (KLF2). Binding of KLF2 to the *qkI* promoter was confirmed by promoter-luciferase reporter gene (de Bruin et al., 2016b).

In the context of prostate cancer, the expression of the *qkI* gene was found to be regulated by the androgen receptor (Zhang et al., 2018). Androgen receptor binding elements were found in the *qkI* promoter region and luciferase assays as well as siRNA mediated knockdown of AR, demonstrated that AR positively regulates *qkI* expression in AR positive cell lines and clinical

prostate cancer samples (Zhang et al., 2018). However, an actual physical association of AR with the *qkI* promoter is yet to be demonstrated. Therefore, these studies show that at the level of transcription, the expression of *qkI* is regulated by different transcription factors and implies that more research is required to identify the different transcriptions factors regulating *qkI* expression in different tissues/cells.

Moreover, a recent report has shown that a MYB-QKI fusion protein is the driver mutation in angiocentric gliomas (Bandopadhayay et al., 2016). Interestingly, the *MYB* gene is not expressed normally in the brain suggesting that the 3' end of the *qkI* gene might harbour brain specific enhancers.

1.2.7.2 Alternative splicing/ mRNA stability and translation

The 3' coding exons of *qkI* are subject to extensive alternative splicing to generate several transcripts. The first evidence for alternative splicing regulation of the *qkI* gene stems from changes in mRNA expression profiles during development with QKI-5 being most abundant during embryogenesis followed by an increase in QKI-6 and QKI-7 expression. Moreover, looking at the ENU-induced mutants, $qk^{l\text{-}1}$ which lacks the QKI-5 isoform and q^{kk2} which has a point mutation in the KH domain, it was demonstrated that there is a lack of *qkI-6* and *qkI-7* expression. This suggests that QKI-5 regulates the generation of *qkI-6* and *-7* transcripts through alternative splicing or transcript stabilization (Bohnsack et al., 2006).

Furthermore, QKI-5 appears to be the default splice variant since it is the predominant isoform during embryonic development and in many adult tissues (Lu et al., 2003, Hardy et al., 1996). It is worth noting that exon 7c, specific to QKI-5, is found at the most 3'-end and yet appears to be the default splice site (Bockbrader and Feng, 2008). The *qkI* gene itself contains several QREs across its sequence which could imply that QKI itself could regulate its own alternative splicing and/or RNA stability.

1.2.7.3 Post-translational modifications

Several signaling pathways regulate the function of QKI proteins. The QKI proteins contain multiple proline rich Src-homology 3 (SH3)-binding motifs implying that QKI could bind to signaling proteins that contain SH3 domains and therefore connect signaling pathways to RNA

metabolism (Zhang et al., 2003). Moreover, tyrosine phosphorylation of QKI by Src family kinases negatively impacts its binding to MBP mRNAs (Zhang et al., 2003), a well-characterized mRNA ligand of QKI (Larocque et al., 2002, Li et al., 2000). This post-translational modification decreased the affinity of QKI proteins to their target RNA *in vivo* and *in vitro* (Zhang et al., 2003). Moreover, Fyn kinase and QKI activity have been shown to antagonistically regulate the alternative splicing of MBP mRNA isoforms (Lu et al., 2005). This is in line with similar observations where tyrosine phosphorylation of other STAR family proteins such as Sam68 reduces their affinity to their target mRNAs as well as suppresses alternative splicing (Stoss et al., 2004, Paronetto et al., 2007). Moreover, it is postulated that the increase in Fyn activity upon OL differentiation may help release the nuclear retention of MBP by QKI-5. The importance of this regulation is highlighted by the fact that Src-PTKs can be linked to extracellular signals which can in turn modulate several aspects of OL development. For example, growth factors such as insulin-like growth factor-I (IGF-I) and platelet-derived growth factor (PDGF) can activate Fyn kinase which in turn regulates QKI function (Cui et al., 2005, Miyamoto et al., 2008).

Serine/threonine phosphorylation has not been observed for QKI yet, however this modification on Sam68 (a STAR family prototype) functions to improve its RNA binding affinity (Matter et al., 2002). QKI-5 has also been shown to be arginine methylated *in vivo* by Protein Arginine Methyltransferase 1 (Cote et al., 2003). The functional consequences of arginine methylation of QKI remain to be investigated. Other PTMs have been identified for a few of the STAR family proteins such as the lysine acetylation of Sam68, which functions to increase its RNA binding (Babic et al., 2004). Therefore, it is plausible to speculate that QKI could undergo much more PTMs than already identified which in turn could function to regulate several aspects of its function. These combined features of QKI allow for extracellular signals to regulate RNA processes, defining the QKI proteins as STAR proteins.

1.2.7.4 microRNA

QKI-5 and *Xenopus Qk* (*Xqua*) have a highly conserved 3'-UTR with over 300 nucleotides being 90% identical. Vertebrate *qkI* genes have also two entirely different 3'-UTRs (for QKI-6/QKI-7 and QKI-5) that are also highly conserved. A web-based bioinformatics analysis of human *quaking* (*HqK*) 3'-UTRs has ranked QKI at the 11th position on the list of the top 20 microRNA binders (Artzt and Wu, 2010). This study has also showed that QKI tops the list of

STAR proteins in terms of theoretical number of bound microRNAs by 3 to 6.5-fold indicating that this high binding number is unique to QKI and not a general feature of the STAR proteins (Artzt and Wu, 2010). Moreover, some microRNAs that are predicted to bind in the 3'-UTR of QKI have been shown to be specifically expressed in neural tissues (Christensen and Schratt, 2009), myocardial, microvascular and endothelial tissues (Urbich et al., 2008) and some immune cells (Lu and Liston, 2009).

Recent reports have also demonstrated that QKI expression is regulated by miRNAs. NF-κB and TGF-β/Smad signaling activities have been shown to lead to increased expression of miR-148a in glioblastoma cell lines *in vivo* and *in vitro* and in Glioblastoma Multiforme (GBM), which in turn targets and reduces the expression of QKI (Wang et al., 2015a). This results in enhanced and prolonged activation of the TGFβ/Smad signaling cascade that significantly correlates with miR-148a levels in a cohort of human glioblastoma tumors (Wang et al., 2015a). miR-29a is another miRNA that was identified to regulate *qkI* expression in glioblastoma stem cells (Xi et al., 2017). Several other miRNAs were identified to regulate *qkI* expression in different types of cancers including colorectal cancer (miR-574-5p and miR-155) (Ji et al., 2013, He et al., 2015), leukemia (miR-155) (Tili et al., 2015), cervical cancer (miR-574-5p) (Ma et al., 2016), esophageal squamous cell carcinoma (miR-143-3p) (He et al., 2016) and in arsenic-induced hepatic cancer (Chen et al., 2018).

Moreover, a role for microRNA regulation of *qkI* expression during development of neural progenitors has been reported (Shu et al., 2017). miR-214-3p was found to be highly expressed in neural progenitors *in vivo* and *in vitro* and functions to inhibit self-renewal and promote neurogenesis (Shu et al., 2017). This miRNA targets *qkI* mRNA expression by binding to the 3'-UTR in progenitor cells of the proliferative ventricular zone leading to reduced QKI levels and further differentiation into neurons (Shu et al., 2017). Notably, miR-214 has been shown to negatively regulate QKI expression is several cellular processes such as angiogenesis (van Mil et al., 2012), neural dendritic morphogenesis (Irie et al., 2016) and smooth muscle cell differentiation (Wu et al., 2017). miR-29a was shown to target *qkI* expression during monocyte to macrophage differentiation (Wang et al., 2015b). Targeting *qkI* expression during hypoxia/reoxygenation injury in cardiomyocytes by miR-208a/b was shown to exacerbate the injury (Wang et al., 2017b). These studies highlight the potential of microRNA regulation of QKI expression in controlling its spatial and temporal activities.

1.2.8 Functions of the QKI proteins

1.2.8.1 RNA trafficking

In the 1990s, a role for RNA trafficking regulation was proposed for QKI since cultured qk^v oligodendrocytes fail to translocate MBP mRNAs to their processes (Barbarese, 1991). Indeed, this was later confirmed by Larocque et al, 2002 by using OLs cultures overexpressing QKI-5, which recreated the MBP nuclear retention defects observed in qk^v mice (Figure 1.4) (Larocque et al., 2002). However, overexpression of QKI-6/7 in these oligodendrocytes transduced with QKI-5 rescues the nuclear retention of MBP mRNA, indicating that the cytoplasmic QKI proteins likely play a role in nuclear RNA export and derepression of nuclear retention by QKI-5 (Larocque et al., 2002). All three major QKI isoforms bound to the 3'-UTR of MBP and the binding site was mapped between nucleotides 680 to 790 (Larocque et al., 2002). These findings provided the first evidence for a role of QKI proteins in controlling RNA trafficking and further confirmed that the qk^v mice dysmyelination phenotype is associated with a deficiency in QKI RNA binding proteins.

A recent report has highlighted a novel role for QKI in macrophage polarization (Wang et al., 2017c). Cytokines and microbial agents polarize macrophages into either M1-type (pro-inflammatory) or M2-type (anti-inflammatory). Lipopolysaccharide (LPS) induces macrophage activation via toll-like receptor 4 (TLR4) leading to a pro-inflammatory response. Treatment of peritoneal macrophages with LPS leads to reduced QKI expression (Wang et al., 2017c). Silencing QKI led to a shift in macrophage polarization towards an M1 state, concomitant with increased expression of pro-inflammatory genes, whereas QKI-5 overexpressing cells showed an increase in anti-inflammatory markers. Loss of QKI mediated its effects by increasing NF-κB activation via enhanced nuclear translocation of p65 along with enhanced phosphorylation (Wang et al., 2017c). Aryl hydrocarbon receptor (Ahr) a negative regulator of TLR signaling was showen to harbour a QRE in its 3'-UTR. Loss of QKI expression was shown to also lead to a reduced mRNA stability and protein expression of Ahr and hence an increased TLR signaling (Wang et al., 2017c). These results were recapitulated in mice lacking QKI expression in macrophages (a conditional knockout model). LPS injection of these mice was lethal by 72h post-injection whereas transfer of peritoneal macrophages overexpressing QKI-5 leads to resistance to LPS-induced lethality (Wang et al., 2017c).

1.2.8.2 Translation

QKI-6 functions as a translational repressor through a mechanism similar to *C. elegans* Gld-1 to repress translation of *Gli1* mRNA (Saccomanno et al., 1999, Lakiza et al., 2005). In these studies, QKI-6 was shown to bind to TGE (*tra-2* and *Gli* elements) *in vivo* and *in vitro*, in a similar manner to Gld-1 and mediate translational repression. Later on, microtubule associated protein 1B (Map1b) was found to be regulated by QKI proteins in glial cells where it plays a role in myelin development (Figure 1.4) (Meixner et al., 2000). QKI binds to the 3'-UTR of Map1b to enhance its expression which is found to be reduced in qk^{v} mice. The QKI binding to Map1b was mapped to a 1.5 kb fragment containing multiple QREs (Zhao et al., 2006a). Cytoplasmic QKI-6 was also shown to bind to a QRE in the 3'-UTR of hnRNP A1 and supress its translation which in turn can regulate alternative splicing of myelin associated glycoprotein (MAG) independent of the nuclear QKI-5 (Zhao et al., 2010). QKI-6 was shown to selectively interact with human and mouse hnRNP H in a QRE dependent manner to negatively regulate its level by suppressing its translation (Mandler et al., 2014).

Krox-20 (also known as early growth 2, Egr-2) is a zinc finger transcription factor that has been shown to play a role in Schwann cell differentiation and myelination in the peripheral nervous system (Nabel-Rosen et al., 2002). It harbors a QRE in its 3'-UTR that was shown using electrophoretic mobility shift assays to be bound by QKI proteins (Galarneau and Richard, 2005). The expression of a reporter gene harboring the Egr-2 3'-UTR was shown to be inhibited by QKI-5 and promoted by QKI-6 and QKI-7 (Nabel-Rosen et al., 2002).

Moreover, it was identified that QKI contributes to endothelial cells barrier function by binding to VE-cadherin and β-catenin which are both essential for endothelial adherent junctions (de Bruin et al., 2016b). Both mRNAs contained QREs in their 3'-UTRs (Galarneau and Richard, 2005) that were bound by QKI (de Bruin et al., 2016b). Luciferase reporter assays using the 3'UTRs of those genes showed an increase in luciferase activity that was blunted when QKI was repressed indicating that QKI can bind and increase translation of those genes (de Bruin et al., 2016b). Reduced QKI levels attenuated VE-cadherin and β-catenin expression, without affecting their mRNA levels. This led to a reduced endothelial barrier function *in vitro* and resulted in increased bradykinin-induced vascular leakage *in vivo* in qk^{v} *mice* (de Bruin et al., 2016b). Taken together, this provides support for a crucial role for QKI in maintaining endothelial barrier function.

A recent report has identified a novel role for QKI proteins in regulating viral replication (Liao et al., 2018). Dengue is a viral disease caused by four dengue viruses (DENV1-4) which are enveloped, positive-strand RNA viruses (Liao et al., 2018). A comprehensive screen identified QKI as a host cell protein that physically interacts with the 3'-UTR of DENV4. A QRE was mapped in the 3'-UTR to be downstream of the stop codon whose mutation leads to increased viral RNA accumulation. Depletion of QKI using siRNA lead to increased viral particle production indicating that QKI negatively impacts viral replication (Liao et al., 2018). Dual luciferase assays indicated that QKI functions to inhibit translation of DENV4 RNA leading to reduced viral particle production.

1.2.8.3 mRNA stability, turnover and decay

QKI deficiency has been shown to cause destabilization of many mRNAs that play key roles in OL differentiation and myelin synthesis. An example is the destabilization of MBP mRNA in qk^v mice (Li et al., 2000). There are four major MBP mRNA splice variants (21.5, 18.5, 17.2 and 14 kDa MBP) with the following relative mRNA abundance: 14 > 18.5> 17.2 >21.5. All these isoforms were expressed in qk^v brain albeit to a much lesser extent then in wild-type brain, especially the variants containing exon 2 (18.5 and 14) (Li et al., 2000). Reduction in MBP protein levels was found to be more severe than that of MBP mRNA. Transcriptional output of the *Mbp* gene was similar between wild-type and qk^v mice with reduced MBP mRNAs only in the cytoplasm (Li et al., 2000). Polysome profiling of MBP mRNA showed almost identical translational profile between wild-type and qk^v mice indicating that MBP mRNAs are actively translated. QREs were found in the 3'-UTR of MBP mRNAs that were bound by QKI indicating that QKI might potentially play a role in stabilizing the MBP mRNAs (Li et al., 2000).

The first direct evidence for the role of QKI proteins in regulating RNA stability stems from a study in 2005 where the authors show that primary rat OPCs transduced with QKI-6 and QKI-7 exited cell cycle and differentiated (Larocque et al., 2005). This was due to binding of QKI proteins to a QRE in the 3'-UTR (between nucleotides 618 and 647) of the cyclin dependent kinase inhibitor $p27^{kip1}$ mRNA, which is a well-known OL cell differentiation factor that binds and prevents activation of cyclin E-CDK2 or cyclin D-CDK4 complexes. This in turns controls cell cycle progression at the G1 phase to promote cell cycle arrest and cellular differentiation (Larocque et al., 2009, Larocque et al., 2005). The binding of QKI was shown to stabilize $p27^{kip1}$ mRNA

following transcriptional inhibition (Figure 1.4) (Larocque et al., 2005). Similar experiments have later identified actin interacting protein-1 (AIP-1) as a target of QKI during OL development, where the binding of QKI to a QRE (between nucleotides 2902-2944) in the 3'-UTR of AIP-1 decreases its stability which was also shown to occur during normal differention of OLs to allow proper process extension (Doukhanine et al., 2010). Other targets of QKI during OL development were later identified (including hnRNP A1 and Sirt-2) and were shown to be bound by QKI to QREs in the 3'-UTRs which lead to increased mRNA stability (Zearfoss et al., 2011, Thangaraj et al., 2017).

An anti-apoptotic role for the QKI isoforms was also identified in neonatal cardiomyocytes and adult rat hearts, where QKI-5 and QKI-6 were found to inhibit the pro-apoptotic transcription factor FOXO1 following stimulated ischemia/reperfusion (Guo et al., 2011). In line with these observations, QKI was found to regulate FOXO1 post-transcriptionally by binding to the 3'-UTR of FOXO1 mRNA and directly decreasing its mRNA stability (Yu et al., 2014). Subsequent studies using *ob/ob* diabetic mice showed that QKI deficiency leads to over activation of FOXO1, which in turn aggravates ischemia/ reperfusion injury by increasing nitrosative and endoplasmic reticulum stress in diabetic myocardium (Guo et al., 2014).

In Zebrafish, QKI has also been shown to be important for the initial steps of myofibril assembly in skeletal muscles as its loss leads to formation of lower density myofibrils that are characterized as shorter in length, less thick with myosin aggregate-like structure (Bonnet et al., 2017). QKI is required for the initial steps of myofibril formation through myosin assembly into filamentous structures. Using RNA-seq, the authors have shown that QKI is required for accumulation of muscle-specific tropomyosin-3 transcript which has been shown to mediate the control of myofibril formation (Bonnet et al., 2017). Rescue experiments reintroducing tropomyosin-3 into QKI null zebrafish were sufficient to restore myofibril formation. QKI mediates this regulation by binding to its QRE in the 3'-UTR of topomysin-3 mRNA to control its transcript level which leads to organized myofibrils (Bonnet et al., 2017).

Using the model of induced pluripotent stem cells (iPSCs) toward endothelial cell differentiation, it was shown that QKI-5 was significantly induced. QKI-5 binds to the 3'-UTR of STAT3 and lead to its stabilization which then leads to vascular endothelial growth factor receptor 2 (VEGFR-2) activation and increased secretion of vascular endothelial growth factor (Cochrane et al., 2017). Moreover, it has been demonstrated that QKI-5 plays a role in the induction and

stabilization of CD144 and activation of VEGFR-regulatory binding sites AP1 and STAT3 and induction of STAT3 phosphorylation. Overexpression of QKI-5 in iPSCs was sufficient to induce vascular tube formation both *in vitro* and *in vivo*. Injecting iPSC derived endothelial cells overexpressing QKI-5 intramuscularly following induction of hindlimb ischemia improved neovascularization and promoted higher blood flow (Cochrane et al., 2017). Similar results were obtained from human iPSCs overexpressing QKI-5 when injected subcutaneously in severe combined immunodeficient mice. These results highlight a pivotal role for QKI in endothelial cells differentiation from human iPSCs (Cochrane et al., 2017).

1.2.8.4 microRNA processing

In a study that validated QKI as a transcriptional target of p53, QKI was found to exert its tumor suppressor functions in glioblastoma multiforme by stabilizing a subset of microRNAs (Chen et al., 2012). miR-20a was identified as a target of QKI, which in turn targets transforming growth factor β receptor-2 (TGFβR2). QKI was found to bind and stabilize mature miR-20a *in vivo* and *in vitro* resulting in the inhibition of TGFβR2 mRNA translation (Chen et al., 2012). However, miR-20a does not contain a QRE and therefore it remains unclear as to how QKI selectively recognizes miR-20a. Moreover, QKI was shown to regulate the processing of miRNAs in glial cell lines (Wang et al., 2013). Specifically, pri-miR-7-1 harbors three putative QREs and was tightly bound by QKI-5 and QKI-6 in the nucleus. In the presence of QKI, pri-miR-7-1 was tightly bound to the Drosha microprocessor complex implying that QKI may hinder Drosha processing which in turn resulted in sequestering pri-miR-7-1 in the nucleus (Figure 1.4). This led to increased levels of epidermal growth factor receptor (EGFR) which is a known target of miR-7 (Wang et al., 2013). Given that other proteins including RNA binding proteins regulate the processing of miRNAs at different steps, the aforementioned opposing effect of QKI on miRNAs could be explained by a context dependent regulation whereby the presence or absence of other protein interactors could function to influence the mechanism of action of QKI.

QKI has also been shown to regulate miRNA processing during erythropoiesis by binding to a distal QRE in the primary miR-124-1 and recruiting the microprocessor through interaction with DGCR8, microprocessor complex subunit (Wang et al., 2017a). When erythropoiesis proceeds, a decrease in QKI-5 levels releases the microprocessor from pri-124-1 and reduces mature miR-124-1 which is required to allow erythrocyte maturation since miR-124-1 targets

TAL1 and c-MYB which are two transcription factors involved in normal erythropoiesis (Wang et al., 2017a).

Therefore, QKI proteins function to regulate miRNA formation and activity and are themselves regulated by miRNAs, together forming a regulatory network that could provide explanations to pathogenic mechanisms leading to human diseases.

1.2.8.5 circular RNA production

In 2015, it was shown that the QKI isoforms regulate circular RNAs (circRNAs) formation by associating with neighboring QREs (Conn et al., 2015). The biogenesis and function of circRNAs is not well understood. It is known, however, that a non-canonical form of alternative splicing gives rise to circRNAs, where the splice donor site of one exon is back spliced to a splice acceptor site of an upstream exon (Nigro et al., 1991). Genome-wide RNA analysis now reveals that circRNAs are abundant, stable and evolutionary conserved (Jeck et al., 2013). Greater than 14% of transcribed genes produce circRNAs with abundance exceeding that of the associated linear mRNA by 10-fold (Jeck et al., 2013). circRNAs can exhibit cell-type specific expression patterns, suggesting that their expression may be regulated (Salzman et al., 2013). Complementary intronic sequences flanking the exon of interest have been shown to mediate circularization (Jeck et al., 2013, Zhang et al., 2014a). Yet this proposed intron-pairing mechanism did not provide an explanation to the cell type specific expression patterns observed for circRNAs (Jeck et al., 2013, Salzman et al., 2013). More importantly, circRNA biogenesis has been shown to compete with canonical splicing (Ashwal-Fluss et al., 2014). A screen for RNA binding proteins that regulate circRNAs during epithelial to mesenchymal transition (EMT) in human mammary epithelial cells has identified QKI as a major regulator (Conn et al., 2015). circRNAs are derived from > 3500 genes during EMT. Using siRNAs targeting ~20 RBPs, changes in circRNAs levels were observed exclusively when the expression of QKI was reduced, indicating that QKI is required to generate circRNAs. The QKI proteins were shown to regulate the formation of circRNAs from the *SMARCA5* locus by binding a QRE flanking the circRNA-forming splice sites (Conn et al., 2015). The introduction of QREs in the regions flanking an exon is sufficient to promote circularization of exons that normally would not produce a circle (Figure 1.4) (Conn et al., 2015). A recent report showed that varied levels of circRNA expression occurs in different brain regions with the olfactory bulb, prefrontal cortex, cerebellum and hippocampus expressing specific sets of circRNAs (Rybak-Wolf et al., 2015). Given the high expression of QKI in several cell types and

areas in the brain, it is plausible to speculate that QKI regulates circRNA biogenesis in the brain. circRNAs may function as microRNA (miRNA) sponges, are involved in regulating splicing and transcription and play roles in changing parental gene expression. This new class of non-coding RNAs also plays roles in human diseases including vascular and neurological disease as well as cancer (Qu et al., 2015).

A transcriptomic analysis in cardiac tissue from doxorubicin-treated mice identified QKI to be downregulated (Gupta et al., 2017). Further inhibition of QKI by siRNA led to increased sensitivity to doxorubicin due to increased apoptosis (Gupta et al., 2017). The authors have demonstrated that QKI expression regulates a subset of circular RNAs found in the heart (*Ttn*, *Fhod3* and *Strn3*) which may serve as downstream mediators of the observed protective effect of QKI (Gupta et al., 2017). The levels of these circular RNAs were also downregulated following doxorubicin treatment in mice. Overexpressing QKI-5 in cardiomyocytes leads to a decrease in apoptosis levels following doxorubicin whereas this effect is not seen if the same cells were treated with siRNA against circular *Ttn* indicating that indeed the effects of QKI-5 are mediated through regulation of circular RNA (Gupta et al., 2017).

1.2.8.6 Cytoplasmic polyadenylation

Cytoplasmic polyadenylation represents one of the post-transcriptional regulations that positively regulate gene expression. Using a transcriptional pulse-chase analysis, QKI was identified as one of the proteins that promote polyadenylation (Yamagishi et al., 2016). Specifically, QKI-7 was shown to promote poly(A) extension by recruiting the non-canonical poly(A) polymerase PAPD4 through its unique C-terminal tail (Yamagishi et al., 2016). This increase in poly(A) length was not due to inhibition of deadenylases nor due to an increase in new mRNA synthesis. Knocking down PAPD4 abrogates QKI-7 dependent increase in poly(A) length. Three known targets of QKI (hnRNP A1, $p27^{kip1}$ and β -catenin) were validated in this study to be bound by QKI-7 which in turn promote polyadenylation and translation (Yamagishi et al., 2016). Moreover, the anti-mitotic agent lovastatin which is known to arrest cells in the G1 phase of cell cycle through increase in $p27^{kip1}$ levels was shown to mediate this effect through increasing the length of its poly(A) tail via QKI and PADP4 (Yamagishi et al., 2016).

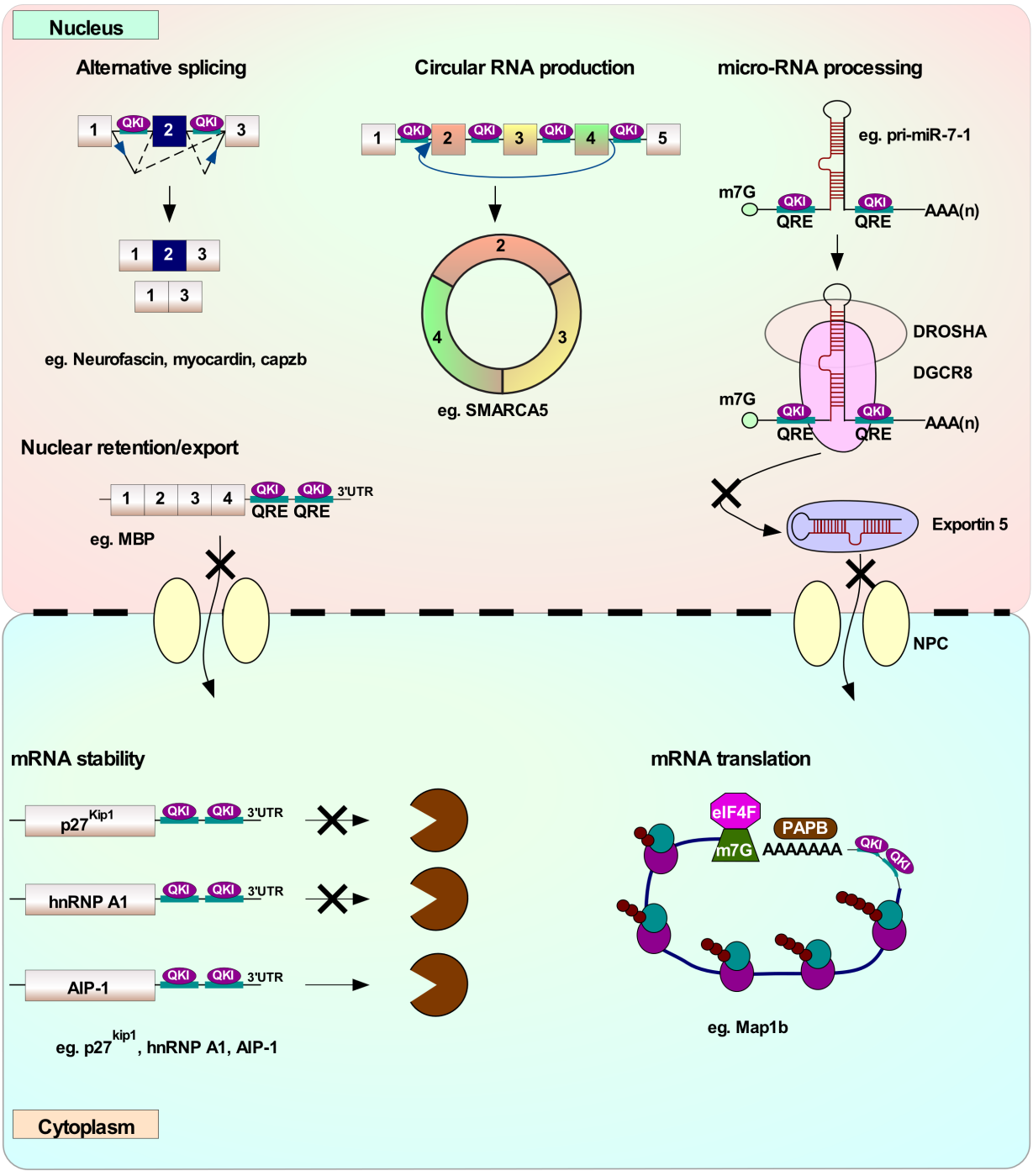

Figure 1.4: The role of QKI in regulating several aspects of RNA metabolism. Alternative splicing: a schematic depicting a pre-mRNA with exon 2 as the alternate exon. QKI functions as a trans-acting factor to regulate alternative splicing by binding to Quaking response elements (QRE, shown in green), that are adjacent to the alternate exon. The binding of QKI to its QRE could either lead to exon inclusion or skipping. Solid lines depict constitutive splicing whereas dashed lines

depict alternate splicing depending on either inclusion or exclusion. Circular RNA production: circular RNA formation occurs due to a noncanonical form of alternative splicing, where the splice donor site of one exon is back spliced to a splice acceptor site of an upstream exon. The binding of QKI to QREs adjacent to exons giving rise to the circRNA can mediate the circRNA formation. Micro-RNA processing: one of the mechanisms by which QKI regulates miRNAs is by binding to its QRE in the pri-microRNA which then functions to sequester the pri-miRNA in the nucleus and inhibits further processing (example: pri-miR-7-1), which in turn inhibits the formation of a mature miRNA and thus nuclear export into the cytoplasm. mRNA stability: QKI binding to its QREs in the 3′-UTRs of mRNA could lead to either increasing or decreasing the stability of the mRNA. mRNA translation: QKI has been shown to bind to its QREs in the 3′-UTR and function to enhance the translation of its bound mRNA. Permission to reprint is granted from John Wiley and Sons (Darbelli and Richard, 2016).

1.2.9 Role of QKI in alternative splicing

Alternative splicing is a major regulatory mechanism through which cells increase their transcriptomic diversity by generating multiple splice variants from one individual gene, allowing expansion of the proteome. In the following sections, the general mechanism and the role of QKI proteins in alternative splicing are discussed.

1.2.9.1 General mechanism of RNA splicing

A multi-mega Dalton complex known as the spliceosome catalyzes the splicing reaction. Several small nuclear ribonucleoproteins (snRNPs) represent the major building blocks of the spliceosomal machinery and they include U1, U2, U4/U6 and U5 snRNPs. Each snRNP consists of an snRNA (or two in the case of U4/U6) along with different complex-specific proteins. Seven Sm proteins are found in each of U1, U2, U4 and U5 (Wahl et al., 2009). Intron identification is determined by the presence of "GU" at the 5' splice site, "A" at branch point and "AG" at 3' splice site (Carpenter et al., 2014). Watson-Crick base pairing between the U1 snRNA and the pre-mRNA 5' splice site (5'SS) of the intron leads to stable binding of the initiation unit. In higher eukaryotes, members of the serine-arginine rich (SR) proteins stabilize the interaction. The 3' splice site (3'SS) sequence is recognized by SF1 and the U2 snRNP auxiliary factor (U2AF). SF1 and the large subunit of U2AF (U2AF65) interact and cooperatively bind the branch point sequence (BPS) and the adjacent polypyrimidine tract, respectively (Berglund et al., 1998). The small subunit of U2AF (U2AF35) binds to the 3' splice site AG dinucleotide (Moore, 2000). Altogether, this forms the early complex E which then converts to pre-splicing complex A by incorporating the U2 snRNP through interaction of the U2 snRNP-associated SF3b155 with the C-terminal RNA recognition motif of U2AF65 (Gozani et al., 1998). This leads to binding and association of the U2 snRNP with the BPS and displaces SF1 from the BPS. Following the formation of complex A, U4/U6 and U5 snRNPs are recruited as a preassembled U4/U6/U5 tri-snRNP, leading to formation of complex B (Wahl et al., 2009). Major conformational and compositional rearrangements allow complex B to be catalytically active to carry the first transesterification step of splicing (Wahl et al., 2009). This is done by destabilizing and releasing U1 and U4 to give activated complex B which then undergoes the first catalytic step generating complex C. Additional rearrangements take place allowing the second catalytic step to occur, followed by release of mRNA as well as the U2, U5 and U6 snRNPs and the intron lariat (Wahl et al., 2009) (Figure 1.5).

In higher eukaryotes, splice site selection is determined by many factors including the strength of the splice site, the presence of flanking pre-mRNA intronic and exonic splicing enhancer or silencer (known as *cis*-acting elements) and *trans*-acting regulator factors (Wahl et al., 2009). Moreover, chromatin modifications (Allemand et al., 2008), small RNA pathway components such as the Argonaute family members (Meister, 2013) as well as the speed of RNA polymerase II have been shown to influence splicing.

The selection of the splice site has long been known to be regulated by nonspliceosomal RNA-binding proteins. Generally, these proteins can be divided into canonical proteins such as hnRNPs and SR proteins as well as tissue specific RNA binding proteins such as Nova and Rbfox family (Darnell, 2013, Weyn-Vanhentenryck et al., 2014). In the following section, regulation of alternative splicing by the *qkI* gene is discussed.

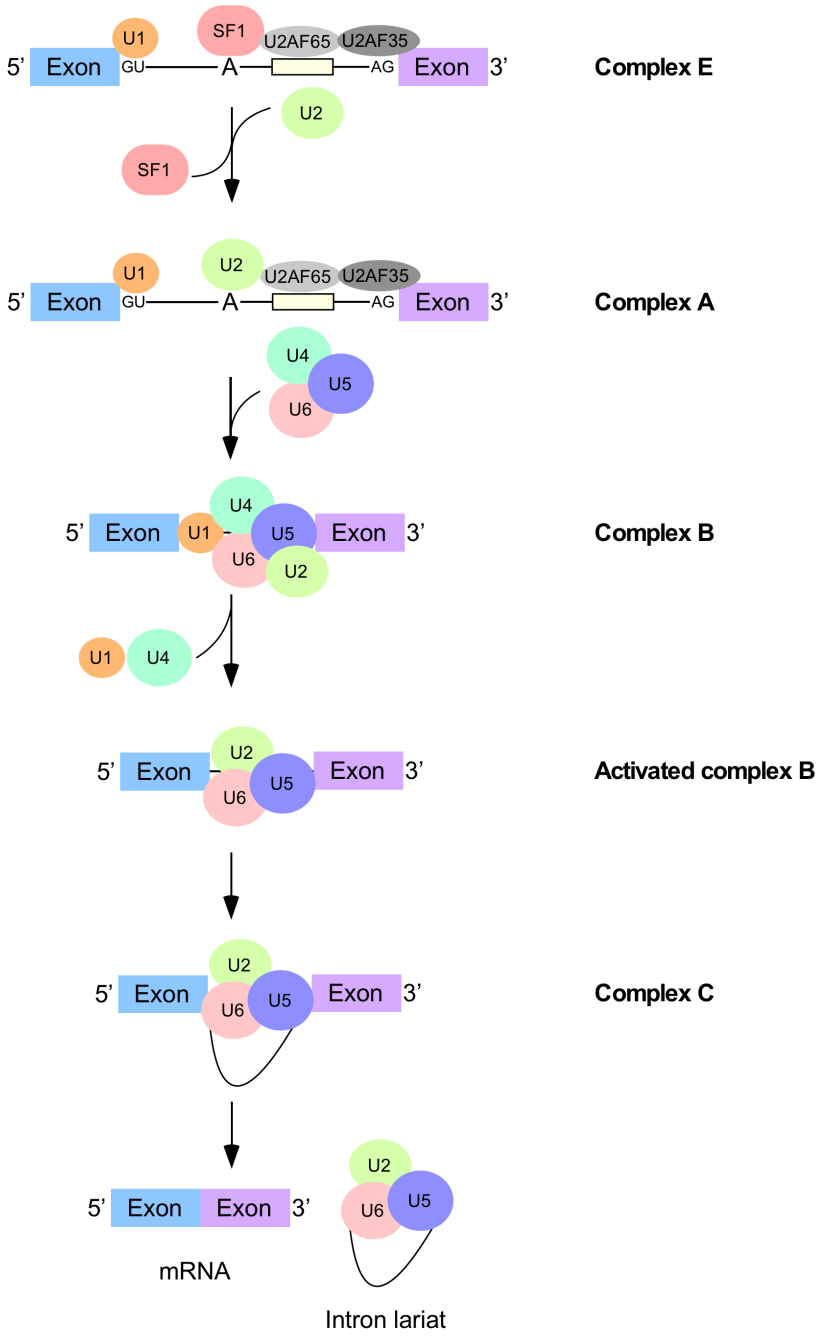

Figure 1.5: A simplified schematic of the general mechanism of alternative splicing. Canonical assembly and disassembly of the spliceosome. snRNPs interaction are shown but not those of non-snRNPs. Exons and introns sequences are indicated by boxes and lines, respectively. The names of the complexes are indicated on the right.

1.2.9.2 Regulation of pre-mRNA splicing by QKI proteins

The first insights into a role of QKI proteins in regulating alternative splicing stems from abnormalities in RNA metabolism seen in qk^v mice. First, MAG displays changes in alternative splicing (Frail and Braun, 1985) as well as MBP (Carnow et al., 1984). MAG is a myelin specific transmembrane protein which contains 13 exons with exon 12 being alternatively spliced by either inclusion or skipping. Exon 12 contains an in-frame stop codon leading to generation of two MAG isoforms. A long isoform designated L-MAG (lacks exon 12) and a short one designated S-MAG (includes exon 12). L-MAG is the major isoform in young mice whereas S-MAG is more abundant in adults (Wu et al., 2002). In qk^v mice, L-MAG has very low expression and S-MAG is overexpressed. It was found that QKI-5 regulates alternative splicing of MAG by repressing exon 12 inclusion (Wu et al., 2002). QKI-5 exerts its negative regulatory effect by binding to a QKI-5 alternative splicing element (QASE) as a 53-nt region in the downstream intron (Wu et al., 2002). Moreover, in proteolipid protein (PLP), exon 3 has two alternative 5' splice sites (3a and 3b), and in qk^v mice, exon 3b 5' splice site usage is significantly increased in comparison to wild-type mice (Wu et al., 2002). In MBP, exons 2, 5 and 6 are also alternatively spliced to generate different splice variants and in qk^v mice, relatively more exon 6 and less of exon 5 are included compared to wild-type mice (Wu et al., 2002).

Recently, a role has been identified for the QKI isoforms beyond the nervous system, as differential expression of QKI in vascular smooth muscle cells (VSMC) was found to impact the vascular response to injury. The primary function of adult VSMCs is to contract, which allows the regulation of vascular tone (van der Veer et al., 2013). However, damage to the artery wall promotes VSMC dedifferentiation from a contractile to a proliferative state. While this critical conversion of VSMC function occurs in response to extra-and intracellular cues, it is well established that the transcriptional co-activator Myocardin is primarily responsible for driving gene expression profiles required to modulate VSMC phenotype (van der Veer et al., 2013). Interestingly, QKI was shown to bind to the *myocardin* pre-mRNA and trigger an alternative splicing event that impacts both myocardin expression and function (Figure 1.4). Importantly, attenuated expression of QKI (in qk^v mice) was found to limit VSMC proliferation and effectively reduce narrowing of the blood vessel (van der Veer et al., 2013). This biology suggests that the alterations in the expression of QKI in other SMC-rich tissues, such as the testis and bladder, could be associated with pathological outcomes.

Interestingly, comprehensive studies by Hall and co-workers revealed that the QKI isoforms play a critical role in regulating skeletal muscle differentiation. QKI-5 was shown to regulate the inclusion of 406 cassette exons during the differentiation of C2C12 muscle cells, whose adjacent introns show enrichment for ACUAA motifs (Hall et al., 2013). A position dependent regulation of alternative splicing was also identified for QKI where it could function as either an activator or a repressor depending on the position of the ACUAA motif. Similar to other RNA binding proteins such as Nova (Ule et al., 2006), QKI was found to generally repress an exon when it is bound upstream and to activate an exon when bound downstream (Hall et al., 2013). By examining the QKI splicing regulatory network, poly-pyrimidine tract binding protein (PTB) was shown to coregulate 42% of the QKI-regulated alternative splicing events (Hall et al., 2013). These two proteins could function to either reinforce or oppose each other. An example of this is the regulation of *Capzb* exon 9 alternative splicing. The inclusion of this exon is activated during differentiation of myotubes into myoblasts and this is consistent with an increase in QKI expression and a decrease in PTB resulting in decreased repression of exon 9 (Hall et al., 2013). PTB has higher expression levels in myotubes and binds upstream of exon 9 and represses inclusion. However, when myotubes start the differentiation process, the expression level of PTB decreases and QKI increases. QKI binds downstream of exon 9 and mediates its inclusion (Hall et al., 2013). Moreover, it was also observed that by mapping the splicing regulatory networks of QKI and PTB that there is a close physical proximity of their binding motifs. This implies that there might be a competition to occupy these motifs, which function to modulate the splicing of exons (Hall et al., 2013). This work provided the first evidence regarding a role for QKI in regulating the splicing network in vertebrate muscle development in concert with PTB. Further investigations are warranted to address whether these two RBPs cooperate or compete for binding to regulate alternatively spliced exons. A recent report published by the same group has demonstrated that in C2C12 myoblasts, the presence of the core 311 amino acids common in all QKI isoforms in the nucleus is sufficient to mediate alternative splicing (Fagg et al., 2017) indicating that nuclear localization is the determinant for QKI regulation of alternative splicing. Targeting expression of QKI-5 by siRNA has led to loss of expression of QKI-6/QKI-7 indicating that cells cannot express these two isoforms unless QKI-5 is expressed first (Fagg et al., 2017).

Elegant studies demonstrated a critical role for QKI during human monocyte to macrophage differentiation (de Bruin et al., 2016a). While QKI mRNA was found to be abundantly

expressed in naïve human monocytes, QKI protein was virtually undetectable. However, the conversion to both pro- and anti-inflammatory macrophages with Granulocyte-macrophage colony-stimulating factor (GM-CSF) or macrophage colony-stimulating factor (M-CSF), respectively, was associated with a potent increase in the expression of all three QKI protein isoforms. Moreover, the expression of all three QKI isoforms were found to be highly expressed in $CD68^+$ macrophages in advanced atherosclerotic lesions. Supporting this essential role in regulating macrophage function was provided firstly by gene enrichment analyses, which identified inflammatory responses to injury and lipid metabolism as being key pathways influenced by changes in QKI expression. Indeed, in the setting of a unique QKI-haploinsufficient patient, the authors confirmed that a reduction of QKI expression limits monocyte to macrophage differentiation, and results in significantly reduced uptake of β-very low density lipoprotein (VLDL) and oxLDL (low density lipoprotein), limiting their ability to become foam cells (de Bruin et al., 2016a). Importantly, their genome-wide RNA analysis revealed altered expression levels of >1000 mRNA species in monocytes and macrophages, along with striking changes in the splicing during this differentiation process. In keeping with the findings by Hall and co-workers, computational assessment of alternatively spliced mRNAs revealed an ACUAA enrichment proximal to the splicing event, while changes in gene expression were commonly associated with the presence of QREs (de Bruin et al., 2016a). These studies point towards a role for QKI in the development of atherosclerosis, as well as other inflammatory-mediated diseases. Furthermore, the direct targeting of QKI, or expression/splicing events mediated by QKI, could function as novel therapeutic targets for limiting inflammatory processes.

A transcriptome analysis of mRNA obtained from cultured neural stem cells that either express QKI or in which QKI was knocked down has shown that QKI is involved in neural stem cell differentiation. More than 800 alternative splicing events were shown to be deregulated in neural stem cells in absence of QKI (Hayakawa-Yano et al., 2017). Overexpressing QKI-5 in embryonic neural stem cells using *in utero* electroporation inhibited neuronal migration and induced mitosis (Hayakawa-Yano et al., 2017). To identify *in vivo* targets, the authors used high throughput-CLIP in E14.5 mouse brains. QKI-5-RNA interactions were distributed in introns and deep intergenic regions of the mouse genome with robust QKI-5 association with UACUAA (Hayakawa-Yano et al., 2017). A position-dependent alternative splicing for QKI-5 in neural stem cells was observed with QKI-5 binding on a 3' end of an upstream intron mediating exon skipping,

whereas binding to the 5' end of a downstream intron results in exon inclusion (Hayakawa-Yano et al., 2017). Performing gene ontology analysis using the 892 predicted QKI-5 targets revealed an association of QKI-5 targets with pathways of cell adhesion and tight junctions. QKI-5 was shown to regulate cell polarity of the apical surface of neural stem cells by regulating the cadherin-catenin pathway through RNA processing. The role of QKI-5 in cell adhesion was confirmed in conditional knockout mice deleting QKI expression in neural stem cells using Nestin-Cre (Hayakawa-Yano et al., 2017). Loss of QKI-5 led to impaired maintenance of cell polarity signals resulting in disruption of adherence junctions and detachment of neural stem cells from the ventricular zone (VZ) leading to ectopic neurogenesis (Hayakawa-Yano et al., 2017).

1.2.10 Role of QKI in human diseases

1.2.10.1 Multiple Sclerosis

Multiple Sclerosis (MS) is a disease characterized by the pathological loss of the myelin sheath insulating neuronal axons. An activated immune system targets components of the myelin sheath and results in repeated depletion of myelin surrounding axons within the brain. This leads to the disorganization of nodes of Ranvier and loss of action potentials within axons followed by neurological dysfunction. In active MS lesions, the presence of oligodendrocytes associated with thinly myelinated axons is indicative of CNS remyelination (Raine and Wu, 1993). Experimental analyses have shown striking similarities between myelin generation during development and remyelination (Podbielska et al., 2013). QKI proteins are known for their function in regulating oligodendrocyte development and differentiation in mice. Little is known, however, about the role of the human QKI proteins during myelination. However, the similarity of the genomic organization, splicing pattern and the conservation of the amino acid sequence of *qkI* in humans and rodents, suggest that human QKI could play an identical role in myelination of the human CNS (Figure 1.6) (Kondo et al., 1999). Another link to a role of QKI in MS is the presence of multiple microRNA binding sites in the 3'-UTR of QKI that correspond to three out of four of the top most dysregulated microRNAs in MS (Keller et al., 2009).

A study in rat brains has demonstrated that the transition from premyelinating to myelinating oligodendrocytes during development is accompanied by elevated levels of QKI proteins (Wu et al., 2001). The same study also showed that in adult rat brains, a subset of oligodendrocytes displays characteristics of actively myelinating oligodendrocytes that are

normally seen during development which are also characterized by increased levels of QKI proteins (Wu et al., 2001). This supports the role of QKI in adult myelination. Some of the therapeutic strategies for MS involve targeting the immune system and aim to reduce the immune system attacks on the myelin sheath. However, very few therapies aim to enhance remyelination and promote the proliferation/differentiation of oligodendrocytes at the lesion sites. Although the function of QKI in adult myelination is uncharacterized, given the role of QKI in glial development and myelination in rodents, a functional importance for QKI in human myelination/remyelination is likely and merits further investigation.

1.2.10.2 Schizophrenia

Pathological changes in myelin are observed in brains of patients with schizophrenia along with decreased expression of oligodendrocyte/myelin genes (for review see (McInnes and Lauriat, 2006)). An ancestral haplotype that segregates with affected individuals in a single large family from northern Sweden was mapped to chromosome 6q25-6q27 (Lindholm et al., 2004). Fine mapping of this locus in a later study identified a region spanning 0.5 Mb, where the *HqK* gene is located, to be shared among the majority of affected individuals in a larger pedigree from northern Sweden (Aberg et al., 2006b). Moreover, decreased mRNA levels of QKI-7 and QKI-7b splice variants were observed in 55 schizophrenic patients compared to healthy controls (Aberg et al., 2006b, Haroutunian et al., 2006). Alterations in the balance of the *Hqk* splice variants, especially *Hqk-7b*, were shown to tightly correlate with alterations of transcript expression of several oligodendrocyte/myelin related genes including MAG, MBP, PLP1, SRY-box 10 (SOX10) and transferrin in several human brain regions of these 55 schizophrenic patients (Figure 1.6) (Aberg et al., 2006a) (McCullumsmith et al., 2007). Several of these genes harbor QKI binding sites and are validated targets of QKI *in vivo* (Artzt and Wu, 2010, Feng and Bankston, 2010). Aberrant alternative splicing of several genes associated with schizophrenia has also been observed (Morikawa and Manabe, 2010). Defects in QKI expression in schizophrenia could lead to downstream alternative splicing defects of several myelin genes, which in turn could play a role in the etiology of schizophrenia. Moreover, structural defects in nodal and paranodal regions along the axons are observed in adult mice following an induced loss of QKI expression in oligodendrocytes (Chapter 2) (Darbelli et al., 2016). Abnormal functions of neuronal networks are thought to be central for schizophrenia etiology (Davis et al., 2003). In this scenario, QKI could

contribute to the disease since its loss would lead to abnormal functional domains along the axon (at the node of Ranvier) that could compromise neuronal function and neurotransmitter release. Patients treated with typical neuroleptics have increased levels of QKI mRNA compared to patients with atypical neuroleptics (Aberg et al., 2006b) indicating that antipsychotics could affect QKI levels and in turn modulate the myelin sheath and therefore impact the onset of disease.

Fasciculation and Elongation Protein Zeta-1 (FEZ1) is a known neuronal schizophrenia risk factor (Lewis et al., 2003). A recent study has reported the expression of FEZ1 in rodent and human oligodendrocytes (Chen et al., 2017) that is upregulated during precursor differentiation. Two QREs were found in the 3'-UTR of FEZ1 to bind the cytoplasmic QKI-6 (Chen et al., 2017). Moreover, in the qk^{v} mouse optic nerve, reduction of FEZ1 mRNA was observed and rescued by FLAG-QKI-6 (Chen et al., 2017). This study has provided the first link between FEZ1 and QKI in the context of risk association to schizophrenia.

Moreover, decreased function of QKI has also been linked to white matter impairment and myelin deficits in other cognitive disorders including major depression patients and suicide populations (Aberg et al., 2006a, Klempan et al., 2009).

1.2.10.3 6q Terminal deletion

A breakpoint mutation has been identified in a unique human patient that maps to the *qkI* locus (Backx et al., 2010). The female patient carries a balanced reciprocal translocation t(5;6) (q23.1;q26) that leads to a breakpoint in *HqK* in the intron between exons 2 and 3 (Figure 1.6). The fact that the patient displays a phenotype similar to subjects with 6q terminal deletion syndrome (which is commonly associated with intellectual disabilities, hypotonia, seizures, brain anomalies and specific dysmorphic features including a shortened neck, large and low-set ears and downturned corners of the mouth), suggests that QKI haploinsufficiency is associated with 6q terminal deletion phenotype. Although no ataxia or myelination defects were observed in the patient, this could be explained by the heterozygosity of the *qkI* allele. Nonetheless, the phenotypes associated with the loss of a single QKI allele provide direct evidence for the involvement of QKI in brain development and function. As previously described, monocyte to macrophage differentiation from this patient is impaired, consistent with a role for the QKI isoforms in differentiation processes (de Bruin et al, 2016a). Taken together with the recent research

implicating *qkI* involvement in schizophrenia, further studies are warranted to uncover the role of QKI in additional neurological disorders.

1.2.10.4 Cancer

Human chromosomal alterations at 6q23.3 to 6q26 were found at high frequencies in astrocytic tumors, suggesting the presence of tumour suppressor genes in this region (Miyakawa et al., 2000). The first implications for a role of *qkI* in cancer came from a report examining the expression of the human *HqK* gene in brain tumour samples (Li et al., 2002). A high incidence of expression alterations was identified in gliomas, but not in Schwannomas or Meningiomas (Li et al., 2002). Some samples were devoid of all QKI expression, whereas others displayed differential loss of one of the major transcripts (Li et al., 2002). Two subsequent studies using anaplastic astrocytomas and glioblastoma multiforme identified a 6q25-26 deletion including both *HqK* and *PACRG* genes (Figure 1.6) (Ichimura et al., 2006, Mulholland et al., 2006). A single nucleotide polymorphism analysis using 55 glioblastoma multiforme samples found a deletion on chromosome 6 encompassing the *QKI* region in 16 samples (~30%) (Yin et al., 2009). Several cases of angiocentric gliomas have been identified to involve a deletion in the *MYB* locus (Ramkissoon et al., 2013). Interestingly, one pediatric ganglioglioma demonstrated a 6q23.3q26 deletion that was predicted to result in a MYB-QKI fusion (Roth et al., 2014). It was later confirmed that MYB-QKI fusion is a specific and single candidate driver event in angiocentric gliomas (Bandopadhayay et al., 2016) which was shown to promote tumorigenesis by MYB activation by truncation, enhancer translocation to drive aberrant MYB-QKI expression as well as the hemizygous loss of QKI (Bandopadhayay et al., 2016). The breakpoint was identified to be in intron 4 of QKI whereas MYB breakpoint varied from intron 9-15 (Bandopadhayay et al., 2016). More recently, it was shown that QKI plays a role in regulating stemness of cancer cells (Shingu et al., 2017). Following the loss of QKI in $Pten^{-/-}Trp53^{-/-}$ in neural stem cells of the subventricular zone, the mice develop glioblastoma with penetrance of 92% and a median survival of 105 days (Shingu et al., 2017). This occurs due to a decreased endolysosomal-mediated degradation of receptors needed to maintain self-renewal, leading to increased levels of these receptors on cell membrane allowing cancer stem cells to cope with low ligand levels outside their niche (Shingu et al., 2017).

qkI promoter hypermethylation was later found to account for reduced QKI expression in colon, gastric and prostate cancer (Bian et al., 2012, Yang et al., 2010, Zhao et al., 2014, Iwata et al., 2017). In a human astrocyte glioma cell line, silencing the expression of the *qkI-7* splice variant led to reduced expression of genes involved in interferon induction (Jiang et al., 2010). QKI was also found to play a role in controlling cell cycle and self-renewal (Yang et al., 2011, Lu et al., 2014). Several reports have shown QKI to either regulate or be regulated by several miRNAs in cancer (Chen et al., 2012, Ji et al., 2013, Wang et al., 2015b, He et al., 2015, Tili et al., 2015). QKI has also been found to modulate alternative splicing and to suppress aberrant splicing patterns in cancer and therefore was found to associate with poorer cancer prognosis (Brosseau et al., 2014, Zong et al., 2014, Danan-Gotthold et al., 2015, Wen et al., 2015). QKI along with RBFOX2 and MBNL1/2 splicing factors have been shown to account for many splicing alterations observed across human solid tumours (Danan-Gotthold et al., 2015). 20% of ovarian tumour microenvironment-associated splicing patterns are deregulated following down-regulation of QKI and RBFOX2 (Brosseau et al., 2014). The histone variant MacroH2A1 alternative splicing is also regulated by QKI to produce MacroH2A1.1 which can interact with NAD^+-derived small molecules such as poly(ADP-ribose) to reduce lung and cervical cancer cell proliferation (Novikov et al., 2011). Reduced QKI levels observed in many cancers leads to generation of MacroH2A1.2 which is unable to bind NAD^+-derived molecules and hence lack the ability to suppress cancer growth (Novikov et al., 2011). QKI was also shown to compete with the core splicing factor SF1 for binding to the branch point sequence and hence inhibit tumour-associated splicing events, as is the case with the splicing of *NUMB* gene to regulate cell proliferation in lung cancer cells (Zong et al., 2014). A recent genome-wide analysis has identified that a substantial fraction of cancer-associated splicing events in non-small cell lung cancer were targets of QKI (de Miguel et al., 2016), and that low expression of nuclear QKI-5 leads to a poor prognosis and decreased survival (de Miguel et al., 2016). Post-transcriptional regulation of several genes involved in regulating cancer, including FOXO1 and cyclin D1, has also been demonstrated to be controlled by QKI (Yu et al., 2014, Fu and Feng, 2015). Taken together, these newly identified roles for QKI in cancer suggest that QKI may be a possible early biomarker for cancer development prognosis and deserve further attention as a therapeutic target.

1.2.10.5 Ataxia

According to the Allen mouse brain atlas, *qkI* is abundantly expressed in Purkinje neurons in the cerebellum (Lein et al., 2007). About a decade ago, a protein-protein interaction network of human inherited ataxias and disorders of Purkinje cell degeneration (Lim et al., 2006) supports the idea that QKI is part of this interactions network. Another evidence for the role of QKI in ataxia stems from the fact that several highly-expressed microRNAs that control Ataxin levels in Purkinje cells also have theoretical binding sites in the 3'-UTR of QKI-7 (Lee et al., 2008).

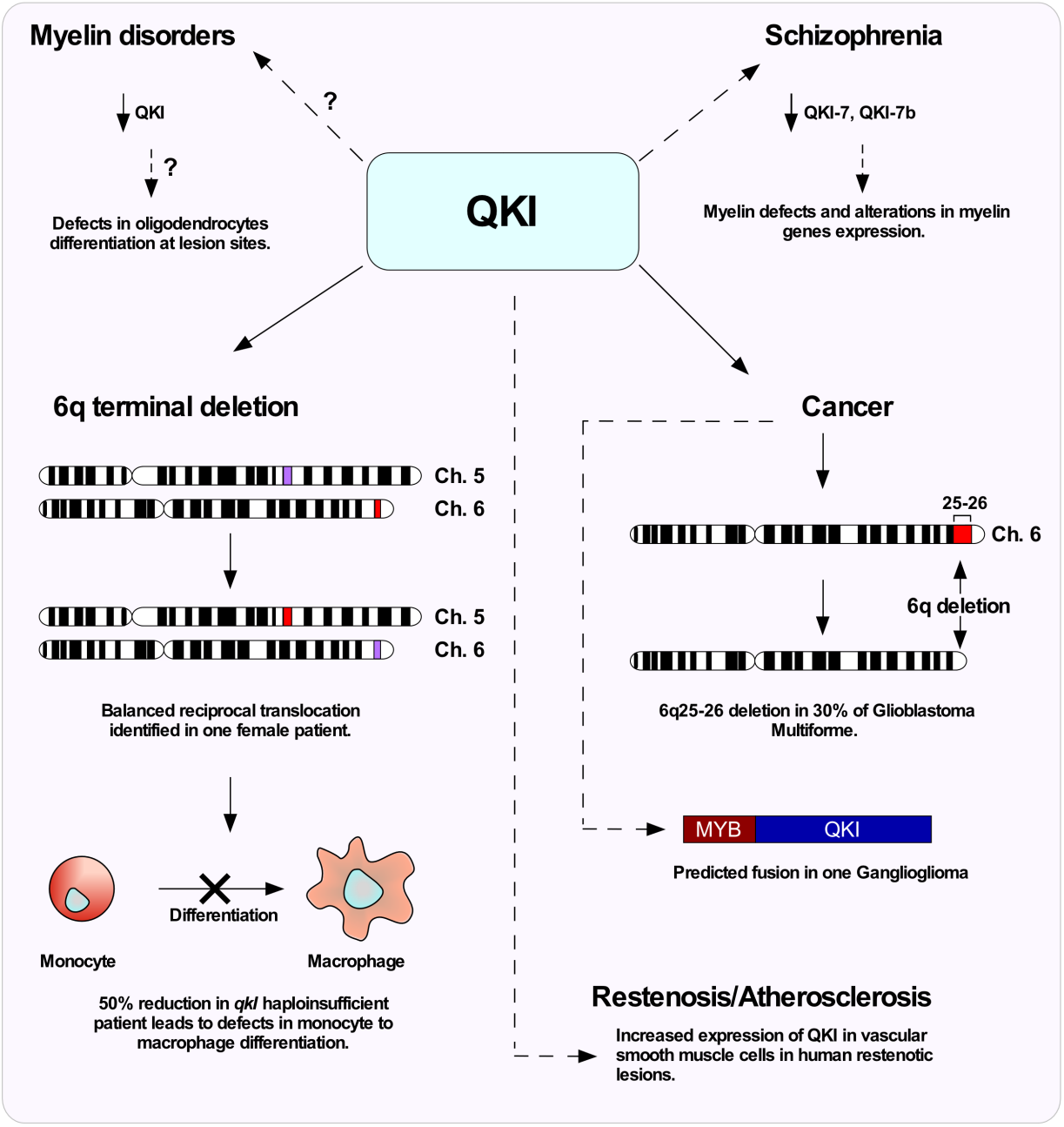

Figure 1.6: The role of QKI in human diseases. Myelin disorders: QKI loss has been associated with defects in myelin formation and maintenance in rodents. Given the high conservation of the qkI gene between rodents and mice, a role for QKI in human myelination is predicted. The reduction in QKI levels at lesion sites could result in failure of newly generated oligodendrocyte precursors to differentiate and myelinate causing remyelination to fail. Schizophrenia: schizophrenic patients have been demonstrated to display pathological changes in myelin structure as well as decreased expression of myelin/oligodendrocyte genes. A reduction in QKI-7 and QKI-

7b levels has been observed in schizophrenic patients. However, whether the decrease in QKI levels leads to reduced expression of myelin genes (and hence pathological myelin structure) or the abnormality in oligodendrocyte gene expression and function leads to oligodendrocyte death and hence reduced QKI levels remain to be investigated. 6q terminal deletion: a patient has been identified to harbor a balanced reciprocal translocation between chromosomes 5 and 6 that disrupts the qkI gene. The patient suffers from phenotypes similar to 6q terminal deletion with intellectual disabilities, hypotonia, seizures, brain anomalies and specific dysmorphic features. Defects in monocyte differentiation into macrophages are observed in the patient. Cancer: chromosomal deletions mapping to 6q25-6q26 have been associated with cancer and were found in 30% of Glioblastoma multiforme. In addition, one pediatric ganglioglioma demonstrated a 6q23.3q26 deletion that was predicted to result in a MYB–QKI fusion. Restenosis/Atherosclerosis: increased QKI levels are observed in vascular smooth muscle cells in human restenotic lesions as well as in monocytes/macrophages in atherosclerotic lesions. Legend: solid lines indicate direct evidence. Dashed lines indicate a predicted association. Permission to reprint is granted from John Wiley and Sons (Darbelli and Richard, 2016).

1.3 Oligodendrocyte development and myelin formation

1.3.1 Myelin

Rapid impulse propagation is required for proper functioning of the nervous system. In vertebrates, this is achieved by insulating axons with myelin, whereas invertebrates and non-jawed vertebrates can do so by enlarging axonal diameter (Zalc et al., 2008). Myelin is the structure that allowed vertebrates to exist and it emerged in cartilaginous fish more than 500 million years ago (Zalc et al., 2008). In non-myelinated invertebrate axons, electrical impulses are propagated at a speed proportional to the axon diameter (averaging between 0.5-30um for both vertebrate and invertebrate) at about 1 meter per second or less (Zalc et al., 2008, Nave and Werner, 2014). For vertebrates however, and due to physical constraints imposed by the skull and vertebral column, they evolved myelin; a tightly compacted membrane to insulate axons. Myelin decreases transverse capacitance and increases transverse resistance of axonal membrane (Zalc et al., 2008, Nave and Werner, 2014). This allows action potential to propagate at about 50 to 100 meters per second along axons with diameters similar to most invertebrates (Zalc et al., 2008, Nave and Werner, 2014).

1.3.2 Structure and Composition of myelin

Myelin was named so by Virchow (Virchow, 1854). It is produced by myelinating glial cells, oligodendrocytes (OLs) in the CNS and Schwann cells in the PNS. It is a spiral structure that is made of an extension of the plasma membrane of myelinating glial cells in the CNS that each forms a segment of sheathing around an axon (Baumann and Pham-Dinh, 2001). It has a periodic structure appearing as alternating concentric electron dense and electron light layers, initially shown in 1949 (Sjöstrand, 1949) with 12 nm periodicity. The dense line is formed as the cytoplasmic surfaces come in close proximity during compaction whereas the light layer (also known as intraperiod line) is formed by the extracellular opposition of the two fused outer leaflets (Figure 1.7). Each myelin segment or internode is about 150-200 um in length (Butt and Ransom, 1989). The spaces between the internodes where myelin is lacking are known as nodes of Ranvier (Bunge, 1968). The myelin lamellae end near the node of Ranvier in little expanded loops containing cytoplasm known as paranodal loops (details in section 1.4.2).

Myelin is the most abundant structure in the vertebrate nervous system constituting ~40-50% of the CNS on a dry weight basis (Baumann and Pham-Dinh, 2001). It has a unique composition (rich in lipids with low water content to allow electrical insulation) with the myelin dry weight consisting of 70% lipids and 30% proteins as opposed to cellular membrane that usually have high protein-to-lipid ratio. The structure, thickness, low water and high lipid content are the factors that contribute to the insulating properties of myelin that favor rapid nerve conduction velocity (Baumann and Pham-Dinh, 2001). The specific constituents of myelin, glycolipids and proteins (discussed in the following sections) are made by either OLs or Schwann cells. Section 1.3.5 will discuss oligodendrocytes in detail.

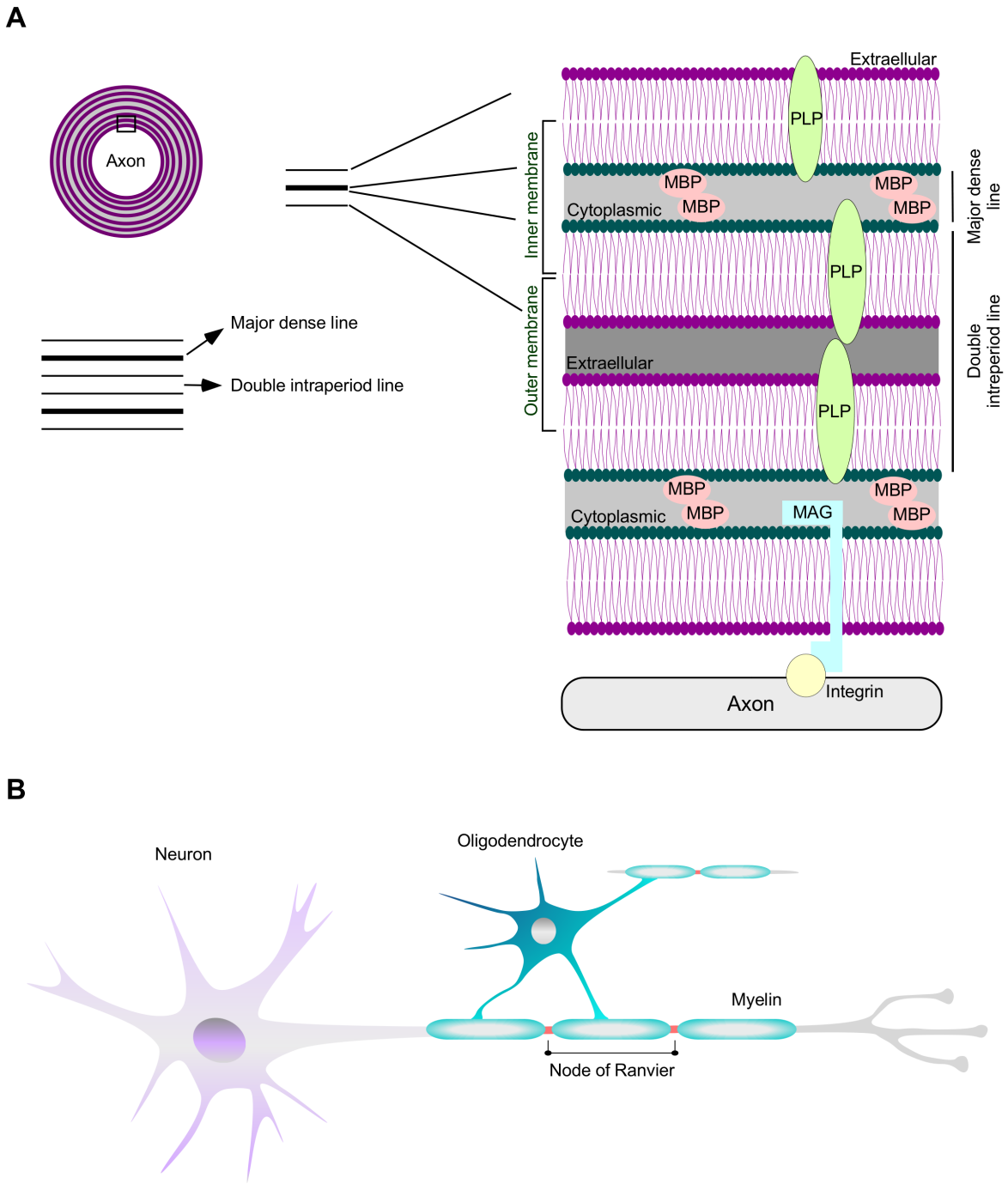

Figure 1.7: Myelin structure. A. The myelin wrapping around axons is shown in top left. The compact myelin is formed by apposition of the external faces of the membrane of the myelinating cell forming the "double intraperiodic line". The apposition of the interface leaflets followed by cytoplasm expulsion forms the "major dense line" (bottom left). The myelin proteins involved in these processes are depicted as well (right). B. A neuron and the myelin sheaths along its axon.

Myelin in the CNS is made by oligodendrocytes. A single oligodendrocyte can generate multiple myelin sheaths.

1.3.2.1 Myelin lipids

Myelin has a very high lipid content compared to other membranes. The most quantitatively significant lipids in myelin are cholesterol, galactosylceramide and ethanolamine plasmalogens which altogether make up about 65% of the total lipid dry weight. The molar ratio of cholesterol, phospholipids and glycosphingolipids in myelin are in the range of 40%:40%:20% compared to 25%:65%:10% in most membranes (O'Brien and Sampson, 1965). Cholesterol synthesis dictates myelin assembly since it provides stability to myelin by regulating both fluidity and permeability of the membrane (Schmitt et al., 2015) as well as being essential to retain major CNS myelin proteins within the myelin membrane. Galactosylceramides/sulfatides are the typical myelin lipids. Following biosynthesis of ceramide, the transfer of sugar moieties generates glucosyl- and galactosylceramide that can be further transformed into gangliosides and sulfatides, respectively (Schmitt et al., 2015). The lack of enzymes needed for generation of galactosylceramide/sulfatides leads to major myelin abnormalities at the paranode where axonal/oligodendroglial cell adhesion molecules meet, indicating that these glycolipids are essential for stability and maintenance of myelin (Schafer et al., 2004). Gangliosides, which are sialylated glycosphingolipids, appear to participate in axon-glia interaction possibly due to organizing axonal paranodal cell adhesion molecules (Yamashita et al., 2005). Ethanolamine plasmalogens function in membrane stabilization, free-radical quenching and immune modulation (Han and Gross, 1990, Lessig and Fuchs, 2009). Phosphoinositides in which phosphatidylinositol-4,5-bisphosphate (PI(4,5)P2) is the most abundant, function to interact with a range of different proteins to regulate cellular processes. PI(4,5)P2 interacts with MBP which could trigger structural rearrangements of MBP to promote self-interaction of MBP to drive myelin membrane compaction (Aggarwal et al., 2013). Therefore, these lipids function altogether to pack myelin into a stable insulating sheath.

1.3.2.2 Myelin proteins

Several myelin proteins are components specific to myelin and OLs. The most abundant in the CNS are MBP, PLP and 2′,3′-cyclic nucleotide 3′-phosphodiesterase (CNPase), which are low molecular weight proteins that make up about 80% of total proteins (Campagnoni and Macklin, 1988). Glycoproteins are also present in myelin and among them are MAG and myelin oligodendrocyte glycoprotein (MOG).

Myelin basic proteins (MBP) are a family of proteins generated by the alternative splicing of the *mbp* gene (exons 2, 5 and 6) and constitute about 8% of proteins in myelin (Jahn et al., 2009, Takahashi et al., 1985). The splice variants give rise to isoforms of different molecular masses that are 21.5, 18.5, 17 and 14 kDa in mouse (Campagnoni and Macklin, 1988). The 18.5 and 14 kDa (which lack exon 2) are the most abundant isoforms in adult mice (95% of total MBPs). The isoforms containing exon 2 (21.5 and 17 kDa) are more predominant during early mouse development with the same expression patterns observed in humans. These proteins could be post-translationally modified by acetylation, phosphorylation and methylation (Campagnoni and Macklin, 1988). Direct evidence for the role of MBP in myelin compaction stems from the *shiverer* mutant mouse which contains a large deletion in the *mbp* gene. The myelin appears largely uncompacted, leading to a tremor phenotype with absent major dense lines in the myelin (Privat et al., 1979). When myelination starts, MBP proteins are locally translated at the distal tips of OLs and localized on the cytoplasmic face of the myelin membrane and function to facilitate compaction of opposing cytoplasmic leaflets of myelin lamellae. MBP bears a 19 net positive charge at neutral pH and therefore can bind to negatively charged lipid heads to neutralize the repulsive negative charges in order to allow compaction to occur (Chang et al., 2016). Moreover, upon interaction with the membrane, MBP can self-associate forming a cohesive network as well as expel proteins over a certain size (Aggarwal et al., 2011).

PLP is the myelin component that plays a role in myelin compaction on the extracellular side to form the intraperiod lines seen under electron microscopy. It comprises 17% of total CNS myelin proteins (Jahn et al., 2009). It is a transmembrane protein found on the extracellular side of the membrane. The gene is alternatively spliced (alternative 3' splice site of exon 3) to generate two major isoforms PLP and DM-20 with PLP being most abundant in adults whereas DM-20 is expressed during embryonic development (Baumann and Pham-Dinh, 2001). Oligodendrocytes of *plp* null mice are still able to myelinate axons and form compact myelin sheath, however, several

structural abnormalities are observed in the intraperiod lines leading to axonal degeneration (Boison and Stoffel, 1994, Griffiths et al., 1998).

CNPase (2′,3′-cyclic nucleotide 3′-phosphodiesterase) makes up ~4% of total CNS myelin protein (Jahn et al., 2009). It hydrolizes artificial substrates, and 2', 3'-cyclic nucleotides into their 2'-derivatives, yet the biological role of this enzymatic activity in the CNS remains under investigation. It is found mostly in noncompacted myelin and in the paranodal loops (Baumann and Pham-Dinh, 2001). CNPase knockout mice develop axonal swelling and neurodegeneration throughout the brain leading to hydrocephalus and premature death, with no apparent ultrastructural myelin abnormalities (Lappe-Siefke et al., 2003). Alternative splicing of two transcription start sites generates two splice variants (CNP1 and CNP2) (O'Neill et al., 1997). A dynamic competition between CNP and MBP has been proposed (Chang et al., 2016) where MBP occupies compacted myelin and CNP occupies uncompacted myelin and that intracellular compaction may be governed by mutual exclusion between these two proteins (Chang et al., 2016).

MAG (myelin associated glycoprotein) is one of the minor myelin constituents (~1%). Two alternative splice variants exist, S-MAG (exon 12 included) which is more abundant in adult rodents, and L-MAG (exon 12 excluded) which is more abundant during CNS myelination (Pedraza et al., 1991). MAG is localized at the periaxonal membrane of the internode, the innermost layer of myelin and is therefore in direct contact with axons. It has a membrane spanning domain, with an extracellular region containing five immunoglobulin-like domains with sites for NH2-linked glycosylation and an intracellular carboxy-terminal (Baumann and Pham-Dinh, 2001). Its structure and localization suggest that it might be involved in adhesion and signalling between OLs and neurons (Wang et al., 2002). The L-MAG isoform could be phosphorylated on its cytoplasmic domain that appears to interact with two signal transduction elements, phospholipase C and p59Fyn (Jaramillo et al., 1994). CNS forms almost normally in *Mag* null mice, however, a prominent defect in periaxonal cytoplasmic collar is evident with myelin sheaths containing cytoplasmic organelles indicating a delay or a block in myelin compaction (Montag et al., 1994).

MOG (myelin oligodendrocyte glycoprotein) is another minor component of the CNS myelin. It is a transmembrane protein which contains a single immunoglobulin-like domain with a single site for glycosylation that allows it to form dimers (Baumann and Pham-Dinh, 2001). It is found in the outermost lamella of compact myelin sheaths in the CNS. MOG is a surface marker

for oligodendrocyte maturation (Scolding et al., 1989). Its localization has implicated MOG as a cytotoxic T lymphocyte target in myelin autoimmune diseases such as multiple sclerosis (de Rosbo and Ben-Nun, 1998). The famously studied animal model of MS, experimental autoimmune encephalomyelitis (EAE), uses a MOG-derived peptide as the immunizing antigen (Amor et al., 1994, Lebar et al., 1986).

1.3.3 Initiation of myelination and myelin compaction

Myelin is a spiral extension of the glial plasma membrane. Axonal contact is the first event that triggers axonal myelination. This initial contact induces several molecular rearrangements in the future myelinating cell. These molecular events include the association of fyn tyrosine kinase with lipid rich membrane microdomains (Czopka et al., 2013, Kramer-Albers and White, 2011), suppression of RhoA activity, local enrichment of phosphoinositides in the glial membrane (i.e., phosphatidylinositol 2 and 3 (PIP2 and PIP3)) (Snaidero et al., 2014), directed mRNA transport and activation of local mRNA synthesis (Barbarese et al., 1999) and cytoskeletal reorganization (Bauer et al., 2009).

During postnatal development, the myelin membrane of an OL may grow by as much as 5,000 um^2 per day (Pfeiffer et al., 1993). A mature myelin layer is composed of 160 membrane layers, and internodes extend up to 1.7 mm in the CNS (Hildebrand et al., 1993). Longitudinal and radial expansion of the myelin segment occurs during secondary axon elongation during body growth (Simpson et al., 2013), yet internodes are formed within days. Recently, *in vivo* time lapse imaging of zebrafish embryos has shed some light on the process of developmental myelination (Snaidero et al., 2014). This model shows that longitudinal and radial expansions occur simultaneously as new membrane is continuously added to the growing tip of the inner layer. Concurrently, the innermost layer is laterally expanding and squeezes in between the preceding layer and the axon (Snaidero et al., 2014), an event termed “wrapping”. The same study has also demonstrated that intracellular compaction starts from the outermost layers and extends inward. To allow compaction to occur, adhesive proteins as well as removal of molecules that prevent compaction are necessary. Highly charged phospholipids such as PIP2 are inhibitory to tight glial membrane appositions. Positively charged basic proteins such as MBP have high affinity to PIP2 and upon binding, MBP neutralizes those phospholipids, pulling together the two bilayers in a zipper fashion (Aggarwal et al., 2013) and forming the major dense lines. Extracellular adhesion

is allowed due to homotypic interaction of PLP, yet lack of PLP is compensated for by its close homolog GPM6b (Boison and Stoffel, 1994, Werner et al., 2013). Compaction also drives out molecules with cytoplasmic domains larger than a certain threshold size and therefore glycosylated proteins are generally absent from compacted CNS myelin (Aggarwal et al., 2011).

1.3.4 Discovery of glial cells

In 1846, Virchow discovered that there were cells other than neurons in the CNS. He called those cells "nervenkitt" (nerve glue), i.e., neuroglia due to thinking that those cells were connective tissue of the brain (Virchow, 1846). Microscopic studies later allowed for the characterization of the major glial cell types using metallic impregnation developed by Ramon y Cajal and Rio Hortega. Cajal used gold impregnation to identify astrocytes among neuronal cells, as well as a third element which was not impregnated by this technique (Ramon y Cajal, 1913). Using silver carbonate impregnation, Rio Hortega found two other cells types, the oligodendrocyte (which he first called interfascicular glia) (Rio Hortega, 1921), and another cell type that he distinguished from the two macroglia cells and that he called microglia (Rio Hortega, 1928). These results were later confirmed by Wilder Penfield who also proposed that myelin was generated by oligodendrocytes (Penfield, 1924). However, it was looking at myelin ultrastructure that provided the definitive proof that myelin is produced by oligodendrocytes and not axons (Geren, 1954). The role of glial cells was thought to be to support the function of nerve cells, however, expanding discoveries have highlighted several roles for glia that are different from providing nerve support.

1.3.5 Development of oligodendrocytes in the Central Nervous System

Oligodendrocyte and Schwann cell development is an intrinsically and extrinsically highly regulated process in the CNS and PNS. Although many similarities exist in the developmental program between CNS and PNS, several major differences have been described. For this thesis, OL development in the CNS will be discussed.

1.3.5.1 Oligodendrocyte morphology

Rio Hortega coined the termed *oligodendroglia* (Rio Hortega, 1921) to describe the neuroglia cells that show few short processes. An oligodendrocyte is mainly a myelin forming cell,

however, there exists satellite OLs (Penfield, 1932) that may not be involved in myelination but are found to be perineuronal and may serve to regulate the microenvironment around the neurons (Ludwin, 1997). OLs are smaller in size compared to astrocytes with greater density of both the cytoplasm and nucleus. They lack intermediate filaments and glycogen, and contain a large number of microtubules (Lunn et al., 1997). One OL can extend many processes, each of which contacts and envelopes a stretch of axon followed by compaction (Bunge et al., 1962, Bunge, 1968). Adjacent myelin segments on an axon could belong to different OLs. A number of distinct stages of OL development have been identified based on expression of various components and markers as well the mitotic and migratory status of the OL (Baumann and Pham-Dinh, 2001).

1.3.5.2 Origin and specification of oligodendrocyte precursor cells (OPCs)

Neuronal and glial subtypes of the CNS are generated from neural progenitors that stem from the ventral neuroepithelium in the neural tube. At the start of neurogenesis, proliferating neural progenitors become restricted to the ventricular zone (VZ) at the inner surface of the neural tube (Paridaen and Huttner, 2014). When the neural progenitors start differentiating into post-mitotic neurons, they migrate away from the VZ and become localized in the outer portion of the neural tube (Barateiro et al., 2016). The decision to differentiate into glial pathways is made spatially and temporally within a restricted population of neural progenitors in the VZ. OPCs are generated in sequential waves from specific regions and platelet derived growth factor receptor α (PDGFRα) was identified as an OPC marker (Pringle and Richardson, 1993). In the mouse spinal cord (SC), the first wave of OPCs starts around embryonic day (E) 12.5 in the ventral neuroepithelium within a progenitor domain that also gives rise to motor neurons (pMN) prior to generating OPCs (Pringle et al., 1996). Motor neurons generation is completed by E10.5. The process of OPC generation depends on sonic hedgehog (Shh) signalling which in turn activates the basic Helix-Loop-Helix (bHLH) transcription factor Olig2 which is crucial for OL development (Lu et al., 2002). A second wave of OPCs emanates from more dorsal progenitor domains starting at E15.5 (Cai et al., 2005). After birth, a third wave of OPCs begins, yet the specific origins of this one remain unclear (Rowitch and Kriegstein, 2010). The ventrally derived OPCs in the SC account for 85.00% of adult OLs, whereas dorsally derived OPCs account for only 10-15% (Mitew et al., 2014).

In the forebrain, an initial wave of OPCs is seen ~E12.5 starting from the VZ of the medial ganglionic eminence (MGE) and the anterior entopeduncular areas of the ventral telencephalon (Tekki-Kessaris et al., 2001). By E18, those OPCs have spread to most of the developing telencephalon. Yet in the brain, the first wave is replaced by dorsally generated precursors as development progresses. A second and third waves emanating from lateral and caudal ganglionic eminences at E15.5 (NK2 homeobox 1 (Nkx2.1)-expressing cells) and from the cortex (Empty spiracles homeobox 1 (Emx1)-expressing cells) after birth, respectively, give rise to majority of adult OLs in mice (Kessaris et al., 2006, Mitew et al., 2014).

Several extracellular signals regulate OPC specification. Shh is secreted by the floor plate and notochord and binds to the Notch-1 receptor on the surface of neural precursor cells (NPCs) to activate its coreceptor smoothened. This leads to induced expression of Nkx6 and Olig2 in ventral progenitors to trigger the first embryonic wave of OPC specification (Pringle et al., 1996). Lack of Shh leads to absence of ventrally derived OPCs (Orentas et al., 1999). An increase in OPC specification is observed following blockade of either Wnt/beta-catenin signalling or bone morphogenic protein (BMP) pathway, indicating that these pathways antagonize Shh signalling (Hsieh et al., 2004, Langseth et al., 2010). Dorsally, fibroblast growth factor-2 (FGF-2), acting through either FGF receptor 1 or 2, independently specifies OPCs on the spinal cord and forebrain by phosphorylation of ERK1/ERK2 downstream of mitogen activated protein kinase (MAPK) (Chandran et al., 2003, Furusho et al., 2011).

As for transcription factors such as Pax6, Olig2, Nkx2.2, NKx6.1/6.2, they are required to define the germinal zones of the pMN domain of the spinal cord during development depending on Shh and BMP gradients (Liu et al., 2003, Vallstedt et al., 2005). Shh acts through inducing GLI-Kruppel family members 1 and 2 (Gli1/2) activators and repressing Gli3 repressor to induce Olig2 and Nkx2.2 to promote OPC specification (Qi et al., 2003, Tan et al., 2006). Achaete-scute family bHLH transcription factor 1 (Mash1/Ascl1) has a fundamental role in OL specification as its knockout mice have decreased OPC generation (Parras et al., 2007).

Lastly, Olig2 is the best characterized transcription factor regulating OPC specification. It is induced ventrally by Shh (Lu et al., 2002). *Olig2* knockout mice fail to generate OPCs, astrocyte and motor neurons in most regions of the CNS. To generate motor neurons in pMN, Olig2 homodimerizes, which is dependent of phosphorylation of Serine 147 (Li et al., 2011). However, its dephosphorylation leads to generation of OPCs (Li et al., 2011). Moreover, phosphorylation

of a triple serine motif in the N-terminus of Olig2 is associated with its role in NPCs and OPCs as a pro-mitotic and anti-differentiation factor (Lu et al., 2002, Lee et al., 2005).

OPCs are characterized by their bipolar morphology, their active proliferation as well as their migratory properties. Widely used markers for OPCs include A2B5, chondroitin sulfate proteoglycan called NG2 as well as PDGFRα (Baumann and Pham-Dinh, 2001).

1.3.5.3 OPC proliferation and migration

OPC proliferation plays a crucial role in CNS development since optimum OLs numbers are critical to ensure that the myelinating capacity of OLs matches axonal demand for myelination. A low number of highly proliferative OPCs migrate away from the pMN zone in the developing neural tube and undergo extensive local proliferation to colonize the future white matter (Miller et al., 1997). Many regulators of OPC migration also regulate OPC proliferation ensuring proper temporal coordination of the overall OPC development. Moreover, most signals promoting proliferation inhibit differentiation. For example, PDGF-A is a major regulator of OPC proliferation and its receptor PDGFRα is a marker of proliferating OPCs (Noble et al., 1988, Raff et al., 1988). Lack of PDGF-A in mice leads to very few OPCs and OLs (Calver et al., 1998, Fruttiger et al., 1999), indicating that the levels of PDGF-A directly regulate OPC proliferation. Activated PDGFRα receptor leads to its co-association with αvβ3 integrin, whose activation enhances OPC proliferation through phosphatidylinositol 3 kinase/ protein kinase C signalling (Baron et al., 2002). Another growth factor that plays a role in OPC proliferation is bFGF which has also been shown to promote proliferation and prevent OPC differentiation *in vitro* (Fok-Seang and Miller, 1994) yet bFGF null mice show no changes in OPC proliferation (Murtie et al., 2005). Chemokine (C-X-C motif) ligand 1 (CXCL1) is a common regulator of OPC proliferation and migration, which acts as a stop signal for migrating OPCs while promoting proliferation of *in vitro* OPCs in synergy with PDGF-A (Robinson et al., 1998). An evidence for a role of CXCL1 *in vivo* stems from CXCL1 receptor (CXCR2) null mice which display reduced numbers of OPCs in the spinal cord (Tsai et al., 2002).

Following emergence from sites of oligodendrogenesis, OPCs migrate and proliferate over extended distances to populate the CNS before their final differentiation into myelin-forming OLs. In the spinal cord, newly generated OPCs migrate ventro-dorsally and medio-laterally (ventrally derived OPCs), and dorso-laterally (dorsally derived OPCs) to populate areas of future white

matter (Miller et al., 1997, Ono et al., 1995, Mitew et al., 2014). In the telencephalon, OPCs generated from MGE migrate away and colonize the forebrain (Kessaris et al., 2006). It was originally suggested that OPCs migrate along preformed axonal tracts (Ono et al., 1997) indicating that cell-bound ligands might act as short range cues for OPCs migration. Yet studies have shown that following optic nerve transection, OPCs still migrate normally suggesting that migration does not require viable retinal ganglion cells and that secreted factors, acting as long-range cues, might play a role in OPCs migration (Ueda et al., 1999). It is now known that extracellular matrix components (such as fibronectin and laminin among others (Armstrong et al., 1990)), secreted mitogenic growth factors (PDGF-A (Armstrong et al., 1990) and FGF (Simpson and Armstrong, 1999)), axon guidance cues such as Netrin-1 (Jarjour et al., 2003, Spassky et al., 2002), as well as chemokines (such as CXCL1 and CXCL12 (Dziembowska et al., 2005, Tsai et al., 2002)) are involved in regulating OPC migration.

PDGF signals through Fyn and cdk5 to promote WASP family Verprolin-homologous protein 2 (WAVE2) phosphorylation and migration (Miyamoto et al., 2008) whereas the migratory effect of FGF-2 is mainly through FGF receptor 1 (FGFR1) (Bansal et al., 1996). These two molecules have also been shown to act as potent chemoattractants to help direct OPCs (Noble et al., 1988). The fine tuning of OPC migration can vary depending on developmental stage, region in CNS and specific factors/receptors expressed. For example, netrin-1 acting through its receptor Deleted in colorectal cancer (DCC) is a chemoattractant in the first wave of OPC migration in the optic nerve. Yet, it functions as a chemorepellent in the second wave through Unc5a receptor (Spassky et al., 2002). However, in the developing spinal cord, netrin-1 secreted from the floor plate acts mainly as a chemorepellent to promote dispersal of OPCs (Jarjour et al., 2003, Tsai et al., 2003, Tsai et al., 2006).

1.3.5.4 OLs survival and differentiation

Using mice overexpressing PDGF-A, an increase in proliferation rate of OCP was observed (Calver et al., 1998). Subsequently, this increase was compensated by increased levels of apoptosis (Calver et al., 1998). Similar findings were seen for insulin growth factor-1 (IGF-1), ciliary neurotrophic factor (CNTF) and neurotrophin-3 (NT-3) (Barres et al., 1992, Barres et al., 1994, Barres et al., 1993). On the other hand, mice lacking tenascin-C, an extracellular matrix component, show diminished proliferation rate of OPCs, which leads to reduced apoptosis levels

(Garcion et al., 2001). These studies indicate that survival mechanisms regulate the number of OLs during development. Moreover, earlier studies have shown that as much as 50% of OPCs generated in the developing rat optic nerve undergo apoptosis during differentiation (Barres et al., 1992).

The above findings indicate that these signaling molecules are normally present in subsaturating amounts and suggest that the observed OPC death that occurs during development may reflect a competition for survival signals that are limited in amount or availability (Barres and Raff, 1994). Some of these survival signals include PDGF-A, neuregulin-1, laminin-2α, and IGF-1 (Barres et al., 1992, Barres and Raff, 1999). PDGF-A promotes survival through interacting with the integrin α6β1 whose blockade impairs OPC survival *in vitro* (Frost et al., 1999). Axonal Neuregulin-1 binds to the ErbB receptor on the OL and signals through PI3K/Akt pathway to induce survival (Fernandez et al., 2000, Flores et al., 2000). Laminin-2α knockout mice develop fewer OLs in the spinal cord and it was shown that laminin-2α can bind to α6β1 integrin which associates with ErbB to activate MAPK signaling and reinforce Neuregulin-1 pro-survival and differentiation signaling (Chun et al., 2003, Colognato et al., 2004). Moreover, binding of IGF-1 to its receptor IGF-1R also activates PI3K/Akt signaling to promote survival (Pang et al., 2007). After settling along fiber tracts that will become the future white matter, OPCs become post-mitotic, multiprocessed cells, less motile and express the marker O4 (Baumann and Pham-Dinh, 2001).

The final step of OL development is their differentiation into myelinating OLs. Once they are correctly positioned, they can terminally differentiate into post-mitotic premyelinating OLs. Following exit from cell cycle, dramatic changes in morphology and gene expression occur. Myelinating OLs is the final stage of OLs differentiation with premyelinating OLs being a highly transient stage where cells transition rapidly to myelination or undergo apoptosis (Barres et al., 1992). Mature myelinating OLs express MBP, MAG, and PLP. The late stage of maturation corresponds with the presence of MOG (Baumann and Pham-Dinh, 2001).

OLs differentiation and myelination are coupled to each other and therefore, extracellular and intracellular signals that regulate differentiation often regulate myelination. The leucine-rich repeat and immunoglobulin domain containing 1 (LINGO-1) is a transmembrane protein that was originally identified as a myelin associated inhibitor of neurite outgrowth (Mi et al., 2004). It was later found that LINGO-1 on axonal membrane, bind in trans to LINGO-1 on OPCs to inhibit

differentiation by inhibiting Fyn kinase signaling and activating RhoA GTPase (Jepson et al., 2012, Mi et al., 2005, Mi et al., 2005, Mitew et al., 2014).

The G-protein coupled receptor 17 (GPR17) is an OL specific receptor expressed in late stage OPC. GPR17 activation strongly inhibits OL differentiation by increasing expression and inducing translocation of inhibitory transcriptional factors, ID2 and ID4, to the nucleus (Chen et al., 2009). These two bHLH transcription factors interact with Olig proteins to inhibit their transcriptional activities (Samanta and Kessler, 2004). A premature onset of myelination is seen in GPR17 knockout mice indicating its inhibitory role of differentiation *in vivo* (Chen et al., 2009, Mitew et al., 2014). Notch signaling has also been shown to regulate OL differentiation. Jagged-1 and Delta-1 are expressed on axons and bind the Notch-1 receptor expressed on OPCs. This leads to cleavage of the notch intracellular domain which translocates to the nucleus and increases expression of *Hes1* and *Hes5* transcription factors that inhibit differentiation (Wang et al., 1998, Mitew et al., 2014). Wnt signaling also plays a role in inhibiting OPC differentiation. Neuronal Wnt binds to its receptor Frizzled, expressed by OPCs which induces β-catenin to translocate to the nucleus where it interacts with the inhibitory transcriptional factor Tcf4 and blocks differentiation. (Huang et al., 2012, Shimizu et al., 2005, Mitew et al., 2014).

Signals that promote OPC differentiation include triiodothyronine/thyroid hormone 3 (T3) and IGF-1. T3 inhibits proliferation and promotes differentiation of rodent OPCs (Barres et al., 1994). Moreover, in humans, hypo- and hyperthyroidism lead to deficient and precocious myelination, respectively (Marta et al., 1998, Rodriguez-Pena et al., 1993, Mitew et al., 2014). In addition to the role of IGF-1 in OL proliferation/survival, its overexpression leads to increased overall brain growth and myelination with an increase in the number of mature OLs and myelin gene expression. This indicates that IGF-1 may play a role in promoting differentiation with IGF-1 or IGF-1R knockout mice showing the opposite phenotype (Ye et al., 1995, Ye et al., 2002, Zeger et al., 2007).

Regulation of transcription factors activity/expression is the result of the upstream mentioned pathways. Pathways that inhibit OPCs differentiation lead to activation of inhibitory transcription factors including ID2, ID4, Hes1, Hes5, Tcf4 and Sox6 (Chen et al., 2009, Samanta and Kessler, 2004, Wang et al., 1998, Shimizu et al., 2005). Whereas, signals that promote OPC differentiation converge onto regulatory mechanisms that release OPCs from those inhibitory signals. Some of these factors include Ascl1/Mash1 whose knockout mice show a deficiency in

the generation of post-mitotic OL (Parras et al., 2007). Conditional ablation of Olig2 in the OPCs postnatally leads to a substantial decrease in OL differentiation, as Olig2 has been shown to recruit chromatin remodeling enzyme BRG1 to regulate key genes during differentiation including *Sox10*, *Sip1/Zhfx1b* and the pro-myelinating transcription factor *Myelin regulator factor* (*Myrf*) (Yu et al., 2013, Mei et al., 2013). Yu et al, 2013 has also found that depending on the stage of OL development, Olig2 can target different genes.

1.3.6 CNS myelination

Following their differentiation, OLs begin to myelinate. In the PNS, a strict size-dependency exists. Only axons with 1 um diameter or larger are myelinated, whereas smaller diameter axons are not. However, in the CNS, axons as small as 300 nm are myelinated and axonal caliber is a direct determinant of myelin thickness with larger caliber axons having thicker myelin (Waxman and Sims, 1984, Hildebrand et al., 1993). The number of wraps is related to axon diameter so that the ratio (called *g*-ratio) of axon diameter to that of myelinated axon is constant (Friede, 1972). Changes to myelin thickness in response to changes in axon caliber support the idea that axon selection for myelination is not intrinsically programmed but mediated by signals on the axon surface (Elder et al., 2001). Yet, it was shown recently that cultured OLs can begin myelinating synthetic axon-like tubes (inert glass nanofibers) as small as 400 nm, lacking the usual neuron-glia signaling cues (Lee et al., 2012). This study highlights the importance of biophysical elements of axonal-oligodendroglial interactions in myelination. Moreover, it appears the OLs have a very small window of opportunity to select which adjacent axons to myelinate (~5 h in developing zebrafish) irrespective of the total number of sheaths being made (Czopka et al., 2013, Watkins et al., 2008).

The intricacy of the myelination program by OLs necessitates a complex and dynamic system of signaling mechanisms. Extracellular signals have various roles in controlling process extension/ initial axonal contact as well as myelin thickness, whereas transcription factors play key roles in regulating myelin-related genes expression.

The process of myelin formation begins with the extension of numerous cytoplasmic protrusions (filipodia) from immature, post-mitotic OLs (Mitew et al., 2014). As these microfilament-rich filipodia are searching for myelin-competent axons, they are invaded by microtubules to enlarge them and convert them to lamellipodia highlighting the importance of

myelin cytoskeletal reorganization during myelination (Mitew et al., 2014). Neuron-derived signals have been shown to regulate OPC differentiation, membrane extension, axon target selection and myelin thickness (Klingseisen and Lyons, 2017, Michalski and Kothary, 2015).

Poly-sialylated neural cell adhesion molecule (PSA-NCAM) expressed on axons is one of the inhibitory signals of myelination. It is developmentally downregulated to coincide with the onset of myelination (Decker et al., 2000, Fewou et al., 2007). PSA molecules negatively regulate CNS myelination as their removal induces a transient increase in the number of myelinated axons in the optic nerve (Charles et al., 2000). Other inhibitors of myelination include Jagged-1 and Lingo2. Jagged-1 interacts with Notch-1 receptors to inhibit OL differentiation (Wang et al., 1998, Watkins et al., 2008), whereas Lingo2 associates with Nogo receptor on OL to inhibit myelination and process outgrowth (Mi et al., 2005).

Besides axon caliber being a potent stimulator of initial myelination, pro-myelination axonal signals include laminin-α2 that binds the β1 integrin receptor on OL to promote initial process extension (Colognato et al., 2002). This leads to dephosphorylation of non-receptor tyrosine kinase Fyn at the inhibitory Tyr531 site which leads to activation of downstream signaling molecules that results in initiation of actin polymerization (Hu et al., 2009, Liang et al., 2004). It is noteworthy that Fyn kinase is downstream of several signaling pathways (such as binding of axonal L1 ligand to OL contactin, or binding of netrin-1 to DCC) (Laursen et al., 2009, Rajasekharan et al., 2009). The outcome of Fyn activation leads to inactivation of RhoA leading to hyperextension of OPC processes and increased branch formation (Liang et al., 2004). The importance of Fyn kinase is highlighted by its genetic ablation that leads to hypomyelination with significantly fewer myelinated axons, mature OLs and thinner myelin sheath (Goto et al., 2008).

Regulators of myelin thickness include laminin-α2, β1 integrin (Lee et al., 2006), axonal neuregulin-1 (type 3) that binds to OL ErbB receptor (Taveggia et al., 2008). Moreover, neuregulin-1 regulation of myelin thickness provides a potential mechanism linking neuronal activity with myelin production since levels of neuregulin-1 are regulated by neuronal activity (Ziskin et al., 2007). Brain-derived neurotrophic factor (BDNF) also has promyelinating effects acting through ERK1/2 as deletion of its receptor TrkB in OLs leads to reduced thickness of myelin sheath (Xiao et al., 2012, Xiao et al., 2010, Wong et al., 2013b). The mechanistic target of rapamycin kinase (mTOR) pathway also appears to play a role in regulating myelin thickness as its constitutive activation leads to hypermyelination (Flores et al., 2008, Narayanan et al., 2009).

Several transcription factors regulate terminal differentiation and myelination. Olig1, for example, is expressed when OPCs are specified, yet appears dispensable for OPC function. Olig1 knockout mice generate early OLs that fail to myelinate (Xin et al., 2005). As OLs mature, Olig1 changes from nuclear to cytoplasmic localization (depending on phosphorylation status) and this shift in localization has been shown to be required to promote full membrane extension (Niu et al., 2012). Nkx2.2 is an inhibitory factor that is downregulated when Olig1 is translocated to the cytoplasm at the onset of myelination (Cai et al., 2010). Nkx2.2 is required to generate post-mitotic OLs yet it can inhibit MBP transcription (Cai et al., 2010, Wei et al., 2005), therefore its downregulation is necessary for myelin gene expression. Another vital transcription factor for myelinating OLs is Sox10. Ablation of Sox10 in mice leads to stalling at the premyelination stage (Stolt et al., 2002). Lastly, Myrf is a transcription factor that is specifically induced during OL differentiation (Emery et al., 2009). The induction of Myrf is carried out by Sox10 acting at an intronic enhancer in *Myrf* gene with mice lacking Sox10 showing a complete loss of Myrf expression (Hornig et al., 2013). Myrf functions to allow progression of premyelinating OL to mature myelinating state (Emery et al., 2009). ChIP-seq experiments have shown that Myrf binds near known myelin genes and other genes that are highly expressed by OLs (Bujalka et al., 2013, Cahoy et al., 2008).

1.3.7 QKI expression in the CNS

Early studies of QKI expression in the mouse embryonic brains and spinal cords show that QKI proteins are expressed in the neural progenitors of the VZ at E10.5-E15.5 (Hardy, 1998b). A recent report has found that QKI-5 and QKI-6 are expressed in the VZ as early as E9.5 when neural tube closure has occurred (Hayakawa-Yano et al., 2017) with QKI-5 being localized primarily in the nucleus while QKI-6 is cytoplasmic. These two proteins are coexpressed in Pax6-positive neural stem cells (Hayakawa-Yano et al., 2017). When the neural progenitors start differentiating into neuroblasts and migrate away from the VZ around E13.5, they lose the expression of QKI proteins. At E12.5 in the spinal cord, however, a restricted subdomain in the ventral VZ expresses dramatically high levels of QKI-5 which disappears by E14.5. Therefore, the expression in this subdomain is transient and followed by a migrating wave of cells leaving this domain and maintaining expression of QKI. Those cells migrate laterally and ventrally and become more numerous and display a redistributed QKI-5 expression into the cytoplasm (Hardy, 1998b). Similar

observations were made at E12.5 in the hindbrain (Hardy, 1998b). Neural progenitors down-regulate QKI expression as they acquire neuronal fate whereas QKI^+ cells emerging from the VZ after the main period of neurogenesis take on a glial fate. This indicates that elevated QKI levels correspond to generation of a glial fate. Moreover, the QKI^+ cells migrating away lack expression of neuronal proteins map2 and β-III tubulin and are $BrdU^+$ (Hardy, 1998b). Therefore, proliferating neural progenitors in the VZ downregulate QKI expression as they differentiate into neurons. On the contrary, a subset of differentiating neural progenitors that derive from a specific subdomain within the VZ, maintains expression of QKI proteins as they leave the VZ and those cells have features of glial cells. The only exception to this is the spinal cord motor neurons in the ventral horn that contain moderate levels of QKI-5 from E10.5 to E15.5 (Hardy, 1998b, Hayakawa-Yano et al., 2017).

In neonatal mice forebrain, similar QKI^+ cells are found in the subventricular zone (SVZ) which is a known area of post-natal gliogenesis (Levison and Goldman, 1993, Hardy, 1998b). These cells also express nestin, incorporate BrdU and do not express neuronal markers suggesting they are of glial identity. By P6, astrocytes and oligodendrocytes also express QKI proteins indicating that glial progenitors as well as glial subtypes express QKI (Hardy, 1998b).

In wild-type mice, all three major QKI isoforms are abundantly expressed in myelinating cells of the CNS and PNS as well as in astrocytes (Hardy et al., 1996). In the brain, QKI proteins were found in both grey and white matters including the cerebellum and optic nerve (Hardy et al., 1996). In the cerebellum, QKI-5 and QKI-6 are detected in Bregmann glia of the Purkinje cell layer at levels comparable to those in oligodendrocytes (Hardy et al., 1996). No immunoreactivity is detected for QKI proteins in any CNS neurons (Hardy et al., 1996). QKI expression is also seen in developing and adult Müller glia and a predominant QKI-5 expression is detected in the adult mouse retina suggesting that QKI could play a role in retinal cell fate development and maturation in both glia and neurons (Suiko et al., 2016).

The expression of the *qkI* transcripts has been shown to be regulated developmentally in the brain with *qkI-5* being the most abundant transcript during embryonic development and in the first two post-natal weeks (Hardy et al., 1996). The levels of *qkI-5* decline after and *qkI-6* and *qkI-7* levels increase throughout postnatal development, specifically during accelerated myelin formation, and continue into adulthood (Hardy et al., 1996). QKI-5 is found to be restricted to the

nucleus whereas QKI-6 and QKI-7 are concentrated in the cytoplasm with some low levels of QKI-6 seen in the nucleus (Hardy et al., 1996).

As discussed earlier, several mRNA targets of QKI proteins are genes involved in myelination including genes that are involved in OLs differentiation and several structural myelin genes as well. During OL maturation and myelin formation, the marked decrease in QKI-5 levels and the increase in QKI-6 and QKI-7 is thought to attenuate nuclear retention of QKI target mRNAs, many of which are structural myelin proteins.

Developmental analysis of QKI isoforms expression in the auditory nerve has revealed a similar pattern to what is reported by Ebersol et al 1996, with QKI-6 and QKI-7 being significantly upregulated during post-natal development, whereas QKI-5 is downregulated in the auditory nerve (Panganiban et al., 2018). The same report has demonstrated that myelin abnormalities occur in the auditory nerve following noise-exposure (Panganiban et al., 2018). The authors identify QKI to be differentially expressed following noise-exposure leading to myelinating glia dysfunction, demyelination, paranodal defects and a defective auditory nerve function (Panganiban et al., 2018).

1.4 The Paranode

1.4.1 Structural domains along the axon

Myelin formed by OLs in the CNS and Schwann cells in the PNS wraps around the axons in segments that are separated by the node of Ranvier leading to formation of distinct domains along the axon (Poliak and Peles, 2003). These domains are different molecularly, structurally and functionally and include, the node of Ranvier, the paranode and the juxtaparanode (Figure 1.8).

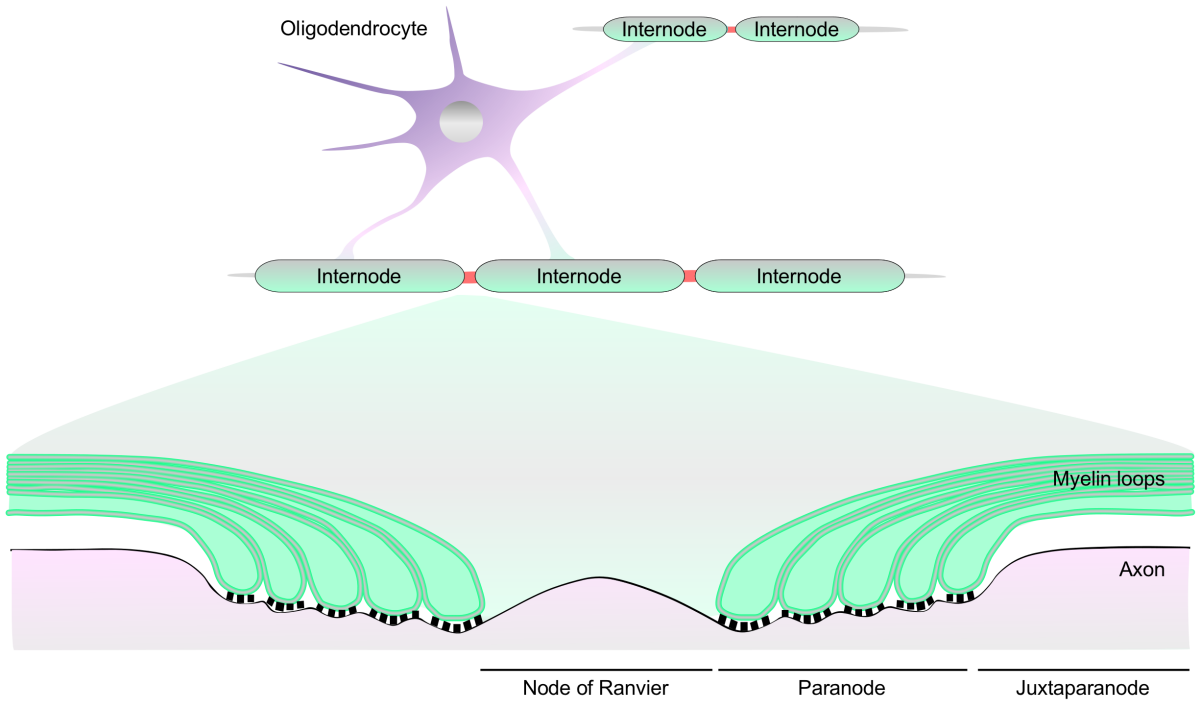

Figure 1.8: Structural domains along the axon. Unmyelinated regions between myelin segments (internodes) are the nodes of Ranvier (shown in red). Myelin loops terminating at the axon lead to the formation of three distinct structural domain: the node, the paranode and the juxtaparanode.

1.4.1.1 The Node

Along myelinated axons, membrane depolarization is confined to non-myelinated nodal regions between adjacent myelin segments allowing for rapid propagation of action potential from one node to the next. The nodes of Ranvier are small periodical gaps along the axon representing interruptions in the myelin sheath, with high clustering of voltage gated sodium channels (Na_v) to allow high influx of Na^+ ions leading to membrane depolarization (Waxman and Ritchie, 1993). The Na_v function to regenerate action potential that has started at the axon initial segment (AIS) which is critical to allow rapid, saltatory conduction. During development, $Na_v1.2$ is recruited to immature nodes but switched to $Na_v1.6$ in the adults (Boiko et al., 2001). These sodium channels interact with adhesion molecules (forming a transmembrane complex) and cytoskeletal adapter proteins (on the cytoplasmic side). The adhesion proteins include Neurofascin-186 (Nfasc-186, the 186kDa isoform of Neurofascin), Nfasc-140 and Contactin-1 in the CNS and Nfasc-186 and Neural-Glial-related cell adhesion molecule (NrCAM) in the PNS (Zhang et al., 2015, Davis et al.,

1996, Lambert et al., 1997). Ankyrin-G and βIV-spectrin adapter proteins link this transmembrane complex to the axonal actin cytoskeleton (Kordeli et al., 1995, Berghs et al., 2000, Kazarinova-Noyes et al., 2001, Komada and Soriano, 2002, Zonta et al., 2008, Ghosh et al., 2017). All these components contribute to recruitment and stabilization of the Na_v channels at the node (Figure 1.9) (Ghosh et al., 2017, Sherman and Brophy, 2005). Voltage gated potassium channels (K_v) are also found at the node and function to allow membrane repolarization (Cooper, 2011).

In the PNS, the secreted extracellular matrix component gliomedin has been shown to instruct nodal assembly and clustering of Na_v channels (Eshed et al., 2007, Eshed et al., 2005). In the CNS, on the other hand, OLs or OL conditioned media have been shown to be able to induce Na_v clustering, therefore providing support that this assembly is as well instructed by a secreted factor (Kaplan et al., 1997). However, such a secreted factor in the CNS is yet to be identified. Moreover, the required axonal cytoskeleton assembles prior to myelination suggesting that intrinsic signals also play a role in inducing nodal formation (Lambert et al., 1997).

Nfasc-186 is the first axonal protein to cluster at the node and in *Nfasc* null mice, none of the remaining nodal components are clustered (Sherman and Brophy, 2005). Reintroducing the Nfasc-186 isoform in these mice was sufficient to rescue nodal formation (Sherman and Brophy, 2005, Zonta et al., 2008). Neurofascin proteins are discussed in detail in section 1.4.3.

1.4.1.2 The Paranode

The paranodes are the domains flanking the node of Ranvier (Figure 1.8). Cytoplasm-filled glial loops, also known as paranodal loops, contact the cell membrane surrounding the axon, known as the axolemma. Myelin compaction forces the OL cytoplasm to the edges of the membrane sheet as the myelin layers compact (Rosenbluth and Blakemore, 1984). The contact between the paranodal loops and the axolemma are known as axo-glial junction or septate-like junctions (Rosenbluth et al., 1995). Those junctions serve as a separation between nodal and juxtaparanodal components and electrical activities as well as limit lateral diffusion of transmembrane proteins into adjacent axonal domains (Rosenbluth, 1976). Specialized proteins, either neuronal or glial, contribute to formation of axo-glial junctions. These include: contactin, contactin associated protein (Caspr) and the 155-kDa Neurofascin isoform (Nfasc-155) (Charles et al., 2002, Einheber et al., 1997, Peles et al., 1997, Menegoz et al., 1997). By electron

microscopy, those axo-glial contacts are seen as transverse bands (Schnapp and Mugnaini, 1976). The paranode is central to this thesis and will be discussed in more detail in section 1.4.2.

1.4.1.3 The juxtaparanode

The juxtaparanode is the domain lying adjacent to the paranode on each side of the node and this part of the axon is directly under the compacted myelin (Figure 1.8). This domain is enriched in potassium channels with two rectifying *Shaker*-like potassium (K^+) channels, $K_v1.1$ and $K_v1.2$ being the most predominant forms (Wang et al., 1993, Rasband et al., 1999, Rasband et al., 2001). Transient axonal glycoprotein-1 (TAG-1, also known as contactin-2) and Caspr2 are two cell adhesion molecules that are localized to this domain and form a complex that is required for clustering of the potassium channels at the juxtaparanode (Figure 1.9) (Poliak et al., 2003). Contactin-2/Caspr2 bind to oligodendroglial contactin-2, which is also expressed in the myelin sheath (Traka et al., 2002). Caspr2, strictly expressed in axons, is critical for maintenance of K^+ channels and functions to prevent diffusion of these channels to the internode. Disrupting either TAG-1 or Caspr2 prevents accumulation of K^+ channels in the juxtaparanode (Savvaki et al., 2008, Poliak et al., 1999, Poliak et al., 2003). Scaffolding proteins including 4.1B, ankyrin-B, αII-spectrin and βII-spectrin are enriched in this domain as well and function to stabilize the contactin-2/Caspr2 complex (Buttermore et al., 2011, Denisenko-Nehrbass et al., 2003, Ogawa et al., 2006). The role of juxtaparanodal K^+ channels remains unclear as evidence supporting its role in repolarization of action potential and support of nerve impulse transmission is still lacking (Thaxton and Bhat, 2009).

1.4.2 The Paranode

1.4.2.1 Composition of the paranode

As mentioned above, the wrapping and compaction of glial membrane leads to pushing the glial cytoplasm to the edges forming glial loops known as paranodal loops which then attach to the axolemma. This attachment leads to the formation of axo-glial junctions (Thaxton and Bhat, 2009, Salzer, 2003) also known as septate-like junctions due to their similarity to invertebrate septate junctions that form between ensheathing glial cells and axon bundles of the nervous system (Rosenbluth et al., 1995, Banerjee et al., 2006). These axo-glial junctions are electron-dense

structures that form a ladder-like distribution between glial paranodal loops and axolemma, known also as transverse bands (Figure 1.9) (Schnapp et al., 1976). On the axonal side, contactin and Caspr are the major components that bind to the glial 155-kDa isoform of Neurofascin, Nfasc-155 (Peles et al., 1997, Charles et al., 2002, Rios et al., 2000). Contactin is a glycosylphosphatidylinositol (GPI)-anchored protein that is a member of the immunoglobulin superfamily and Caspr is a transmembrane protein (Bhat, 2003). Contactin and Caspr interact in *cis* and this is mediated by the extracellular domain of Caspr and the fibronectin type III-like domain of Contactin. This interaction is also required for transport of Caspr from the endoplasmic reticulum to the axonal membrane (Faivre-Sarrailh et al., 2000, Boyle et al., 2001). Several cytoskeletal scaffolding proteins accumulate at the paranode including αII- and βII-spectrins, protein 4.1B and the adapter protein Ankyrin B (Ohara et al., 2000, Ogawa et al., 2006, Thaxton and Bhat, 2009). The C-terminus of Caspr contains a 4.1/ezrin/radixin/moesin (FERM) binding domain that allows it to interact with protein 4.1B (Menegoz et al., 1997, Peles et al., 1997, Poliak et al., 1999), spectrin and actin indicating that the axoglial junctions function to anchor paranodal loops to the axonal cytoskeleton (Garcia-Fresco et al., 2006, Buttermore et al., 2011). Loss of Contactin, Caspr or Nfasc-155 leads to disruption of axoglial junctions (Bhat et al., 2001, Boyle et al., 2001, Pillai et al., 2009). Neurofascin-155 is of central importance in this thesis and will be discussed in detail in section 1.4.3.

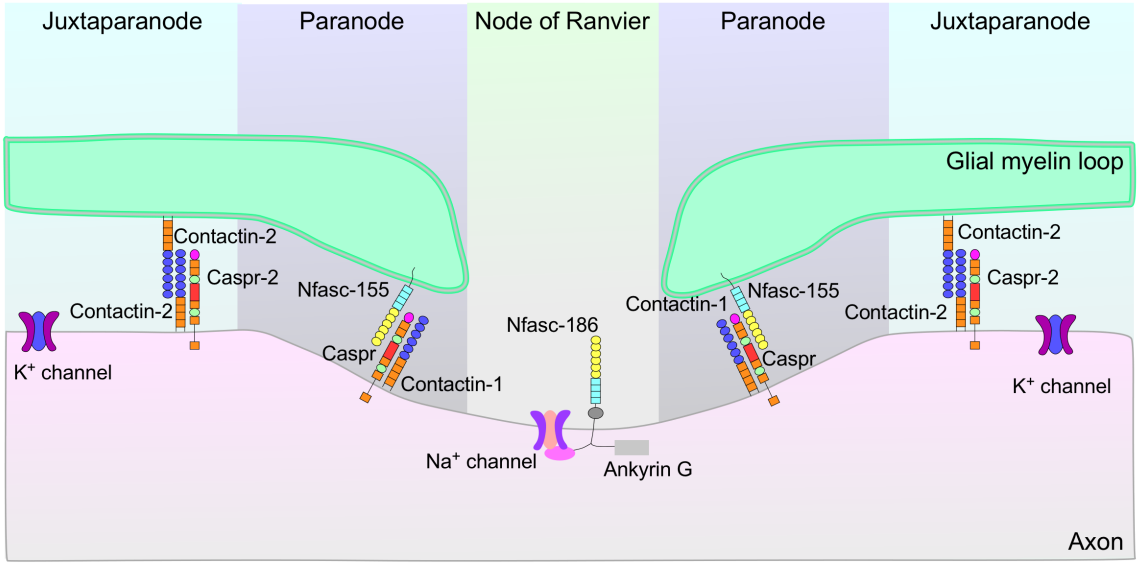

Figure 1.9: Molecular components of the structural domain along the axon. Nfasc-186 is located at the node along with the voltage-gated sodium channel and Ankyrin G. Nfasc-155 is at the

paranode and connects the myelin sheath to axonal Caspr and contactin-1. At the juxtaparanode, contactin-2 expressed by both axons and glia and helps in clustering the potassium channels. (Permission to reprint is granted from Springer Nature, Adapted from (Derfuss et al., 2010))

1.4.2.1 Function of the paranode and axoglial junctions

The first evidence for the role of axoglial junctions stems from studies on frog brain that demonstrated that the paranode functions as a fence to prevent diffusion of ion channels from the juxtaparanode towards the nodal domain (Rosenbluth, 1976). This barrier function is allowed due to the linkage between paranodal components and the axonal cytoskeleton. Although no ion channels cluster at the paranode, maintenance of its function is crucial for proper axonal function to maintain separation of electrical activity between the juxtaparanode and the node.

Studies of knockout mice of *Contactin*, *Caspr* and *Nfasc-155* showed a lack of the electron dense transverse bands by electron microscopy with a severe disorganization of paranodal loops (Bhat et al., 2001, Boyle et al., 2001, Pillai et al., 2009). The spacing between adjacent paranodal loops as well as the space between the paranodal loops and the axolemma were found to also be significantly increased. This provides evidence for the role of axoglial septate junctions in securing the attachment of paranodal loops to axolemma.

In the absence of intact paranodes, ion channels fail to segregate properly and be restricted to their appropriate domains. The distribution of voltage gated sodium channels as well as potassium channels was more diffuse at the nodes/juxtaparanodes and invaded the paranodes (Bhat et al., 2001, Boyle et al., 2001, Pillai et al., 2009). This led to detrimental effects on the conduction of action potential with severe defects in both conduction velocity and amplitude in *Caspr*, *Contactin* and *Nfasc-155* null mice (Bhat et al., 2001, Boyle et al., 2001, Pillai et al., 2009). Therefore, paranodes have a pivotal role in maintaining the barrier between nodal and juxtaparanodal domains to ensure proper electrophysiological properties of myelinated axons.

Lastly, paranodal complexes are crucial for maintaining organization of axonal cytoskeleton. Lack of *Nfasc-155* or *Caspr* leads to axonal swelling with complete disorganization of the normally parallel arrays of axonal cytoskeleton as well as organelle accumulation in the paranodal regions, indicating disrupted axonal transport (Garcia-Fresco et al., 2006, Pillai et al., 2009). Increased levels of phosphorylated neurofilaments, a hallmark of cytoskeletal disruption, was also observed (Pillai et al., 2009). Axonal swelling and cytoskeletal abnormalities are

normally found prior to axonal degeneration in many neuropathies (Lappe-Siefke et al., 2003). Therefore, proper paranodal association with the axon is crucial for proper organization and stabilization of axonal cytoskeleton which is vital for maintaining healthy axons.

1.4.3 Neurofascin

1.4.3.1 Discovery of Neurofascin

Neurofascin (*Nfasc*) is a cell adhesion protein that was discovered in the chick brain in 1987 by Rathjen et al who hinted to a role for Neurofascin in neurite-neurite interactions (Rathjen et al., 1987). Davis et al in 1994 identified Nfasc as an ankyrin-binding glycoprotein functioning to link extracellular interactions to intracellular cytoskeleton (Davis and Bennett, 1994, Ebel et al., 2014). Neurofascin belongs to the L1 subgroup of the immunoglobulin superfamily of cell adhesion molecules (IgCAMs). Extensive alternative splicing and post-translational modifications along with spatial and temporal regulation lead to highly complex expression patterns. The Neurofascin gene spans ~171 kb and alternative splicing generates many isoforms. The major studied isoforms are Nfasc-186 (Neurofascin of 186 kDa), Nfasc-155 (Neurofascin of 155 kDa) and Nfasc-140 (Neurofascin of 140 kDa) which will be discussed in detail in the following section.

1.4.3.2 Gene, alternative splicing, structure and expression of Neurofascin

Analysis of *Nfasc* gene revealed that it contains 33 exons in total. It has four types of major structural components (from N- to C-terminus): Six Ig-like repeats of the C2 subgroup (Ig1-Ig6), five fibronectin type III-like repeats (FN1-FN5), a transmembrane domain and a cytoplasmic domain of 113 amino acids (Figure 1.10) (Volkmer et al., 1992, Davis et al., 1993). A specific subset of Nfasc isoforms contains an additional structural element known as the PAT/mucin-like domain, consisting of mainly proline, alanine and threonine (Volkmer et al., 1992).

Alternatively spliced exons encode three major structural domains: the third and fifth FNIII-like domains and the PAT domain (Hassel et al., 1997). Minor alternatively spliced exons include one located at the NH2-terminus (exon 4, 18 bp), between Ig-like domains 2 and 3 (exon 8, 51 bp), at the junction between the Ig-like and the FNIII-like domains (exon 17, 45 bp) and within the cytosolic domain (exon 32, 12 bp) (Figure 1.10) (Ebel et al., 2014). Five major isoforms of Nfasc have been identified, Nfasc-155, Nfasc-166, Nfasc-180, Nfasc-186 and recently, Nfasc-

140. These isoforms are characterized by inclusion of specific alternatively spliced exons. Nfacs-155 has fibronectin III-like domains 1-4 and lacks the PAT domain (Kriebel et al., 2012). Nfasc-166 has FNIII-like domain 1, 2 and 4. Nfasc-180 includes the same FNIII-like domains as Nfasc-166 and also includes the PAT domain (Kriebel et al., 2012). Nfasc-186 on the other hand has FNIII-like domains 1, 2 and 4, PAT domain as well as an additional FNIII-like domain 5 (Figure 1.10) (Kriebel et al., 2012). Alternatively, spliced exons are mutually exclusive. Exons 4, 17, 25-28 are found in Nfasc-186 (Suzuki et al., 2017) whereas exons 8, 21/22 are found in Nfasc-155 (Figure 1.10). Recently, Rbfox RNA-binding protein was shown to be responsible for neuronal isoforms selection through inclusion of exons 25-28 (Suzuki et al., 2017).

Nfasc-166, -180 and -186 are found in neurons, whereas Nfasc-155 is expressed in OLs. In the embryonic chick brain, Nfasc-166 is the first isoform to emerge in the extending fibre tracts axons in the CNS and PNS, indicating a possible role in neurite outgrowth (Rathjen et al., 1987, Hassel et al., 1997, Pruss et al., 2006). In rodents, Nfasc-180 was found to be expressed in hippocampal neurons at the axon initial segment and regulate the organization of post synaptic components (Kriebel et al., 2011, Burkarth et al., 2007). Later in development, Nfasc-180 becomes replaced with Nfasc-186 that is expressed at the AIS and nodes of Ranvier (Davis et al., 1996, Kriebel et al., 2011). On the other hand, Nfasc-155 is expressed in myelinating glia at the axo-glial contact sites (paranodal loops) (Poliak and Peles, 2003) and accordingly, its expression coincides with onset of myelination (Collinson et al., 1998, Basak et al., 2007). Neurofascin has also been shown to undergo homo and heterophilic interactions (Pruss et al., 2004, Pruss et al., 2006, Volkmer et al., 1996).

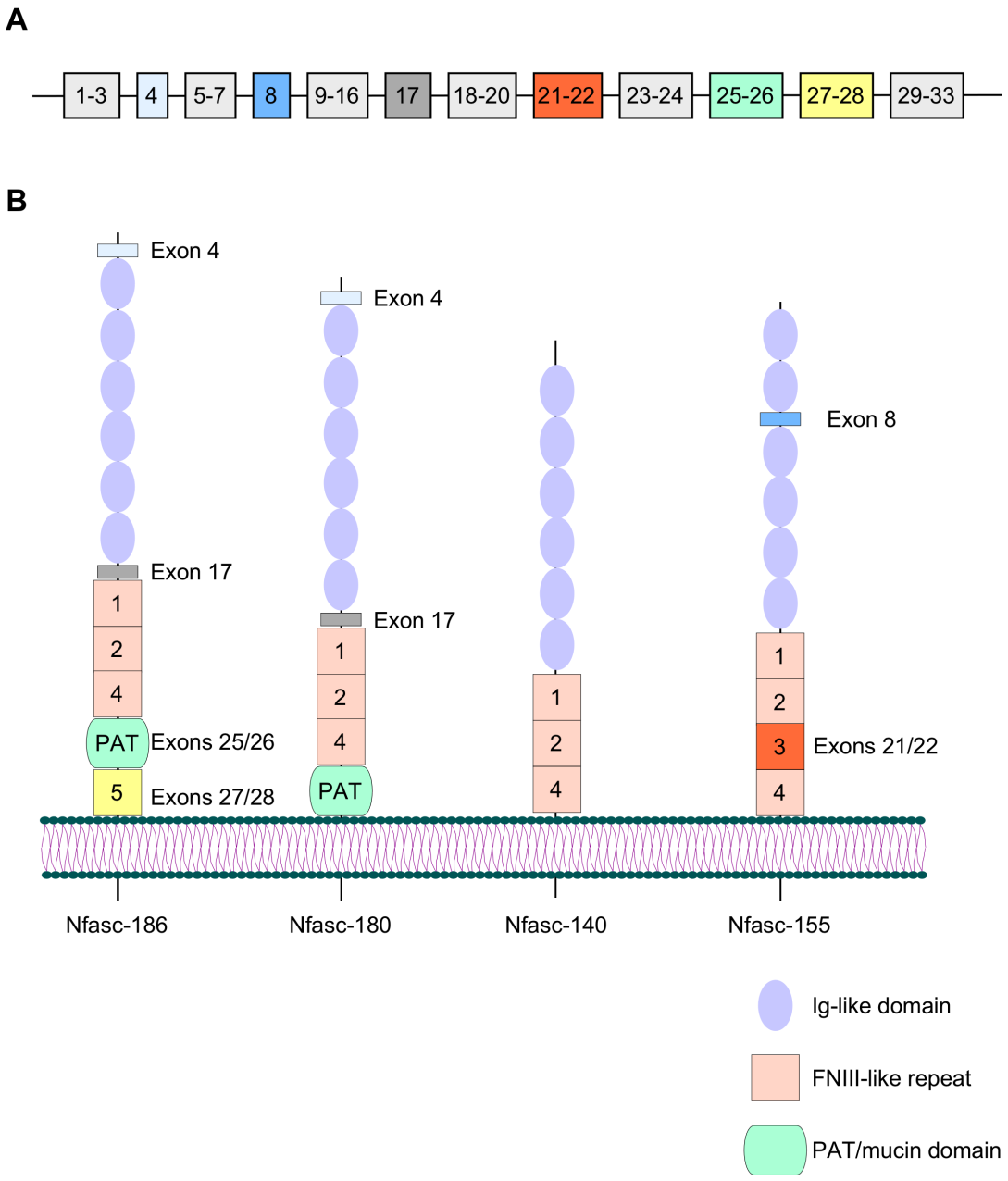

Figure 1.10: Neurofascin gene. A. Schematics representation of the genomic locus of Neurofascin with alternatively spliced genes highlighted to correspond to colors of distinct functional domains. B. Domain structures of neurofascin isoforms (Chick Nfasc-166 is not shown). Immunoglobulin (Ig)-like domains and fibronectin type III (FNIII)-like repeats are represented. PAT refers to the proline-alanine-threonine rich sequence, also known as the mucin-like domain. Permission to reprint is granted from Springer Nature (Adapted from (Ebel et al., 2014)).

1.4.3.3 Function of Neurofascin

Nfasc-166 and Nfasc-180 have been shown to play a role in neurite outgrowth. Homophilic and heterophilic interactions of Neurofascin induce axonal outgrowth (Pruss et al., 2004, Volkmer et al., 1996), with different neurons exhibiting different interactions. Nfasc-166 and Nfasc-180 have opposing functions in regulating neurite outgrowth. Nfasc-166 expressed in dorsal root ganglion neurons during development, becomes replaced with Nfasc-180 later on (Pruss et al., 2006, Koticha et al., 2005). Moreover, Neurofascin is also implicated in the formation and clustering of postsynaptic scaffold protein gephyrin that is located on the postsynaptic site of inhibitory synapses (Fritschy et al., 2008). Gephyrin plays a role in the clustering of glycine, and GABAA receptors (Kneussel et al., 1999, Levi et al., 2004). Nfasc-180 has been demonstrated to induce formation of gephyrin clusters in immature neurons at the axon hillock (Burkarth et al., 2007). Later on in development, Nfasc-180 shifts localization to the AIS to regulate clustering of gephyrin, therefore, implicating Neurofascin in the regulation of GABAergic innervation (Ebel et al., 2014).

Nfasc-140 is the newest member discovered in the Neurofascin family. It is a neuronal isoform that is strongly expressed during embryonic development and diminishes during the initial stages of nodal formation (Zhang et al., 2015). It lacks mucin and FNIII5 domain that are characteristics of Nfasc-186 and lacks FNIII3 domain that is characteristic of Nfasc-155. It has been shown to function similarly to Nfasc-186 to cluster Na_v channels at the developing node using transgenic rescue in *Nfasc* null mice (Zhang et al., 2015). More interestingly, it has been shown to be reexpressed in demyelinated white matter lesion of post-mortem brain tissues from human subjects with multiple sclerosis (Zhang et al., 2015).

Nfasc-155 expression is induced at the onset of myelination in the PNS and CNS (Collinson et al., 1998). It interacts with the axonal membrane proteins Caspr and contactin-1 to form axoglial septate like junctions (Tait et al., 2000, Rios et al., 2000). The recruitment of axonal contactin-1 to the membrane has been shown to be dependent on Nfasc-155 (Sherman and Brophy, 2005) with the contactin-1 and Caspr interactions being required for transport and intracellular processing of contactin-1 (Gollan et al., 2003). Myelination is inhibited by blocking the interaction between Nfasc-155 and Caspr/Contactin-1 (Charles et al., 2002). Genetic ablation of either Nfasc-155, Caspr or Contactin-1 leads to disruption of paranodal septate-like junctions, loss of ion channel segregation and impaired nerve conduction (Boyle et al., 2001, Bhat et al., 2001, Pillai et

al., 2009 Thaxton et al., 2010). Reconstituting glial Nfasc-155 in *Nfasc* null mice is sufficient to rescue clustering of Na_v channels at the node in the CNS (Zonta et al., 2008). This highlights a significant role for paranodal septate-like junctions in restricting diffusion of nodal complexes to maintain proper axonal conduction.

Nfasc-186 localizes to the AIS and node of Ranvier and plays a role in assembly and stabilization of these axonal domains. Ankyrin G is the master regulator of AIS assembly (Hedstrom et al., 2007, Zhou et al., 1998). Mice lacking cerebellar ankyrin G fail to assemble AIS in Purkinje cells (Jenkins and Bennett, 2001, Ango et al., 2004) and lose clustering of Nfasc-186 and ion channels at the AIS. $Na_v1.6$ channels are targeted to the AIS and the nodes by Ankyrin G through an ankyrin G-binding domain (Garrido et al., 2003, Gasser et al., 2012). Although Nfasc-186 is not required for the initial organization of the AIS, AIS maturation is dependent on Nfasc-186 as its ablation in Purkinje neurons leads to failure of mature $Na_v1.6$ channels to cluster at the AIS (Zonta et al., 2011, Buttermore et al., 2012). The maintenance of AIS protein complexes in adult animals is carried out by Nfasc-186 exclusively. Adult inducible loss of Nfasc-186 in cerebellar Purkinje cells leads to its rapid loss from AIS but not from the nodes (Zonta et al., 2011). This causes disintegration, impairment of motor learning and abolition of spontaneous tonic discharge which is a typical feature of Purkinje cells (Zonta et al., 2011). Surprisingly, nodal Nfasc-186 was much more stable and the nodes were much less susceptible to disintegration. Conditional neuronal ablation of Nfasc-186 leads to disrupted nodal clustering with intact paranodes that invade the nodal region (Thaxton et al., 2011). This indicates further that Nfasc-186 is required for CNS and PNS nodal organization. Along with other studies, the loss of Nfasc-186 was shown to lead to impaired nodal assembly of Na_v channels, spectrin BIV, and Ankyrin G suggesting that Nfasc-186 is upstream of Ankyrin G clustering at the node (Koticha et al., 2006, Thaxton et al., 2011).

As for the node formation, differences between CNS and PNS have been reported and are likely due to differences in glial contribution. In the PNS, Schwann cells extend microvilli to the nodal segment and express gliomedin that interacts with Nfasc-186 to assemble the nodal complexes (Eshed et al., 2005). Knockdown of gliomedin results in disrupted clustering of nodal proteins including Na_v channels and Nfasc-186 (Eshed et al., 2005). Absence of Nfasc-186 also leads to disruption of Na_v channels clustering at the node, however, Schwann cell expression of Nfasc-155 in *Nfasc* null dorsal root ganglion cocultures allows for clustering of mature nodes

(Feinberg et al., 2010). Moreover, at the node, Nfasc-186 seems to act as the master regulator. When it localizes to the node, Nfasc-186 recruits Ankyrin G through its FIGQY motif and Na_v channels then bind to Ankyrin G, and their β1 subunit binds to Nfasc-186 as well (Malhotra et al., 2000, Garrido et al., 2003, Garver et al., 1997, Gasser et al., 2012). The interaction between the β1 subunit of Na_v and Nfasc-186 has been reported to occur through either the first Ig-like or the second FNIII-like repeat (Ratcliffe et al., 2001). In the CNS, however, nodal organization is not as well understood. Periodal astrocytes which fill the extracellular space adjacent to the nodes, are thought to be the equivalent of Schwann cells microvilli (Raine, 1984). However, a CNS equivalent of gliomedin remains to be identified. One possible candidate is brevican yet its knockout mice show no major defects in nodal organization (Brakebusch et al., 2002). Ablation of *Nfasc* in the CNS and PNS of mice results in complete disorganization of nodes and paranodes resulting in death at P6 (Sherman and Brophy, 2005). Restoring Nfasc-186 expression in these mice can rescue Ankyrin G and $Na_v1.6$ localization at the CNS node, independent of the paranode (Zonta et al., 2008). Interestingly, transgenic rescue of Nfasc-155 in these mice can rescue nodal complex in the CNS indicating that functional paranodes can compensate for lack of Nfasc-186 (Zonta et al., 2008). Yet, nodes still form in absence of paranodal components Caspr, Contactin-1 and Nfasc-155 (Pillai et al., 2009, Boyle et al., 2001, Bhat et al., 2001). Therefore, nodes can form independently of axo-glial junctions.

Nfasc proteins could be post-translationally modified. Nodal Nfasc-186 remains unphosphorylated allowing its interaction with Ankyrin G. When Nfasc-186 is phosphorylated, it loses its interaction with Ankyrin G and interacts with doublecortin (a tubulin binding protein) (Kizhatil et al., 2002) which leads to internalization of Nfasc-186 at the soma and dendritic sites (Yap et al., 2012). However, Nfasc-155 remains phosphorylated indicating that its recruitment to the membrane is independent of Ankyrin G (Jenkins et al., 2001).

1.4.3.4 Neurofascin and disease

Proper nodal and paranodal functions are essential for proper conduction of action potentials. In MS patients, sodium channel clusters are no longer stable at the node which is thought to contribute to axonal degeneration leading to loss of function in MS patients (Craner et al., 2004). A study of post-mortem tissues from MS patients showed a loss and alteration of Nfasc-

155 in actively demyelinating areas of the white matter. The destabilization of paranodal Nfasc-155 results in disruption of axoglial junctions leading to potassium channel invasion into the paranode (Howell et al., 2006). Nfasc-186 expression is disrupted in MS white matter lesion and becomes diffusely distributed along demyelinated axons in a manner similar to sodium channels (Howell et al., 2006). Later in 2007, the first evidence for neurofascin as a target in autoimmune diseases emerged. Autoantibodies against the extracellular domain of Nfasc-155 and Nfasc-186 were identified in plasma of MS patients (Mathey et al., 2007). In other autoimmune disorders such as acute motor axonal neuropathy, alterations at the node are observed that lead to disruption of proper action potential propagation (Susuki et al., 2007). Autoantibodies against neurofascin were found in sera of patients affected by Guillain Barre syndrome which includes a group of inflammatory neuropathies (Pruss et al., 2011). In experimental allergic neuritis, an animal model of acute inflammatory demyelinating polyneuropathy, disorganization of nodal neurofascin and gliomedin were seen prior to demyelination and this was associated with autoantibodies against these two proteins (Lonigro and Devaux, 2009). Chronic inflammatory neuropathies are a group of diseases with autoimmune pathology in the peripheral nerve. Acute and Chronic inflammatory demyelinating polyradiculoneuropathy (AIPD or CIPD) are one of the main diseases and they are characterized by autoantibodies against Nfasc-186 and/or Nfasc-155 where most patients show symptoms associated with a conduction block indicative of nodal/paranodal disorganization (Delmont et al., 2017, Fehmi et al., 2017). Moreover, autoantibodies against Nfasc-186 or Nfasc-155 are also found in combined central and peripheral demyelination (CCPD) (Kawamura et al, 2013, Fehmi et al, 2017). Lastly, several neurodegenerative diseases display axonal swellings that result from axonal domains disorganization. These include amyotrophic lateral sclerosis, Charcot-Marie Tooth, Wallerian degeneration, Alzheimer's disease as well as cerebrospinal ataxia (Stokin et al., 2005, Brownlees et al., 2002, Collard et al., 1995). The swelling observed in these diseases is similar to what is observed in paranodal mutant mice indicating that axonal domain disorganization is an early sign of degeneration.

Chapter 2

Quaking regulates Neurofascin 155 expression for myelin and axoglial junction maintenance

2.1 Preface

Previous studies investigating the role of Quaking proteins in OLs development have relied mostly on *in vitro* systems. The work in Chapter 2 focuses on characterizing the *qkI* conditional allele as well as assess the functional consequences for the loss of QKI proteins in OLs during development and adulthood. Moreover, I characterized the alternative splicing changes following loss of QKI and identified Neurofascin as a novel target of QKI.

2.2 Title page

Quaking regulates *Neurofascin 155* expression for myelin and axoglial junction maintenance

Abbreviated title: QKI regulates Nfasc155 alternative splicing

Lama Darbelli[1], Gillian Vogel[1], Guillermina Almazan[2] and Stéphane Richard[1]*

[1]Terry Fox Molecular Oncology Group and the Bloomfield Center for Research on Aging, Lady Davis Institute for Medical Research, Sir Mortimer B. Davis Jewish General Hospital, and Departments of Oncology and Medicine, McGill University, Montréal, Québec, Canada.

[2]Department of Pharmacology and Therapeutics, McGill University, Montréal, Québec, Canada.

*Corresponding author: Lady Davis Institute, 3755 Côte Ste-Catherine Road, Montréal, Québec, Canada H3T 1E2. Phone: (514) 340-8260, Fax: (514) 340-8295

E-mail: stephane.richard@mcgill.ca

Keywords: Myelin, QUAKING, RNA binding protein, alternative splicing, axoglial junctions, Neurofascin, oligodendrocyte differentiation

2.3 Abstract

RNA binding proteins required for the maintenance of myelin and axoglial junctions are unknown. Herein, we report that deletion of the Quaking (QKI) RNA binding proteins in oligodendrocytes (OLs) using *Olig2-Cre* results in mice displaying rapid tremors at post-natal day 10 followed by death at the third post-natal week. Extensive central nervous system hypomyelination was observed as a result of OL differentiation defects during development. The QKI proteins were also required for adult myelin maintenance, as their ablation using *PLP-CreERT* resulted in hindlimb paralysis with immobility at around 30 days post 4-hydroxytamoxifen injection. Moreover, deterioration of axoglial junctions of the spinal cord was observed and is consistent with a loss of Nfasc155 isoform that we confirmed as an alternative splice target of the QKI proteins. Our findings define roles for the QKI RNA binding proteins in myelin development and maintenance, as well as in the generation of Nfasc155 to maintain healthy axoglial junctions.

Significance statement

Neurofascin 155 is responsible for axoglial junction formation and maintenance. Using a genetic mouse model to delete Quaking (QKI) RNA-binding proteins in oligodendrocytes, we identify QKI as the long-sought regulator of Neurofascin alternative splicing further establishing the role of QKI in oligodendrocyte development and myelination. We establish a new role for QKI in myelin and axoglial junction maintenance using an inducible genetic mouse model that deletes QKI in mature oligodendrocytes. Loss of QKI in adult oligodendrocytes leads to phenotypes reminiscent of the experimental autoimmune encephalomyelitis (EAE) mouse model with complete hindlimb paralysis and death by 30 days post induction of QKI deletion.

2.4 Introduction

Quaking viable mice (qk^v) display tremors by post-natal day 10 (P10). The genetic defect in qk^v is a ~1 Mb deletion encompassing the *qkI* gene promoter that reduces the expression of QKI proteins in myelinating glia (Ebersole et al., 1996a). qk^v mice exhibit severe dysmyelination in the central and peripheral nervous system (PNS) with abnormalities in nodal, internodal and paranodal regions with spotty disruption of paranodal junctions (Rosenbluth and Bobrowski-Khoury, 2013, Chenard and Richard, 2008), however the exact cause of these defects remains unknown.

The *qkI* gene encodes KH-type RNA binding proteins that generates 3 major alternative splicing mRNAs (5, 6, and 7 kb) encoding QKI-5, -6, and -7 that differ in their C-terminal 30 amino acids (Ebersole et al., 1996b). QKI-5 is exclusively nuclear, while QKI-6 is distributed throughout the cell, and QKI-7 is predominantly cytoplasmic (Wu et al., 1999). The QKI isoforms dimerize (Chen and Richard, 1998, Beuck et al., 2012, Teplova et al., 2013), and interact with RNA in a sequence-specific manner. The following bipartite sequence, ACUAAY-(N_{1-20})-UAAY was identified and termed the QKI Response Element (QRE) (Galarneau and Richard, 2005). Transcriptome-wide CLIP (crosslinking and immunoprecipitation) confirmed the QRE *in vivo* and also showed that QKI associates predominantly with intronic sequences (Hafner et al., 2010), implying a nuclear role for the QKI isoforms.

It was recognized that qk^v mice harbour many RNA-associated defects. The QKI isoforms regulate the mRNA export (Larocque et al., 2002) and stability of the MBP mRNAs (Li et al., 2000). The QKI isoforms also regulate the mRNA stability of Krox-20 (Egr-2) (Nabel-Rosen et al., 2002), the cyclin-dependent kinase inhibitor $p27^{KIP1}$ (Larocque et al., 2005) and the actin interacting protein 1 (AIP-1) (Doukhanine et al., 2010). The qk^v mice display alternative splicing defects of myelin components including myelin associated glycoprotein (MAG), proteolipid protein (PLP) (Wu et al., 2002) and Sirt2 (Zhu et al., 2012) and these have been shown to be regulated indirectly by QKI-6 that regulates the mRNA translational control of hnRNPA1 (Zhao et al., 2010, Zearfoss et al., 2011), and hnRNP F/H (Mandler et al., 2014). However, nuclear QKI-5 has been shown to regulate alternative splicing in vascular smooth muscle cells and skeletal muscle (van der Veer et al., 2013, Hall et al., 2013), but a role for QKI-5 in the regulation of alternative splicing in myelinating cells has yet to be demonstrated.

To circumvent the embryonic lethality of *qkI* mice (Li et al., 2003) and the large deletion the qk^v mice, we now report a *qkI* conditional allele designed to delete all 3 major isoforms. This new

allele led to the identification of *Neurofascin* as an alternative splicing target of QKI-5. *Neurofascin* (*Nfasc*) is extensively alternatively spliced with two major isoforms: Nfasc155 expressed in myelinating cells and Nfasc186 expressed in neurons (Ebel et al., 2014), however, the RNA binding proteins that regulate this alternative splicing event remain unknown. Nfasc155 is up-regulated at the onset of myelination, where it interacts with axonal Caspr and Contactin to form septate-like junctions also known as axoglial junctions (Collinson et al., 1998 Gollan et al., 2003, Tait et al., 2000, Charles et al., 2002). Genetic ablation of Caspr, Contactin-1 or Nfasc155 leads to disrupted paranodal axoglial junctions, failure to properly segregate ion channels, and impaired action potential conduction (Boyle et al., 2001, Bhat et al., 2001, Pillai et al., 2009, Thaxton et al., 2010, Sherman and Brophy, 2005).

Herein, we show that deletion of the QKI isoforms in OLs using *Olig2-Cre* leads to severe CNS hypomyelination with tremors by P10 and death by the third post-natal week. Ablation of *qkI* in adult mice using *PLP-CreERT* resulted in hindlimb paralysis, thoracic kyphosis and immobility ~30 days post-4-hydroxytamoxifen (OHT) administration. Our work defines QKI-5 as a regulator of *Nfasc* alternative splicing required for axoglial junction development and maintenance.

2.5 Materials and methods

***qkI* conditional allele.** All mouse procedures were performed in accordance with McGill University guidelines, which are set by the Canadian Council on Animal Care. The mouse *qkI* conditional allele was constructed using a previously described targeting vector (Yu et al., 2009). The targeting construct contained *loxP* sites flanking exon 2 of the *qkI* gene. Briefly, the sequenced plasmid was linearized and electroporated into 129/Sv ES cells. Three independent ES cell clones with homologous integration at the targeting site were injected into C57BL/6J blastocysts and chimeras obtained. These chimeras were subsequently crossed with C57BL/6J females and those mice with successful germline transmission of the targeted allele were crossed with C57BL/6J mice expressing Flp recombinase to remove the neomycin resistance cassette resulting in a floxed allele ($qkI^{FL/+}$). These mice were then intercrossed to obtain $QKI^{FL/FL}$ homozygote animals. Genomic DNA was isolated from ear biopsies and a DNA fragment was amplified using the following primers: (5'-ACA GAG GCT TTT CCT GAC CA-3') and (5'-TTC AGA ACC CCC ACA TTA CC-3') resulting in a band of ~191 bp in the wild type allele and ~309 bp in the floxed allele. To generate the embryonic or inducible *qkI* conditional knockout mice, $qkI^{FL/+}$ mice were crossed with transgenic mice expressing either *Olig2-Cre* or *PLP-CreERT*, respectively. To detect the *Olig2-Cre* (Ligon et al., 2007) and *PLP-CreERT* transgenes (Doerflinger et al., 2003), generic Cre recombinase primers were used: 5'-GCG GTC TGG CAG TAA AAA CTA TC-3' and 5'-GTG AAA CAG CAT TGC TGT CAC TT-3'. To verify recombination between the loxP sites, the following primers were used: 5'-CCT GGA ATG GTG CTT TCC TA-3' and 5'-TTC AGA ACC CCC ACA TTA CC-3'. For tamoxifen treatment, a solution of 10 mg/ml tamoxifen (Sigma) was dissolved in corn oil and eight-week-old mice were injected intraperitoneally once daily for 5 consecutive days with 1 mg/25g.

Immunoblotting. Mice were scarified in accordance with a protocol approved by the Animal Care Committee at McGill University and tissues were immediately flash frozen on dry ice and stored at −80°C. Tissues were lysed in cold RIPA buffer (Sigma Aldrich) with protease inhibitor cocktail (Roche). Samples were incubated on ice for 30 min, sonicated and centrifuged at 10,000 rpm for 15 min at 4°C. Supernatants were collected and protein concentration measured using protein assay reagent (BioRad). Samples were stored at −80°C or used immediately for immunoblotting. 40µg protein/well was separated by SDS-PAGE, transferred to nitrocellulose membranes using

immunoblot TurboTransfer system (BioRad) and immunoblotted with the indicated primary antibody: (QKI-5/-6/-7 (Millipore), β-tubulin (Sigma), GFAP (Sigma), Nefl (Sigma), NeuN (Chemicon), Nfasc155 and Nfasc186 (Millipore), pan-Nfasc (a kind gift from Dr. Peter J. Brophy, University of Edinburgh, Scotland), MBP (Sternberger), Na_v (Sigma) and Caspr (Abcam) followed by horseradish peroxidase conjugated secondary antibody and visualized by ECL Plus reagent (Perkin Elmer).

Reverse transcription, semi-quantitative and quantitative- PCR. Total RNA from tissues were isolated in appropriate amounts of TRIzol® reagent according to the manufacturer's instructions (Invitrogen). Thirty μg of RNA were DNase I (Promega) treated for 30 min at 37°C. One μg of RNA was reverse transcribed using oligo(dT) primer and M-MLV reverse transcriptase according to manufacturer's protocol (Promega). cDNAs were then amplified by semi-quantitative PCR and the DNA fragments separated by agarose gel electrophoresis. For real-time PCR, primers were designed and efficiency tested according to the MIQE guidelines. Real-time PCR was performed in triplicates with a 1:4 dilution of cDNA using SyBR Green PCR Mastermix (Qiagen, Valencia, CA) on 7500Fast Real-Time PCR System (Applied Biosystems, Foster City, CA). All quantification data were normalized to GAPDH using the ΔΔCt method.

Primary mouse and rat OL cultures and siRNA Transfection. Primary oligodendrocyte progenitor cells (OPCs) were prepared from newborn Sprague-Dawley rat brains as described previously (Almazan et al., 1993). The cells were plated on poly-D-lysine-coated dishes and grown in serum-free DMEM-F12 mixture (1:1) medium supplemented with 10 mm HEPES, 0.1% bovine serum albumin, 25 μg/ml of human transferrin, 30 nm triiodothyronine, 20 nm hydrocortisone, 20 nm progesterone, 10 nm biotin, 5 μg/ml of insulin, 16 μg/ml of putrescine, 30 nm selenium, and 10 ng/ml of each of PDGFAA and basic FGF. The progenitors are proliferative under these conditions, whereas removal of the mitogens initiates their differentiation. Culture medium was changed every 2 days under all experimental conditions. OPCs were induced to differentiate following withdrawal of growth factors for 4 days and transfected with an siRNA designed to target QKI (5′-GGA CUU ACA GCC AAA CAA C-3′) and luciferase control siRNA (5′-CGU ACG CGG AAU ACU UGA-3′) with 5′-tagged Alexa-488 fluorophore (Invitrogren). Primary OPCs were transfected using the Lipofectamine RNAiMax reagent (Invitrogen) according to the

manufacturer's instructions. The cells were harvested 48 h post-transfection. Primary mouse OPCs were isolated from a pool of 5-6 wild type or QKI$^{FL/FL;PLP\text{-}CreERT}$ P1 pups. The same isolation procedure as the rat OPCs was followed. Mouse OPCs were induced to differentiate for 4 days prior to treatment with tamoxifen.

Minigene assays. *Neurofascin* gene exons 20 to 23 with the intervening introns were amplified from mouse brain genomic DNA by PCR using the forward primer 5′- GGG GCTAGC CACC ATG GAC TAC AAA GAC GAT GAC GAC AAG CCT ATG AAT GCT ACC TCT GCC TTT GGC-3', containing a FLAG epitope tag and an *Nhe*I site, and the reverse primer 5'-CCG GGC TCG AGT TAG GGC ACG TAT CTG AGG ATG TAT C -3, containing an *Xho*I site. The DNA fragment was then subcloned into the corresponding site of pVAX1. The mutation of the QKI Response Elements (QRE) within intron 21 of the minigene was performed in a two-step PCR using primers 5′- CCC AGC CCC ACG GAC CCA CCT TCT TGC GGG TCA GGG AAA GGG GTA GCA GCC -3′ (forward primer) and 5′- CTT TCC CTG ACC CGC AAG AAG GTG GGT CCG TGG GGC TGG GTG C -3′ (reverse primer) for QRE1 and PCR primers 5'- GTC ACT ACC ACC ACG GGT CAC GAG CCT GGC CCT GCT GCC TCG CCA C-3' (forward primer) and 5'- AGG GCC AGG CTC GTG ACC CGT GGT GGT AGT GAC TGG TCC TCC CTT TGC-3' (reverse primer) for QRE2 mutation. HEK293T cells were plated in 6-well plates and transfected with 2 μg of the indicated minigene with 2 μg of pcDNA3.1 expression vectors encoding QKI-5, QKI-6, QKI-7, QKI5:V157E. These plasmids have been previously described (Chen and Richard, 1998, Larocque et al., 2002). The common forward primer for RT-PCR detection of *Neurofascin* minigene transcripts was: (5′- TGA CGA CAA GCC TAT GAA TGC TAC -3′). The reverse primer for RT-PCR detection was as follows: (5′- CTA GAC TCG AGT TAG GGC ACG TAT C -3').

RNA binding assays. Brains were lysed in cell lysis buffer (20 mM Tris-HCl pH 8.0, 150 mM NaCl, 1% Triton X-100, 40 U/ml RNase Inhibitor and supplemented with Roche Complete Mini EDTA-free protease inhibitor) and incubated at 4°C with 4 μL of 100 μM biotinylated RNA (IDT) for 60 min and then subsequently Streptavidin beads were added for 30 min with end-over-end mixing. The beads were washed 3-times with lysis buffer with increasing salt concentrations (150

mM, 300 mM or 500 mM) and once with 1X PBS. Protein samples were analyzed by SDS-PAGE and immunoblotting.

Layered and Integrated system for splicing annotation (LISA). Total RNA was extracted from brains of $QKI^{FL/FL;-}$ and $QKI^{FL/FL;Olig2\text{-}Cre}$ P14 mice (n=3 for each genotype), reverse transcribed, and analyzed by high-throughput PCR amplification at the Université de Sherbrooke RNomics Platform as previously described (Klinck et al., 2008; Venables et al., 2009). A highly curated database has identified a genome-wide selection of 1328 alternative splicing events from the mouse RefSeq database whose isoform sizes differ by between 10 and 450 nucleotides at a particular event. Spliced isoforms were characterized by end-point PCR in an automated fashion with the primers flanking the alternative splicing events, such that following amplification and analysis by microcapillary electrophoresis on Caliper LC-90 instruments (Caliper Life Sciences, Hopkinton, MA), the relative ratio of the isoforms can be calculated. A percent splicing index (PSI) was assigned to each exon depending on its inclusion/exclusion.

Electron Microscopy. Mice were anesthetised and perfused with ice-cold PBS followed by 2.5% glutaraldehyde in 0.1 M sodium cacodylate buffer. Tissues were dissected out and post-fixed with 1% aqueous OsO_4 (Mecalab) with 1.5% aqueous potassium ferrocyanide for 2 h. Tissues were embedded with Epon (Mecalab). Tissue sections were trimmed and cut at 90-100 nm sections with UltraCut E ultramicrotome (Reichert-Jung) and put onto a 200 mesh copper grid. (Electron Microscopy Sciences). Sections were then stained with uranyl acetate (Electron Microscopy Sciences) followed by Reynold's lead (Electron Microscopy Sciences). Images were captured using FEI Tecnai 12 120 kV transmission electron microscope (TEM) equipped with an AMT XR80C 8 megapixel CCD camera (McGill University, Anatomy and Cell Biology Department). A total of 2 mice per genotype were analyzed. The g-ratio measurements were calculated using ImageJ software. At least 100 axons per genotype were calculated.

Immunohistochemistry. Mice were anaesthetized with a cocktail mix (Ketamine-xylazine-acepromazine) and perfused with ice-cold PBS followed by 4% paraformaldehyde. Brains tissues were post-fixed in PFA for 3 days and then cryoprotected in 30% sucrose and embedded in OCT compound (Tissue-Tek, Markham, ON) over dry ice in ethanol. Tissues were cryostat sectioned at

a thickness of 10 μm and collected on Superfrost +/+ slides (Fisher, Ottawa, ON). Tissue sections were blocked in 10% normal goat serum in PBS with 0.3% Triton-X 100 for 1 h followed by primary antibody: Olig2, MBP, PDGFRα, CC1, QKI-5, QKI-6, and QKI-7 (Dilution at 1:200) incubation overnight at 4°C. Slides were then incubated with Alexa-fluor 488 or 546 immunoglobulin G (Invitrogen, Carlsbad, CA) at a dilution of 1:200 for 2 h at room temperature. Pictures were taken using Zeiss LSM Pascal Confocal Imaging System with identical settings for wild type and knockout antibody pairs. For staining of spinal cord and sciatic nerves, mice were sacrificed and the tissues were fixed in 4% PFA in 0.1 M phosphate buffer (PB) for 30 min. Spinal cords were then washed extensively with PB buffer and placed in 30% sucrose overnight. Teased sciatic nerves were washed with PB buffer and teased. Spinal cords were sectioned on cryostat at 20 um sections. Spinal cord sections and teased sciatic nerves were blocked and permeabilized using 0.1 M PB buffer, 10% normal goat serum, and 0.3% Triton X-100 for 1 hour followed by primary antibodies diluted in blocking buffer: Nfasc155, AnkG and caspr at 1/50 overnight at 4°C. Tissues were washed 3X 5 mins each in the blocking buffers. Secondary antibodies were diluted in blocking buffer at 1/200 and slides were stained for 1 hour. Pictures were taken using Zeiss AxioImager 2 upright microscope. Images were processed with Photoshop. The intensity histogram was adjusted on greyscale images from each individual channel and subsequently coloured images were merged. Brightness/contrast adjustments were then applied across the entire set of images and equally to controls. For fluromyelin staining, brain sections were blocked with 10% normal goat serum in PBS for 1 h at room temperature followed by 1 h fluoromyelin incubation in blocking solution (Life Technologies, dilution at 1:300). Images were acquired using AxioImager 2 upright microscope (Carl Zeiss).

Statistical Analysis. All data presented were produced in at least three independent experiments with the exceptions indicated in the Figure legends. Statistical analysis was performed using the Prism GraphPad software unless otherwise stated. Significance of differences was evaluated with either Student's *t*-test, when only two groups were compared (g ratio, axon diameter, nodal gap, and paranode-length), or with one-way ANOVA for more than two groups (RT-qPCR). One-way ANOVA was followed by Bonferroni's post hoc analysis. * $p < 0.05$, ** $p < 0.01$ and *** $p < 0.001$

2.6 Results

2.6.1 Ablation of qkI in oligodendrocytes of mice leads to severe ataxia and death at the third post-natal week.

Whole body ablation of *qkI* leads to embryonic lethality around E10 (Li et al., 2003), thus preventing the assessment of the role of QKI isoforms in mammalian myelination using a loss-of-function approach. We generated a conditional mouse knockout allele of *qkI* where exon 2 was flanked by loxP sites (Figure 2.1A, QKI^{FL}). Exon 2 encodes part of the KH RNA binding domain, common to all QKI isoforms and its deletion should generate a frame-shift resulting in a null allele. $QKI^{FL/FL}$ mice were generated and crossed with mice expressing Cre recombinase under the control of the *Olig2* promoter (Olig2-Cre), to induce recombination in the OL lineage from early developmental stages (Schuller et al., 2008). The deletion of exon 2 and the appearance of the 1 loxP allele was observed by genomic PCR using DNA extracted from the brain, but not other organs of $QKI^{FL/FL;Olig2\text{-}Cre}$ mice (Figure 2.1B, C). $QKI^{FL/FL;Olig2\text{-}Cre}$ mice were smaller in size (Figure 2.1D) and at post-natal day 10 (P10) displayed progressive neurological defects with tremors, seizures and severe ataxia followed by death by the third post-natal week (Figure 2.1E). In the brain, the QKI isoforms are expressed in the glial lineage with high abundance in OLs (Hardy et al., 1996). We observed that in P14 mice, the major QKI expressing cell was indeed the OL, since brains of $QKI^{FL/FL;Olig2\text{-}Cre}$ mice were essentially devoid of the QKI-5, QKI-6 and QKI-7 isoforms at this time point, as visualized by immunoblotting and RT-qPCR (Figure 2.2A, B). The loss of QKI isoform expression also led to a complete loss of the myelin basic proteins (MBPs), in brains of $QKI^{FL/FL;Olig2\text{-}Cre}$ mice, but not $QKI^{FL/FL;-}$ (wild type) or $QKI^{FL/+;Olig2\text{-}Cre}$ (heterozygous) mice (Figure 2.2A). We detected the expected 50% reduction in QKI mRNA and protein levels in heterozygous mice (Figure 2.2A, B), however, no overt phenotype was observed and normal levels of MBPs were expressed. Immunohistochemical analysis of P14 brain sections of $QKI^{FL/FL;Olig2\text{-}Cre}$ mice confirmed the loss of MBP as the staining revealed only the occasional MBP-positive (MBP^{+}) OL in the corpus callosum compared to the intense MBP staining in the $QKI^{FL/FL;-}$ mice (Figure 2.2C). Similarly, QKI^{+} OLs were abundant in the corpus callosum of $QKI^{FL/FL;-}$ mice, whereas this staining pattern was severely diminished in the brains of $QKI^{FL/FL;Olig2\text{-}Cre}$ mice (Figure 2.2C). These findings show that the loss of QKI in OLs leads to tremors and death by the third post-natal week.

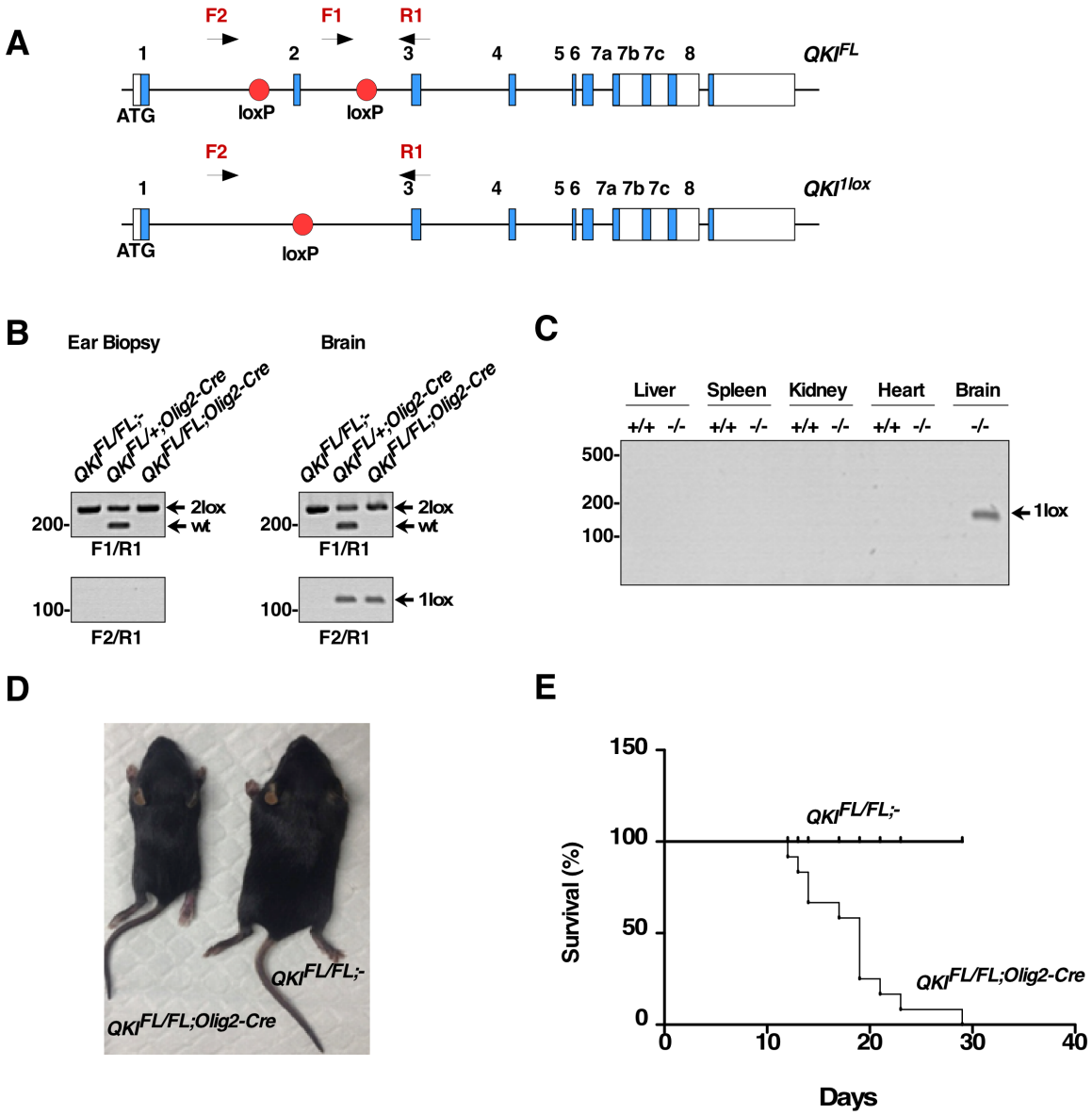

Figure 2.1. *QKI*$^{FL/FL;Olig2\text{-}Cre}$ mice display tremors and die at the third post-natal week.

(A) Schematic of the conditional construct engineered to target exon 2 of the *qkI* gene. *QKI*^{FL} depicts the insertion of the loxP sequences flanking exon 2 and *QKI*^{1lox} is the locus predicted after homologous recombination between the loxP sites. Primers F1/R1 are designed to detect the loxP site insertion. Primers F2/R1 are designed to detect the loss of exon 2 following recombination, and the generation of the 1 loxP site.

(B) PCR amplification of genomic DNA from ear biopsies and brains to detect the1lox band confirming Cre-mediated recombination.

(C) PCR from genomic DNA from the respective tissues showing that the 1lox PCR band is only detected in $QKI^{FL/FL;Olig2\text{-}Cre}$ brains.

(D) Photographs of $QKI^{FL/FL;-}$ and $QKI^{FL/FL;Olig2\text{-}Cre}$ mice at P14.

(E) Kaplan-Meier survival plot of $QKI^{FL/FL;-}$ (n=12) and $QKI^{FL/FL;Olig2\text{-}Cre}$ (n=12) mice. The statistical significance for survival was assessed by log-rank ($p < 0.0001$).

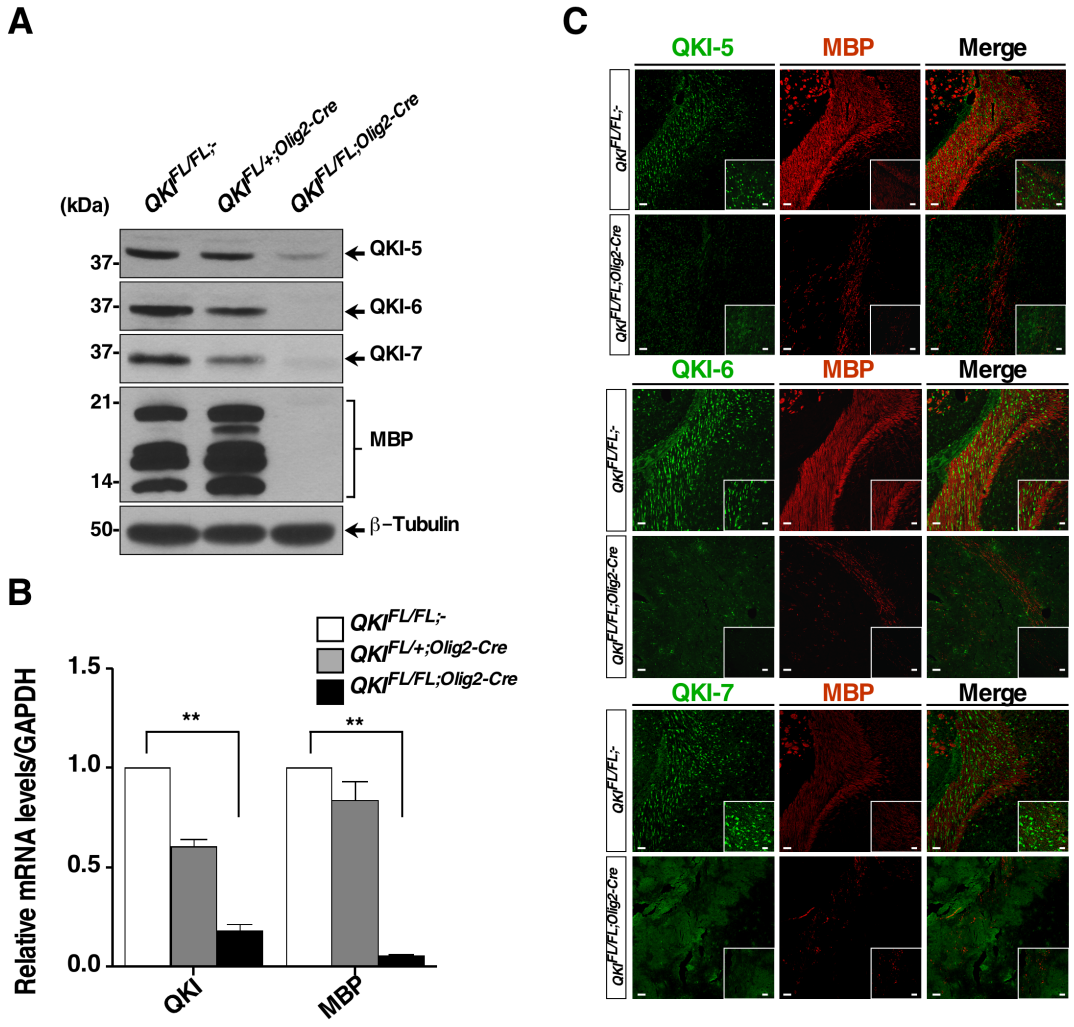

Figure 2.2. Recombination in *QKI*$^{FL/FL;Olig2\text{-}Cre}$ mice leads to loss of QKI proteins expression in OLs.

(A) Total brain lysates from P14 wild type (*QKI*$^{FL/FL;-}$), heterozygotes (*QKI*$^{FL/+;Olig2\text{-}Cre}$) and knockout (*QKI*$^{FL/FL;Olig2\text{-}Cre}$) mice were immunoblotted with anti-QKI-5, -6, -7, -MBP and -β-tubulin antibodies. Molecular mass markers are shown on the left in kDa. **(B)** RT-qPCR analysis for *QKI* and *MBP* mRNAs in P14 whole brains for the indicated genotypes (n=3 per genotype). The results are represented in terms of fold change after normalizing the mRNA levels to *GAPDH* mRNA. Each value represents the mean ± SEM. ** denotes $p < 0.01$. **(C)** Representative images of coronal sections of P14 brains of wild type (*QKI*$^{FL/FL;-}$) and knockout *QKI*$^{FL/FL;Olig2\text{-}Cre}$ mice stained with anti-QKI-5, -QKI-6, -QKI-7 and anti-MBP antibodies (n > 3). The area shown is the corpus callosum. Scale bar = 50μm. Inset denotes higher magnification (Scale bar = 25μm).

2.6.2 Hypomyelination in the CNS of QKI$^{FL/FL;Olig2\text{-}Cre}$ mice

The brains of the *QKI*$^{FL/FL;Olig2\text{-}Cre}$ mice were smaller, however, the gross anatomy appeared normal. The severe reduction in MBP staining in the brains of *QKI*$^{FL/FL;Olig2\text{-}Cre}$ mice implied a defect in central nervous system (CNS) myelination. To examine this in detail, coronal brain sections were stained with fluoromyelin. A complete loss of myelin in the brains of *QKI*$^{FL/FL;Olig2\text{-}Cre}$ was visualized in comparison to *QKI*$^{FL/FL;-}$ mice (Figure 2.3A, B). We also confirmed the absence of myelin by electron microscopy in the CNS using cross-sections of P14 optic nerves and spinal cords from *QKI*$^{FL/FL;Olig2\text{-}Cre}$ mice (Figure 2.3C-F). There were normal levels of myelin lamellae in wild type *QKI*$^{FL/FL;-}$ mice with a *g*-ratio of ~0.7, while a *g*-ratio of ~1.0 was observed in the optic nerve and spinal cord of *QKI*$^{FL/FL;Olig2\text{-}Cre}$ mice, confirming the absence of myelin lamellae (Figure 2.3G, H). We noticed that axons in the optic nerves of *QKI*$^{FL/FL;Olig2\text{-}Cre}$ mice had a small diameter (Figure 2.3C, D), while in the spinal cords certain axons were larger and displayed axonal swelling (Figure 2.3E, F), as often observed in the absence of myelin (Rosenfeld and Friedrich, 1986). These data show that the lack of QKI in developing OLs leads to hypomyelination.

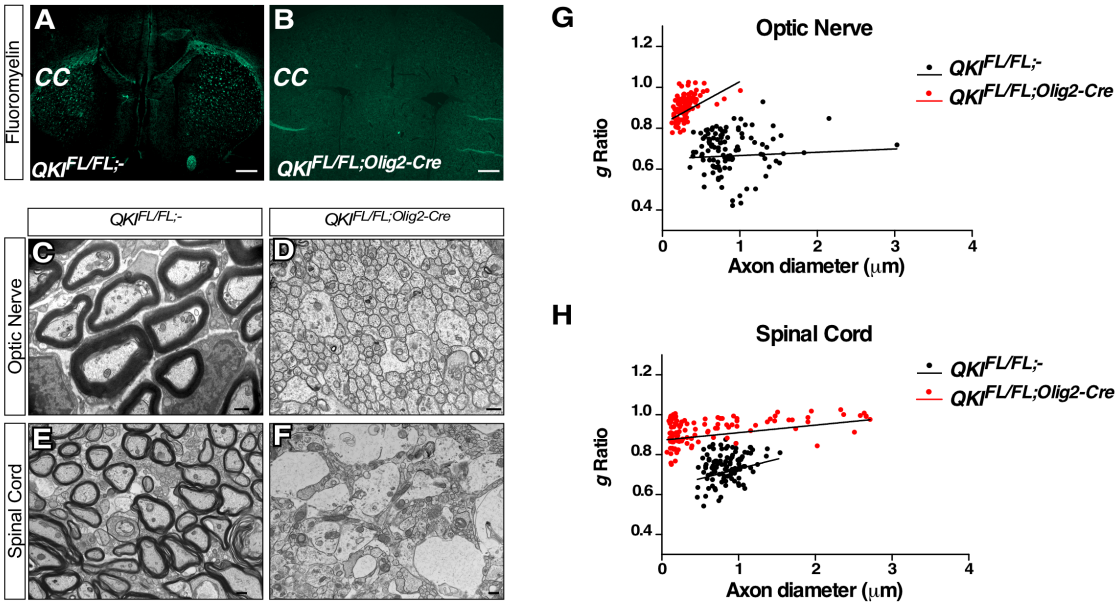

Figure 2.3. Ablation of QKI in oligodendrocytes leads to hypomyelination.

(A-B) Representative images of coronal sections from brains of *QKI*$^{FL/FL;-}$ and *QKI*$^{FL/FL;Olig2\text{-}Cre}$ mice stained with fluoromyelin. CC denotes the corpus callosum. Scale bar = 500μm.

(C-D) Representative cross-section electron micrograph images of optic nerves from (n=2/ genotype) P14 $QKI^{FL/FL;-}$ and $QKI^{FL/FL;Olig2\text{-}Cre}$ mice. Scale bar =500nm.

(E-F) Representative cross-section electron micrograph images of spinal cords from (n=2/ genotype) P14 $QKI^{FL/FL;-}$ and $QKI^{FL/FL;Olig2\text{-}Cre}$ mice. Scale bar =500nm.

(G) A scatter plot of the *g* ratio determined from electron micrographs of cross-sections of P14 optic nerves from $QKI^{FL/FL;-}$ and $QKI^{FL/FL;Olig2\text{-}Cre}$ mice for n=108 axons. (*g* ratio: $p < 0.0001$, axon diameter: $p < 0.0001$).

(H) A scatter plot of the *g* ratio determined from electron micrographs of cross-sections of P14 spinal cords from $QKI^{FL/FL;-}$ and $QKI^{FL/FL;Olig2\text{-}Cre}$ mice for n=108 axons. (*g* ratio: $p < 0.0001$, axon diameter: $p < 0.05$).

2.6.3 Oligodendrocyte differentiation defects in QKI$^{FL/FL;Olig2\text{-}Cre}$ mice

To assess whether the lack of MBP in the brain of *QKI*$^{FL/FL;Olig2\text{-}Cre}$ mice was due to either a defect in differentiation of oligodendrocyte precursor cells (OPCs) or a complete absence of the OL population, we evaluated the various stages of OL maturation by immunofluorescence. Brain immunostaining for the pan-OL marker Olig2 showed a slight reduction in Olig2$^+$ cells in the corpus callosum of *QKI*$^{FL/FL;Olig2\text{-}Cre}$ mice (Figure 2.4A, D). OPCs positive for PDGFRα appeared unaffected by the loss of QKI in OLs (Figure 2.4B, D). However, CC1$^+$ cells were absent in the brains of *QKI*$^{FL/FL;Olig2\text{-}Cre}$ mice, which is a marker for post-mitotic mature OLs (Figure 2.4C, D). In the *QKI*$^{FL/FL;Olig2\text{-}Cre}$ mice, the protein levels of glial fibrillary acidic protein (GFAP), an astrocyte marker, and neurofilament light polypeptide (Nefl) as well as neuronal nuclei (NeuN), known neuronal markers, were comparable between genotypes as confirmed by immunoblotting (Figure 2.4E). These findings show that the loss of QKI prevents OL maturation with minimal to no effect on the neuronal and astrocytic populations in the brain.

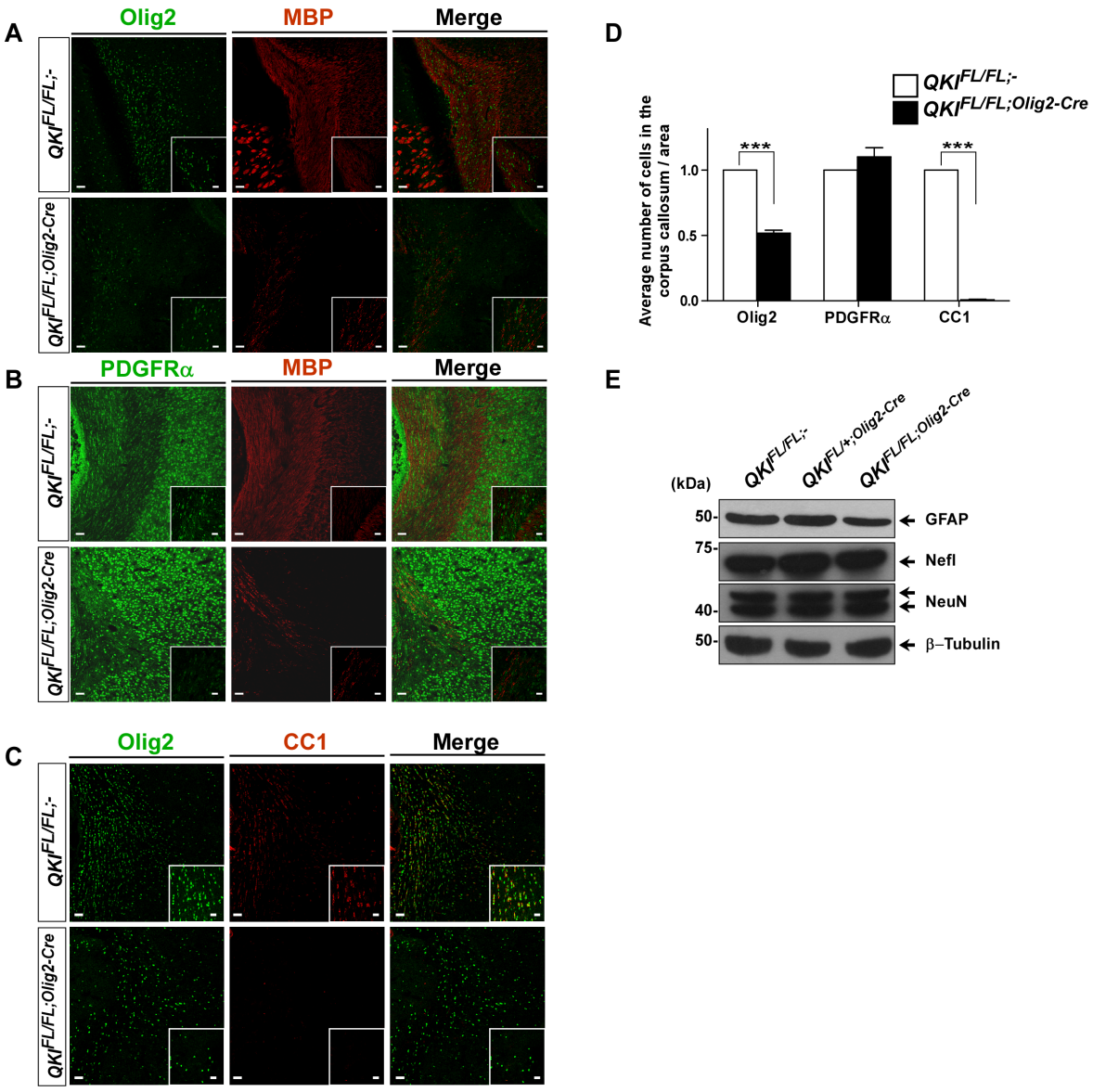

Figure 2.4. Ablation of QKI in oligodendrocytes leads to loss of mature oligodendrocytes.

(A) Representative images of coronal sections of P14 brains of wild type ($QKI^{FL/FL;-}$) and knockout $QKI^{FL/FL;Olig2\text{-}Cre}$ mice stained with anti-Olig2 and anti-MBP antibodies (n > 3). The area shown is the corpus callosum. Scale bar = 50μm. Inset denotes higher magnification (Scale bar = 25μm).

(B) Representative images of coronal sections of P14 brains of wild type ($QKI^{FL/FL;-}$) and knockout $QKI^{FL/FL;Olig2\text{-}Cre}$ mice stained with anti-PDGFRα and anti-MBP antibodies (n > 3). The area shown is the corpus callosum. Scale bar = 50μm. Inset denotes higher magnification (Scale bar = 25μm).

(C) Representative images of coronal sections of P14 brains of wild type ($QKI^{FL/FL;-}$) and knockout $QKI^{FL/FL;Olig2\text{-}Cre}$ mice stained with anti-Olig2 and anti-CC1 antibodies (n > 3). The area shown is the corpus callosum. Scale bar = 50μm. Inset denotes higher magnification (Scale bar = 25μm). **(D)** Total number of $Olig2^{+}$, $PDGRF\alpha^{+}$ and $CC1^{+}$ cells in the corpus callosum in $QKI^{FL/FL;-}$ and $QKI^{FL/FL;Olig2\text{-}Cre}$. Data are shown as mean ± SEM. (n = 3 brains for each phenotype, $^{***}P < 0.001$). (**E**) Total brain lysates from P14 wild type ($QKI^{FL/FL;-}$), heterozygotes ($QKI^{FL/+;Olig2\text{-}Cre}$) and knockout ($QKI^{FL/FL;Olig2\text{-}Cre}$) mice were immunoblotted with anti-GFAP, -Nefl, -NeuN and –β-tubulin antibodies. Molecular mass markers are shown on the left in kDa.

2.6.4 Alternative splicing defects in QKI$^{FL/FL;Olig2\text{-}Cre}$ brains

We used brain RNA from P14 wild type and *QKI*$^{FL/FL;Olig2\text{-}Cre}$ mice to identify alternative splicing defects using LISA (*Layered and Integrated system for Splicing Annotation*), a high-throughput RT-PCR RNomics platform based annotation of alternative splicing events (Venables et al., 2009). We performed the initial screen termed the "detection screen" using primers targeting 1328 characterized alternative splice events and the percent splice index (PSI) was calculated for each event. From this list, 96 alternatively spliced events (ASEs) (with a ΔPSI of at least 0.10) were selected for the "validation screen" and n=3 mice per genotype were used and their PSI values were calculated. This screen yielded 31 ASEs that were significantly altered with the loss of QKI (Table 2.1). We searched for neighboring QKI response elements (QREs; *ACUAAY-N$_{20}$-UAAY*) (Galarneau and Richard, 2005) adjacent to the alternatively spliced exons and we identified at least one QRE near each splice event, suggesting that these splicing events are directly regulated by QKI (Table 1). The alternative splicing of MAG, PLP and Sirt2 were previously shown to be deregulated in *qk*^{v} mice and served as positive controls (Wu et al., 2002, Zhu et al., 2012, Mandler et al., 2014). We identified new splicing events of myelin components regulated by QKI including *Nfasc*, *MBP, MOBP*, *Mpzl1* and *Magi1* (Table 2.1).

Table 2.1: Top alternatively spliced events identified using LISA in *QKI*$^{FL/FL:Olig2\text{-}Cre}$ mice. The top identified genes in LISA screen that exhibit deregulated alternative splicing attributable to loss of QKI expression in *QKI*$^{FL/FL;Olig2–Cre}$ mice.

Gene	Exon Number	PSI[a] WT	PSI KO	Δ PSI	|Δ PSI|	QRE[b]	WT vs KO p-value
Nfasc	2	0.233	0.945	0.712	0.712	GCTAACCCACTGGAactaac	5.412E-8
Nfasc	17	0.193	0.974	0.781	0.781	TCTAACCCTGATAACCTGCTAAC	1.407E-6
Magi1	15	0.890	0.517	-0.373	0.373	ACGAATAAACTCTCTTTGCCCTATGTTAAC, CCTAACTAGTTGCAGTAAT	2.775E-5
Prom1	4	0.280	0.811	0.531	0.531	GTCTTAGGTCAAT	7.690E-5
Lhfpl3	5	0.225	0.729	0.504	0.504	ACTAACACATGAAAC	1.627E-4
Mpzl1	5, 6	0.270	0.099	-0.171	0.171	ACTAACATTTACTAAAAAC, CCTAACATATGTCTGTAAT	2.064E-4
Cadm1	9	0.684	0.323	-0.361	0.361	AGGAAGAACTTTTAACATCTGA	2.456E-4
Bin1	7,8	0.642	0.884	0.242	0.242	ACTAACCTGCTCCGAAAT, ACAAACCCTCTCTTTGTAAT	2.772E-4
Vldlr	16	0.179	0.011	-0.168	0.186	ACTAACTGCCGCTTAAATAAT	6.189E-4
Plp1	3	0.502	0.012	-0.490	0.490	CAATAACAAGGGGTGGGGGACAATT	6.791E-4
Phka1	19	0.613	0.896	0.283	0.283	TCTAACTCTCAATCTGTGAGGTTGTATAAT, ACTGATTATTTTAAAAATTATTTAAT	7.481E-4
Mbp	2	0.964	0.409	-0.555	0.555	CAACAAAGAAGAAATTTCTAA	9.313E-4
Ctnnd1	18	0.834	0.678	-0.156	0.156	TCTAATGTTGCAGAATAGTGTTTAAT	1.005E-3
Pcdh15	4	0.589	0.897	0.308	0.308	ACTACTAAATAGTTCTATGCTAAT	2.111E-3
Mon2	29	0.746	0.858	0.112	0.112	CCTAACCCTGTCCTAAT	2.331E-3
Nfasc	8	0.418	0.007	-0.411	0.411	CCTAATCCACTTTGTCTAAC	2.606E-3
Bnip2	10	0.392	0.127	-0.265	0.265	CAATAACTCTTCCCTACC	2.613E-3
Myo9b	37	0.746	0.836	0.090	0.090	ACTAACCTAGAGCTGCTGGTT	4.063E-3
Smarcb1	2	0.717	0.788	0.071	0.071	CCTAACACTAAG	5.568E-3
Neo1	20	0.559	0.666	0.107	0.107	ACTGACTCACCAGATTCAAGAGTTAAC	6.321E-3

Nfasc	20,21	0.197	0.000	-0.197	0.197	TAACCACCTTCTTGCTAAC, CACTAACCACTAAC	6.660E-3
Mobp	4	0.975	0.885	-0.090	0.090	ACTAACATGGGGGATCTGTCCACAGTACC AAGCCTGTGTAAT, CAATCCATAGGACTGGAAGTCACTAAT	8.288E-3
Grm5	8	0.656	0.470	-0.186	0.186	ACTAAATAAATCTTTTCTGGTTAAT	9.840E-3
Pdlim5	5	0.234	0.127	-0.107	0.107	CAACTCATTGTTTTTCTTGAAGACATATTT GAGCTGCTAAC	1.082E-2
Nhsl1	5	0.048	0.448	0.400	0.400	ACTAACCTCATGTGGTGCTGTCAAAT	1.500E-2
Sirt2	2	0.111	0.248	0.137	0.137	ACTACCATCCCTGACTCTGAAATAAT	1.919E-2
Tnk2	12	0.850	0.715	-0.135	0.135	CTAAACCCTTCCCTCTGTGATCT	2.143E-2
Grik1	15	0.219	0.317	0.097	0.097	CAATTTGCTCTTGGGGTGTCTTGTTTTATG CTACTAAT	3.439E-2
Sytl2	10	0.611	0.719	0.108	0.108	GCTAATGAACTAATCCATTAAT,TCTAATG GTTGTGGATAAT	4.256E-2
Musk	13	0.353	0.105	-0.248	0.248	CCTAATGCTCTCCTAAT, ATTAATGCTACACTTTATACATAGATAAC	4.380E-2
Oxr1	11	0.700	0.607	-0.093	0.093	AGTAACTTTAAT	4.733E-2

2.6.5 QKI regulates alternative splicing of Neurofascin pre-mRNA

Neurofascin (Nfasc) was identified as a top hit with multiple exons showing splicing deregulation in $QKI^{FL/FL;Olig2\text{-}Cre}$ mice (Table 2.1). Alternative splicing of *Nfasc* produces cell adhesion proteins termed NFasc155 and NFasc186, which are the major isoforms (Sherman and Brophy, 2005). The regulation of *Nfasc* alterative splicing is unknown. Nfasc155 is OL-specific and exons 21/22 encode a fibronectin III-like domain unique to this isoform (Collinson et al., 1998), while exon17 is unique to neuronal Nfasc186 (Collinson et al., 1998). In $QKI^{FL/FL;Olig2\text{-}Cre}$ mice, we observed a lack of *Nfasc* exons 21/22 inclusion, and an increase in exon 17, as well as deregulation of exons 2 and 8 (Table 2.1). We confirmed the exclusion of *Nfasc* exons 21/22 and the inclusion of exon17 by RT-PCR in the brains of $QKI^{FL/FL;Olig2\text{-}Cre}$ mice using primers flanking these exons (Figure 2.5A). These findings were also confirmed by RT-qPCR (Figure 2.5B), while the overall *Nfasc* transcript levels were unaffected (Figure 2.5B). Nfasc155 protein was absent, while Nfasc186 remained unchanged, by immunoblotting whole brain lysates (Figure 2.5C). The loss of Nfasc155 did not lead to reduced expression of the voltage gated sodium channel (Na_v) nor Caspr (Figure 2.5C), consistent with previous findings of $Nfasc155^{-/-}$ mice in OLs (Pillai et al., 2009).

We analyzed the genomic sequence surrounding exons 21/22 of *Nfasc155* for the presence of QREs. Two putative QREs were identified in intron 21 that could be responsible for the alternative splicing of the exons 21/22. QRE1 (UAAC-N_9-GCUAAC) deviates by a single mismatch (underlined) from the consensus QRE, while QRE2 is a perfect binding site. To examine whether these QREs are indeed functional, biotinylated RNAs harbouring wild type and mutated binding sequences were synthesized for each *Nfasc* QRE. RNA pull-down assays were performed with brain cell lysates from wild type mice and the enrichment of QKI-5 was observed by immunoblotting in the presence of increasing concentrations of sodium chloride. Both QRE1 and QRE2 affinity purified QKI-5, although QRE2 bound with a higher relative affinity. Mutations within the sequences prevented binding (Figure 2.5D). To show that QKI isoforms regulate *Nfasc* alternative splicing via these QREs, we next generated a minigene with a *Nfasc* genomic fragment spanning the exons 21/22 cassette (Figure 2.5E). The minigene was co-transfected in HEK293T cells with expression vectors encoding QKI-5, -6, -7 or an RNA binding defective version of QKI-5 (QKI-5:V157E). QKI-5 expression led to inclusion of exons 21/22, however little to no inclusion was observed with QKI-6, QKI-7 nor the RNA binding defective version of QKI-5 (QKI-5:V157E) (Figure 2.5E). The overexpression of the QKI-6 isoform led to a slight inclusion of exons 21/22

which could be explained by the endogenous expression of QKI-5 in HEK293T cells which could dimerize with QKI-6 and lead to inclusion of these exons (Figure 2.5E). Mutation of QRE2, but not QRE1, prevented this inclusion, suggesting that QRE2 is the major binding site utilized by QKI-5. Equivalent QKI protein expression was confirmed by immunoblotting (Figure 2.5F). These observations demonstrate that *Nfasc* is a direct alternative splicing target of QKI.

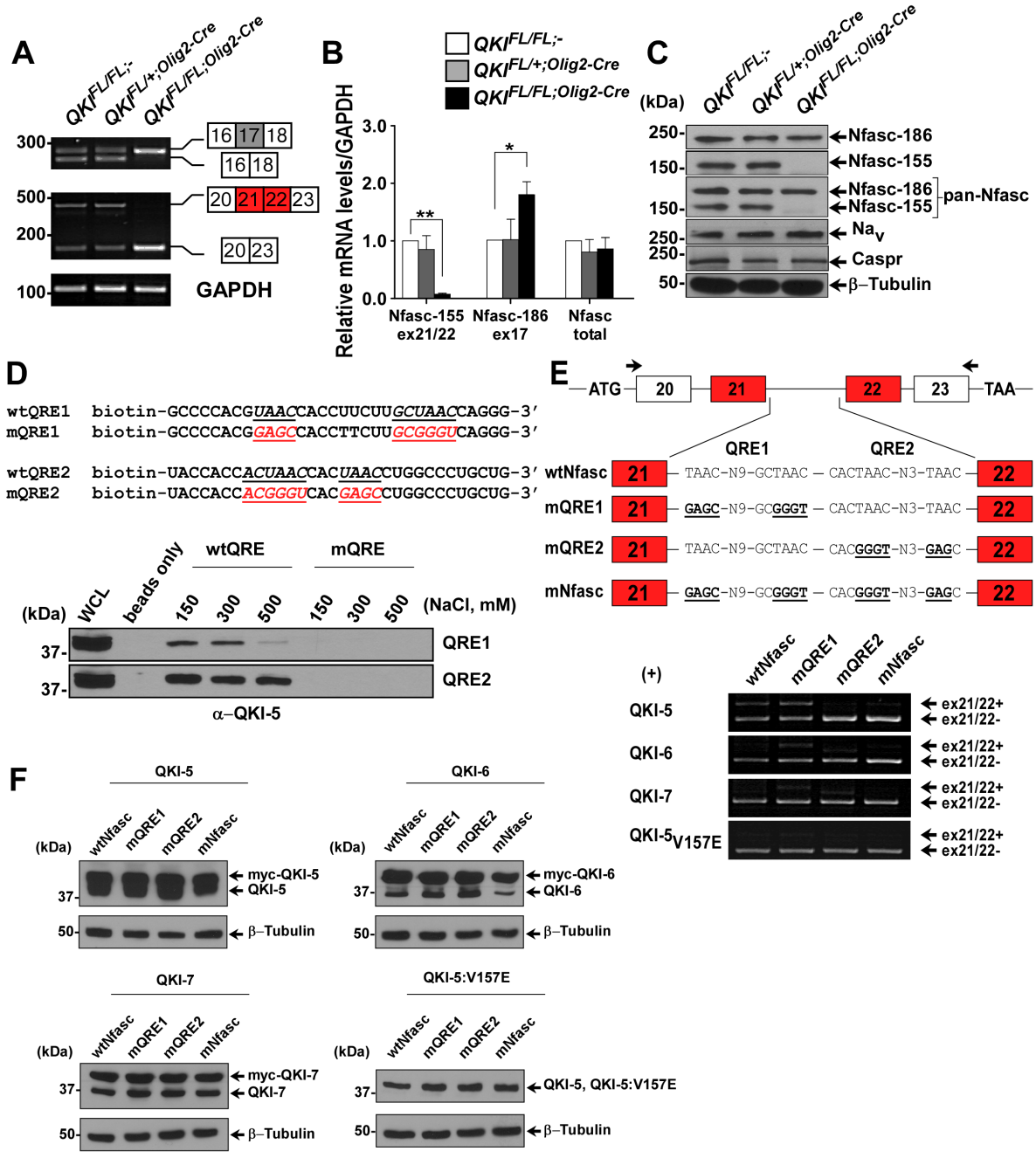

Figure 2.5. QKI regulates alternative splicing of *Nfasc* pre-mRNA.

(A) RT-PCR analysis from P14 mice brains with the indicated primers flanking exon 17 (inclusion denotes Nfasc186) and exons 21,22 (inclusion denotes Nfasc155).

(B) RT-qPCR using primers spanning the exon-exon junction for ex17 of Nfasc186, exons 21/22 of Nfasc155 and primers that detect the total mRNA of Nfasc. The results are represented in terms of fold change after normalizing the mRNA levels to *GAPDH* mRNA from n= 3. Each value represents the mean ± SEM. * denotes $p < 0.05$. ** denotes $p < 0.01$.

(C) Western blot analysis of total brain lysates immunoblotted with anti-Nfasc155, -Nfasc186, -pan-Nfasc, -Na_v, -caspr and anti-β-tubulin. Molecular mass markers are shown on the left in kDa.

(D) Immunoblot analysis of RNA-pull down assay from brains of wild type P14 mice using biotinylated RNA harbouring either wild type or mutated QREs (mutated sequences indicated) using QKI-5 antibody. Increasing salt concentrations were used to compete with the binding.

(E) Schematics of the genomic DNA region used to generate the *Nfasc155* minigene, the location of the primer set used for RT-PCR are marked by arrows. Wild type sequences as well as sequences harbouring mutant QRE1, QRE2 or both are shown. HEK293T cells were transfected with the *Nfasc* minigene plasmid and either expression vectors for -QKI-5, -QKI-6, -QKI-7, or -QKI-5:V157E. Total RNA was isolated 48h later and analyzed by RT-PCR.

(F) Protein expression of transfected plasmids in HEK293T cells is determined by immunoblotting using the indicated antibodies. Myc-tagged QKI proteins migrate higher than endogenous QKI isoforms.

2.6.6 Loss of QKI in the CNS and PNS of adult mice leads to paralysis

We subsequently investigated the role of QKI proteins in myelin maintenance in adult mice using the 4-hydroxytamoxifen (OHT) inducible-Cre line (*PLP-CreERT,* (Doerflinger et al., 2003)). Eight-week old $QKI^{FL/FL;PLP\text{-}CreERT}$ mice and age-matched wild type littermates were injected with OHT for 5 consecutive days. The presence of the *qkI* 1lox band was readily detected in brains of $QKI^{FL/FL;PLP\text{-}CreERT}$ mice, as early as 5 days post-OHT treatment (Figure 2.6A). $QKI^{FL/FL;PLP\text{-}CreERT}$ mice progressively developed hindlimb paralysis with visible thoracic kyphosis at ~post-OHT injection day 20 (Figure 2.6B, C). Numerous $QKI^{FL/FL;PLP\text{-}CreERT}$ mice reached a clinical endpoint of accelerated breathing and immobility around 30 days post-OHT necessitating sacrifice. As early as post-OHT day 15, the mice also displayed a characteristic shaking phenotype when held by the tail. These findings show that deletion of QKI in myelinating glia of adult mice results in paralysis and immobility.

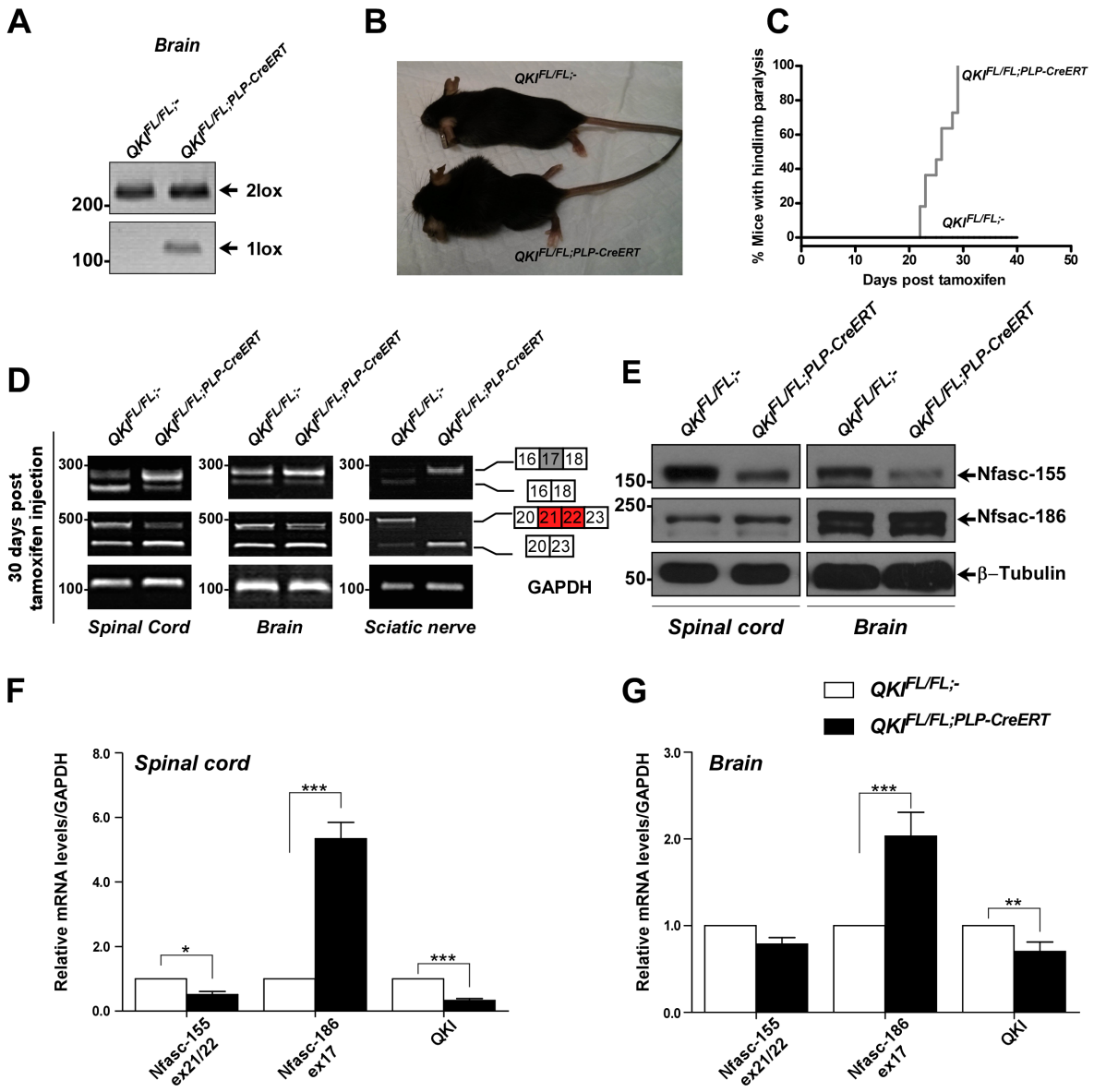

Figure 2.6. *QKI*$^{FL/FL;\ PLP\text{-}CreERT}$ mice display *Nfasc* pre-mRNA splicing defects.

(A) PCR amplification of genomic DNA from brains of eight-week old wild type and *QKI*$^{FL/FL;PLP\text{-}CreERT}$ mice injected with OHT for 5 consecutive days to confirm the Cre-mediated recombination and the presence of a 1lox band. Mice were sacrificed and brains collected at 30 days post OHT injection.

(B) Photographs of *QKI*$^{FL/FL;-}$ and *QKI*$^{FL/FL;PLP\text{-}CreERT}$ mice 30 days post-OHT injection.

(C) Kaplan-Meier plot of onset of paralysis in *QKI*$^{FL/FL;-}$ (n=11) and *QKI*$^{FL/FL;PLP\text{-}CreERT}$ (n=11) mice. The statistical significance was assessed by log-rank ($p < 0.0001$).

(D) RT-PCR analysis of spinal cords, brains, and sciatic nerves from wild type and $QKI^{FL/FL;PLP\text{-}CreERT}$ mice injected with OHT at 30 days post-injection using primers flanking exon 17 (inclusion denotes Nfasc186) or exons 21,22 (inclusion denotes Nfasc155).

(E) Immunoblot analysis of lysates obtained from spinal cord and brain samples of eight-week old wild type and $QKI^{FL/FL;PLP\text{-}CreERT}$ mice injected with OHT for 5 consecutive days and harvested at 30 days post OHT injection. Blots were against anti-Nfasc-155, -Nfasc-186 and –β-tubulin.

(F) RT-qPCR analysis from spinal cord samples (n=4) of eight-week old wild type and $QKI^{FL/FL;PLP\text{-}CreERT}$ mice injected with OHT for 5 consecutive days and collected at 30 days post OHT injection. Primers were specific for *qkI*, *Nfasc155 ex21/22, and Nfasc186 ex17* mRNAs. The results are represented in terms of the mean of the fold change after normalizing the mRNA levels to *GAPDH* mRNA ± SEM. * denotes $p < 0.05$. *** denotes $p < 0.001$.

(G) RT-qPCR analysis from brain samples (n=4) of eight-week old wild type and $QKI^{FL/FL;PLP\text{-}CreERT}$ mice injected with OHT for 5 consecutive days and collected 30 days post OHT injection. Primers were specific for *qkI*, *Nfasc155 ex21/22, and Nfasc186 ex17* mRNAs. The results are represented in terms of the mean of the fold change after normalizing the mRNA levels to *GAPDH* mRNA ± SEM. ** denotes $p < 0.01$. *** denotes $p < 0.001$.

2.6.7 QKI regulates Nfasc pre-mRNA alternative splicing in mature OLs

We next examined whether the loss of QKI in mature OLs could affect the Nfasc155 isoform expression. Indeed, we observed exclusion of Nfasc155 exons 21/22 in $QKI^{FL/FL;PLP\text{-}CreERT}$ mice, as early as 5 days post-OHT injection in the brains, spinal cords and sciatic nerves with a concomitant inclusion of exon 17 (data not shown) and persisting at 30 days post-OHT injection as shown by RT-PCR (Figure 2.6D) and RT-qPCR (Figure 2.6F, G). The exclusion of exons 21/22 was paralleled with an appreciable reduction in Nfasc155 protein observed at 30 days post-OHT injection with no visible increase in Nfasc186 (Figure 2.6E). We next isolated primary OL precursor (OPC) cells from P1 $QKI^{FL/+;-}$ and $QKI^{FL/FL;PLP\text{-}CreERT}$ mice and induced them to differentiate for 4 days prior to treating them with increasing concentrations of OHT. Genomic PCR confirmed recombination between the loxP sites in OLs with the generation of the 1lox allele (Figure 2.7A, B, upper panels). The exclusion of exons 21/22 and the inclusion of exon 17 was observed in differentiated cultures treated with OHT of $QKI^{FL/FL;PLP\text{-}CreERT}$ OLs, as compared with $QKI^{FL/+;-}$ OLs using RT-PCR (Figure 2.7A, B, bottom panels) and RT-qPCR (diff, Figure 2.7C), while no change was observed in undifferentiated cultures without OHT treatment (Figure 2.7A, C).

We investigated whether we could observe these *Nfasc* alternative splicing defects in primary rat OLs using fluorescently labelled (GLO) siRNAs targeting QKI. The transfection efficiency was >50% (data not shown). An increase in exons 21/22 exclusion (Figure 2.7D; ex20/23 fragment) and the inclusion of exon 17 was indeed observed (Figure 2.7D; ex16/17/18 fragment) even with the lowest siQKI-GLO concentration, while a decrease in the complementary isoforms was difficult to observe due to their elevated abundance upon inducing differentiation (Figure 2.7D). A significant decrease in Nfasc155 protein levels was observed with increasing concentrations of siQKI-GLO, however, we were unable to detect the appearance of Nfasc186 in the primary rat OLs (Figure 2.7E). We confirmed that the siQKI reduced the expression of the QKI isoforms and this was evident at 40 nM, as assessed by immunoblotting (Figure 2.7F). Taken together, our findings show that QKI regulates *Nfasc* alternative splicing to maintain Nfasc155 expression in mature OLs.

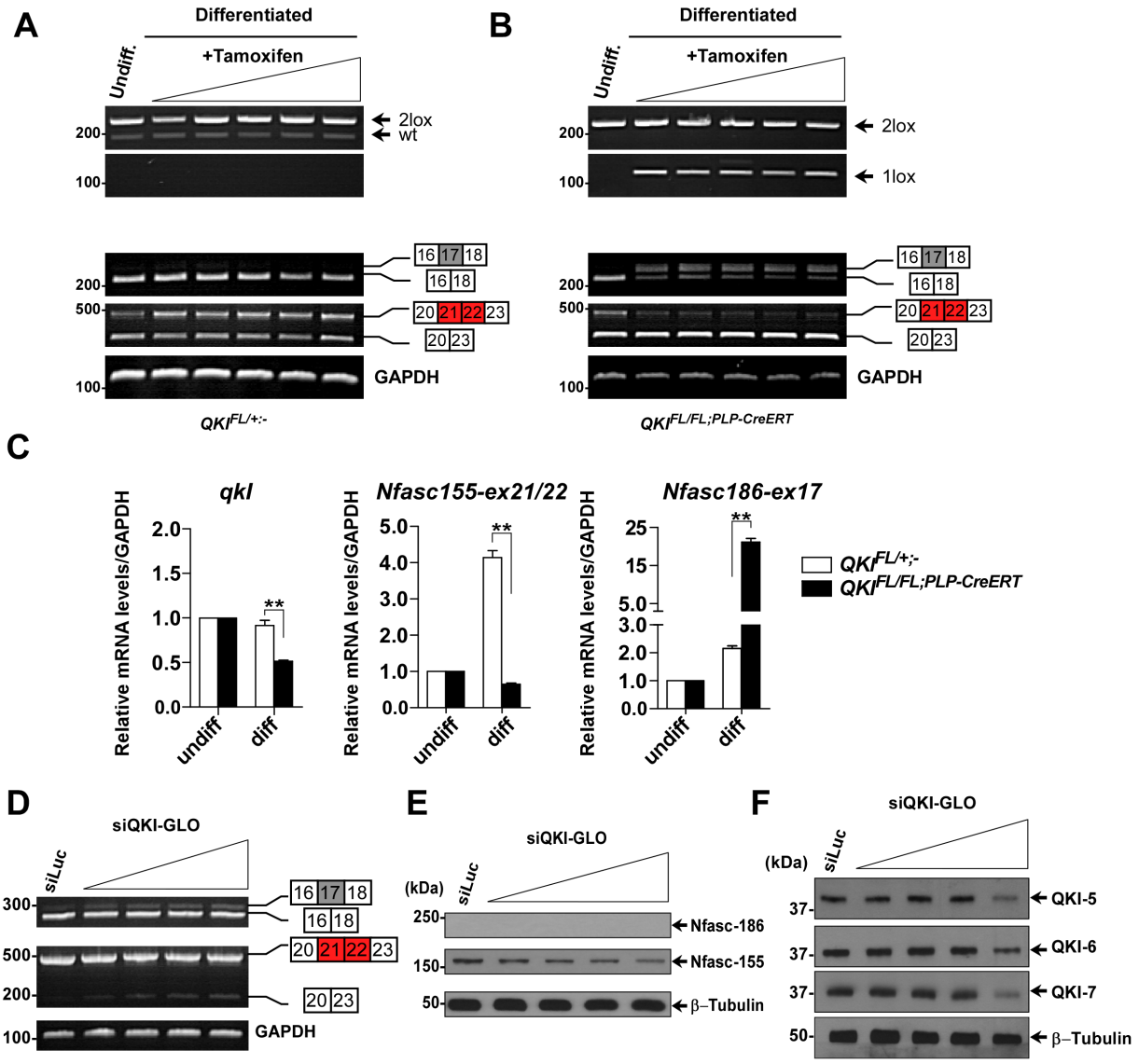

Figure 2.7. Loss of QKI in differentiated primary mouse and rat oligodendrocytes leads to defects in *Nfasc* pre-mRNA splicing.

(A-B) (Top panel) PCR amplification of genomic DNA from primary mouse OPCs isolated from wild type and *QKI*$^{FL/FL;PLP\text{-}CreERT}$ mice. Cultures were induced to differentiate for 4 days prior to OHT treatment with increasing concentrations (50, 100, 150, 200 and 250nM) for 5 days to confirm the Cre-mediated recombination. The presence of a 1lox band indicates recombination between LoxP sites. (Bottom panel) RT-PCR analysis from wild type and *QKI*$^{FL/FL;PLP\text{-}CreERT}$ differentiated cultures after 5 days treatment with OHT using primers flanking exon 17 (inclusion denotes Nfasc186) or exons 21,22 (inclusion denotes Nfasc155).

(C) RT-qPCR analysis for wild type and $QKI^{FL/FL;PLP\text{-}CreERT}$ differentiated cultures after treatment with OHT using primers for *QKI* mRNA, and Nfasc155 exons 21/22 and Nfasc186 exon 17. Cultures were isolated from pooled $QKI^{FL/+}$ (n=5) or $QKI^{FL/FL;PLP\text{-}CreERT}$ (n=5) P1 mice. The results are represented as the average fold change obtained from the individual treatment after normalizing the mRNA levels to *GAPDH* mRNA. Each value represents the mean ± SEM. * denotes $p < 0.05$. ** denotes $p < 0.01$.

(D) RT-PCR from differentiated rat OPCs transfected with either siLuc-GLO or increasing concentrations of siQKI-GLO using primers for exon 17 (Nfasc186-specific) and exons 21/22 (Nfasc155-specific). GAPDH is used as a control.

(E) Immunoblot analysis from undifferentiated and differentiated rat OPCs for 4 days and then transfected with increasing concentrations of siQKI-GLO (5nM, 10nM, 20nM and 40nM) blotted using anti-Nfasc186, -Nfasc155 and –β-tubulin.

(F) Immunoblot analysis from differentiated rat OPCs for 4 days and then transfected with increasing concentrations of siQKI-GLO (5nM, 10nM, 20nM and 40nM) blotted using anti-QKI-5,-QKI-6, -QKI-7, and –β-tubulin.

2.6.8 Paranodal defects in QKI$^{FL/FL;Olig2\text{-}Cre}$ and QKI$^{FL/FL;PLP\text{-}CreERT}$ mice

We next sought to assess the integrity of the nodes of Ranvier and the paranodes using immunofluorescence and electron microscopy. Ultrastructure analysis of optic nerves and spinal cords showed that wild type mice had properly formed and spaced paranodal loops (Figure 2.8A, C). While in *QKI$^{FL/FL;Olig2\text{-}Cre}$* mice, the optic nerves were translucent, a sign of hypomyelination (not shown) and paranodal loops were difficult to observe being large with little periodicity (Figure 2.8B, D).

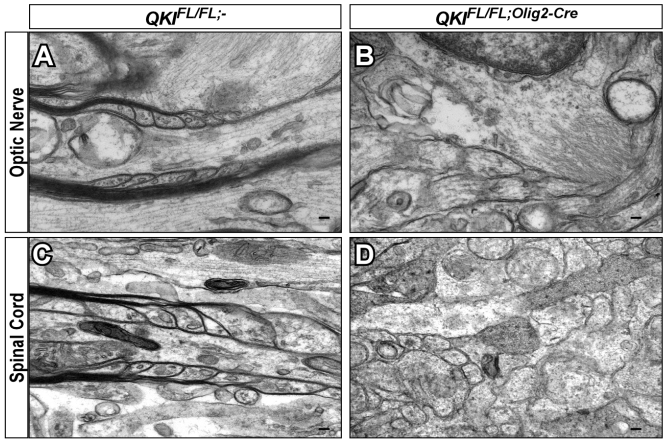

Figure 2.8. Ultrastructural paranodal defect in *QKI$^{FL/FL;Olig2\text{-}Cre}$* mice.

(A-D) Representative electron micrograph images of longitudinal sections of optic nerves and spinal cords (n=2/genotype) from wild type *QKI$^{FL/FL;-}$* and *QKI$^{FL/FL;Olig2\text{-}Cre}$* mice. Scale bar=100nm.

Next, using spinal cords and sciatic nerves from adult $QKI^{FL/FL;PLP\text{-}CreERT}$ mice, we could assess the role of the QKI proteins in axoglial junction maintenance. In wild type mice, immunostaining for paranodal Nfasc155 and Caspr along with the nodal Ankyrin G (AnkG) at 30 days post-OHT injection showed normal localization of Nfasc155 and Caspr at the paranodes with AnkG being restricted to the nodes (Figure 2.9A, B). However, several paranodal defects were observed in the $QKI^{FL/FL;PLP\text{-}CreERT}$ mice. In the spinal cord, we were able to observe either a loss of one paranode, both paranodes or increased distance in between the paranodes. We quantified the total number of each observed defect using both anti-Nfasc155 and anti-Caspr. Loss of both Nfasc-155^{+} paranodes was the most observed defect. In the sciatic nerves, a significant number of paranodes displaying increasing nodal gap and shorter paranode length compared with wild type mice was observed (Figure 2.9B, bottom panel). We also confirmed the paranodal defects in these mice by electron microscopy in spinal cord samples. Wild type mice displayed regular paranodal loops that terminate at the axon with tight axoglial junctions and minimal spacing between the paranodal loop and the axolemma (Figure 2.10A, B). In $QKI^{FL/FL;PLP\text{-}CreERT}$ mice, many terminal paranodal loops were found to be everting away from the axon and displayed irregular formations in which the loops abut each other instead of the axons (Figure 2.10C). Absence of transverse bands is evident in these mice along with an increase in the paranodal junction gap width (Figure 2.10D). These findings show that the loss of QKI expression in $QKI^{FL/FL;PLP\text{-}CreERT}$ mice leads to defective axoglial junctions as well as confirms the requirement for the ongoing expression of QKI to maintain expression of Nfasc-155 and hence paranode integrity.

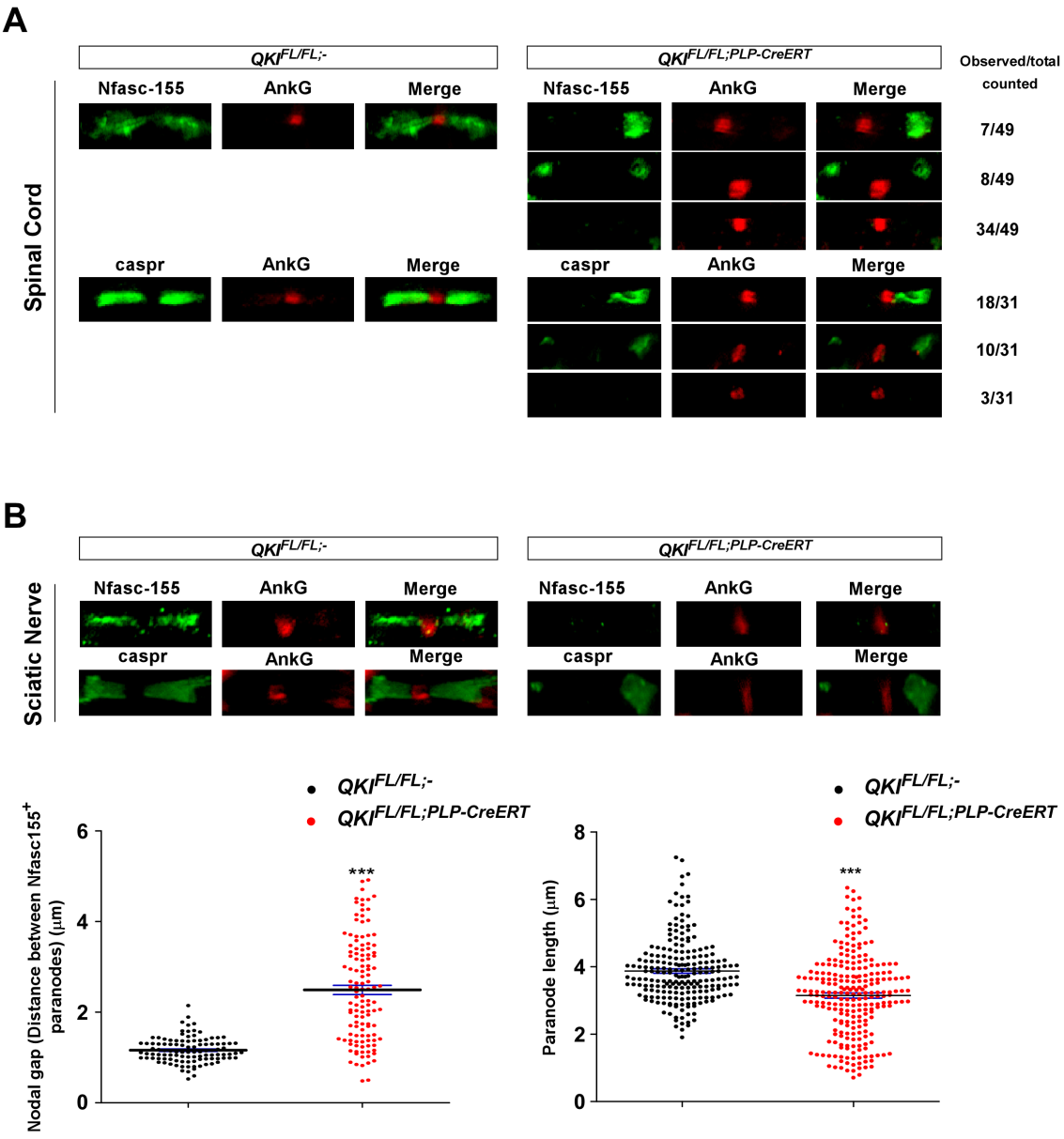

Figure 2.9. QKI-deficient mice exhibit axoglial junction defects.

(A) Immunostaining images of spinal cord sections from eight-week old *QKI*$^{FL/FL;-}$ and *QKI*$^{FL/FL;PLP\text{-}CreERT}$ mice injected with OHT and harvested 30 days post-injection and stained for Caspr, Nfasc155 and AnkG. Nfasc155 and Caspr colocalized to paranode structures and AnkG localized at the node. Number of defective paranodes observed in the spinal cord of *QKI*$^{FL/FL;PLP\text{-}CreERT}$ for each type of defect is shown on the right.

(B) (Upper panel) Immunostaining images of teased sciatic nerves from eight-week old $QKI^{FL/FL;-}$ and $QKI^{FL/FL;PLP\text{-}CreERT}$ mice injected with OHT and harvested 30 days post-injection and stained for Caspr, Nfasc155 and AnkG. Nfasc155 and Caspr colocalized to paranode structures and AnkG localized at the node. (Bottom panel) Vertical scatter plot showing nodal gap size between $Nfasc155^{+}$ paranodes. 106 wild type and 122 $QKI^{FL/FL;PLP\text{-}CreERT}$ nodal gaps were quantified. ($p < 0.001$). (Right) Vertical scatter plot displaying paranode length of $QKI^{FL/FL}$ mice versus $QKI^{FL/FL;PLP\text{-}CreERT}$. 212 wild type and 244 $QKI^{FL/FL;PLP\text{-}CreERT}$ paranodes were quantified, ($p < 0.001$).

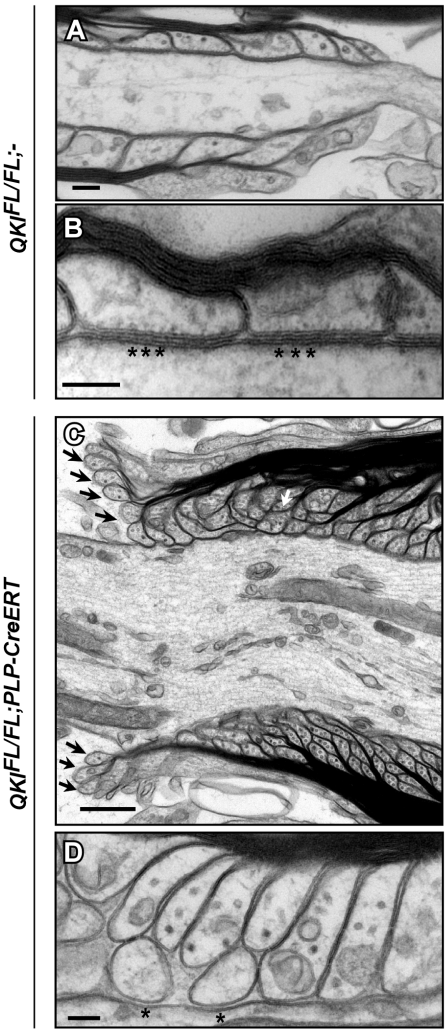

Figure 2.10. Ultrastructural paranodal defect in QKI-deficient mice.

(A-B) Representative electron micrograph images of longitudinal sections of spinal cords from wild type mice at 30 days post-OHT injection showing the attachment of paranodal loops to the axolemma and the formation of septate-like junctions (stars). Scale bar = 100nm.

(C) Representative electron micrograph images of longitudinal sections of spinal cords from $QKI^{FL/FL;PLP\text{-}CreERT}$ mice displaying detached paranodal loops (black arrows) and the failure of several loops to terminate at the axolemma and instead abut each other (white arrow). Scale bar= 500nm.

(D) Electron micrographs of $QKI^{FL/FL;PLP\text{-}CreERT}$ longitudinal spinal cord sections at 30 days post-OHT injection showing the lack of septate-like junctions (stars) and increased space between the paranodal loops and the axolemma. Scale bar= 100nm.

2.7 Discussion

In the present manuscript, we report a mouse conditional null allele of the QKI RNA binding proteins. Deletion of QKI in OLs with *Olig2-Cre* caused the mice to develop rapid tremors at P10 followed by death at the third post-natal week. The mice had a severe hypomyelination phenotype with OLs unable to fully mature beyond the PDGFRα^{+} stage. Removal of QKI expression in adult mice using *PLP-CreERT* resulted in hindlimb paralysis and immobility by ~30 days post-OHT injection. In these mice, we observed defects in axoglial junctions. High-throughput quantitative PCR identified several alternative splicing defects including that of the axoglial protein, *Neurofascin (Nfasc)*. Our findings define roles for QKI in myelin development and maintenance, as well as in the *Nfasc* isoform balance to maintain intact axoglial junctions.

The onset of tremors in the $QKI^{FL/FL;Olig2\text{-}Cre}$ mice at P10 and death at the third post-natal week is similar to null alleles of Nfasc155 (Sherman and Brophy, 2005, Pillai et al., 2009), Caspr (Bhat et al., 2001) and Contactin (Berglund et al., 1999) in that they die at the third week post-natally, they do differ, however, in that $QKI^{FL/FL;Olig2\text{-}Cre}$ completely lack myelin whereas the other mice have normal myelin. These findings suggest that a major function of the QKI proteins is to generate the Nfasc155 isoform for proper development of the axoglial junctions. Moreover, we identify a regulatory pathway through which QKI regulates *Nfasc* pre-mRNA splicing to generate Nfasc155. The binding of QKI to an RNA element (QRE2) in *Nfasc* intron 21 is required to promote inclusion of exons 21/22, which encode the third fibronectin-like domain unique to Nfasc155. A position-dependent asymmetric regulation of alternative splicing has been proposed for QKI with binding to QREs upstream of skipped exons and downstream of included exons in muscle (Hall et al., 2013). The fact that QRE2 is upstream of included exon 22, suggests that QKI does not exclusively function in a position-dependent asymmetric regulation like nSR100 (Raj et al., 2014). The absence of QKI in primary OLs led to the production of Nfasc186 mRNA, but not protein. These observations suggest that the Nfasc neuronal isoforms may be the default mRNA produced in the absence of the QKI proteins. It is likely that QKI functions in collaboration with other splicing factors to regulate the *Nfasc* splicing events. Indeed RBFOX2, PTB and SF1 have been shown to influence the alternative splicing activity of QKI in tumour microenvironment (Brosseau et al., 2014), muscle differentiation (Hall et al., 2013) and lung tumorigenesis (Zong et al., 2014), respectively. We also note the presence of eight QREs in the *Nfasc155* mRNA. These observations suggest that the QKI isoforms may also regulate *Nfasc* mRNA export, transport,

mRNA stability and translation.

The *qkI* conditional allele provides a role for the QKI proteins in axoglial junction formation and maintenance. Although paranodal defects were observed in myelin mutants such as *Shiverer* and qk^{v} (Rosenbluth and Bobrowski-Khoury, 2013), these are likely a consequence of the severe dysmyelination and loss of mature OLs. We show that our observed paranodal defects are not solely an outcome of dysmyelination, but due to the lack of the generation of the Nfasc155 isoform. This was confirmed with primary rat and mouse $QKI^{FL/FL;PLP\text{-}CreERT}$ OLs. *In vivo* deletion of the QKI proteins in $QKI^{FL/FL;PLP\text{-}CreERT}$ mice further substantiated the requirement of QKI to maintain axoglial junctions. Despite adult mice possessing established axonal domains, removal of QKI resulted in the rapid loss of Nfasc155 mRNA and protein along with the observed paranodal axoglial junction defects. A similar defect is observed in adult OL-specific loss of $Nfasc155^{-/-}$ (Sherman and Brophy, 2005, Pillai et al., 2009). This suggests that axoglial components are continuously being replenished to maintain the integrity of the nodes and paranodes and further demonstrate an ongoing requirement for glial QKI expression to maintain Nfasc155 protein. A complete absence of Nfasc155 at the paranodes in $Nfasc155^{FL/FL;PLP\text{-}CreERT}$ mice was only seen after 90 days post OHT injection, whereas by day 20 post-OHT injection, only a 50% reduction in Nfasc155 levels was observed (Pillai et al., 2009). Consistent with this observation, $QKI^{FL/FL;PLP\text{-}CreERT}$ mice display the expected 50% reduction in Nfasc155 staining with a significant increase in nodal gap. However, unlike $Nfasc155^{FL/FL;PLP\text{-}CreERT}$ mice, the $QKI^{FL/FL;PLP\text{-}CreERT}$ mice exhibit progressive paralysis with immobility ~30 days post-OHT injection, preventing further analysis of axoglial junction defects. Therefore, the death of the $QKI^{FL/FL;PLP\text{-}CreERT}$ mice cannot be explained solely by the loss of Nfasc155, indicating that deregulated control of RNA metabolism of other QKI targets also contribute to the phenotypes of these mice.

In humans, QKI has been associated with neurological disorders. Decreased expression of the QKI proteins is associated with Schizophrenia along with other myelin abnormalities (Haroutunian et al., 2006, Katsel et al., 2005). Abnormally spliced *Nfasc* has been identified in Schizophrenic brains (Wu et al., 2012), suggesting that reduced levels of QKI may be responsible for this event. Proper formation and maintenance of paranodal domains is critical, as disruption of Nfasc localization has been shown to lead to early changes that precede demyelination in multiple sclerosis (Howell et al., 2006). Thus, the regulation of *Nfasc* alternative splicing by QKI may be disrupted in certain demyelination disorders and Schizophrenia. A breakpoint mutation in humans

mapping to the QKI locus leads to a phenotype similar to 6q terminal deletion syndrome with characteristics such as intellectual disabilities, hypotonia, seizures, brain anomalies and specific dysmorphic features (Backx et al., 2010). Our findings suggest that the loss of QKI leads to paranodal defects, which may be associated with certain neurological disorders.

In conclusion, we show using a new conditional allele of *qkI* that not only does QKI play a role in myelin development via the regulation of OL differentiation, but also in myelin maintenance in adult mice. Our studies identify a novel role for the QKI proteins in axoglial junction maintenance by regulating the expression of the *Nfasc155* splice isoform. These findings define the QKI RNA binding protein as a critical regulator of many RNA processes in myelinating glia including alternative splicing.

2.8 Acknowledgments

We thank Jun Fang and Jeannie Mui for technical assistance with the primary cultures and EM, respectively. We thank Roscoe Klinck, Durand Mathieu and Philippe Thibault from the Université de Sherbrooke RNomics platform. We also acknowledge Kelly Sears and Hojatollah Vali for helpful discussions. The work was supported by a grant from the Multiple Sclerosis Society of Canada to S. R. L.D. is a recipient of a CIHR doctoral award (Funding reference number: GSD-140319)

2.9 Author contributions

L.D. and S.R. designed research; L.D. and G.V. performed research; L.D., G.V., G.A, and S.R. analyzed data; L.D. and S.R. wrote the paper.

Chapter 3

Transcriptome profiling of mouse brains with qkI-deficient oligodendrocytes reveals major alternative splicing defects including self-splicing

3.1 Preface

Based on our previously published genome-wide alternative splicing changes following loss of QKI expression in oligodendrocytes (Chapter 2), we were interested in identifying global changes in gene expression that are not restricted to known alternative splicing events. The work in chapter 3 focuses on transcriptomic profiling of *qkI*-deficient OLs to identify QKI RNA targets. This chapter also provides the first evidence for a role of QKI in regulating the alternative splicing of its own pre-mRNA.

3.2 Title page

Transcriptome profiling of mouse brains with *qkI*-deficient oligodendrocytes reveals major alternative splicing defects including self-splicing

Lama Darbelli[1#], Karine Choquet[2#], Stéphane Richard[1*], and Claudia L. Kleinman [2*]

[1]Segal Cancer Centre and the Bloomfield Center for Research on Aging, Lady Davis Institute for Medical Research, Sir Mortimer B. Davis Jewish General Hospital, and Departments of Oncology and Medicine, McGill University, Montréal, Québec, Canada.
[2]Segal Cancer Centre, Lady Davis Institute for Medical Research, Sir Mortimer B. Davis Jewish General Hospital, and Department of Human Genetics, McGill University, Montréal, Québec, Canada.

# authors contributed equally
*Corresponding authors: Lady Davis Institute, 3755 Côte Ste-Catherine Road, Montréal, Québec, Canada H3T 1E2. Phone: (514) 340-8260, Fax: (514) 340-8295
E-mail: claudia.Kleinman@mcgill.ca ; **stephane.richard@mcgill.ca**

The authors declare no competing financial interests.

3.3 Abstract

The *qkI* gene encodes a family of RNA binding proteins alternatively spliced at its 3' end, giving rise to three major spliced isoforms: QKI-5, QKI-6 and QKI-7. Their expression is tightly regulated during brain development with nuclear QKI-5 being the most abundant during embryogenesis followed by QKI-6 and QKI-7 that peak during myelination. Previously, we generated a mouse conditional *qkI* allele where exon 2 is excised using *Olig2-Cre* resulting in QKI-deficient oligodendrocytes (OLs). These mice have dysmyelination and die at the third post-natal week. Herein, we performed a transcriptomic analysis of P14 mouse brains of QKI-proficient *($QKI^{FL/FL;-}$)* and QKI-deficient ($QKI^{FL/FL;Olig2\text{-}Cre}$) OLs. QKI deficiency results in major global changes of gene expression and RNA processing with >1,800 differentially expressed genes with the top categories being axon ensheathment and myelination. Specific downregulated genes included major myelin proteins, suggesting that the QKI proteins are key regulators of RNA metabolism in OLs. We also identify 810 alternatively spliced genes including known QKI targets, *MBP* and *Nfasc*. Interestingly, we observe in $QKI^{FL/FL;Olig2\text{-}Cre}$ a switch in exon 2-deficient *qkI* mRNAs favoring the expression of the *qkI-5* rather than the *qkI-6* and *qkI-7*. These findings define QKI as regulators of alternative splicing in OLs including self-splicing.

3.4 Introduction

The quaking (*qkI*) gene encodes a family of alternatively spliced isoforms of RNA binding proteins that function as master regulators of cell differentiation (Darbelli and Richard, 2016). The deletion of these QKI isoforms in neural progenitors, muscles and monocytes causes severe differentiation defects (Darbelli et al., 2016, de Bruin et al., 2016a, Hall et al., 2013). A mouse conditional null allele of *qkI* has been generated by deleting exon 2 encoding part of the KH domain (Darbelli et al., 2016). The deletion of the QKI isoforms in OLs using *Olig2-Cre* ($QKI^{FL/FL;Olig2\text{-}Cre}$) leads to severe CNS hypomyelination with tremors by post-natal day 10 (P10) and death at the third post-natal week. Ablation of *qkI* in adult mice using *PLP-CreERT* results in hindlimb paralysis, thoracic kyphosis and immobility by the third to fourth week post-4-hydroxytamoxifen (OHT) administration (Darbelli et al., 2016). This work defines the QKI isoforms as major regulators of OL differentiation and maintenance. QKI also plays a pivotal role in monocytes, as its deletion using RNA interference blocked their differentiation into macrophages (de Bruin et al., 2016a). Moreover, a *qkI* haploinsufficient patient (Backx et al., 2010), also exhibits monocyte to macrophage differentiation defects(de Bruin et al., 2016a). Indeed, in humans, the essential role of QKI is evidenced by a marked intolerance to loss-of-function (LoF) genetic variants: an analysis of protein-coding genetic variation in >60,000 human exomes (Lek et al., 2016) shows that LoF variants are observed 14 times less frequently than expected by chance, with an associated probability of LoF intolerance of 0.96.

The *qkI* gene encodes KH-type RNA binding proteins that generates 3 major alternatively spliced mRNAs (5, 6, and 7 kb) encoding QKI-5, -6, and -7 that differ in their C-terminal 30 amino acids (Ebersole et al., 1996b). QKI-5 contains a nuclear localization signal in its unique C-terminal sequence and is exclusively nuclear (Wu et al., 1999). Thus QKI-5 participates in nuclear roles such as in the regulation of alternative splicing. QKI-6 is distributed throughout the cell and forms heterodimers with QKI-5 and may perform both nuclear and cytoplasmic functions (Pilotte et al., 2001). QKI-7 is predominantly cytoplasmic and both QKI-6 and QKI-7 are thought to function in mRNA export, mRNA stability and protein synthesis (Larocque et al., 2002, Li et al., 2000, Zearfoss et al., 2011, Larocque et al., 2005, Zhao et al., 2010, Doukhanine et al., 2010). During embryonic brain development, QKI-5 isoform is the most abundant and its expression declines after the first two post-natal weeks, while the QKI-6 and QKI-7 isoforms are expressed later in

embryogenesis and peak during myelination at the third post-natal week (Ebersole et al., 1996a; Hardy, 1998a). What regulates the *qkI* gene and its alternative splicing is unknown.

The QKI isoforms all share identical KH domains flanked by QUA1 and QUA2 sequences that mediate sequence-specific recognition of an RNA element termed the QKI response element (QRE) with the following sequence ACUAAY-(N_{1-20})-UAAY (Galarneau and Richard, 2005). Transcriptome-wide CLIP (crosslinking and immunoprecipitation) demonstrate that the QKI isoforms *in cellulo* bind the QREs and also showed that QKI associates predominantly with intronic sequences implying that alternative splicing regulation is one of its main nuclear functions (Hafner et al., 2010). The QKI isoforms were shown to regulate pre-mRNA splicing of myelin components (Wu et al., 2002), and later this function of QKI was shown not to be restricted to brain, as QKI-5 also fulfills this role in vascular smooth muscle cells, monocytes and skeletal muscle (de Bruin et al., 2016a, Hall et al., 2013, van der Veer et al., 2013).

Herein, we report a transcriptomic analysis by RNA-Seq of entire brains of $QKI^{FL/FL;Olig2\text{-}Cre}$ mice compared to $QKI^{FL/FL;-}$ mice. The results are consistent with the hypomyelination phenotype of the mice and show that mRNAs encoding myelin components are severely downregulated (Darbelli et al., 2016). We also identify alternative splicing defects especially in genes encoding myelin components. Interestingly, we noted that the absence of the QKI proteins also altered the alternative splicing of the *qkI* gene. Deletion of the *qkI* exon 2 generates a null allele, but switches the production of the $qkI^{\Delta exon2}$ mRNAs from being mainly *qkI-6* and *qkI-7* in wild type P14 brains to *qkI-5* in the brains of $QKI^{FL/FL;Olig2\text{-}Cre}$ mice. This work defines a self-splicing mechanism by which the *qkI* gene autoregulates its own alternative splicing in oligodendrocytes.

3.5 Materials and Methods

Isolation of brain RNA

All mouse procedures were performed in accordance with McGill University guidelines, which are set by the Canadian Council on Animal Care. Experimental protocols involving animal use were approved by the McGill University Animal Care Committee. $QKI^{FL/FL;Olig2\text{-}Cre}$ and $QKI^{FL/FL;-}$ mice were generated as described (Darbelli et al., 2016). Exon 2 of the *qkI* gene is flanked with loxP sites and the recombination with Cre results in a null. Total RNA was extracted from brains of $QKI^{FL/FL;-}$ and $QKI^{FL/FL;Olig2\text{-}Cre}$ P14 mice (n=3 for each genotype) with appropriate amounts of TRIzol® reagent according to the manufacturer's instructions (Invitrogen). 30 µg of RNA were DNase I (Promega) treated for 30 mins at 37°C.

RNA-Sequencing analysis

Total RNA from $QKI^{FL/FL;-}$ and $QKI^{FL/FL;Olig2\text{-}Cre}$ brains (n=3 females for each genotype) were purified using polyA selection and converted into cDNA by Illumina TruSeq and sequenced on a HiSeq 2000 (Illumina) with paired ends 100 bp in length (Genome Quebec, Canada) at an average of 133 million reads/sample. Illumina sequencing adapters were removed from the reads, and all reads were required to have a length of at least 32 bp. Sequencing runs were processed with Illumina CASAVA software. Trimmomatic v0.32 (Bolger et al., 2014) was used to trim reads, including removal of low-quality bases at the end of reads (phred33<30), clipping of the first three bases and clipping of Illumina adaptor sequences using the palindrome mode. We performed quality trimming with a sliding window, cutting once the average quality of a window of four bases fell below 30. We discarded reads shorter than 32 base pairs after trimming. Trimmed reads were aligned to the reference genome mm10 using STAR v2.3.0e (Dobin et al., 2013). Quality control was performed using metrics obtained with FASTQC v0.11.2, SAMtools(Li et al., 2009), BEDtools (Quinlan and Hall, 2010) and custom scripts. This showed a good proportion of high quality reads and mapping rates higher than 90% in all samples. Bigwig tracks were produced with custom scripts, using BEDtools and UCSC tools. Data were visualized using the Integrative Genomics Viewer (IGV)(Thorvaldsdottir et al., 2013).

Gene expression analysis

Expression levels were estimated by featureCounts v1.5.0 using exonic reads (Liao et al., 2014) and normalized using DESeq2 (Love et al., 2014). Global gene expression changes were assessed by unsupervised hierarchical clustering of samples and PCA, as previously described (Binan et al., 2016). Differential expression analysis between $QKI^{FL/FL;-}$ and $QKI^{FL/FL;Olig2\text{-}Cre}$ mice was performed using DESeq2 (Love et al., 2014) for all UCSC known genes. Genes were considered differentially expressed if they had an adjusted p-value < 0.05 and a base mean > 100. Expressed genes were defined as all genes with the DESeq2 base mean higher than the first expression quartile.

Alternative splicing analysis

We used rMATS v3.2.2 to identify alternative splicing (AS) events (Shen et al., 2014). Since rMATS requires reads of equal lengths, we performed the analysis on untrimmed reads after verifying that the adaptor content was low in the FASTQC reports. We ran rMATS with standard parameters and analyzed both outputs: AS events identified using reads mapping to splice junctions and reads on target (JC+ROT), and AS events identified using reads mapping to splice junctions only (JC). The list of putative AS events was obtained by including all events with an adjusted p-value (FDR) < 0.05 in either JC+ROT or JC. We also computed differential exon usage with DEXSeq v1.12.2 (Anders et al., 2012). To generate counts compatible with DEXSeq, we used featureCounts to count reads mapping to all annotated exons in Ensembl GRCm38.84 and converted them to the standard DEXSeq input format using scripts available online from Vivek Bhardwaj (Subread_to_DEXSeq, https://github.com/vivekbhr/Subread_to_DEXSeq). Differential exon usage analysis between WT and *QKI* KO mice was performed using standard DEXSeq parameters. Exons with a minimum length of 15 nucleotides and with an adjusted p-value > 0.05 were considered statistically significant.

To obtain a reduced set of stringent, robust ASE candidates, we combined predictions from DEXSeq and rMATS, since the underlying methods and the type of information (read counts, splice junction reads, etc) used by each approach are quite dissimilar. Significant events called both by rMATS (p-value < 0.05) and by DEXSeq (adjusted p-value < 0.05) were intersected based on genomic location. For this, we first merged the two rMATS outputs (JC+ROT and JC) so that each AS event was represented by one entry. We then used the BEDTools intersect function to

identify the genomic regions of overlap between the results from rMATS and DEXSeq, keeping the information from rMATS (Table S3). Since a number of exons are present as multiple entries in the rMATS outputs (for each isoform they belong to), we then intersected (BEDTools intersect) the results from rMATS and DEXSeq with the GENCODE VM11 annotation to identify all unique AS exons. AS events that were identified by rMATS and DEXSeq but that were not annotated in GENCODE VM11 were then added to the list. Exons with identical genomic coordinates were merged and counted only once. This approach allowed us to count the number of unique AS events without duplicates. To obtain a more comprehensive list of AS exons, we generated the union of the DEXSeq (adjusted p-value < 0.05) and rMATS (adjusted p-value < 0.05). For both the stringent and the comprehensive lists, we then used the GENCODE annotation to distinguish SE events corresponding to cassette exons compared to first or last exons. Exons were considered to be "cassette exons" if they were not the first or last exon in any of the gene isoforms or "mixed exons" if they were not the first or last exon in at least one isoform. SE events identified by rMATS that were not included in the GENCODE annotation were counted as "mixed" exons. This annotation is indicated in the last columns of Tables S3 and S5. Exons that were first or last exons in all isoforms were excluded from further analyses.

Gene Ontology

GO term enrichment analysis was performed Gorilla (Eden et al., 2009). The lists of differentially expressed genes and genes containing AS events were compared to a background list of expressed genes, consisting of all expressed genes in the complete dataset (see Gene expression analysis above). For differentially expressed genes, upregulated and downregulated genes with a base mean higher than 100 and an absolute fold change greater than 2 were used for the analysis. For AS, we used the genes in which stringent AS events (detected by DEXSeq and rMATS, see above) were observed.

Motif enrichment analysis

We searched for the motif ACUAA in windows of 200 nucleotides neighbouring each side of the identified SE events corresponding to "cassette" or "mixed" exons (see Alternative splicing analysis above). To verify enrichment of this motif in SEs and compute empirical p-values, we generated a set of control exons (n=88,217) that met the following criteria: "cassette" or "mixed"

exons, good coverage at the exon and gene level (coverage > lowest quartile of exon or gene coverage normalized by exon or gene length), not alternatively spliced (DEXSeq adjusted p-value > 0.99 and rMATS p-value < 0.05) and with a minimum length of 15 nucleotides. To compute empirical p-values, we performed 1,000 iterations, where in each iteration we randomly selected a number of control exons equal to the number of observed AS events, and computed the frequency of occurrence of the ACUAA motif within neighbouring windows of 200nt in these controls exons. Motif analyses were performed successively for all SEs, SEs with higher inclusion (QKI repressed) in $QKI^{FL/FL;Olig2\text{-}Cre}$ mice and SEs with higher exclusion in $QKI^{FL/FL;Olig2\text{-}Cre}$ mice (QKI activated). To determine the position of the core motif relative to the exon, we used the FIMO tool[37] (MEME suite) and searched for exact matches to ACUAA.

Transfections

HEK293T cells were plated in 6-well plates and transfected with 2μg of the indicated GFP expression vectors encoding QKI-5, QKI-6, QKI-7, QKI5:E148G and QKI5:V157E. The common forward primer for RT-PCR detection of *qkI* alternative splicing was in exon 6 and is the following: 5'- CCT CAC CCA ACT GCT GCA ATA G-3'. The reverse primer to detect exon 7 of QKI-7 inclusion is: 5'- CAT GAC TGG CAT TTC AAT CC-3'. Human constitutive exon: forward, 5'- GTC GGG GAA ATG GAA ACG AAG- 3' and reverse, 5'- GGT TGA AGA TCC CGC AGA AG-3'. Human GAPDH forward: 5'- CCG CAT CTT CTT TTG CGT CG-3', Human GAPDH reverse: 5'- TGG GTG TCG CTG TTG AAG TC -3'

Reverse transcript - qPCR

1μg of RNA was reverse transcribed using oligo(dT) primer and M-MLV reverse transcriptase according to the manufacturer's protocol (Promega). cDNAs were then amplified by PCR using the following conditions: 95^{o}C for 30 seconds, 60^{o}C for 30 seconds, 72^{o}C for 1 minute and repeated for 30 cycles. The PCR products were then separated by agarose gel electrophoresis. For real-time PCR, primers were designed and efficiency tested according to the MIQE guidelines. Real-time PCR was performed in triplicates with a 1:4 dilution of cDNA using SyBR Green PCR Mastermix (Qiagen, Valencia, CA) on 7500Fast Real-Time PCR System (Applied Biosystems, Foster City, CA). All quantification data were normalized to GAPDH using the ΔΔCt method. All quantification data were normalized to GAPDH using the ΔΔCt method or for the *qkI* isoforms

they were normalized to a constant exon region.

Primers:

Mouse 1: 5'- TCC TTG AGT ACC CTA TTG AAC CC -3'; Mouse 2: 5'- GGG CTG AAA TAT CAG GCA TGA C -3'; Mouse 3: 5'- TTA GCC TTT CGT TGG GAA AGC -3'; Mouse 4: 5'- GGT CTG CGG TCA CAA TCC TTT G -3'; Mouse 5: 5'- TAG GTT AGT TGC CGG TGG C -3'; Mouse 6: 5'- GGC CTT CTT ACC GTT CG -3'; . Mouse constitutive exon (exon 1 in all isoforms): forward, 5'-GTC GGG GAA ATG GAA ACG AAG- 3' and reverse, 5'- GGT TGA AGA TCC CGC AGA AG-3'. Mouse GAPDH forward 5'- CCC AGC TTA GGT TCA TCA GG-3'. Mouse GAPDH reverse: 5'- CAA TAC GGC CAA ATC CGT TC-3'. Mouse Bcas1 forward: 5'-GAC ACT GGT TTC ACC TAA CAA G-3'. Mouse Bcas1 reverse: 5'-GTA GCC TTT GTC TTC CCT C-3'. Mouse Bacs1 constitutive forward: 5'-CCC TCT GAT GGC GTT TCT CA-3'. Mouse Bcas1 constitutive reverse: 5'-CCA CGG AGT TTG ACG TTT GG-3'. Mouse Sema6a forward: 5'-GAG ACT GTC ACA ATT CCT TCG -3'. Mouse Sema6a reverse: 5'- GAA CAA GCT GGT CGT TGC-3'. Mouse Sema6a constitutive forward: 5'-CCA AAC ATG CCA ACA TCG C-3'. Mouse Sema6a constitutive reverse: 5'-TGA CAG TCC TGA GGG TAG GG-3'. Mouse Capzb forward: 5'-CTG GTG GAG GAC ATG GAA AAC-3'. Mouse Capzb reverse: 5'-CTG CTG CTT TCT CTT CAA GG -3'. Mouse Capzb constitutive forward: 5'-GTG GTG GAA GTG CAG GAG-3'. Mouse Capzb constitutive reverse: 5'-AGC CGG ATT TGT TGG TTT GC-3'.

3.6 Results

3.6.1 QKI-depleted oligodendrocytes downregulate genes involved in myelination.

To define the genome-wide alterations in gene expression and alternative splicing patterns in the absence of the QKI proteins, we isolated RNA from brains of $QKI^{FL/FL;-}$ and $QKI^{FL/FL;Olig2\text{-}Cre}$ mice (n=3 females/genotype) and performed RNA-sequencing at an average of 133 million reads/sample (Online Supplementary Table S1). Sequencing and quality control metrics showed high quality reads, with a mean alignment rate greater than 90%. More than 95% of reads mapped to genes and there was low ribosomal and mitochondrial gene content (Online Supplementary Table S1). We first assessed the global impact of oligodendrocyte (OL)-specific depletion of the QKI RNA binding proteins by unsupervised clustering analysis of samples based on expression profiles. $QKI^{FL/FL;-}$ and $QKI^{FL/FL;Olig2\text{-}Cre}$ mice consistently formed distinct, robust clusters (Figure 3.1A). Indeed, Principal Component Analysis (PCA) based on gene expression data showed that the first component (PC1) clearly separates $QKI^{FL/FL;-}$ and $QKI^{FL/FL;Olig2\text{-}Cre}$ mice and explained 75% of the variance (Figure 3.1A). Bootstrapped hierarchical clustering also separated the two groups with high bootstrap values (Supplementary Figure 3.1A). The clustering is very robust and is not affected by the number of genes or the algorithm used (Supplementary Figure 3.1B). Taken together, these results indicate that QKI-depletion in oligodendrocytes induces major changes in gene expression in the brain. In fact, differential expression analysis showed statistically significant differences in 1,899 genes, representing 10.55% of expressed genes (n=18,004). Of these, 229 had an absolute fold change greater than 2 (Figure 3.1B, Online Supplementary Table S2). A high proportion (70%) of the significant genes is downregulated, in line with a scenario where a well-defined population of cells is depleted in the brain samples. Quantitative RT-PCR analysis of 19 genes (Supplementary Figure 3.1C) showed strong correlation between RNA-seq fold change and RT-qPCR data (r^2=0.8049, Figure 3.1C). Gene Ontology (GO) analysis using the conservative list of 229 differentially expressed genes (with absolute fold change greater than 2) suggests that the downregulated biological processes are enriched for genes implicated in myelination and ensheathment of neurons (Figure 3.2A,B), consistent with the hypomyelination phenotype of these mice (Darbelli et al., 2016). The upregulated genes, on the other hand, are enriched for biological processes involving extracellular matrix organization and cell adhesion and include a number of genes related to neuronal biology, once again reflecting the loss of oligodendrocyte populations in QKI-depleted mice and increase in proportion of cell populations

of neuronal origin (Figure 3.2A,B). Examples include genes related to axon guidance, such as Ntn4, or genes associated with neurological phenotypes, such as Col5a3 (Online Supplementary Table S2).

Loss of QKI did not lead to major changes in transcript levels of genes involved in oligodendrocyte lineage specification and precursor proliferation, including *Olig2*, *Nkx6.1*, *Id2*, *Id4*, and *Sox5/6* (Online Supplementary Table S2), consistent with maintenance of PDGFRα^{+} OLs in $QKI^{FL/FL;Olig2\text{-}Cre}$ mice (Darbelli et al., 2016). QKI did appear to regulate RNA metabolism of transcription factors involved in OL differentiation and expression of myelin genes, including *Sox10*, *Myrf*, or myelin genes, including *Mag*, *Plp*, *Mbp*, *Mobp*, and *Sirt2* (Figure 3.1C), consistent with the hypomyelination phenotype of the mice. The sequencing of the entire brain would reveal secondary events occurring, for example in neurons, as it is well-known that OLs tightly regulate the contacts and metabolism of neurons (Funfschilling et al., 2012). However, genes involved in neuronal specification and differentiation, including Neurogenin proneural genes, Achaete scute-like 1, as well as neurogenic differentiation (Wilkinson et al., 2013), were not affected by the loss of QKI. Therefore, loss of QKI in OLs exerts changes in gene expression that are specific to OL lineage transcripts.

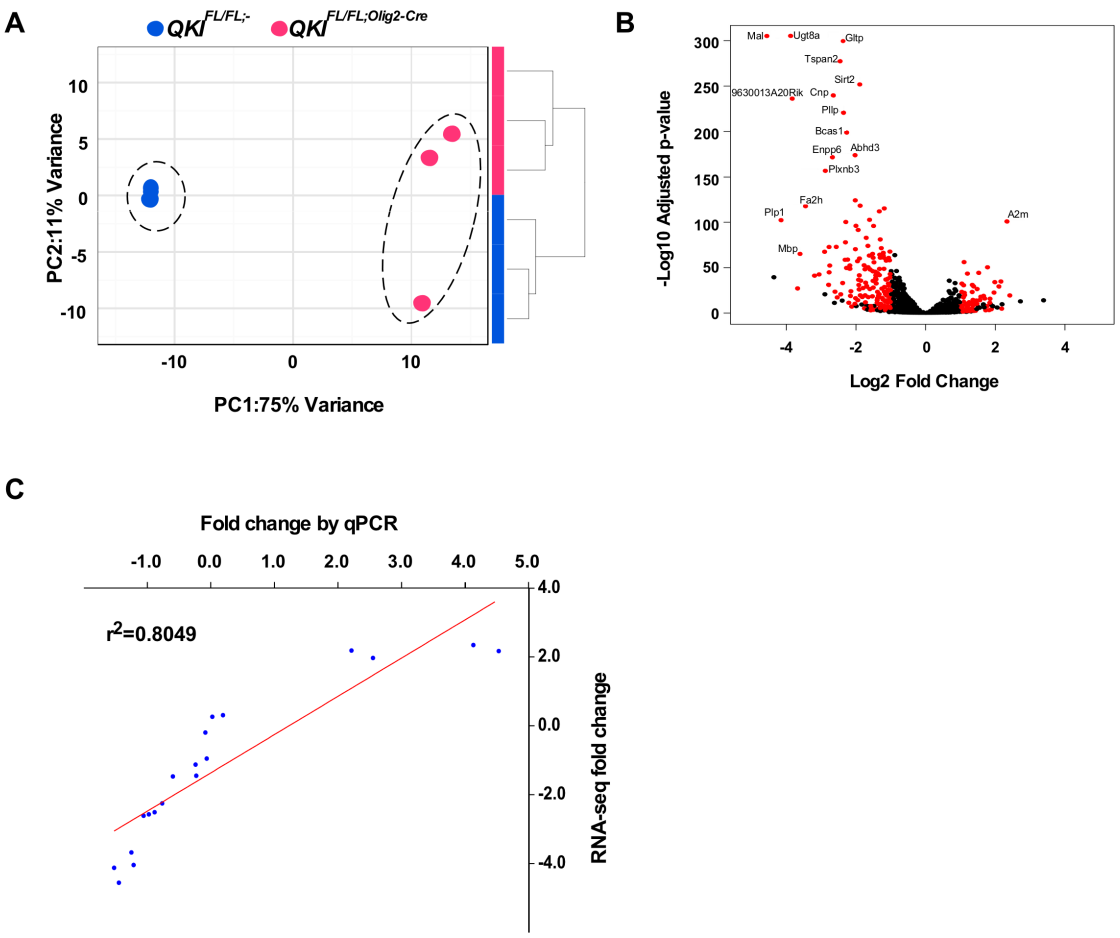

Figure 3.1. Gene expression profiles comparing brains of *QKI*$^{FL/FL;Olig2\text{-}Cre}$ *and* *QKI*$^{FL/FL;-}$ mice.

(A) Global effects of *QKI* KO on cells were evaluated by unsupervised clustering of samples based on expression profiles of 1,000 most variant genes. WT and KO mice form robust, distinct clusters, both with hierarchical clustering (right) and Principal Component Analysis (left). **(B)** Volcano plot representing the results of differential expression analysis. Genes with adjusted p-value < 0.05, absolute fold change > 2 and base mean > 100 are colored in red. **(C)** Validation of RNA-seq data by qPCR with 19 transcripts. RNA-seq data strongly correlated with qPCR data (r^2 = 0.8049 , *p* <0.0001, Pearson correlation coefficient).

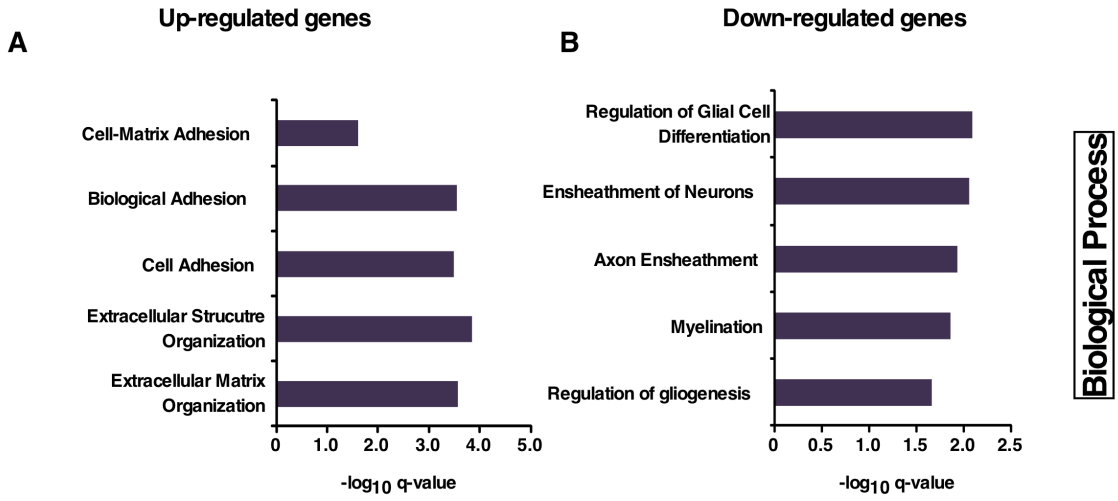

Figure 3.2. Gene ontology analysis.

Gene Ontology analysis shows enriched Biological Processes in the lists of upregulated genes (left) and downregulated genes (right) in *QKI* KO. Genes with adjusted p-value < 0.05, absolute fold change > 2 and a base mean > 100 were used for the analysis.

3.6.2 Alternative splicing changes observed in QKI$^{FL/FL;Olig2\text{-}Cre}$ mice

A previous search of alternative splicing events (ASE) within a defined subset of genes allowed us to identify 31 QKI-regulated ASEs in oligodendrocytes (Darbelli et al., 2016). Here, we extended the search genome-wide to identify novel events and to assess the extent of AS regulation by QKI, using two different, complementary methods to infer splicing information from RNA-Seq data (DEXSeq and rMATs) (Anders et al., 2012, Shen et al., 2014). Genome-wide loss of QKI resulted in widespread AS changes, with 1,438 ASEs detected in 810 genes (Online Supplementary tables S3-S5). Of the 31 identified with the candidate approach, 19 events were confirmed by RNA-seq including ASEs of *Nfasc, Magi, Lhfpl3, Mpzl1, Cadm1, Bin1, Vldlr, Plp1, Phka1, Mbp, Mobp, Grm5, Nhsl1,* and *Sirt2* (Online Supplementary Table S6). These data indicate that our RNA-seq analysis identified *bona fide* QKI RNA targets and that the majority of AS exons are novel events that have not been previously reported in *QKI$^{FL/FL;Olig2\text{-}Cre}$* mice. A stringent list of ASEs, detected by both methods is presented in Online Supplementary Table S3. The majority of the observed events were skipped exons (SE), with only a handful of alternative 5' or 3' splice sites detected (Figure 3.3A, Online Supplementary Tables S3, S5), suggesting that loss of QKI may result in significant changes at the proteome level. Importantly, most SE events corresponded to skipped cassette exons (Figure 3.3A). Among AS events identified by DEXSeq only, approximately half affected first or last exons (Figure 3.3A). Since alternative promoter or terminator usage is generally not regulated via the splicing machinery, we excluded them from further analyses and concentrated on cassette exons only. We showed previously that the QKI isoforms bind optimally to QKI response elements (QREs) with a sequence of ACUAAY (N1-20) UAAY (Galarneau and Richard, 2005). Therefore, we searched for the core sequence ACUAA as a minimal sequence and whether it is enriched upstream and/or downstream of the skipped cassette exons (SCE) events (Figure 3.3B,C, Supplementary Figure 3.2). More than 40% of SCE events from the stringent list had the exact sequence motif ACUAA in the neighbouring regions (Online Supplementary Table S7). In particular, this was the case for almost 50% of SCE events with lower inclusion level in *QKI$^{FL/FL;Olig2\text{-}Cre}$* mice (QKI activated). In both cases, this represents statistically significant enrichment (p-value < 0.001) over the distribution of the ACUAA motif frequency in a random set of control sequences (Figure 3.3B, Supplementary Figure 3.2B). Furthermore, over 30% of the complete set of 842 detected SCE events had the sequence motif in neighbouring sequences (Online Supplementary Table S8), again representing a significant enrichment over the

control distribution (Figure 3.3C, Supplementary Figure 3.2C,D). In addition, we determined whether the motif was present upstream or downstream of the AS exon. Similar to previous reports (Hall et al., 2013), we observed that the QRE core sequence tends to be located more often upstream of ASEs that are repressed by QKI and downstream of ASEs that are activated by QKI (Online Supplementary Tables S7, S8, Supplementary Figure 3.2G).

We performed GO analysis on the stringent list of candidates. Interestingly, the top enriched GO terms for biological processes included regulation of gliogenesis and myelination with myelin structural constituents and paranodal junction being one of the top molecular functions and cellular components, respectively (Figure 3.3D,E,F). Moreover, many of the top AS candidates are associated with neurological disease(s) and/or are involved in neurite outgrowth, neurogenesis, oligodendrocyte differentiation and myelination (Table 3.1). In some cases, we found almost complete exon skipping in $QKI^{FL/FL;Olig2\text{-}Cre}$, such as for exon 7 of *Bcas1,* exon 18 of *Sema6a* and exon 9 of *Capzb* (Figure 3.4A,B,C, left panels, sashimi plots are shown in supplementary Figure 4A,B,C), which we have validated by semi-quantitative PCR showing complete exon exclusion in the $QKI^{FL/FL;Olig2\text{-}Cre}$ mice (Figure 3.4A,B,C, middle panels). We have also quantified the exon inclusion levels normalized over a constitutive exon present in all isoforms for each of those three genes and a significant reduction was observed ($p<0.001$, Figure 3.4D,E,F).

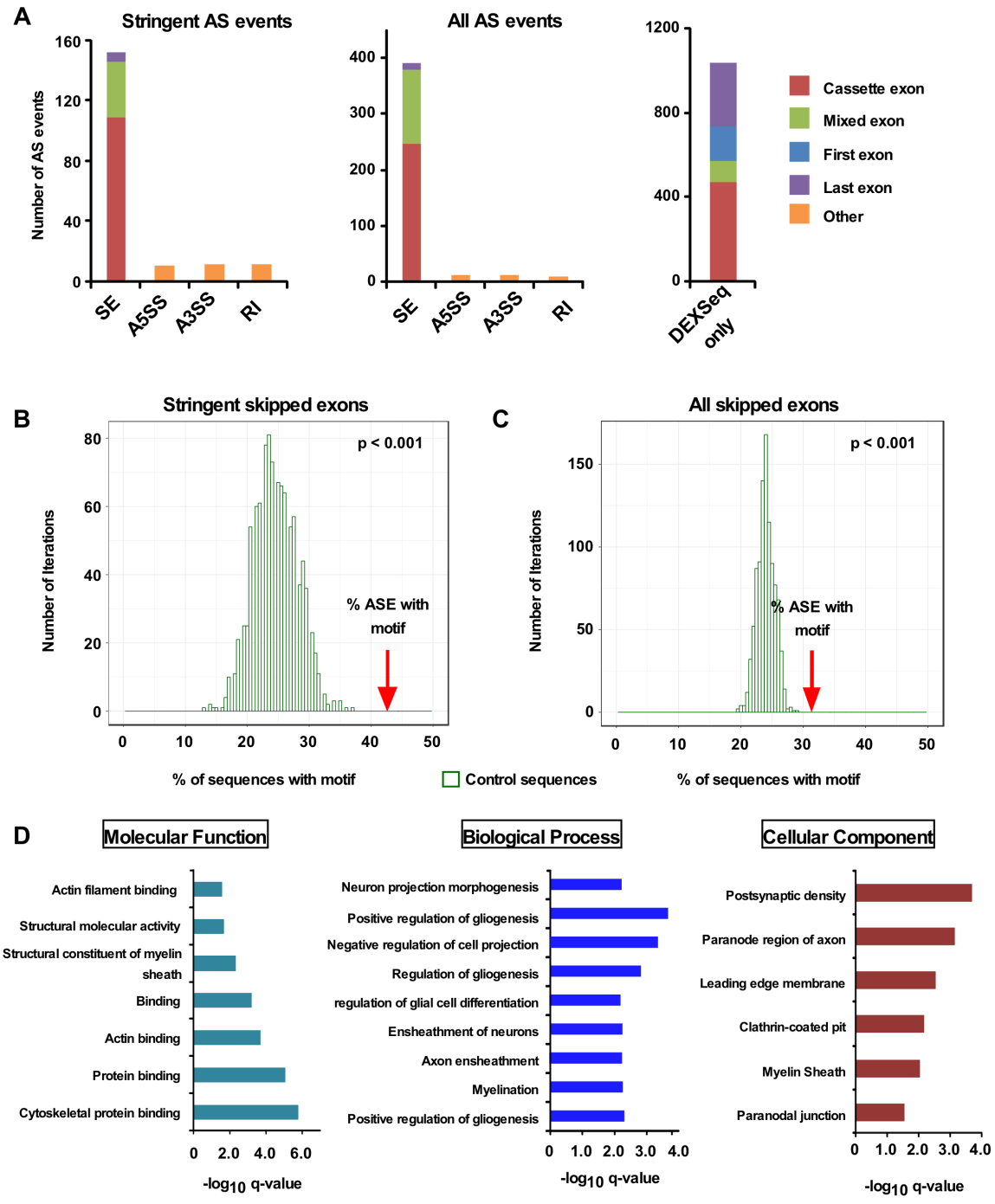

Figure 3.3. Brain alternative splicing patterns of mice with QKI-deficient oligodendrocytes. **(A)** Types of alternative splicing events identified in *QKI*$^{FL/FL;Olig2\text{-}Cre}$ mice. For skipped exons (SE), the type of exon affected is also indicated. Exons were considered to be "cassette exons" if they were not the first or last exon in any of the gene isoforms or "mixed exons" if they were not

the first or last exon in at least one isoform. Abbreviations: SE: skipped exon, A5SS: alternative 5' splice site, A3SS: alternative 3' splice site, RI: retained intron. **(B, C)** Motif enrichment analysis. Percentage of sequences with the motif ACUAA in introns neighboring SE events compared to a set of background sequences for the stringent SE candidates called by both methods **(B)** or for all SE candidates **(C)**. The occurrence of the motif was counted in a random set of non-alternatively spliced control sequences of the same size of the set of SE events. This was repeated 1,000 times to get the distribution of the motif occurrence in control sequences. The p-value corresponds to the empirical p-value of the enrichment for the set of SE events compared to the control distribution. **(D)** Gene Ontology analysis shows enriched molecular function, biological processes and cellular component in the list of genes where the stringent alternative splicing events were found. For Molecular Function, all GO terms with q-value < 0.01 are represented. For Biological Process and Cellular Component, GO terms with q-value < 0.01 and enrichment > 5 are represented.

Table 3.1. Alternative splicing events in *QKI*$^{FL/FL;Olig2\text{-}Cre}$ mice identified by RNA-seq. A large number of novel AS events observed in *QKI*$^{FL/FL;Olig2\text{-}Cre}$ mice are located in genes associated with neurological diseases and/or involved in important brain function, with the top 15 represented in this table. Abbreviations: SE: skipped exon, A5SS: alternative 5' splice site, A3SS: alternative 3' splice site, RI: retained intron.

Gene Symbol	Gene Description	Splicing inclusion change in QKI$^{FL/FL;Olig2\text{-}Cre}$	Event Type	Associated neurological diseases / brain function	Reference (PMID)
Vcan	versican	inclusion	SE	Neurite outgrowth	24955366
Gpm6b	glycoprotein m6b	exclusion	A3SS	Myelination	23322581
Ptprz1	protein tyrosine phosphatase, receptor type Z, polypeptide 1	inclusion/exclusion	SE	Oligodendrocyte differentiation and myelination	23144976
Mag	myelin-associated glycoprotein	inclusion	SE	Associated with demyelinating leukodystrophy	26179919
Sema6a	semaphorin 6A	exclusion	SE	Oligodendrocyte differentiation and myelination	22777942
Ndrg2	N-myc downstream regulated gene 2	inclusion	SE	Mainly expressed in astrocytes, regulates neurogenesis, associated with neurodegeneration	26341979
Ank3	ankyrin 3, epithelial	exclusion	SE	Genetic risk factor for psychiatric disorders; cytoskeletal scaffolding and synaptic protein	25374361
Daam2	dishevelled associated activator of morphogenesis 2	inclusion	SE	Suppresses oligodendrocyte differentiation during development, elevated in Guillain-Barré syndrome	25754822 26293489
Epb4.1l2	erythrocyte protein band 4.1-like 2	inclusion	SE	Organization of internodes in peripheral myelin	22291039
Map4k4	mitogen-activated protein kinase kinase kinase kinase 4	inclusion	SE	Neurite outgrowth and retraction	18007665
Myo6	myosin VI	exclusion	SE	Hippocampal synaptic transmission	16819522
Map4	microtubule-associated protein 4	inclusion	SE	Microtubule-stabilizing activity in oligodendrocytes and astrocytes	15642108
Bcas1	breast carcinoma-amplified sequence 1	exclusion	SE	Among most abundant transcripts in myelin	27173133
Fgfr3	fibroblast growth factor receptor 3	inclusion	RI	Involved in neurogenesis, associated with hypochondroplasia, medial temporal lobe dysgenesis and focal epilepsy	26180198 24630288
Map2	microtubule-associated protein 2	exclusion	SE	Microtubule-stabilizing activity and regulation of microtubule networks in dendrites	15642108

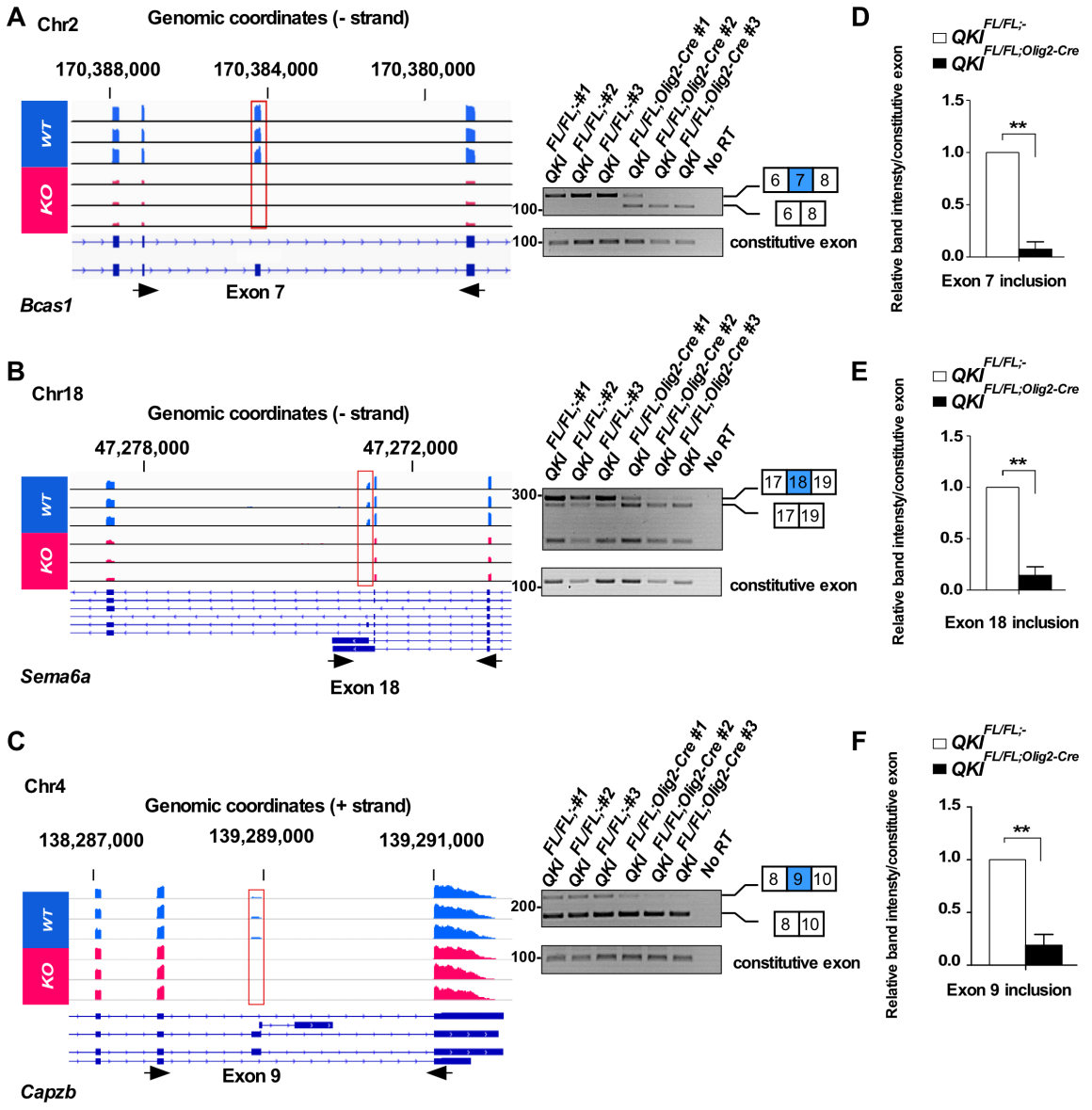

Figure 3.4. Alternative splicing event in *Bcas1, Sema6a* and *Capzb* in *QKI*$^{FL/FL;Olig2\text{-}Cre}$ and *QKI*$^{FL/FL;-}$ mice.

(A, B, C) IGV views of the exon skipping events in *Bcas1*, *Sema6a* and *Capzb*. All samples are represented on the same scale for each screenshot. Black arrows represent the primers used for validation by RT-PCR. Right: Validation of exon skipping events by semi-quantitative PCR in n = 3 mice per genotype. e constitutive exon is present in all isoforms of the gene and is not alternatively spliced. **(D, E, F)** pixel densities of PCR bands from 3 independent mice brain RNA samples were quantified using ImageJ software, normalized over wild-type mice and represented as mean ± SEM (Student *t*-test, **p < 0.001).

3.6.3 Quaking regulates the alternative splicing of its pre-mRNA

Remarkably, among the most significant events detected were exons of *qkI* itself, indicating a switch of isoform usage in $QKI^{FL/FL;Olig2\text{-}Cre}$ mice. The alternative splicing of exons 7 and 8 in the 3'UTR of the *qkI* gene generates the different QKI isoforms. In fact, exons 7c and 8 as well as the 3' UTR of the *qkI-5* isoform were significantly upregulated, while exons 7a, 7b and the 3' UTRs of *qkI-6* and *qkI-7* isoforms were significantly downregulated in $QKI^{FL/FL;Olig2\text{-}Cre}$ mice compared to $QKI^{FL/FL;-}$ mice (Figure 3.5A, sashimi plots are shown in supplementary Figure 3.4D). We also searched the *qkI* gene for QREs and we were able to identify many that mapped in intronic or exonic sequences. We identified 24 QREs present in the 3' alternatively spliced region of *qkI* that harbour either a perfect QRE or differ by 1 mismatch (Figure 3.5B and Online Supplementary Table S9). We next designed primer pairs aimed at amplifying the different *qkI* isoforms with their locations and expected products shown in Online Supplementary Table S10. We validated the alternative splicing of *qkI* pre-mRNA by RT-PCR using RNA from brains of three mice each for $QKI^{FL/FL;-}$ and $QKI^{FL/FL;Olig2\text{-}Cre}$. Since exon 6 of *qkI* mRNA is common to all the isoforms, we designed a primer (Figure 3.6A; primer #1) that is located in this exon and performed PCR with primers that map to either *qkI-5* (Figure 3.6A; primer#4), *qkI-6* (Figure 3.6A; primer#3) or *qkI-7* (Figure 3.6A; primer#2) specific exon 7 as well as in *qkI-5* specific exon 8 (Figure 3.6A; primer#5) and 3'-UTR (Figure 3.6A; primer#6). *qkI-5*, *qkI-6* and *qkI-7* share overlapping sequences in the 3'-end and therefore theses primers amplify regions in each of these transcripts with the size of the PCR product indicating which *qkI* isoform is being amplified. In $QKI^{FL/FL;Olig2\text{-}Cre}$ mice, we observed a decrease in the *qkI-7* isoform as evident by the lower PCR product obtained from primers #1 and #2 that corresponds to exon 6; exon 7a (Figure 3.6B). The upper band in Figure 3.6B corresponds to a product if the intron was retained (unspliced pre-mRNA) and shows a non-significant increase in $QKI^{FL/FL;Olig2\text{-}Cre}$ mice. Primers #1 and #3 show a decrease in the *qkI-6* isoform (the lower PCR product in Figure 3.6C that corresponds to exon 6; exon 7b). The upper band corresponds to the 3'-UTR of *qkI-7* which shows a significant decrease in the $QKI^{FL/FL;Olig2\text{-}Cre}$ mice. Primers #1 and #4 show a significant increase in *qkI-5* isoform (Figure 3.6D, lower band, exon 6; exon 7c) with a significant decrease in the 3'-UTR of *qkI-6* (Figure 3.6D, upper band). A significant increase in *qkI-5* isoform is shown using primers #1 and #5 (Figure 3.6E, exon 6; exon 7c; exon 8) as well as an increase in the 3'-UTR of *qkI-5* using primers #1 and #6 (exon 6; exon 7c; exon 8; 3'-UTR). We have also quantified the exon inclusion/exclusion levels normalized over

a constitutive exon of *qkI* (in exon 1) shown on the right of each semi-quantitative PCR (Fig 6b,c,d,e). The observed decrease in the inclusion of exons 7a (*qkI-7*) and 7b (*qkI-6*) and the increase in the inclusion of exon 7c of *qkI*-5 were confirmed by RT-qPCR (Supplementary Figure 3.3A). The deletion of exon 2 generates a frame-shift resulting in a null allele and therefore a complete lack of QKI proteins as previously shown (Darbelli et al., 2016). The loss of QKI-6 and QKI-7 specific exons and 3'-UTRs in $QKI^{FL/FL;Olig2\text{-}Cre}$ brains indicates that expression of the nuclear QKI-5 isoform is required to promote the inclusion of exons 7a (*qkI-7*) and 7b (*qkI-6*) as well as their 3'-UTRs. To confirm this, we transfected plasmids expressing green fluorescent protein (GFP) alone or GFP-QKI-5, -QKI-6, -QKI-7, mutated versions of QKI-5 that either cannot dimerize (GFP-QKI-5:E148G), or a version that cannot bind RNA (GFP-QKI-5:V157E) in HEK293T cells and assessed the inclusion of exon 7b of QKI-7 by RT-PCR. We observed an increase in the *Hqk-7* isoform (exon 6; exon 7b) only when GFP-QKI-5 was transfected, but not when GFP-QKI-6, GFP-QKI-7 or the mutated versions of QKI-5 were transfected (Figure 3.7A, B). We have also quantified exon 7b (*Hqk-7*) inclusion levels normalized over a constitutive exon of *qkI* (exon 1), and observed a significant increase in exon 7b inclusion when QKI-5 was transfected (Figure 3.7B, right). The increase observed when GFP-QKI-7 was transfected is due to the primer being in exon 7b of the cDNA in pGFP-QKI-7, recognizing the ectopically expressed isoform. Equivalent QKI protein expression was confirmed by immunoblotting (Figure 3.7C). These findings show that QKI-5 promotes the inclusion of exon 7b of *Hqk-7* in *cellulo*.

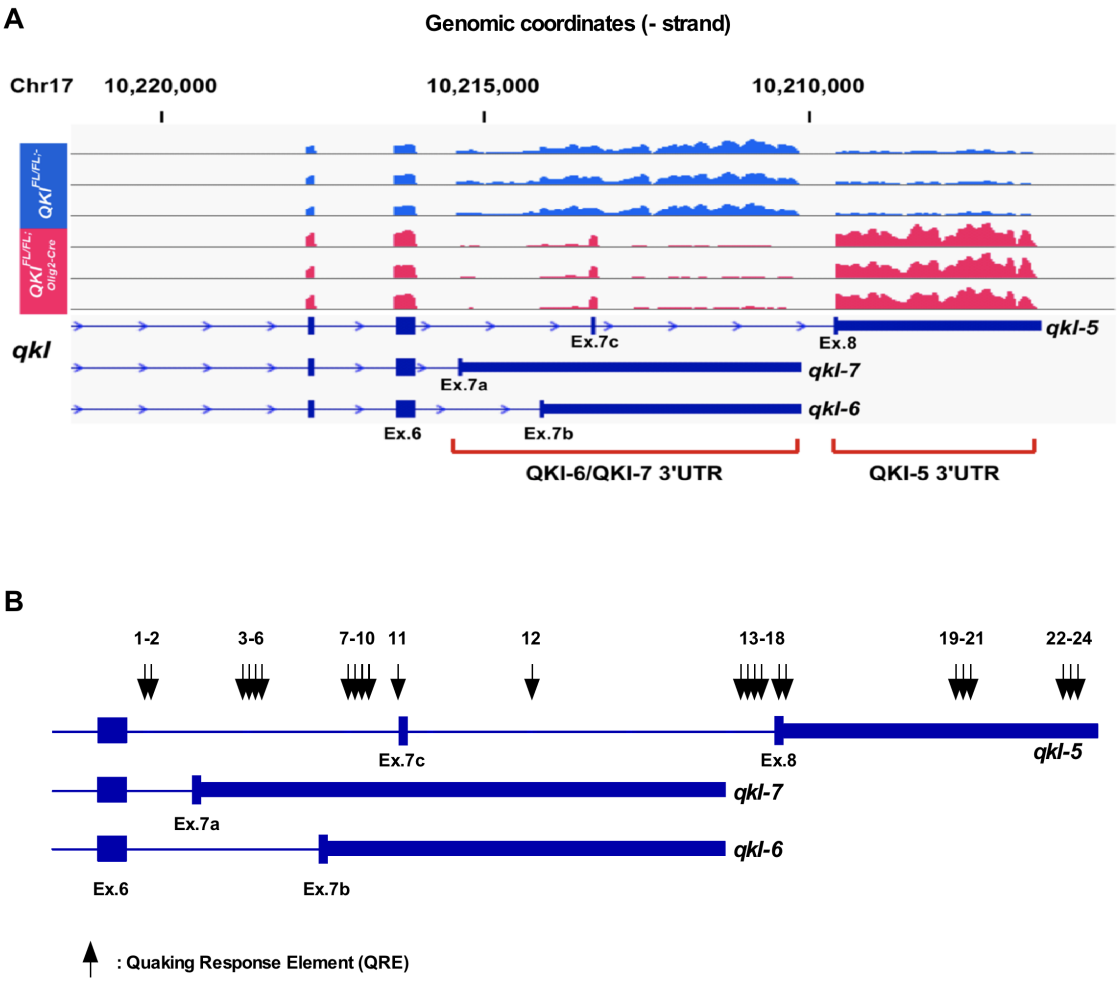

Figure 3.5. Alternative splicing patterns of *qkI* in *QKI*$^{FL/FL;Olig2\text{-}Cre}$ *and QKI*$^{FL/FL;-}$ mice.
(A) IGV view of the alternative splicing events in *qkI*. All samples are represented on the same scale for each screenshot. **(B)** A schematic of the 3'-UTR of mouse *qkI* gene showing the location of Quaking Response Elements (QREs) identified. QREs are either a perfect match to consensus QRE or differ by one mismatch.

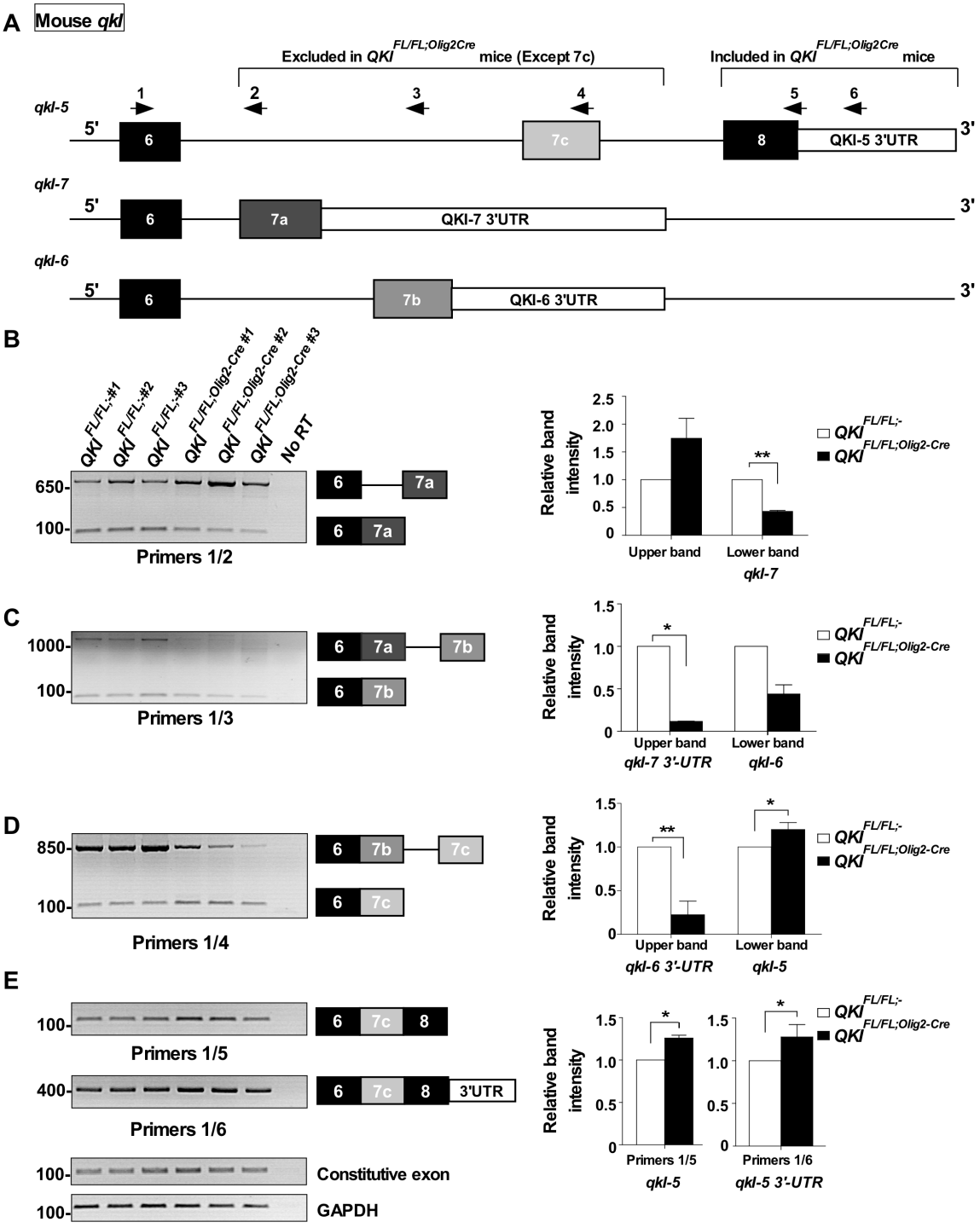

Figure 3.6. QKI proteins regulate self-splicing in mice.

(A) A schematic of the 3'-UTR of mouse *qkI* gene. Arrows indicate location of primers used for splicing analysis. Primer 1 is in exon 6 that is common to all QKI isoforms.

(B) (Left) RT-PCR analysis using primers #1 and #2 from n=3 mice brain RNA/ genotype. The lower band corresponds to *qkI-7* isoform (exon 6; 7a) whereas the upper band corresponds to the unspliced pre-mRNA. (Right) The pixel densities of PCR bands from 3 independent mice brain RNA samples were quantified using ImageJ software, normalized over constitutive exon , and then normalized over wild-type mice represented as mean ± SEM (Student *t*-test, ** $p<0.001$).

(C) (Left) RT-PCR analysis using primers #1 and #3 from n=3 mice brain RNA/genotype. The lower band corresponds to *qkI-6* isoform (exon 6; 7b) whereas the upper band corresponds to *qkI-7* 3'-UTR. (Right) The pixel densities of PCR bands from 3 independent mice brain RNA samples were quantified using ImageJ software, normalized over constitutive exon and then normalized over wild-type mice and represented as mean ± SEM (Student *t*-test, * $p<0.05$).

(D) (Left) RT-PCR analysis using primers #1 and #4 from n=3 mice brain RNA/ genotype. The lower band corresponds to *qkI-5* isoform (exon 6; 7c) whereas the upper band corresponds to *qkI-6* 3'-UTR. (Right) The pixel densities of PCR bands from 3 independent mice brain RNA samples were quantified using ImageJ software, normalized over constitutive exon and then normalized over wild-type mice and represented as mean ± SEM (Student *t*-test, * $p<0.05$, ** $p>0.01$).

(E) (Left) RT-PCR analysis using primers #1 and #5 (*qkI-5* isoform: exon 6; 7c; exon8), primers #1 and #6 (*qkI-5* isoform: exon 6; 7c; exon8; 3'-UTR), constitutive *qkI* exon 1, and GAPDH from n=3 mice brain RNA/ genotype. (Right) The pixel densities of PCR bands from 3 independent mice brain RNA samples were quantified using ImageJ software, normalized over constitutive exon and then normalized over wild-type mice and represented as mean ± SEM (Student *t*-test, * $p<0.05$).

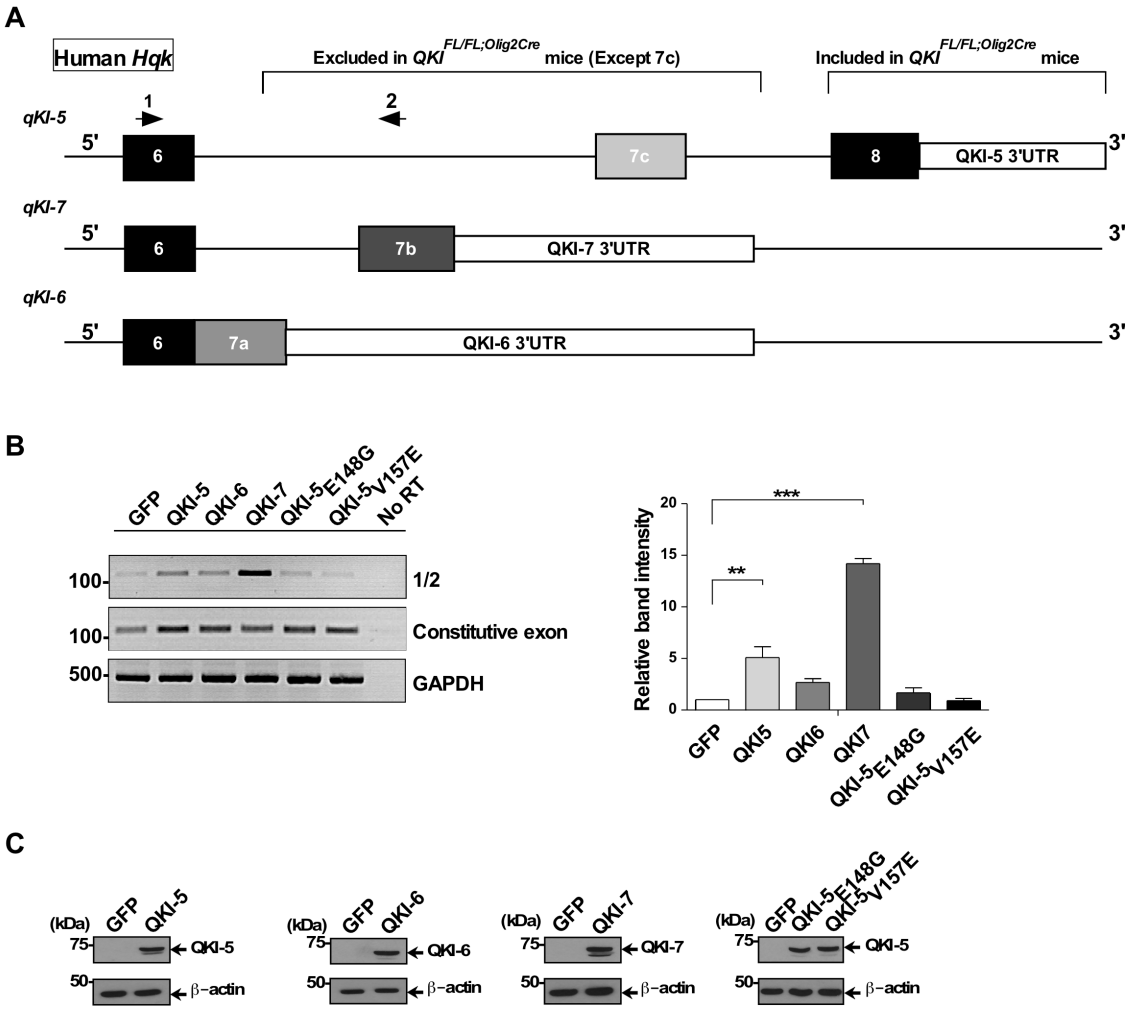

Figure 3.7. QKI-5 regulates self-splicing *in vitro* in human cells.

(A) A schematic of the 3'-UTR of human *Hqk* gene. Arrows indicated location of primers used for RT-PCR/splicing analysis. **(B)** (Left) HEK293T cells were transfected with expression vectors encoding green fluorescent protein (GFP) alone or expression vectors for GFP-QKI-5, -QKI-6, -QKI-7, -QKI-5:V157E or -QKI-5:E148G. Total RNA was isolated 72h later and analyzed by RT-PCR (n=3). The pixel densities of PCR bands from 3 independent transfections were quantified using ImageJ software, normalized over *Hqk* constitutive exon 1 and represented as mean ± SEM (One-way ANOVA, ** $p<0.01$, *** $p<0.001$). **(C)** Protein expression of transfected plasmids in HEK293T cells is determined by immunoblotting using the indicated QKI antibodies or β-actin antibody for equivalent loading. The molecular mass markers are shown on the left in kDa and the migration of the GFP-QKI isoforms indicated on the right.

3.7 Supplementary figures and legends

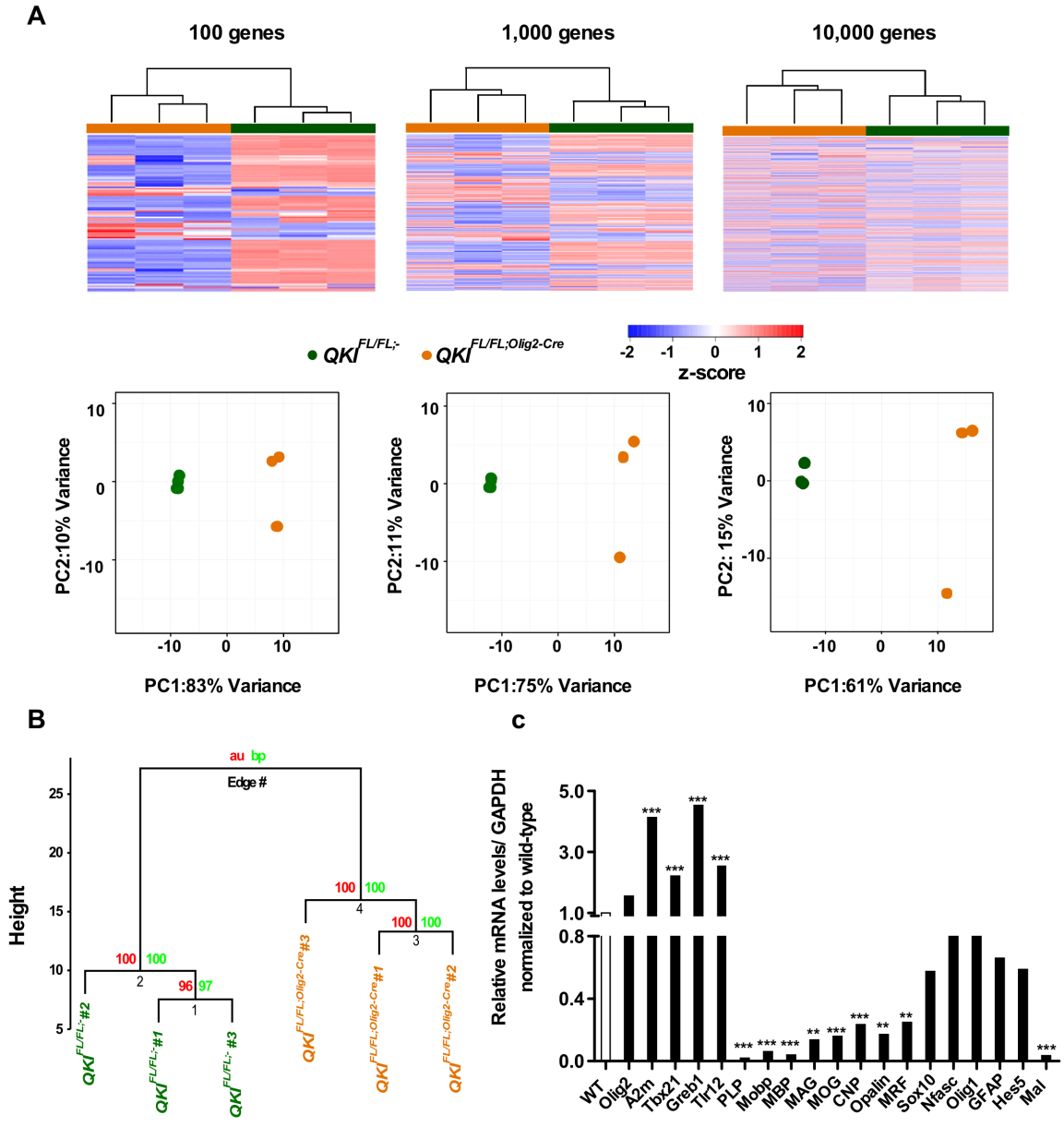

Supplementary Figure 3.1. Global effects of loss of QKI in OLs on gene expression.

(A) Unsupervised hierarchical clustering (top panel) and Principal Component Analysis (bottom panel) based on expression profiles, using a variable number of most variant genes (from 100 to 10,000). **(B)** Multiscale bootstrapping of gene expression clustering using the 1,000 most variant genes, performed with the R package pvclust (Bioinformatics 22(12:1540-2), 2006). In red, the approximately unbiased (AU) p-value is represented. With all algorithms, the two groups

consistently form distinct, robust clusters, indicating major expression changes associated with genotype. **(C)** RT-qPCR for the indicated genes using P14 brain RNA from n=3 mice/genotype. The results are represented in terms of fold change after normalizing the mRNA levels to a GAPDH and normalized after to wild-type. Each value represents the mean ± SEM.

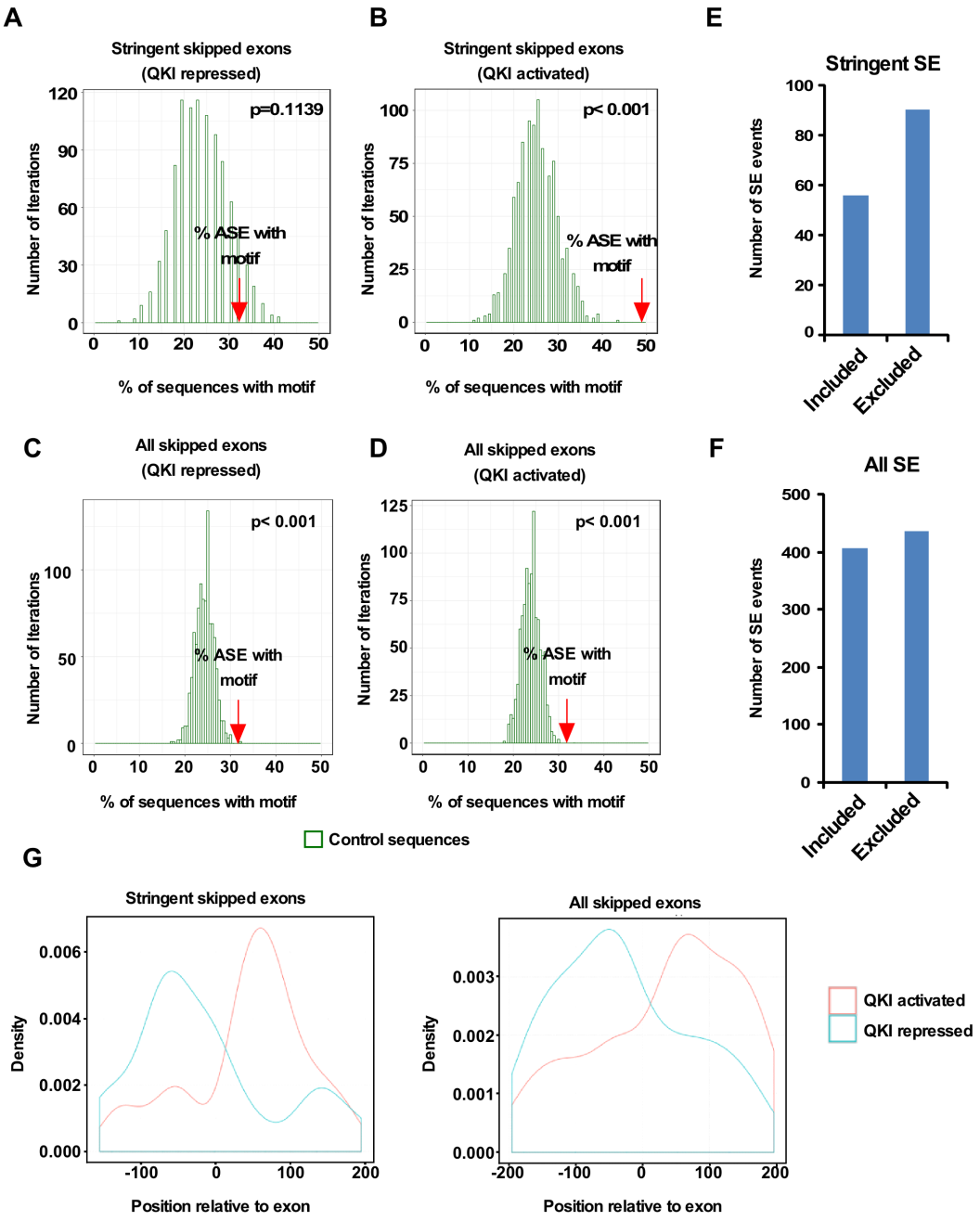

Supplementary Figure 3.2. Motif enrichment analysis for QKI activated and QKI repressed SE events.

(A, B) Percentage of sequences with the motif ACUAA in introns neighboring SE events compared to a set of background sequences for the stringent SE candidates called by both methods or for all SE candidates **(C, D).** QKI activated exons correspond to the ones that have lower inclusion level in $QKI^{FL/FL;Olig2\text{-}Cre}$ mice, while QKI repressed exons have higher inclusion level in $QKI^{FL/FL;Olig2\text{-}Cre}$ mice. The p- value corresponds to the empirical p-value of the enrichment for the set of SE events compared to the control distribution. **(E, F)** Number of SE that are included or excluded in $QKI^{FL/FL;Olig2\text{-}Cre}$ mice compared to $QKI^{FL/FL;-}$ mice in the stringent events **(E)** and all events **(F)**. **(G)** Density plot of the location of ACUAA sequence relative to exon for QKI repressed and QKI activated exons. Position of the QRE relative to the exon was computed with FIMO.

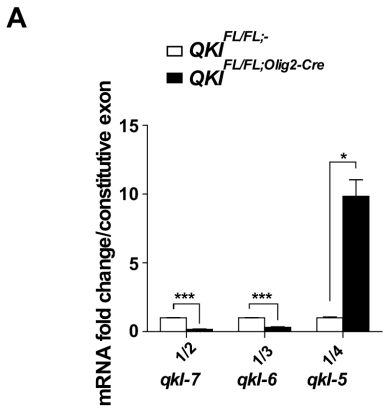

Supplementary Figure 3.3. Alternative splicing of the 3'-UTR of the *qkI* gene.

(A) RT-qPCR using indicated primers. The results are represented in terms of fold change after normalizing the mRNA levels to a constitutive *qkI* exon from n= 3 samples/genotype. Each value represents the mean ± SEM. * denotes $p < 0.05$. *** denotes $p < 0.001$, Student's *t*-test.

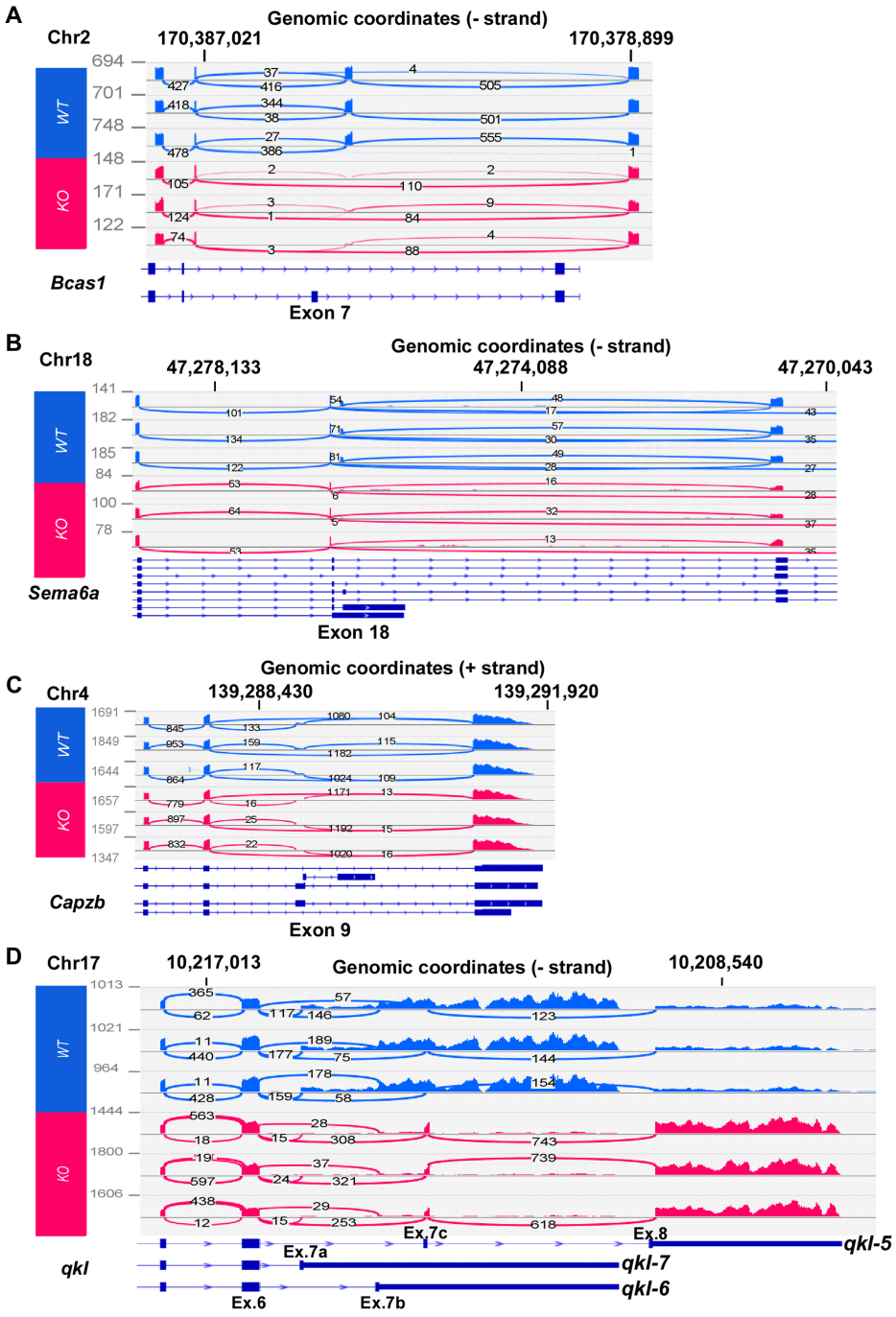

Supplementary figure 3.4. Sashimi plots of alternative splicing events in *Bcas1, Sema6a, Capzb* and *qkI* in $QKI^{FL/FL;Olig2\text{-}Cre}$ and $QKI^{FL/FL;-}$ mice.

Sashimi plots produced with IGV illustrating the exon skipping events in *Bcas1, Sema6a* and *Capzb*, with the number of reads supporting each exon junction. The number of reads in each

sample is indicated in grey on the left of the plot. For *Sema6a* and *qkI*, only junctions with more than 5 and 10 supporting reads, respectively, are indicated to maintain legibility.

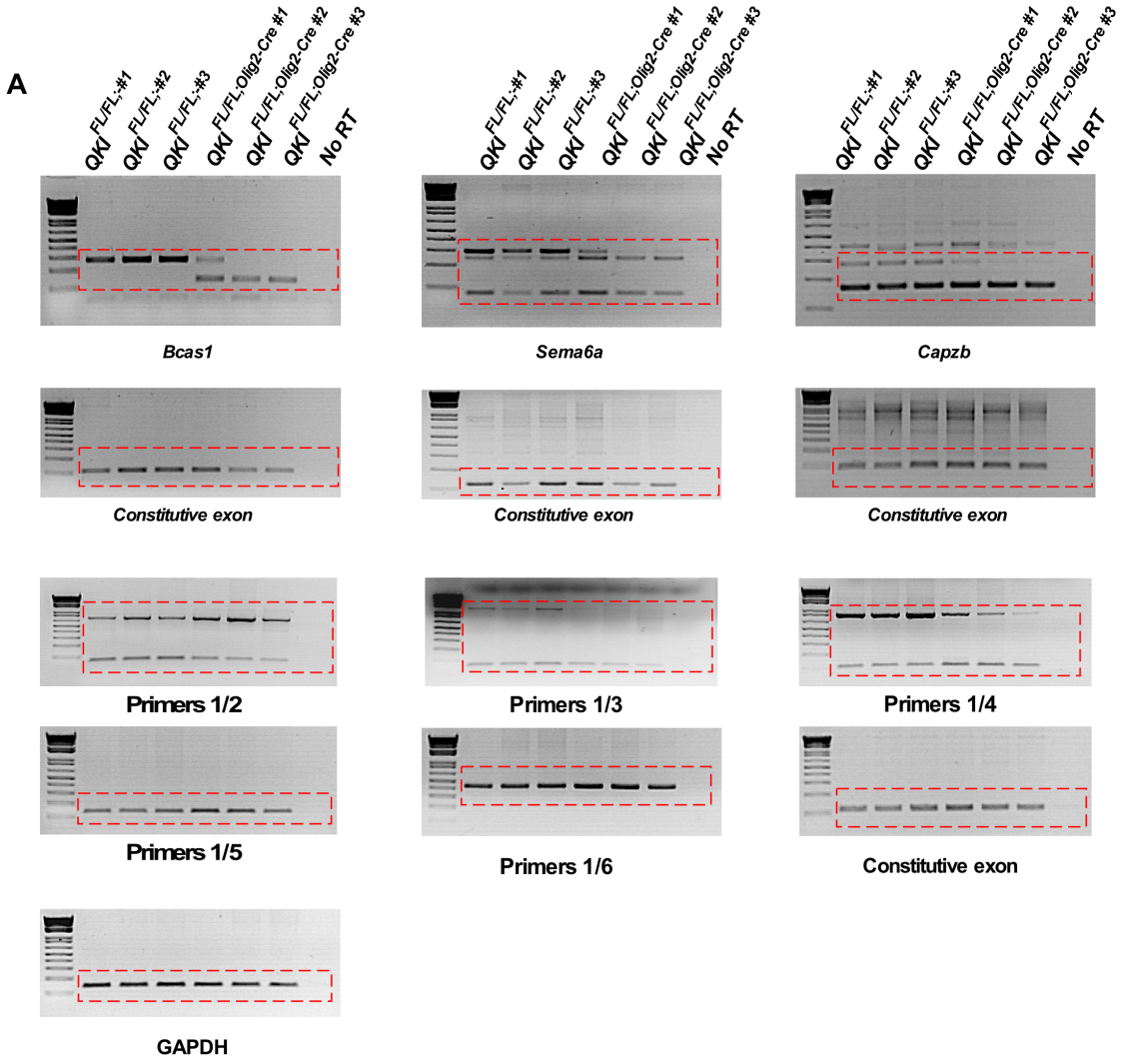

Supplementary Figure 3.5. Original PCR gels.

Original PCR gel images from $QKI^{FL/FL;-}$ and $QKI^{FL/FL;Olig2\text{-}Cre}$ mice brain RNA.

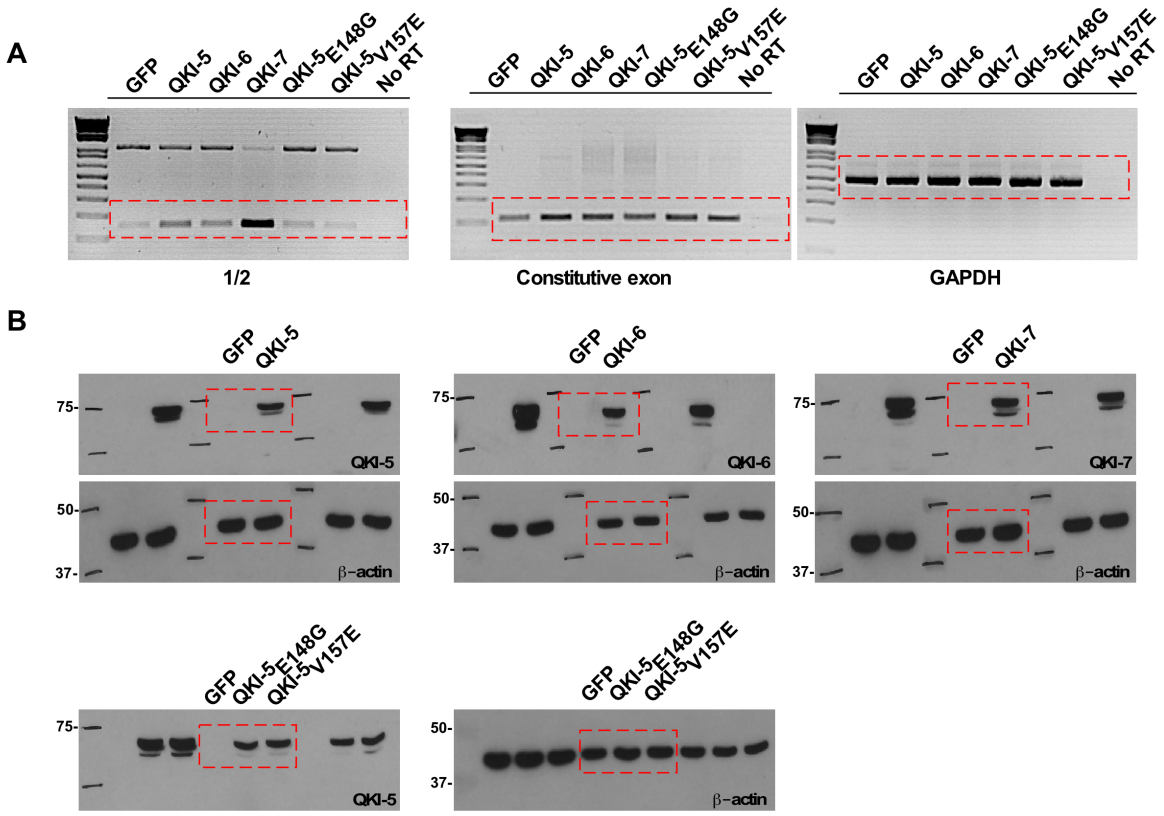

Supplementary Figure 3.6. Original PCR gels and western blots.

(A) Original PCR gel images from HEK293T transfected with the indicated plasmids. **(B)** Original western blots of transfected HEK293T cells with the indicated plasmids blotted for the expression of QKI proteins and β-actin as loading control.

3.8 Discussion

The presence of a QKI response element in >1400 mRNAs suggested that the QKI isoforms regulate many genes (Galarneau and Richard, 2005). In the present manuscript, we perform a transcriptomic analysis using whole brain RNA from $QKI^{FL/FL;-}$ and $QKI^{FL/FL;Olig2\text{-}Cre}$ mice and we identify >1,800 genes that are significantly differentially expressed of which 229 genes show an absolute fold change greater than 2. More than 1,500 alternative splicing candidates were identified using two methods, DEXseq and rMATS. Gene ontology analysis of the 229 genes has identified genes involved in glial cell differentiation (OLs), axon ensheathment, and myelination to be the most downregulated. Surprisingly, we identified *qkI* as the top alternatively spliced event by DEXseq and we show that QKI-5 regulates the alternative splicing of the *qkI-6* and *qkI-7* isoforms. Inspection of the *qkI* pre-mRNA reveals the presence of many QREs distributed across the intronic regions of these pre-mRNAs. Our findings define the QKI isoforms as master regulators of RNA metabolism in oligodendrocytes and show that QKI-5 isoform auto-regulates alterantive splicing of its own gene.

Northern blot analysis shows that the *qkI-5* mRNA is highly expressed during embryogenesis and maintained until approximately P14 at which point its expression declines thereafter. In contrast, the mRNA expression of *qkI-6* and *qkI-7* begins embryonically and peaks at P14 and is maintained into adulthood (Hardy et al., 1996, Ebersole et al., 1996a). Thus, our observation in P14 wild type mice ($QKI^{FL/FL;-}$) that *qkI-6* and *qkI-7* are the main mRNA isoforms observed is expected. What is unexpected is that *qkI-5* is the major isoform observed at P14 in the brains of $QKI^{FL/FL;Olig2\text{-}Cre}$ mice. These findings suggest that the complete absence of the QKI proteins favors the splicing of the *qkI-5* isoform. It also suggests that the partial *qkI* promoter deletion observed in the *quaking viable* mice(Ebersole et al., 1996a) may decrease the transcriptional output of the *qkI* gene such that the levels of *qkI-5* are insufficient to drive the subsequent pre-mRNA splicing of *qkI-6* and *qkI-7* and their expression. Therefore, it is the *qkI* isoform imbalance that blocks cellular differentiation and these findings support the tumor suppressor function of the QKI proteins (Zong et al., 2014), as their deletion or isoform imbalance favors cell proliferation. Furthermore, the haploinsufficient expression of the human *qkI* gene (Backx et al., 2010) is enough to block cellular differentiation, as observed with its monocyte to macrophage differentiation defect (de Bruin et al., 2016a).

We next compared our mouse alternative splice analysis with two other RNA-seq analyses that were performed in human cells. There *qkI* haploinsufficient patient exhibits intellectual disabilities, hypotonia, seizures, brain anomalies and specific dysmorphic features (Backx et al., 2010). She carries a balanced reciprocal translocation (t(5;6)(q23.1;q26), where a break point in one of her *qkI* alleles causes reduced expression of QKI mRNA and protein (de Bruin et al., 2016a). RNA-seq analysis of her monocytes and macrophages compared to her control sibling revealed 1 513 alternative splice events (de Bruin et al., 2016a). These spliced events were indeed enriched for QREs next to these regulated exons (de Bruin et al., 2016a), suggesting these events are mainly direct targets of the QKI isoforms. Low QKI levels is a prognostic marker for poor survival for patients with non-small cell lung cancer (Zong et al., 2014). The human lung/bronchus epithelial cell line, BEAS-2B, was depleted of the QKI isoforms using shRNAs (Zong et al., 2014). RNA-seq was performed and 451 ASE were identified of which 81 were validated by RT-qPCR (Zong et al., 2014). Recently, transcriptomic profiling and alternative splicing analysis was performed in wild type versus *qkI*-deficient neural stem cells either in the presence or absence of *Pten* and *Trp53* identifying 388 and 215 genes that are differentially regulated and alternatively spliced, respectively (Shingu et al., 2017).

Our RNA-seq analysis identified a total of 1,526 ASEs (Online Supplementary Table S3, S4) with 190 events (Supplementary Table S2) that we termed 'stringent', as they were identified by both DEXSeq and rMATS. Comparing our stringent list with Zong et al., 2014, de Bruin et al., 2016 and Shingu et al., 2016, we have 96, 93, and 46 common gene names, respectively. If we compare all ASEs from all 4 gene sets, we can assemble a common signature of 4 genes in QKI-depleted cells (ADD3, Bin1, MAP4K4 and WDFY3). Interestingly, this list of 4 gene names spans mouse, human, oligodendrocytes, neural stem cells, monocyte/macrophages and lung epithelial cells. The other alternative splice targets are, therefore, more tissue- or cell-specific. Other genes commonly identified in three out of four gene sets include HP1BP3, MAP3K7, SBF1, SPAG9 and VLDLR.

In sum, we define the QKI RNA binding proteins as master regulators of RNA metabolism driving oligodendrocyte differentiation. Our RNA-seq analysis clearly defines QKI as regulators of alternative splicing and herein we define many spliced targets including self-regulation.

3.9 Acknowledgments

We thank Drs. Eric Van der Veer and Ruben de Bruin for sharing of unpublished data and stimulating discussions. L.D. is a recipient of a CIHR doctoral award (Funding reference number: GSD-140319). K.C. is a recipient of a doctoral award from the Fonds de Recherche du Québec – Santé (FRQS). The work was supported by a grant from the Multiple Sclerosis Society of Canada to S.R. and by a grant from the Natural Sciences and Engineering Research Council of Canada to C.L.K. C.L.K. receives salary awards from the FRQS. The computing and networking infrastructure were provided by Calcul Québec and Compute Canada.

3.10 Authors contribution

L.D. conceived the study, performed the lab experiments, analyzed the data and wrote the manuscript. K.C. and C.K. performed all the bioinformatic analysis, analyzed the data, and wrote the manuscript. S.R. conceived the study, analyzed data and wrote the manuscript.

Chapter 4

General discussion:

4.1 General summary

Since the discovery of the natural mutant *quaking viable*, much attention has focused on elucidating the role of QKI proteins in the CNS and during myelination. Many of those studies were carried out *in vitro* cell cultures or *in vivo* using qk^v and/or *qkI* null mice with both systems imposing their own limitations to properly address the function of QKI proteins. On one hand, *in vitro* systems may not truly represent the complexity of physiological processes in an organism. On the other hand, qk^v mice show complex, difficult to interpret phenotypes due to a 1 Mb deletion that deletes *parkin, parkin coregulated* genes as well as the *qkI* promoter and lead to differential QKI proteins expression with characteristic phenotypes in the CNS versus the PNS. *qkI* null mice represent an even more difficult system to use due to embryonic lethality therefore hindering any further analyses of later developmental stages.

As shown in this thesis, our lab has overcome these limitations in studying the function of QKI proteins in the CNS by generating the first conditional null mouse where we deleted the expression of QKI specifically in oligodendrocytes during development and later in adulthood. The results shown in this thesis provide evidence that indeed, the loss of QKI proteins in OLs leads to severe fatal hypomyelination represented by tremors and seizures in the mice that die by the third post-natal week. A novel role for QKI in myelin maintenance is established as its ablation in adult mice leads to a progressive hindlimb paralysis and eventually death. In both transgenic mice, deterioration of axoglial junctions with a loss of Nfasc-155 was observed and Nfasc-155 was validated as a target of QKI. This discovery has recently been replicated by Shi et al using a conditional knockout mouse for *Tuberous Sclerosis Complex 1* (*Tsc1*) in the CNS and PNS (Shi et al., 2018). Ablation of *Tsc1* in OLs and Schwann cells was shown to lead to mTORC1 activation along with a strong reduction in *qkI* and *Nfasc-155* mRNAs and proteins. During normal OPCs differentiation, the levels of QKI gradually increase, whereas mTORC1 decreases (Beirowski et al, 2017) Reintroducing exogenous *qkI* gene into OLs was sufficient to restore *Nfasc-155* mRNA and proteins levels further highlighting the importance of proper QKI expression for the generation of the Nfasc-155 isoform (Shi et al., 2018).

A transcriptomic analysis of P14 mice brains that either express or lack QKI proteins identifies major global changes in gene expression and RNA processing in more than 1800 genes. Most of these genes played a role in axon ensheathment and myelination. We also provide the first direct evidence for a function of QKI in regulating its own expression by regulating the alternative splicing of its pre-mRNA.

4.2 The advantages of generating a qkI conditional allele

For decades, gene knockout has been the most efficient method for functional genomic research. Yet, full body knockouts present their own limitations: 1) if a gene is embryonic lethal, then knowledge of its function beyond it being essential for the organism is eliminated, 2) a gene could function differently between tissues and thus making interpretation of the full body knockout more complicated with limited ability to pinpoint the exact function of the gene within a specific tissue or cell type, and 3) full body knockouts do not represent an ideal system for studying human diseases since most genetic disorders develop in a certain cell type or at a specific developmental stage (Zhang et al., 2012).

Our lab has been interested in studying the function of QKI proteins during OLs development. Full body knockout of *qkI* as well as the ENU-induced *qkI* mutants are embryonic lethal at a stage preceding OLs development and myelination. The objective of this thesis was to understand the function of QKI proteins in myelination cells. Therefore, to properly elucidate the role of QKI in OLs, it was necessary to generate a conditional null allele. Our newly generated floxed *qkI* allele has provided direct evidence that indeed QKI proteins are master regulators of OLs development and differentiation (Darbelli et al., 2016). The mosaic expression pattern of QKI in qk^{v} mice and the complete absence of some but not all the isoforms in certain parts of the CNS complicated interpretations of the function of QKI in myelinating cells. Now we know that QKI proteins are essential for proper maturation of OLs which is a crucial step to get to the myelinating OLs. These mice have also added an unprecedented function to the repertoire of QKI roles. Not only these proteins are necessary during development, but their removal in adults after completion of myelination, results in lethal disrupted myelin sheath as well as defects in paranodal loops (Darbelli et al., 2016). This implies that paranodal domain compartments undergo constant turnover and that the continuous expression of QKI during adulthood is required to generate the *Nfasc-155* splice variant and protein. Moreover, our studies in these newly generated mice have

focused on studying alternative splicing, yet there exist many more aspects of RNA metabolism that are regulated by QKI proteins in other systems that are still to be investigated in OLs.

A recent transcriptomic analysis using RNA-seq of acutely purified neurons, OPCs, newly formed OLs, myelinating OLs, microglia, endothelial cells and pericytes from mouse cerebral cortex revealed that QKI proteins are also expressed in other cell types in the CNS (Zhang et al., 2014b). QKI is expressed also in astrocyte, microglia and endothelial cells (Zhang et al., 2014b). Given the vast number of functions ascribed to QKI proteins in terms of regulating RNA metabolism, it most likely that QKI also functions to regulate essential processes in these cells as well. Astrocytes function to provide axon guidance, synaptic support as well as to control blood brain barrier and blood flow. They also function to maintain homeostasis at the synapse, regulate neuronal functions as well as protect neurons from oxidative damage (Blackburn et al., 2009). Therefore, they exhibit essential functions in the CNS. QKI proteins are highly expressed in astrocytes, almost to levels similar to those seen in newly formed OLs (Zhang et al., 2014b). An in vitro study of human primary astrocytic cultures provided evidence that human QKI controls the mRNA levels of Glial fibrillary acidic protein (GFAP), a major component of astrocytic intermediate filaments (Radomska et al., 2013). Yet, the *in vivo* role of QKI in astrocytes remains to be characterized. A recent report has demonstrated that astrocytes are capable of local translation with presence of ribosomes and mRNAs in their distal processes (Sakers et al., 2017). This local translation was enriched for transcripts with known roles for astrocytic processes such as glutamate and GABA metabolism. Moreover, a QKI response element motif was found in a high percentage of those locally translated mRNAs (Sakers et al., 2017). Deleting the QRE in one of the locally translated mRNA leads to increased nuclear retention. Therefore, the functional importance of QKI proteins in astrocytes is starting to be uncovered. Several astrocyte specific Cre lines have been used to target gene expression in astrocytes (Blackburn et al., 2009) that could be combined with the floxed *qkI* mice to provide an invaluable system to assess the function of QKI in astrocytes.

Microglia are the innate resident immune cells of the CNS. They are involved in a variety of functions ranging from mediating immune responses, to clearing cellular debris to being involved in controlling neuronal activity and surveying synaptic functions. A newly generated Cre-ERT mouse line (the CX3CR1-CreERT), can target gene expression specifically in microglia without affecting other peripheral immune cells that express the CX3CR1 receptor. This is due to the evidence that microglia are maintained by their own stem cell pool in the CNS and do not

receive input from the bone marrow (Parkhurst et al., 2013). Emerging evidence has implicated QKI proteins in genome-wide alternative splicing regulation during monocyte to macrophages differentiation in the bone marrow (de Bruin et al., 2016a). These finding imply that the QKI proteins may regulate the function of the resident macrophages of the CNS, which are the microglia. Moreover, microglia play essential roles in neuroinflammatory disease specifically multiple sclerosis. Therefore, targeting QKI expression in these cells in models such as the experimental autoimmune encephalomyelitis would provide invaluable evidence for a possible role for QKI protein in microglial functions.

Endothelial cells are key components of the blood-brain barrier. They maintain homeostasis in the CNS and are involved in pathophysiology of many neurological diseases. Several Cre lines have been established and used in targeting gene expression in endothelial cells (Assmann et al., 2016). These Cre lines, combined with the floxed *qkI* allele, could be used to investigate a potential role for QKI in endothelial cell homeostasis or in disease models mimicking human disease such as Multiple Sclerosis and Alzheimer's disease among other chronic neuroinflammatory or neurodegenerative disease in which brain endothelial cells are involved.

Increasing lines of evidence support an essential function for QKI in humans since its deregulation leads to different diseases (section 1.2.10). Mouse and human *qkI* genes are highly similar with an identical amino acid sequence indicating that QKI most likely plays similar roles in humans and mice. Therefore, the generation of the conditional *qkI* allele would allow for the replication of certain human diseases/genetic disorders in mice. In MS, there are still no therapies to enhance remyelination. Remyelinating events include steps that are similar to what occurs during development ranging from OPC generation to migration to lesion sites to finally differentiation and myelination. The generation of the conditional allele would allow for addressing the question of whether QKI proteins play a role in remyelination. Using the inducible PLP-CreERT, demyelination could be induced using the lysolecithin injections that lead to demyelination and remyelination in the spinal cord within 14 days due to OPC proliferation and migration (Lau et al, 2012). Since the PLP-CreERT knockout mice of QKI die within 30 days, this method would allow to study the extent of demyelination, early myelination and complete remyelination at 4, 7 and 14 days post injection, respectively. The demyelination could be induced as early as 5 days post tamoxifen injection, since in our unpublished data, we could observe recombination as early as 5 days post injection. In this way, the *qkI* conditional allele would

provide an invaluable evidence to the role of QKI proteins in promoting remyelination which could be extrapolated to humans in the hope of finding means to promote remyelination in MS.

More recently, a novel role for QKI in gliomas was discovered. A Myb-QKI fusion protein was identified as a specific and single candidate driver event in angiocentric gliomas (AG), a pediatric low-grade glioma (Bandopadhayay et al., 2016). As the name suggests, these tumours grow surrounding blood vessels, yet the cellular origin of the tumours remains unknown. Angiocentric gliomas exhibit a QKI haploinsufficiency whereas GBM are characterized by biallelic loss of QKI, therefore, possibly indicating that QKI haploinsufficiency accounts for the low-grade nature of AG compared to the aggressive nature of GBM (Bandopadhayay et al., 2016). Moreover, it is likely that the loss of one allele of QKI is what drives the angiocentric pattern of AG, otherwise those tumours would grow similar to other gliomas. The floxed *qkI* allele along with a transgenic mouse expressing a Cre-inducible Myb-QKI fusion protein would provide a vital model to exactly pinpoint the cell type from which these tumours originate.

4.3 Perspectives on regulation of qkI expression and function

Despite decades of research, there remains many aspects of QKI research to uncover. QKI is expressed in multiple tissues starting from embryonic development and exhibit a spatially and temporally regulated expression patterns. Several potential transcription factors binding sites were found in the *qkI* promoter (section 1.2.7.1), yet only two studies have indeed shown specific transcription factors binding to *qkI* promoter and controlling its expression (C/EBPα in monocyte and KLF2 in endothelial cells). Therefore, further studies are necessary to address transcriptional regulation of *qkI* expression in different tissues. Specifically, in OLs, no functional studies have aimed at understanding the transcription of *qkI*.

When examining the *qkI* gene, over 200 QREs can be identified. These QREs are localized both in introns as well as exons. Therefore, it is plausible to speculate that QKI proteins can regulate several aspects of their RNA metabolism. The *qkI* gene displays intriguing alternative splicing patterns that usually change during development. In the developing brain and heart, QKI-5 isoform is the first to be detected (Justice and Bode, 1988, Hardy, 1998b) followed by QKI-6 and QKI-7. Bockbrader et al, in 2008, have sequence analyzed the intron-exon boundaries of *qkI* and observed several interesting features (Bockbrader and Feng, 2008). The alternative splicing of the *qkI* gene occurs mainly at the 3' end of exon 6. All alternatively spliced introns follow the GU-

AG rule, yet, none of the acceptor sites at the intron-exon boundaries downstream of exon 6 satisfy this rule (Bockbrader and Feng, 2008). Interestingly, those mismatched bases at the acceptor sites are evolutionary conserved and found in all vertebrate species. This indicates that those mismatches might result in weaker binding of the spliceosome complex and therefore might need help from specific splicing factors to mediate the alternative splicing (Bockbrader and Feng, 2008). Yet, another intriguing aspect of *qkI* alternative splicing is that QKI-5 isoform, which seems to be the default isoforms during embryogenesis, has its specific exons 7c and 8 at the most 3'-end of the gene and displays the highest number of mismatches at the acceptor sites (Bockbrader and Feng, 2008). The authors of this study have hypothesized that splicing suppressors bind upstream of exon 7c to inhibit inclusion of QKI-6 and QKI-7 specific exons and allow generation of the QKI-5 transcript and that the downregulation of these splicing suppressors allow generation of QKI-6 and QKI-7. However, in chapter 3, we show that the absence of QKI-5 from OLs is sufficient to inhibit the generation of *qkI-6* and *qkI-7* transcripts and that transfection of the QKI-5 isoform in HEK293T cells is sufficient to increase the inclusion of QKI-7 exon 7c (Darbelli et al., 2017). Moreover, the QKI mRNA transcripts are differentially affected in qk^{v} mice. The data presented in chapter 3 provides an explanation to the complete absence of QKI-6/QKI-7 seen in qk^{v} mice as there is no QKI-5 expression detected in the severely affected areas which might lead to the lack *qkI-6* and *qkI-7* transcript production.

The QKI isoforms harbour long 3'-UTRs raising the possibility that these mRNAs could exhibit differential stability. QKI-5 has a unique 3'-UTR whereas QKI-6 and QKI-7 share overlapping regions and contain numerous AT-rich regions that may target those isoforms for the canonical mRNA decay mechanism (Garneau et al., 2007). The predicted QREs in mouse are also found in human indicating the QKI regulation of its stability and expression may be conserved among species.

Due to their localization, differential expression and RNA stability, QKI proteins exert different effects on their target RNA depending on the spatial and temporal expression of that specific RNA target. An example is MBP mRNA that is retained in the nucleus with overexpression of QKI-5, with the nuclear retention being released upon expression of QKI-6/QKI-7 (Larocque et al., 2002). Therefore, a challenge remains which is to delineate the function of each specific QKI isoform in regulating developmental-specific RNA ligands. However, the overlapping 3'-UTRs greatly hinder the targeting of specific QKI isoforms. Moreover, QKI

proteins may regulate several aspects of RNA metabolism for a specific RNA ligand as is the case with MBP. In chapter 3, we have added another layer of regulation of MBP RNA metabolism by identifying it as an alternatively spliced target of QKI. It is also plausible to speculate that QKI proteins may also regulate MBP mRNA stability, transport to distal OL processes as well as translation which are all aspects that merit further investigation.

In 2005, our lab has generated a list of about 1400 potential targets of QKI using *in vitro* assays. However, the bioinformatically defined RNA ligands did not predict OL-specific functional targets involved in OLs development. Our transcriptomic analysis has led to identification of *in vivo* targets of QKI in OLs. Yet the pool of mRNA targets that are critical at each stage of OL development remains elusive. This could be circumvented by following the protocol optimized by Wu JQ and Barres BA labs (Zhang et al., 2014b) to isolate the different stages of OLs during development and perform transcriptomic analysis in the presence and absence of QKI. This would greatly improve our understanding of the QKI specific targets at each stage of OL development.

Several signalling pathways play important roles in regulating oligodendrocyte development and myelination. The STAR family proteins function to link signal transduction to RNA metabolism. Yet, for QKI, Fyn kinase is the only member of the Src-PTKs that has been demonstrated to negatively impact the function of QKI proteins through tyrosine phosphorylation (Lu et al., 2005). However, other kinases have been shown to play important roles during OLs development. Cdk-5 is a serine/threonine kinase that is activated upon OL differentiation and plays an important role in supporting the development of OL processes (Lew et al., 1994, Miyamoto et al., 2008). Forced Akt signalling in transgenic mice leads to overproduction of myelin (Flores et al., 2008) and the MAPK pathway has been shown to play roles in OL migration, proliferation, survival and differentiation (Fragoso et al., 2007). Nonetheless, further investigations are necessary to demonstrate whether any of these signalling pathways could be linked to QKI function.

Lastly, most of QKI research has focused on understanding its diverse roles in regulating aspects of RNA metabolism as well as identifying specific targets of QKI especially using genome-wide analyses. Yet, the molecular mechanisms through which QKI regulates these processes is largely unknown and very little is known about the interacting partners of QKI proteins. Given its vital role in regulating alternative splicing in different tissues and cell types, it is imperative to

investigate how QKI protein may recruit the spliceosome complex or other spliceosome-interacting proteins to mediate alternative splicing. One of the ways to screen for physiological protein-protein interactions (including weak and transient interaction) could be done by performing the highly innovative BioID (Roux et al., 2013). This technique relies on expressing a promiscuous biotin ligase fused to a protein of interest (in this case, QKI) which biotinylates endogenous proteins based on proximity. This allows for subsequent isolation of interacting proteins and identification by mass spectrometry. The advantage of applying this method to identifying interactors of QKI is that individual isoforms can be fused to the biotin ligase to identify unique interacting partners for each of the QKI isoforms. This will help shed some light on the mechanisms by which QKI proteins mediate their functions and will greatly improve our understanding of how QKI proteins carry their functions in different cellular processes and further impact human diseases providing potential targeting mechanisms to either enhance or suppress their function.

4.4 Concluding remarks

In this study, we have provided evidence that indeed QKI proteins are master regulators of OLs development and myelination, generated the first published *qkI* conditional allele, as well as provided a novel function for QKI in regulating myelin maintenance. Additionally, we identified *in vivo* targets of QKI and showed that alternative splicing of paranodal Nfasc-155 is regulated by QKI. Years of research have postulated that QKI proteins can regulate their own RNA metabolism and in Chapter 3, we have provided evidence that indeed QKI proteins can regulate their own alternative splicing.

RNA processing is critical for maintaining cellular and physiological homeostasis. Since Quaking proteins are key components in RNA metabolism, altering their expression would have major implications for human diseases. From the abundance of direct and indirect links to neurological disease, it is apparent that the functions of QKI merits further investigations to fully understand how the deregulation of QKI protein expression could lead to downstream changes resulting in disease pathogenesis. The generation of the *qkI* conditional knockout mice provides new tools to further study the role of the QKI RBPs in different tissues and cell-types. The association of the QKI proteins with human pathologies show that future work is likely to identify

more links with human diseases. This may provide a basis for therapeutic interventions that would target the deregulated QKI isoform in a specific pathology.

References

Aberg, K., Saetre, P., Jareborg, N., and Jazin, E. (2006a). Human QKI, a potential regulator of mRNA expression of human oligodendrocyte-related genes involved in schizophrenia. Proc Natl Acad Sci U S A *103*, 7482-7487.

Aberg, K., Saetre, P., Lindholm, E., Ekholm, B., Pettersson, U., Adolfsson, R., and Jazin, E. (2006b). Human QKI, a new candidate gene for schizophrenia involved in myelination. Am J Med Genet B Neuropsychiatr Genet *141B*, 84-90.

Aggarwal, S., Snaidero, N., Pahler, G., Frey, S., Sanchez, P., Zweckstetter, M., Janshoff, A., Schneider, A., Weil, M.T., Schaap, I.A.*, et al.* (2013). Myelin membrane assembly is driven by a phase transition of myelin basic proteins into a cohesive protein meshwork. PLoS Biol *11*, e1001577.

Aggarwal, S., Yurlova, L., Snaidero, N., Reetz, C., Frey, S., Zimmermann, J., Pahler, G., Janshoff, A., Friedrichs, J., Muller, D.J.*, et al.* (2011). A size barrier limits protein diffusion at the cell surface to generate lipid-rich myelin-membrane sheets. Dev Cell *21*, 445-456.

Allemand, E., Batsche, E., and Muchardt, C. (2008). Splicing, transcription, and chromatin: a menage a trois. Curr Opin Genet Dev *18*, 145-151.

Almazan, G., Afar, D.E.H., and Bell, J.C. (1993). Phosphorylation and disruption of intermediate filament protein in oligodendrocyte precursor cultures treated with calyculin A. J Neurosci Res *36*, 163-172.

Amor, S., Groome, N., Linington, C., Morris, M.M., Dornmair, K., Gardinier, M.V., Matthieu, J.M., and Baker, D. (1994). Identification of epitopes of myelin oligodendrocyte glycoprotein for the induction of experimental allergic encephalomyelitis in SJL and Biozzi AB/H mice. J Immunol *153*, 4349-4356.

Anders, S., Reyes, A., and Huber, W. (2012). Detecting differential usage of exons from RNA-seq data. Genome Res *22*, 2008-2017.

Ango, F., di Cristo, G., Higashiyama, H., Bennett, V., Wu, P., and Huang, Z.J. (2004). Ankyrin-based subcellular gradient of neurofascin, an immunoglobulin family protein, directs GABAergic innervation at purkinje axon initial segment. Cell *119*, 257-272.

Armstrong, R.C., Harvath, L., and Dubois-Dalcq, M.E. (1990). Type 1 astrocytes and oligodendrocyte-type 2 astrocyte glial progenitors migrate toward distinct molecules. J Neurosci Res *27*, 400-407.

Arning, S., Gruter, P., Bilbe, G., and Kramer, A. (1996). Mammalian splicing factor SF1 is encoded by variant cDNAs and binds to RNA. RNA *2*, 794-810.

Artzt, K., and Wu, J.I. (2010). STAR trek: An introduction to STAR family proteins and review of quaking (QKI). Adv Exp Med Biol *693*, 1-24.

Ashwal-Fluss, R., Meyer, M., Pamudurti, N.R., Ivanov, A., Bartok, O., Hanan, M., Evantal, N., Memczak, S., Rajewsky, N., and Kadener, S. (2014). circRNA biogenesis competes with pre-mRNA splicing. Mol Cell *56*, 55-66.

Assmann, J.C., Korbelin, J., and Schwaninger, M. (2016). Genetic manipulation of brain endothelial cells in vivo. Biochim Biophys Acta *1862*, 381-394.

Babic, I., Jakymiw, A., and Fujita, D.J. (2004). The RNA binding protein Sam68 is acetylated in tumor cell lines, and its acetylation correlates with enhanced RNA binding activity. Oncogene *23*, 3781-3789.

Backx, L., Fryns, J.P., Marcelis, C., Devriendt, K., Vermeesch, J., and Van Esch, H. (2010). Haploinsufficiency of the gene Quaking (QKI) is associated with the 6q terminal deletion syndrome. Am J Med Genet A *152A*, 319-326.

Baehrecke, E.H. (1997). who encodes a KH RNA binding protein that functions in muscle development. Development *124*, 1323-1332.

Bandopadhayay, P., Ramkissoon, L.A., Jain, P., Bergthold, G., Wala, J., Zeid, R., Schumacher, S.E., Urbanski, L., O'Rourke, R., Gibson, W.J.*, et al.* (2016). MYB-QKI rearrangements in angiocentric glioma drive tumorigenicity through a tripartite mechanism. Nat Genet *48*, 273-282.

Banerjee, S., Sousa, A.D., and Bhat, M.A. (2006). Organization and function of septate junctions: an evolutionary perspective. Cell Biochem Biophys *46*, 65-77.

Bansal, R., Kumar, M., Murray, K., Morrison, R.S., and Pfeiffer, S.E. (1996). Regulation of FGF receptors in the oligodendrocyte lineage. Mol Cell Neurosci *7*, 263-275.

Barateiro, A., Brites, D., and Fernandes, A. (2016). Oligodendrocyte Development and Myelination in Neurodevelopment: Molecular Mechanisms in Health and Disease. Curr Pharm Des *22*, 656-679.

Barbarese, E. (1991). Spatial distribution of myelin basic protein mRNA and polypeptide in quaking oligodendrocytes in culture. J Neurosci Res *29*, 271-281.

Barbarese, E., Brumwell, C., Kwon, S., Cui, H., and Carson, J.H. (1999). RNA on the road to myelin. J Neurocytol *28*, 263-270.

Baron, W., Shattil, S.J., and ffrench-Constant, C. (2002). The oligodendrocyte precursor mitogen PDGF stimulates proliferation by activation of alpha(v)beta3 integrins. EMBO J *21*, 1957-1966.

Barres, B.A., Hart, I.K., Coles, H.S., Burne, J.F., Voyvodic, J.T., Richardson, W.D., and Raff, M.C. (1992). Cell death and control of cell survival in the oligodendrocyte lineage. Cell *70*, 31-46.

Barres, B.A., Jacobson, M.D., Schmid, R., Sendtner, M., and Raff, M.C. (1993). Does oligodendrocyte survival depend on axons? Curr Biol *3*, 489-497.

Barres, B.A., Lazar, M.A., and Raff, M.C. (1994). A novel role for thyroid hormone, glucocorticoids and retinoic acid in timing oligodendrocyte development. Development *120*, 1097-1108.

Barres, B.A., and Raff, M.C. (1994). Control of oligodendrocyte number in the developing rat optic nerve. Neuron *12*, 935-942.

Barres, B.A., and Raff, M.C. (1999). Axonal control of oligodendrocyte development. J Cell Biol *147*, 1123-1128.

Basak, S., Raju, K., Babiarz, J., Kane-Goldsmith, N., Koticha, D., and Grumet, M. (2007). Differential expression and functions of neuronal and glial neurofascin isoforms and splice variants during PNS development. Dev Biol *311*, 408-422.

Bauer, N.G., Richter-Landsberg, C., and Ffrench-Constant, C. (2009). Role of the oligodendroglial cytoskeleton in differentiation and myelination. Glia *57*, 1691-1705.

Baumann, N., and Pham-Dinh, D. (2001). Biology of oligodendrocyte and myelin in the mammalian central nervous system. Physiol Rev *81*, 871-927.

Beirowski, B., Wong, K.M., Babetto, E., and Milbrandt, J. (2017). mTORC1 promotes proliferation of immature Schwann cells and myelin growth of differentiated Schwann cells. Proc Natl Acad Sci U S A *114*, E4261-E4270

Bennett, W.I., Gall, A.M., Southard, J.L., and Sidman, R.L. (1971). Abnormal spermiogenesis in quaking, a myelin-deficient mutant mouse. Biol Reprod *5*, 30-58.

Berghs, S., Aggujaro, D., Dirkx, R., Jr., Maksimova, E., Stabach, P., Hermel, J.M., Zhang, J.P., Philbrick, W., Slepnev, V., Ort, T.*, et al.* (2000). betaIV spectrin, a new spectrin localized at axon initial segments and nodes of ranvier in the central and peripheral nervous system. J Cell Biol *151*, 985-1002.

Berglund, E.O., Murai, K.K., Fredette, B., Sekerková, G., Marturano, B., Weber, L., Mugnaini, E., and Ranscht, B. (1999). Ataxia and abnormal cerebellar microorganization in mice with ablated contactin gene expression. Neuron *24*, 739-750.

Berglund, J.A., Abovich, N., and Rosbash, M. (1998). A cooperative interaction between U2AF65 and mBBP/SF1 facilitates branchpoint region recognition. Genes Dev *12*, 858-867.

Beuck, C., Qu, S., Fagg, W.S., Ares, M., Jr., and Williamson, J.R. (2012). Structural analysis of the quaking homodimerization interface. J Mol Biol *423*, 766-781.

Bhat, M.A. (2003). Molecular organization of axo-glial junctions. Curr Opin Neurobiol *13*, 552-559.

Bhat, M.A., Rios, J.C., Lu, Y., Garcia-Fresco, G.P., Ching, W., St Martin, M., Li, J., Einheber, S., Chesler, M., Rosenbluth, J.*, et al.* (2001). Axon-glia interactions and the domain organization of myelinated axons requires neurexin IV/Caspr/Paranodin. Neuron *30*, 369-383.

Bian, Y., Wang, L., Lu, H., Yang, G., Zhang, Z., Fu, H., Lu, X., Wei, M., Sun, J., Zhao, Q.*, et al.* (2012). Downregulation of tumor suppressor QKI in gastric cancer and its implication in cancer prognosis. Biochem Biophys Res Commun *422*, 187-193.

Binan, L., Mazzaferri, J., Choquet, K., Lorenzo, L.E., Wang, Y.C., Affar el, B., De Koninck, Y., Ragoussis, J., Kleinman, C.L., and Costantino, S. (2016). Live single-cell laser tag. Nat Commun *7*, 11636.

Blackburn, D., Sargsyan, S., Monk, P.N., and Shaw, P.J. (2009). Astrocyte function and role in motor neuron disease: a future therapeutic target? Glia *57*, 1251-1264.

Bockbrader, K., and Feng, Y. (2008). Essential function, sophisticated regulation and pathological impact of the selective RNA-binding protein QKI in CNS myelin development. Future Neurol *3*, 655-668.

Bode, V.C. (1984). Ethylnitrosourea mutagenesis and the isolation of mutant alleles for specific genes located in the T region of mouse chromosome 17. Genetics *108*, 457-470.

Bohnsack, B.L., Lai, L., Dolle, P., and Hirschi, K.K. (2004). Signaling hierarchy downstream of retinoic acid that independently regulates vascular remodeling and endothelial cell proliferation. Genes Dev *18*, 1345-1358.

Bohnsack, B.L., Lai, L., Northrop, J.L., Justice, M.J., and Hirschi, K.K. (2006). Visceral endoderm function is regulated by quaking and required for vascular development. Genesis *44*, 93-104.

Boiko, T., Rasband, M.N., Levinson, S.R., Caldwell, J.H., Mandel, G., Trimmer, J.S., and Matthews, G. (2001). Compact myelin dictates the differential targeting of two sodium channel isoforms in the same axon. Neuron *30*, 91-104.

Boison, D., and Stoffel, W. (1994). Disruption of the compacted myelin sheath of axons of the central nervous system in proteolipid protein-deficient mice. Proc Natl Acad Sci U S A *91*, 11709-11713.

Bolger, A.M., Lohse, M., and Usadel, B. (2014). Trimmomatic: a flexible trimmer for Illumina sequence data. Bioinformatics *30*, 2114-2120.

Bonnet, A., Lambert, G., Ernest, S., Dutrieux, F.X., Coulpier, F., Lemoine, S., Lobbardi, R., and Rosa, F.M. (2017). Quaking RNA-Binding Proteins Control Early Myofibril Formation by Modulating Tropomyosin. Dev Cell *42*, 527-541 e524.

Boyle, M.E., Berglund, E.O., Murai, K.K., Weber, L., Peles, E., and Ranscht, B. (2001). Contactin orchestrates assembly of the septate-like junctions at the paranode in myelinated peripheral nerve. Neuron *30*, 385-397.

Brakebusch, C., Seidenbecher, C.I., Asztely, F., Rauch, U., Matthies, H., Meyer, H., Krug, M., Bockers, T.M., Zhou, X., Kreutz, M.R.*, et al.* (2002). Brevican-deficient mice display impaired hippocampal CA1 long-term potentiation but show no obvious deficits in learning and memory. Mol Cell Biol *22*, 7417-7427.

Brosseau, J.P., Lucier, J.F., Nwilati, H., Thibault, P., Garneau, D., Gendron, D., Durand, M., Couture, S., Lapointe, E., Prinos, P.*, et al.* (2014). Tumor microenvironment-associated modifications of alternative splicing. RNA *20*, 189-201.

Brownlees, J., Ackerley, S., Grierson, A.J., Jacobsen, N.J., Shea, K., Anderton, B.H., Leigh, P.N., Shaw, C.E., and Miller, C.C. (2002). Charcot-Marie-Tooth disease neurofilament mutations disrupt neurofilament assembly and axonal transport. Hum Mol Genet *11*, 2837-2844.

Bujalka, H., Koenning, M., Jackson, S., Perreau, V.M., Pope, B., Hay, C.M., Mitew, S., Hill, A.F., Lu, Q.R., Wegner, M.*, et al.* (2013). MYRF is a membrane-associated transcription factor that autoproteolytically cleaves to directly activate myelin genes. PLoS Biol *11*, e1001625.

Bunge, M.B., Bunge, R.P., and Pappas, G.D. (1962). Electron microscopic demonstration of connections between glia and myelin sheaths in the developing mammalian central nervous system. J Cell Biol *12*, 448-453.

Bunge, R.P. (1968). Glial cells and the central myelin sheath. Physiol Rev *48*, 197-251.

Burd, C.G., and Dreyfuss, G. (1994). Conserved structures and diversity of functions of RNA-binding proteins. Science *265*, 615-621.

Burkarth, N., Kriebel, M., Kranz, E.U., and Volkmer, H. (2007). Neurofascin regulates the formation of gephyrin clusters and their subsequent translocation to the axon hillock of hippocampal neurons. Mol Cell Neurosci *36*, 59-70.

Butt, A.M., and Ransom, B.R. (1989). Visualization of oligodendrocytes and astrocytes in the intact rat optic nerve by intracellular injection of lucifer yellow and horseradish peroxidase. Glia *2*, 470-475.

Buttermore, E.D., Dupree, J.L., Cheng, J., An, X., Tessarollo, L., and Bhat, M.A. (2011). The cytoskeletal adaptor protein band 4.1B is required for the maintenance of paranodal axoglial septate junctions in myelinated axons. J Neurosci *31*, 8013-8024.

Buttermore, E.D., Piochon, C., Wallace, M.L., Philpot, B.D., Hansel, C., and Bhat, M.A. (2012). Pinceau organization in the cerebellum requires distinct functions of neurofascin in Purkinje and basket neurons during postnatal development. J Neurosci *32*, 4724-4742.

Cahoy, J.D., Emery, B., Kaushal, A., Foo, L.C., Zamanian, J.L., Christopherson, K.S., Xing, Y., Lubischer, J.L., Krieg, P.A., Krupenko, S.A., *et al.* (2008). A transcriptome database for astrocytes, neurons, and oligodendrocytes: a new resource for understanding brain development and function. J Neurosci *28*, 264-278.

Cai, J., Qi, Y., Hu, X., Tan, M., Liu, Z., Zhang, J., Li, Q., Sander, M., and Qiu, M. (2005). Generation of oligodendrocyte precursor cells from mouse dorsal spinal cord independent of Nkx6 regulation and Shh signaling. Neuron *45*, 41-53.

Cai, J., Zhu, Q., Zheng, K., Li, H., Qi, Y., Cao, Q., and Qiu, M. (2010). Co-localization of Nkx6.2 and Nkx2.2 homeodomain proteins in differentiated myelinating oligodendrocytes. Glia *58*, 458-468.

Calabretta, S., and Richard, S. (2015). Emerging Roles of Disordered Sequences in RNA-Binding Proteins. Trends Biochem Sci *40*, 662-672.

Calver, A.R., Hall, A.C., Yu, W.P., Walsh, F.S., Heath, J.K., Betsholtz, C., and Richardson, W.D. (1998). Oligodendrocyte population dynamics and the role of PDGF in vivo. Neuron *20*, 869-882.

Campagnoni, A.T., and Macklin, W.B. (1988). Cellular and molecular aspects of myelin protein gene expression. Mol Neurobiol *2*, 41-89.

Carnow, T.B., Carson, J.H., Brostoff, S.W., and Hogan, E.L. (1984). Myelin basic protein gene expression in quaking, jimpy, and myelin synthesis-deficient mice. Dev Biol *106*, 38-44.

Carpenter, S., Ricci, E.P., Mercier, B.C., Moore, M.J., and Fitzgerald, K.A. (2014). Post-transcriptional regulation of gene expression in innate immunity. Nat Rev Immunol *14*, 361-376.

Chandran, S., Kato, H., Gerreli, D., Compston, A., Svendsen, C.N., and Allen, N.D. (2003). FGF-dependent generation of oligodendrocytes by a hedgehog-independent pathway. Development *130*, 6599-6609.

Chang, K.J., Redmond, S.A., and Chan, J.R. (2016). Remodeling myelination: implications for mechanisms of neural plasticity. Nat Neurosci *19*, 190-197.

Charles, P., Hernandez, M.P., Stankoff, B., Aigrot, M.S., Colin, C., Rougon, G., Zalc, B., and Lubetzki, C. (2000). Negative regulation of central nervous system myelination by polysialylated-neural cell adhesion molecule. Proc Natl Acad Sci U S A *97*, 7585-7590.

Charles, P., Tait, S., Faivre-Sarrailh, C., Barbin, G., Gunn-Moore, F., Denisenko-Nehrbass, N., Guennoc, A.M., Girault, J.A., Brophy, P.J., and Lubetzki, C. (2002). Neurofascin is a glial receptor for the paranodin/Caspr-contactin axonal complex at the axoglial junction. Curr Biol *12*, 217-220.

Chen, A.J., Paik, J.H., Zhang, H., Shukla, S.A., Mortensen, R., Hu, J., Ying, H., Hu, B., Hurt, J., Farny, N.*, et al.* (2012). STAR RNA-binding protein Quaking suppresses cancer via stabilization of specific miRNA. Genes Dev *26*, 1459-1472.

Chen, C., Luo, F., Yang, Q., Wang, D., Yang, P., Xue, J., Dai, X., Liu, X., Xu, H., Lu, J.*, et al.* (2018). NF-kappaB-regulated miR-155, via repression of QKI, contributes to the acquisition of CSC-like phenotype during the neoplastic transformation of hepatic cells induced by arsenite. Mol Carcinog *57*, 483-493.

Chen, T., and Richard, S. (1998). Structure-function analysis of Qk1: a lethal point mutation in mouse quaking prevents homodimerization. Mol Cell Biol *18*, 4863-4871.

Chen, X., Ku, L., Mei, R., Liu, G., Xu, C., Wen, Z., Zhao, X., Wang, F., Xiao, L., and Feng, Y. (2017). Novel schizophrenia risk factor pathways regulate FEZ1 to advance oligodendroglia development. Transl Psychiatry *7*, 1293.

Chen, Y., Wu, H., Wang, S., Koito, H., Li, J., Ye, F., Hoang, J., Escobar, S.S., Gow, A., Arnett, H.A.*, et al.* (2009). The oligodendrocyte-specific G protein-coupled receptor GPR17 is a cell-intrinsic timer of myelination. Nat Neurosci *12*, 1398-1406.

Chenard, C.A., and Richard, S. (2008). New implications for the QUAKING RNA binding protein in human disease. J Neurosci Res *86*, 233-242.

Christensen, M., and Schratt, G.M. (2009). microRNA involvement in developmental and functional aspects of the nervous system and in neurological diseases. Neurosci Lett *466*, 55-62.

Chun, S.J., Rasband, M.N., Sidman, R.L., Habib, A.A., and Vartanian, T. (2003). Integrin-linked kinase is required for laminin-2-induced oligodendrocyte cell spreading and CNS myelination. J Cell Biol *163*, 397-408.

Cochrane, A., Kelaini, S., Tsifaki, M., Bojdo, J., Vila-Gonzalez, M., Drehmer, D., Caines, R., Magee, C., Eleftheriadou, M., Hu, Y.*, et al.* (2017). Quaking Is a Key Regulator of Endothelial Cell Differentiation, Neovascularization, and Angiogenesis. Stem Cells *35*, 952-966.

Collard, J.F., Cote, F., and Julien, J.P. (1995). Defective axonal transport in a transgenic mouse model of amyotrophic lateral sclerosis. Nature *375*, 61-64.

Collinson, J.M., Marshall, D., Gillespie, C.S., and Brophy, P.J. (1998). Transient expression of neurofascin by oligodendrocytes at the onset of myelinogenesis: implications for mechanisms of axon-glial interaction. Glia *23*, 11-23.

Colognato, H., Baron, W., Avellana-Adalid, V., Relvas, J.B., Baron-Van Evercooren, A., Georges-Labouesse, E., and ffrench-Constant, C. (2002). CNS integrins switch growth factor signalling to promote target-dependent survival. Nat Cell Biol *4*, 833-841.

Colognato, H., Ramachandrappa, S., Olsen, I.M., and ffrench-Constant, C. (2004). Integrins direct Src family kinases to regulate distinct phases of oligodendrocyte development. J Cell Biol *167*, 365-375.

Conn, S.J., Pillman, K.A., Toubia, J., Conn, V.M., Salmanidis, M., Phillips, C.A., Roslan, S., Schreiber, A.W., Gregory, P.A., and Goodall, G.J. (2015). The RNA binding protein quaking regulates formation of circRNAs. Cell *160*, 1125-1134.

Cooper, E.C. (2011). Made for "anchorin": Kv7.2/7.3 (KCNQ2/KCNQ3) channels and the modulation of neuronal excitability in vertebrate axons. Semin Cell Dev Biol *22*, 185-192.

Cote, J., Boisvert, F.M., Boulanger, M.C., Bedford, M.T., and Richard, S. (2003). Sam68 RNA binding protein is an in vivo substrate for protein arginine N-methyltransferase 1. Mol Biol Cell *14*, 274-287.

Cox, R.D., Hugill, A., Shedlovsky, A., Noveroske, J.K., Best, S., Justice, M.J., Lehrach, H., and Dove, W.F. (1999). Contrasting effects of ENU induced embryonic lethal mutations of the quaking gene. Genomics *57*, 333-341.

Craner, M.J., Newcombe, J., Black, J.A., Hartle, C., Cuzner, M.L., and Waxman, S.G. (2004). Molecular changes in neurons in multiple sclerosis: altered axonal expression of Nav1.2 and Nav1.6 sodium channels and Na+/Ca2+ exchanger. Proc Natl Acad Sci U S A *101*, 8168-8173.

Cui, Q.L., Zheng, W.H., Quirion, R., and Almazan, G. (2005). Inhibition of Src-like kinases reveals Akt-dependent and -independent pathways in insulin-like growth factor I-mediated oligodendrocyte progenitor survival. J Biol Chem *280*, 8918-8928.

Czopka, T., Ffrench-Constant, C., and Lyons, D.A. (2013). Individual oligodendrocytes have only a few hours in which to generate new myelin sheaths in vivo. Dev Cell *25*, 599-609.

Danan-Gotthold, M., Golan-Gerstl, R., Eisenberg, E., Meir, K., Karni, R., and Levanon, E.Y. (2015). Identification of recurrent regulated alternative splicing events across human solid tumors. Nucleic Acids Res *43*, 5130-5144.

Darbelli, L., Choquet, K., Richard, S., and Kleinman, C.L. (2017). Transcriptome profiling of mouse brains with qkI-deficient oligodendrocytes reveals major alternative splicing defects including self-splicing. Sci Rep *7*, 7554.

Darbelli, L., and Richard, S. (2016). Emerging functions of the Quaking RNA-binding proteins and link to human diseases. Wiley Interdiscip Rev RNA *7*, 399-412.

Darbelli, L., Vogel, G., Almazan, G., and Richard, S. (2016). Quaking Regulates Neurofascin 155 Expression for Myelin and Axoglial Junction Maintenance. J Neurosci *36*, 4106-4120.

Darnell, R.B. (2013). RNA protein interaction in neurons. Annu Rev Neurosci *36*, 243-270.

Daubner, G.M., Brummer, A., Tocchini, C., Gerhardy, S., Ciosk, R., Zavolan, M., and Allain, F.H. (2014). Structural and functional implications of the QUA2 domain on RNA recognition by GLD-1. Nucleic Acids Res *42*, 8092-8105.

Davis, J.Q., and Bennett, V. (1994). Ankyrin binding activity shared by the neurofascin/L1/NrCAM family of nervous system cell adhesion molecules. J Biol Chem *269*, 27163-27166.

Davis, J.Q., Lambert, S., and Bennett, V. (1996). Molecular composition of the node of Ranvier: identification of ankyrin-binding cell adhesion molecules neurofascin (mucin+/third FNIII domain-) and NrCAM at nodal axon segments. J Cell Biol *135*, 1355-1367.

Davis, J.Q., McLaughlin, T., and Bennett, V. (1993). Ankyrin-binding proteins related to nervous system cell adhesion molecules: candidates to provide transmembrane and intercellular connections in adult brain. J Cell Biol *121*, 121-133.

Davis, K.L., Stewart, D.G., Friedman, J.I., Buchsbaum, M., Harvey, P.D., Hof, P.R., Buxbaum, J., and Haroutunian, V. (2003). White matter changes in schizophrenia: evidence for myelin-related dysfunction. Archives of general psychiatry *60*, 443-456.

De Boulle, K., Verkerk, A.J., Reyniers, E., Vits, L., Hendrickx, J., Van Roy, B., Van den Bos, F., de Graaff, E., Oostra, B.A., and Willems, P.J. (1993). A point mutation in the FMR-1 gene associated with fragile X mental retardation. Nat Genet *3*, 31-35.

de Bruin, R.G., Shiue, L., Prins, J., de Boer, H.C., Singh, A., Fagg, W.S., van Gils, J.M., Duijs, J.M., Katzman, S., Kraaijeveld, A.O.*, et al.* (2016a). Quaking promotes monocyte differentiation into pro-atherogenic macrophages by controlling pre-mRNA splicing and gene expression. Nat Commun *7*, 10846.

de Bruin, R.G., van der Veer, E.P., Prins, J., Lee, D.H., Dane, M.J., Zhang, H., Roeten, M.K., Bijkerk, R., de Boer, H.C., Rabelink, T.J.*, et al.* (2016b). The RNA-binding protein quaking maintains endothelial barrier function and affects VE-cadherin and beta-catenin protein expression. Sci Rep *6*, 21643.

de Miguel, F.J., Pajares, M.J., Martinez-Terroba, E., Ajona, D., Morales, X., Sharma, R.D., Pardo, F.J., Rouzaut, A., Rubio, A., Montuenga, L.M.*, et al.* (2016). A large-scale analysis of alternative splicing reveals a key role of QKI in lung cancer. Mol Oncol *10*, 1437-1449.

de Rosbo, N.K., and Ben-Nun, A. (1998). T-cell responses to myelin antigens in multiple sclerosis; relevance of the predominant autoimmune reactivity to myelin oligodendrocyte glycoprotein. J Autoimmun *11*, 287-299.

Decker, L., Avellana-Adalid, V., Nait-Oumesmar, B., Durbec, P., and Baron-Van Evercooren, A. (2000). Oligodendrocyte precursor migration and differentiation: combined effects of PSA residues, growth factors, and substrates. Mol Cell Neurosci *16*, 422-439.

Delmont, E., Manso, C., Querol, L., Cortese, A., Berardinelli, A., Lozza, A., Belghazi, M., Malissart, P., Labauge, P., Taieb, G.*, et al.* (2017). Autoantibodies to nodal isoforms of

neurofascin in chronic inflammatory demyelinating polyneuropathy. Brain *140*, 1851-1858.

Denisenko-Nehrbass, N., Oguievetskaia, K., Goutebroze, L., Galvez, T., Yamakawa, H., Ohara, O., Carnaud, M., and Girault, J.A. (2003). Protein 4.1B associates with both Caspr/paranodin and Caspr2 at paranodes and juxtaparanodes of myelinated fibres. Eur J Neurosci *17*, 411-416.

Derfuss, T., Linington, C., Hohlfeld, R., and Meinl, E. (2010). Axo-glial antigens as targets in multiple sclerosis: implications for axonal and grey matter injury. J Mol Med (Berl) *88*, 753-761.

Di Fruscio, M., Chen, T., and Richard, S. (1999). Characterization of Sam68-like mammalian proteins SLM-1 and SLM-2: SLM-1 is a Src substrate during mitosis. Proc Natl Acad Sci U S A *96*, 2710-2715.

Dobin, A., Davis, C.A., Schlesinger, F., Drenkow, J., Zaleski, C., Jha, S., Batut, P., Chaisson, M., and Gingeras, T.R. (2013). STAR: ultrafast universal RNA-seq aligner. Bioinformatics *29*, 15-21.

Doerflinger, N.H., Macklin, W.B., and Popko, B. (2003). Inducible site-specific recombination in myelinating cells. Genesis *35*, 63-72.

Doukhanine, E., Gavino, C., Haines, J.D., Almazan, G., and Richard, S. (2010). The QKI-6 RNA binding protein regulates actin-interacting protein-1 mRNA stability during oligodendrocyte differentiation. Mol Biol Cell *21*, 3029-3040.

Dziembowska, M., Tham, T.N., Lau, P., Vitry, S., Lazarini, F., and Dubois-Dalcq, M. (2005). A role for CXCR4 signaling in survival and migration of neural and oligodendrocyte precursors. Glia *50*, 258-269.

Ebel, J., Beuter, S., Wuchter, J., Kriebel, M., and Volkmer, H. (2014). Organisation and control of neuronal connectivity and myelination by cell adhesion molecule neurofascin. Advances in neurobiology *8*, 231-247.

Ebersole, T.A., Chen, Q., Justice, M.J., and Artzt, K. (1996a). The quaking gene product necessary in embryogenesis and myelination combines features of RNA binding and signal transduction proteins. Nat Genet *12*, 260-265.

Ebersole, T.A., Chen, Q., Justice, M.J., and Artzt, K. (1996b). The *quaking* gene unites signal transduction and RNA binding in the developing nervous system. Nature Genetics *12*, 260-265.

Eden, E., Navon, R., Steinfeld, I., Lipson, D., and Yakhini, Z. (2009). GOrilla: a tool for discovery and visualization of enriched GO terms in ranked gene lists. BMC Bioinformatics *10*, 48.

Einheber, S., Zanazzi, G., Ching, W., Scherer, S., Milner, T.A., Peles, E., and Salzer, J.L. (1997). The axonal membrane protein Caspr, a homologue of neurexin IV, is a component of the

septate-like paranodal junctions that assemble during myelination. J Cell Biol *139*, 1495-1506.

Elder, G.A., Friedrich, V.L., Jr., and Lazzarini, R.A. (2001). Schwann cells and oligodendrocytes read distinct signals in establishing myelin sheath thickness. J Neurosci Res *65*, 493-499.

Emery, B., Agalliu, D., Cahoy, J.D., Watkins, T.A., Dugas, J.C., Mulinyawe, S.B., Ibrahim, A., Ligon, K.L., Rowitch, D.H., and Barres, B.A. (2009). Myelin gene regulatory factor is a critical transcriptional regulator required for CNS myelination. Cell *138*, 172-185.

Eshed, Y., Feinberg, K., Carey, D.J., and Peles, E. (2007). Secreted gliomedin is a perinodal matrix component of peripheral nerves. J Cell Biol *177*, 551-562.

Eshed, Y., Feinberg, K., Poliak, S., Sabanay, H., Sarig-Nadir, O., Spiegel, I., Bermingham, J.R., Jr., and Peles, E. (2005). Gliomedin mediates Schwann cell-axon interaction and the molecular assembly of the nodes of Ranvier. Neuron *47*, 215-229.

Fagg, W.S., Liu, N., Fair, J.H., Shiue, L., Katzman, S., Donohue, J.P., and Ares, M., Jr. (2017). Autogenous cross-regulation of Quaking mRNA processing and translation balances Quaking functions in splicing and translation. Genes Dev *31*, 1894-1909.

Faivre-Sarrailh, C., Gauthier, F., Denisenko-Nehrbass, N., Le Bivic, A., Rougon, G., and Girault, J.A. (2000). The glycosylphosphatidyl inositol-anchored adhesion molecule F3/contactin is required for surface transport of paranodin/contactin-associated protein (caspr). J Cell Biol *149*, 491-502.

Fehmi, J., Scherer, S.S., Willison, H.J., and Rinaldi, S. (2017). Nodes, paranodes and neuropathies. J Neurol Neurosurg Psychiatry.

Feinberg, K., Eshed-Eisenbach, Y., Frechter, S., Amor, V., Salomon, D., Sabanay, H., Dupree, J.L., Grumet, M., Brophy, P.J., Shrager, P.*, et al.* (2010). A glial signal consisting of gliomedin and NrCAM clusters axonal Na+ channels during the formation of nodes of Ranvier. Neuron *65*, 490-502.

Feng, Y., and Bankston, A. (2010). The star family member QKI and cell signaling. Adv Exp Med Biol *693*, 25-36.

Fernandez, P.A., Tang, D.G., Cheng, L., Prochiantz, A., Mudge, A.W., and Raff, M.C. (2000). Evidence that axon-derived neuregulin promotes oligodendrocyte survival in the developing rat optic nerve. Neuron *28*, 81-90.

Fewou, S.N., Ramakrishnan, H., Bussow, H., Gieselmann, V., and Eckhardt, M. (2007). Down-regulation of polysialic acid is required for efficient myelin formation. J Biol Chem *282*, 16700-16711.

Flamme, I., Frolich, T., and Risau, W. (1997). Molecular mechanisms of vasculogenesis and embryonic angiogenesis. J Cell Physiol *173*, 206-210.

Flores, A.I., Mallon, B.S., Matsui, T., Ogawa, W., Rosenzweig, A., Okamoto, T., and Macklin, W.B. (2000). Akt-mediated survival of oligodendrocytes induced by neuregulins. J Neurosci *20*, 7622-7630.

Flores, A.I., Narayanan, S.P., Morse, E.N., Shick, H.E., Yin, X., Kidd, G., Avila, R.L., Kirschner, D.A., and Macklin, W.B. (2008). Constitutively active Akt induces enhanced myelination in the CNS. J Neurosci *28*, 7174-7183.

Fok-Seang, J., and Miller, R.H. (1994). Distribution and differentiation of A2B5+ glial precursors in the developing rat spinal cord. J Neurosci Res *37*, 219-235.

Fragoso, G., Haines, J.D., Roberston, J., Pedraza, L., Mushynski, W.E., and Almazan, G. (2007). p38 mitogen-activated protein kinase is required for central nervous system myelination. Glia *55*, 1531-1541.

Frail, D.E., and Braun, P.E. (1985). Abnormal expression of the myelin-associated glycoprotein in the central nervous system of dysmyelinating mutant mice. J Neurochem *45*, 1071-1075.

Friede, R.L. (1972). Control of myelin formation by axon caliber (with a model of the control mechanism). J Comp Neurol *144*, 233-252.

Fritschy, J.M., Harvey, R.J., and Schwarz, G. (2008). Gephyrin: where do we stand, where do we go? Trends Neurosci *31*, 257-264.

Frost, E.E., Buttery, P.C., Milner, R., and ffrench-Constant, C. (1999). Integrins mediate a neuronal survival signal for oligodendrocytes. Curr Biol *9*, 1251-1254.

Fruttiger, M., Karlsson, L., Hall, A.C., Abramsson, A., Calver, A.R., Bostrom, H., Willetts, K., Bertold, C.H., Heath, J.K., Betsholtz, C*., et al.* (1999). Defective oligodendrocyte development and severe hypomyelination in PDGF-A knockout mice. Development *126*, 457-467.

Fu, H., Yang, G., Wei, M., Liu, L., Jin, L., Lu, X., Wang, L., Shen, L., Zhang, J., Lu, H*., et al.* (2012). The RNA-binding protein QKI5 is a direct target of C/EBPalpha and delays macrophage differentiation. Mol Biol Cell *23*, 1628-1635.

Fu, X., and Feng, Y. (2015). QKI-5 suppresses cyclin D1 expression and proliferation of oral squamous cell carcinoma cells via MAPK signalling pathway. Int J Oral Maxillofac Surg *44*, 562-567.

Fumagalli, S., Totty, N.F., Hsuan, J.J., and Courtneidge, S.A. (1994). A target for Src in mitosis. Nature *368*, 871-874.

Funfschilling, U., Supplie, L.M., Mahad, D., Boretius, S., Saab, A.S., Edgar, J., Brinkmann, B.G., Kassmann, C.M., Tzvetanova, I.D., Mobius, W*., et al.* (2012). Glycolytic oligodendrocytes maintain myelin and long-term axonal integrity. Nature *485*, 517-521.

Furusho, M., Kaga, Y., Ishii, A., Hebert, J.M., and Bansal, R. (2011). Fibroblast growth factor signaling is required for the generation of oligodendrocyte progenitors from the embryonic forebrain. J Neurosci *31*, 5055-5066.

Galarneau, A., and Richard, S. (2005). Target RNA motif and target mRNAs of the Quaking STAR protein. Nat Struct Mol Biol *12*, 691-698.

Garcia-Fresco, G.P., Sousa, A.D., Pillai, A.M., Moy, S.S., Crawley, J.N., Tessarollo, L., Dupree, J.L., and Bhat, M.A. (2006). Disruption of axo-glial junctions causes cytoskeletal disorganization and degeneration of Purkinje neuron axons. Proc Natl Acad Sci U S A *103*, 5137-5142.

Garcion, E., Faissner, A., and ffrench-Constant, C. (2001). Knockout mice reveal a contribution of the extracellular matrix molecule tenascin-C to neural precursor proliferation and migration. Development *128*, 2485-2496.

Garneau, N.L., Wilusz, J., and Wilusz, C.J. (2007). The highways and byways of mRNA decay. Nat Rev Mol Cell Biol *8*, 113-126.

Garrido, J.J., Giraud, P., Carlier, E., Fernandes, F., Moussif, A., Fache, M.P., Debanne, D., and Dargent, B. (2003). A targeting motif involved in sodium channel clustering at the axonal initial segment. Science *300*, 2091-2094.

Garver, T.D., Ren, Q., Tuvia, S., and Bennett, V. (1997). Tyrosine phosphorylation at a site highly conserved in the L1 family of cell adhesion molecules abolishes ankyrin binding and increases lateral mobility of neurofascin. J Cell Biol *137*, 703-714.

Gasser, A., Ho, T.S., Cheng, X., Chang, K.J., Waxman, S.G., Rasband, M.N., and Dib-Hajj, S.D. (2012). An ankyrinG-binding motif is necessary and sufficient for targeting Nav1.6 sodium channels to axon initial segments and nodes of Ranvier. J Neurosci *32*, 7232-7243.

Geren, B.B. (1954). The formation from the Schwann cell surface of myelin in the peripheral nerves of chick embryos. Exp Cell Res *7*.

Gerstberger, S., Hafner, M., Ascano, M., and Tuschl, T. (2014). Evolutionary conservation and expression of human RNA-binding proteins and their role in human genetic disease. Adv Exp Med Biol *825*, 1-55.

Ghosh, A., Sherman, D.L., and Brophy, P.J. (2017). The Axonal Cytoskeleton and the Assembly of Nodes of Ranvier. Neuroscientist, 1073858417710897.

Gollan, L., Salomon, D., Salzer, J.L., and Peles, E. (2003). Caspr regulates the processing of contactin and inhibits its binding to neurofascin. J Cell Biol *163*, 1213-1218.

Goto, J., Tezuka, T., Nakazawa, T., Sagara, H., and Yamamoto, T. (2008). Loss of Fyn tyrosine kinase on the C57BL/6 genetic background causes hydrocephalus with defects in oligodendrocyte development. Mol Cell Neurosci *38*, 203-212.

Gozani, O., Potashkin, J., and Reed, R. (1998). A potential role for U2AF-SAP 155 interactions in recruiting U2 snRNP to the branch site. Mol Cell Biol *18*, 4752-4760.

Griffiths, I., Klugmann, M., Anderson, T., Yool, D., Thomson, C., Schwab, M.H., Schneider, A., Zimmermann, F., McCulloch, M., Nadon, N.*, et al.* (1998). Axonal swellings and degeneration in mice lacking the major proteolipid of myelin. Science *280*, 1610-1613.

Grishin, N.V. (2001). KH domain: one motif, two folds. Nucleic Acids Res *29*, 638-643.

Guo, W., Jiang, T., Lian, C., Wang, H., Zheng, Q., and Ma, H. (2014). QKI deficiency promotes FoxO1 mediated nitrosative stress and endoplasmic reticulum stress contributing to increased vulnerability to ischemic injury in diabetic heart. J Mol Cell Cardiol *75*, 131-140.

Guo, W., Shi, X., Liu, A., Yang, G., Yu, F., Zheng, Q., Wang, Z., Allen, D.G., and Lu, Z. (2011). RNA binding protein QKI inhibits the ischemia/reperfusion-induced apoptosis in neonatal cardiomyocytes. Cell Physiol Biochem *28*, 593-602.

Gupta, S.K., Garg, A., Bar, C., Chatterjee, S., Foinquinos, A., Milting, H., Streckfuss-Bomeke, K., Fiedler, J., and Thum, T. (2017). Quaking Inhibits Doxorubicin-Mediated Cardiotoxicity Through Regulation of Cardiac Circular RNA Expression. Circulation research.

Haas, S., Steplewski, A., Siracusa, L.D., Amini, S., and Khalili, K. (1995). Identification of a sequence-specific single-stranded DNA binding protein that suppresses transcription of the mouse myelin basic protein gene. J Biol Chem *270*, 12503-12510.

Hafner, M., Landthaler, M., Burger, L., Khorshid, M., Hausser, J., Berninger, P., Rothballer, A., Ascano, M., Jr., Jungkamp, A.C., Munschauer, M.*, et al.* (2010). Transcriptome-wide identification of RNA-binding protein and microRNA target sites by PAR-CLIP. Cell *141*, 129-141.

Hall, M.P., Nagel, R.J., Fagg, W.S., Shiue, L., Cline, M.S., Perriman, R.J., Donohue, J.P., and Ares, M., Jr. (2013). Quaking and PTB control overlapping splicing regulatory networks during muscle cell differentiation. RNA *19*, 627-638.

Han, X.L., and Gross, R.W. (1990). Plasmenylcholine and phosphatidylcholine membrane bilayers possess distinct conformational motifs. Biochemistry *29*, 4992-4996.

Hardy, R.J. (1998a). Molecular defects of the dysmyelinating mutant quaking. J Neurosci Res *51*, 417-422.

Hardy, R.J. (1998b). QKI expression is regulated during neuron-glial cell fate decisions. J Neurosci Res *54*, 46-57.

Hardy, R.J., Loushin, C.L., Friedrich Jr., V.L., Chen, Q., Ebersole, T.A., Lazzarini, R.A., and Artzt, K. (1996). Neural cell type-specific expression of QKI proteins is altered in the *quaking* viable mutant mice. J Neurosci *16*, 7941-7949.

Haroutunian, V., Katsel, P., Dracheva, S., and Davis, K.L. (2006). The human homolog of the QKI gene affected in the severe dysmyelination "quaking" mouse phenotype: downregulated in multiple brain regions in schizophrenia. Am J Psychiatry *163*, 1834-1837.

Hassel, B., Rathjen, F.G., and Volkmer, H. (1997). Organization of the neurofascin gene and analysis of developmentally regulated alternative splicing. J Biol Chem *272*, 28742-28749.

Hayakawa-Yano, Y., Suyama, S., Nogami, M., Yugami, M., Koya, I., Furukawa, T., Zhou, L., Abe, M., Sakimura, K., Takebayashi, H*., et al.* (2017). An RNA-binding protein, Qki5, regulates embryonic neural stem cells through pre-mRNA processing in cell adhesion signaling. Genes Dev *31*, 1910-1925.

He, B., Gao, S.Q., Huang, L.D., Huang, Y.H., Zhang, Q.Y., Zhou, M.T., Shi, H.Q., Song, Q.T., and Shan, Y.F. (2015). MicroRNA-155 promotes the proliferation and invasion abilities of colon cancer cells by targeting quaking. Molecular medicine reports *11*, 2355-2359.

He, Z., Yi, J., Liu, X., Chen, J., Han, S., Jin, L., Chen, L., and Song, H. (2016). MiR-143-3p functions as a tumor suppressor by regulating cell proliferation, invasion and epithelial-mesenchymal transition by targeting QKI-5 in esophageal squamous cell carcinoma. Mol Cancer *15*, 51.

Hedstrom, K.L., Xu, X., Ogawa, Y., Frischknecht, R., Seidenbecher, C.I., Shrager, P., and Rasband, M.N. (2007). Neurofascin assembles a specialized extracellular matrix at the axon initial segment. J Cell Biol *178*, 875-886.

Hildebrand, C., Remahl, S., Persson, H., and Bjartmar, C. (1993). Myelinated nerve fibres in the CNS. Prog Neurobiol *40*, 319-384.

Hogan, E.L., and Greenfield, S. (1984). Animal models of genetic disorders of myelin. (New York: Plenum).

Hornig, J., Frob, F., Vogl, M.R., Hermans-Borgmeyer, I., Tamm, E.R., and Wegner, M. (2013). The transcription factors Sox10 and Myrf define an essential regulatory network module in differentiating oligodendrocytes. PLoS Genet *9*, e1003907.

Howell, O.W., Palser, A., Polito, A., Melrose, S., Zonta, B., Scheiermann, C., Vora, A.J., Brophy, P.J., and Reynolds, R. (2006). Disruption of neurofascin localization reveals early changes preceding demyelination and remyelination in multiple sclerosis. Brain *129*, 3173-3185.

Hsieh, J., Aimone, J.B., Kaspar, B.K., Kuwabara, T., Nakashima, K., and Gage, F.H. (2004). IGF-I instructs multipotent adult neural progenitor cells to become oligodendrocytes. J Cell Biol *164*, 111-122.

Hu, J., Deng, L., Wang, X., and Xu, X.M. (2009). Effects of extracellular matrix molecules on the growth properties of oligodendrocyte progenitor cells in vitro. J Neurosci Res *87*, 2854-2862.

Huang, J.Y., Wang, Y.X., Gu, W.L., Fu, S.L., Li, Y., Huang, L.D., Zhao, Z., Hang, Q., Zhu, H.Q., and Lu, P.H. (2012). Expression and function of myelin-associated proteins and their common receptor NgR on oligodendrocyte progenitor cells. Brain Res *1437*, 1-15.

Ichimura, K., Mungall, A.J., Fiegler, H., Pearson, D.M., Dunham, I., Carter, N.P., and Collins, V.P. (2006). Small regions of overlapping deletions on 6q26 in human astrocytic tumours identified using chromosome 6 tile path array-CGH. Oncogene *25*, 1261-1271.

Irie, K., Tsujimura, K., Nakashima, H., and Nakashima, K. (2016). MicroRNA-214 Promotes Dendritic Development by Targeting the Schizophrenia-associated Gene Quaking (Qki). J Biol Chem *291*, 13891-13904.

Itier, J.M., Ibanez, P., Mena, M.A., Abbas, N., Cohen-Salmon, C., Bohme, G.A., Laville, M., Pratt, J., Corti, O., Pradier, L.*, et al.* (2003). Parkin gene inactivation alters behaviour and dopamine neurotransmission in the mouse. Hum Mol Genet *12*, 2277-2291.

Iwata, N., Ishikawa, T., Okazaki, S., Mogushi, K., Baba, H., Ishiguro, M., Kobayashi, H., Tanaka, H., Kawano, T., Sugihara, K.*, et al.* (2017). Clinical Significance of Methylation and Reduced Expression of the Quaking Gene in Colorectal Cancer. Anticancer Res *37*, 489-498.

Jahn, O., Tenzer, S., and Werner, H.B. (2009). Myelin proteomics: molecular anatomy of an insulating sheath. Mol Neurobiol *40*, 55-72.

Jaramillo, M.L., Afar, D.E., Almazan, G., and Bell, J.C. (1994). Identification of tyrosine 620 as the major phosphorylation site of myelin-associated glycoprotein and its implication in interacting with signaling molecules. J Biol Chem *269*, 27240-27245.

Jarjour, A.A., Manitt, C., Moore, S.W., Thompson, K.M., Yuh, S.J., and Kennedy, T.E. (2003). Netrin-1 is a chemorepellent for oligodendrocyte precursor cells in the embryonic spinal cord. J Neurosci *23*, 3735-3744.

Jeck, W.R., Sorrentino, J.A., Wang, K., Slevin, M.K., Burd, C.E., Liu, J., Marzluff, W.F., and Sharpless, N.E. (2013). Circular RNAs are abundant, conserved, and associated with ALU repeats. RNA *19*, 141-157.

Jenkins, S.M., and Bennett, V. (2001). Ankyrin-G coordinates assembly of the spectrin-based membrane skeleton, voltage-gated sodium channels, and L1 CAMs at Purkinje neuron initial segments. J Cell Biol *155*, 739-746.

Jenkins, S.M., Kizhatil, K., Kramarcy, N.R., Sen, A., Sealock, R., and Bennett, V. (2001). FIGQY phosphorylation defines discrete populations of L1 cell adhesion molecules at sites of cell-cell contact and in migrating neurons. J Cell Sci *114*, 3823-3835.

Jepson, S., Vought, B., Gross, C.H., Gan, L., Austen, D., Frantz, J.D., Zwahlen, J., Lowe, D., Markland, W., and Krauss, R. (2012). LINGO-1, a transmembrane signaling protein, inhibits oligodendrocyte differentiation and myelination through intercellular self-interactions. J Biol Chem *287*, 22184-22195.

Ji, S., Ye, G., Zhang, J., Wang, L., Wang, T., Wang, Z., Zhang, T., Wang, G., Guo, Z., Luo, Y., *et al.* (2013). miR-574-5p negatively regulates Qki6/7 to impact beta-catenin/Wnt signalling and the development of colorectal cancer. Gut *62*, 716-726.

Jiang, L., Saetre, P., Radomska, K.J., Jazin, E., and Lindholm Carlstrom, E. (2010). QKI-7 regulates expression of interferon-related genes in human astrocyte glioma cells. PLoS One *5*.

Jones, A.R., and Schedl, T. (1995). Mutations in gld-1, a female germ cell-specific tumor suppressor gene in Caenorhabditis elegans, affect a conserved domain also found in Src-associated protein Sam68. Genes Dev *9*, 1491-1504.

Justice, M.J., and Bode, V.C. (1988). Three ENU-induced alleles of the murine quaking locus are recessive embryonic lethal mutations. Genet Res *51*, 95-102.

Kaplan, M.R., Meyer-Franke, A., Lambert, S., Bennett, V., Duncan, I.D., Levinson, S.R., and Barres, B.A. (1997). Induction of sodium channel clustering by oligodendrocytes. Nature *386*, 724-728.

Katsel, P., Davis, K.L., and Haroutunian, V. (2005). Variations in myelin and oligodendrocyte-related gene expression across multiple brain regions in schizophrenia: a gene ontology study. Schizophrenia research *79*, 157-173.

Kawamura, N., Yamasaki, R., Yonekawa, T., Matsushita, T., Kusunoki, S., Nagayama, S., Fukuda, Y., Ogata, H., Matsuse, D., Murai, H., *et al.* (2013). Anti-neurofascin antibody in patients with combined central and peripheral demyelination. Neurology *81*, 714-722.

Kazarinova-Noyes, K., Malhotra, J.D., McEwen, D.P., Mattei, L.N., Berglund, E.O., Ranscht, B., Levinson, S.R., Schachner, M., Shrager, P., Isom, L.L., *et al.* (2001). Contactin associates with Na+ channels and increases their functional expression. J Neurosci *21*, 7517-7525.

Keller, A., Leidinger, P., Lange, J., Borries, A., Schroers, H., Scheffler, M., Lenhof, H.P., Ruprecht, K., and Meese, E. (2009). Multiple sclerosis: microRNA expression profiles accurately differentiate patients with relapsing-remitting disease from healthy controls. PLoS One *4*, e7440.

Kessaris, N., Fogarty, M., Iannarelli, P., Grist, M., Wegner, M., and Richardson, W.D. (2006). Competing waves of oligodendrocytes in the forebrain and postnatal elimination of an embryonic lineage. Nat Neurosci *9*, 173-179.

Kizhatil, K., Wu, Y.X., Sen, A., and Bennett, V. (2002). A new activity of doublecortin in recognition of the phospho-FIGQY tyrosine in the cytoplasmic domain of neurofascin. J Neurosci *22*, 7948-7958.

Klempan, T.A., Ernst, C., Deleva, V., Labonte, B., and Turecki, G. (2009). Characterization of QKI gene expression, genetics, and epigenetics in suicide victims with major depressive disorder. Biol Psychiatry *66*, 824-831.

Klinck, R., Bramard, A., Inkel, L., Dufresne-Martin, G., Gervais-Bird, J., Madden, R., Paquet, E.R., Koh, C., Venables, J.P., Prinos, P.*, et al.* (2008). Multiple alternative splicing markers for ovarian cancer. Cancer research *68*, 657-663.

Klingseisen, A., and Lyons, D.A. (2017). Axonal Regulation of Central Nervous System Myelination: Structure and Function. Neuroscientist, 1073858417703030.

Kneussel, M., Brandstatter, J.H., Laube, B., Stahl, S., Muller, U., and Betz, H. (1999). Loss of postsynaptic GABA(A) receptor clustering in gephyrin-deficient mice. J Neurosci *19*, 9289-9297.

Komada, M., and Soriano, P. (2002). [Beta]IV-spectrin regulates sodium channel clustering through ankyrin-G at axon initial segments and nodes of Ranvier. J Cell Biol *156*, 337-348.

Komuro, I., Schalling, M., Jahn, L., Bodmer, R., Jenkins, N.A., Copeland, N.G., and Izumo, S. (1993). Gtx: a novel murine homeobox-containing gene, expressed specifically in glial cells of the brain and germ cells of testis, has a transcriptional repressor activity in vitro for a serum-inducible promoter. EMBO J *12*, 1387-1401.

Kondo, T., Furuta, T., Mitsunaga, K., Ebersole, T.A., Shichiri, M., Wu, J., Artzt, K., Yamamura, K., and Abe, K. (1999). Genomic organization and expression analysis of the mouse qkI locus. Mamm Genome *10*, 662-669.

Kordeli, E., Lambert, S., and Bennett, V. (1995). AnkyrinG. A new ankyrin gene with neural-specific isoforms localized at the axonal initial segment and node of Ranvier. J Biol Chem *270*, 2352-2359.

Koticha, D., Babiarz, J., Kane-Goldsmith, N., Jacob, J., Raju, K., and Grumet, M. (2005). Cell adhesion and neurite outgrowth are promoted by neurofascin NF155 and inhibited by NF186. Mol Cell Neurosci *30*, 137-148.

Koticha, D., Maurel, P., Zanazzi, G., Kane-Goldsmith, N., Basak, S., Babiarz, J., Salzer, J., and Grumet, M. (2006). Neurofascin interactions play a critical role in clustering sodium channels, ankyrin G and beta IV spectrin at peripheral nodes of Ranvier. Dev Biol *293*, 1-12.

Kramer-Albers, E.M., and White, R. (2011). From axon-glial signalling to myelination: the integrating role of oligodendroglial Fyn kinase. Cell Mol Life Sci *68*, 2003-2012.

Kriebel, M., Metzger, J., Trinks, S., Chugh, D., Harvey, R.J., Harvey, K., and Volkmer, H. (2011). The cell adhesion molecule neurofascin stabilizes axo-axonic GABAergic terminals at the axon initial segment. J Biol Chem *286*, 24385-24393.

Kriebel, M., Wuchter, J., Trinks, S., and Volkmer, H. (2012). Neurofascin: a switch between neuronal plasticity and stability. Int J Biochem Cell Biol *44*, 694-697.

Lakiza, O., Frater, L., Yoo, Y., Villavicencio, E., Walterhouse, D., Goodwin, E.B., and Iannaccone, P. (2005). STAR proteins quaking-6 and GLD-1 regulate translation of the

homologues GLI1 and tra-1 through a conserved RNA 3'UTR-based mechanism. Dev Biol *287*, 98-110.

Lambert, S., Davis, J.Q., and Bennett, V. (1997). Morphogenesis of the node of Ranvier: co-clusters of ankyrin and ankyrin-binding integral proteins define early developmental intermediates. J Neurosci *17*, 7025-7036.

Langseth, A.J., Munji, R.N., Choe, Y., Huynh, T., Pozniak, C.D., and Pleasure, S.J. (2010). Wnts influence the timing and efficiency of oligodendrocyte precursor cell generation in the telencephalon. J Neurosci *30*, 13367-13372.

Lappe-Siefke, C., Goebbels, S., Gravel, M., Nicksch, E., Lee, J., Braun, P.E., Griffiths, I.R., and Nave, K.A. (2003). Disruption of Cnp1 uncouples oligodendroglial functions in axonal support and myelination. Nat Genet *33*, 366-374.

Larocque, D., Fragoso, G., Huang, J., Mushynski, W.E., Loignon, M., Richard, S., and Almazan, G. (2009). The QKI-6 and QKI-7 RNA binding proteins block proliferation and promote Schwann cell myelination. PLoS One *4*, e5867.

Larocque, D., Galarneau, A., Liu, H.N., Scott, M., Almazan, G., and Richard, S. (2005). Protection of the p27KIP1 mRNA by quaking RNA binding proteins promotes oligodendrocyte differentiation. Nat Neurosci *8*, 27-33.

Larocque, D., Pilotte, J., Chen, T., Cloutier, F., Massie, B., Pedraza, L., Couture, R., Lasko, P., Almazan, G., and Richard, S. (2002). Nuclear retention of MBP mRNAs in the Quaking viable mice. Neuron *36*, 815-829.

Lau, L.W., Keough, M.B., Haylock-Jacobs, S., Cua, R., Doring, A., Sloka, S., Stirling, D.P., Rivest, S., and Yong, V.W. (2012). Chondroitin sulfate proteoglycans in demyelinated lesions impair remyelination. Ann Neurol *72*, 419-432.

Laursen, L.S., Chan, C.W., and ffrench-Constant, C. (2009). An integrin-contactin complex regulates CNS myelination by differential Fyn phosphorylation. J Neurosci *29*, 9174-9185.

Lebar, R., Lubetzki, C., Vincent, C., Lombrail, P., and Boutry, J.M. (1986). The M2 autoantigen of central nervous system myelin, a glycoprotein present in oligodendrocyte membrane. Clin Exp Immunol *66*, 423-434.

Lee, K.K., de Repentigny, Y., Saulnier, R., Rippstein, P., Macklin, W.B., and Kothary, R. (2006). Dominant-negative beta1 integrin mice have region-specific myelin defects accompanied by alterations in MAPK activity. Glia *53*, 836-844.

Lee, S., Leach, M.K., Redmond, S.A., Chong, S.Y., Mellon, S.H., Tuck, S.J., Feng, Z.Q., Corey, J.M., and Chan, J.R. (2012). A culture system to study oligodendrocyte myelination processes using engineered nanofibers. Nat Methods *9*, 917-922.

Lee, S.K., Lee, B., Ruiz, E.C., and Pfaff, S.L. (2005). Olig2 and Ngn2 function in opposition to modulate gene expression in motor neuron progenitor cells. Genes Dev *19*, 282-294.

Lee, Y., Samaco, R.C., Gatchel, J.R., Thaller, C., Orr, H.T., and Zoghbi, H.Y. (2008). miR-19, miR-101 and miR-130 co-regulate ATXN1 levels to potentially modulate SCA1 pathogenesis. Nat Neurosci *11*, 1137-1139.

Lein, E.S., Hawrylycz, M.J., Ao, N., Ayres, M., Bensinger, A., Bernard, A., Boe, A.F., Boguski, M.S., Brockway, K.S., Byrnes, E.J.*, et al.* (2007). Genome-wide atlas of gene expression in the adult mouse brain. Nature *445*, 168-176.

Lek, M., Karczewski, K.J., Minikel, E.V., Samocha, K.E., Banks, E., Fennell, T., O'Donnell-Luria, A.H., Ware, J.S., Hill, A.J., Cummings, B.B.*, et al.* (2016). Analysis of protein-coding genetic variation in 60,706 humans. Nature *536*, 285-291.

Lessig, J., and Fuchs, B. (2009). Plasmalogens in biological systems: their role in oxidative processes in biological membranes, their contribution to pathological processes and aging and plasmalogen analysis. Curr Med Chem *16*, 2021-2041.

Levi, S., Logan, S.M., Tovar, K.R., and Craig, A.M. (2004). Gephyrin is critical for glycine receptor clustering but not for the formation of functional GABAergic synapses in hippocampal neurons. J Neurosci *24*, 207-217.

Levison, S.W., and Goldman, J.E. (1993). Both oligodendrocytes and astrocytes develop from progenitors in the subventricular zone of postnatal rat forebrain. Neuron *10*, 201-212.

Lew, J., Huang, Q.Q., Qi, Z., Winkfein, R.J., Aebersold, R., Hunt, T., and Wang, J.H. (1994). A brain-specific activator of cyclin-dependent kinase 5. Nature *371*, 423-426.

Lewis, C.M., Levinson, D.F., Wise, L.H., DeLisi, L.E., Straub, R.E., Hovatta, I., Williams, N.M., Schwab, S.G., Pulver, A.E., Faraone, S.V.*, et al.* (2003). Genome scan meta-analysis of schizophrenia and bipolar disorder, part II: Schizophrenia. American journal of human genetics *73*, 34-48.

Li, H., de Faria, J.P., Andrew, P., Nitarska, J., and Richardson, W.D. (2011). Phosphorylation regulates OLIG2 cofactor choice and the motor neuron-oligodendrocyte fate switch. Neuron *69*, 918-929.

Li, H., Handsaker, B., Wysoker, A., Fennell, T., Ruan, J., Homer, N., Marth, G., Abecasis, G., Durbin, R., and Genome Project Data Processing, S. (2009). The Sequence Alignment/Map format and SAMtools. Bioinformatics *25*, 2078-2079.

Li, Z., Takakura, N., Oike, Y., Imanaka, T., Araki, K., Suda, T., Kaname, T., Kondo, T., Abe, K., and Yamamura, K. (2003). Defective smooth muscle development in qkI-deficient mice. Dev Growth Differ *45*, 449-462.

Li, Z., Zhang, Y., Li, D., and Feng, Y. (2000). Destabilization and mislocalization of myelin basic protein mRNAs in quaking dysmyelination lacking the QKI RNA-binding proteins. J Neurosci *20*, 4944-4953.

Li, Z.Z., Kondo, T., Murata, T., Ebersole, T.A., Nishi, T., Tada, K., Ushio, Y., Yamamura, K., and Abe, K. (2002). Expression of Hqk encoding a KH RNA binding protein is altered in human glioma. Japanese journal of cancer research : Gann *93*, 167-177.

Liang, X., Draghi, N.A., and Resh, M.D. (2004). Signaling from integrins to Fyn to Rho family GTPases regulates morphologic differentiation of oligodendrocytes. J Neurosci *24*, 7140-7149.

Liao, K.C., Chuo, V., Ng, W.C., Neo, S.P., Pompon, J., Gunaratne, J., Ooi, E.E., and Garcia-Blanco, M. (2018). Identification and Characterization of Host Proteins Bound to Dengue Virus 3'UTR Reveal an Anti-viral Role for Quaking Proteins. RNA.

Liao, Y., Smyth, G.K., and Shi, W. (2014). featureCounts: an efficient general purpose program for assigning sequence reads to genomic features. Bioinformatics *30*, 923-930.

Ligon, K.L., Huillard, E., Mehta, S., Kesari, S., Liu, H., Alberta, J.A., Bachoo, R.M., Kane, M., Louis, D.N., Depinho, R.A*., et al.* (2007). Olig2-regulated lineage-restricted pathway controls replication competence in neural stem cells and malignant glioma. Neuron *53*, 503-517.

Lim, J., Hao, T., Shaw, C., Patel, A.J., Szabo, G., Rual, J.F., Fisk, C.J., Li, N., Smolyar, A., Hill, D.E*., et al.* (2006). A protein-protein interaction network for human inherited ataxias and disorders of Purkinje cell degeneration. Cell *125*, 801-814.

Lindholm, E., Aberg, K., Ekholm, B., Pettersson, U., Adolfsson, R., and Jazin, E.E. (2004). Reconstruction of ancestral haplotypes in a 12-generation schizophrenia pedigree. Psychiatric genetics *14*, 1-8.

Liu, R., Cai, J., Hu, X., Tan, M., Qi, Y., German, M., Rubenstein, J., Sander, M., and Qiu, M. (2003). Region-specific and stage-dependent regulation of Olig gene expression and oligodendrogenesis by Nkx6.1 homeodomain transcription factor. Development *130*, 6221-6231.

Liu, Z., Luyten, I., Bottomley, M.J., Messias, A.C., Houngninou-Molango, S., Sprangers, R., Zanier, K., Kramer, A., and Sattler, M. (2001). Structural basis for recognition of the intron branch site RNA by splicing factor 1. Science *294*, 1098-1102.

Lonigro, A., and Devaux, J.J. (2009). Disruption of neurofascin and gliomedin at nodes of Ranvier precedes demyelination in experimental allergic neuritis. Brain *132*, 260-273.

Lorenzetti, D., Bishop, C.E., and Justice, M.J. (2004). Deletion of the Parkin coregulated gene causes male sterility in the quaking(viable) mouse mutant. Proc Natl Acad Sci U S A *101*, 8402-8407.

Love, M.I., Huber, W., and Anders, S. (2014). Moderated estimation of fold change and dispersion for RNA-seq data with DESeq2. Genome Biol *15*, 550.

Lu, L.F., and Liston, A. (2009). MicroRNA in the immune system, microRNA as an immune system. Immunology *127*, 291-298.

Lu, Q.R., Sun, T., Zhu, Z., Ma, N., Garcia, M., Stiles, C.D., and Rowitch, D.H. (2002). Common developmental requirement for Olig function indicates a motor neuron/oligodendrocyte connection. Cell *109*, 75-86.

Lu, W., Feng, F., Xu, J., Lu, X., Wang, S., Wang, L., Lu, H., Wei, M., Yang, G., Wang, L.*, et al.* (2014). QKI impairs self-renewal and tumorigenicity of oral cancer cells via repression of SOX2. Cancer Biol Ther *15*, 1174-1184.

Lu, Z., Ku, L., Chen, Y., and Feng, Y. (2005). Developmental abnormalities of myelin basic protein expression in fyn knock-out brain reveal a role of Fyn in posttranscriptional regulation. J Biol Chem *280*, 389-395.

Lu, Z., Zhang, Y., Ku, L., Wang, H., Ahmadian, A., and Feng, Y. (2003). The quakingviable mutation affects qkI mRNA expression specifically in myelin-producing cells of the nervous system. Nucleic Acids Res *31*, 4616-4624.

Ludwin, S.K. (1997). The pathobiology of the oligodendrocyte. Journal of neuropathology and experimental neurology *56*, 111-124.

Lukong, K.E., Chang, K.W., Khandjian, E.W., and Richard, S. (2008). RNA-binding proteins in human genetic disease. Trends Genet *24*, 416-425.

Lukong, K.E., and Richard, S. (2003). Sam68, the KH domain-containing superSTAR. Biochim Biophys Acta *1653*, 73-86.

Lunn, K.F., Baas, P.W., and Duncan, I.D. (1997). Microtubule organization and stability in the oligodendrocyte. J Neurosci *17*, 4921-4932.

Ma, D.L., Li, J.Y., Liu, Y.E., Liu, C.M., Li, J., Lin, G.Z., and Yan, J. (2016). Influence of continuous intervention on growth and metastasis of human cervical cancer cells and expression of RNAmiR-574-5p. J Biol Regul Homeost Agents *30*, 91-102.

Maguire, M.L., Guler-Gane, G., Nietlispach, D., Raine, A.R., Zorn, A.M., Standart, N., and Broadhurst, R.W. (2005). Solution structure and backbone dynamics of the KH-QUA2 region of the Xenopus STAR/GSG quaking protein. J Mol Biol *348*, 265-279.

Malhotra, J.D., Kazen-Gillespie, K., Hortsch, M., and Isom, L.L. (2000). Sodium channel beta subunits mediate homophilic cell adhesion and recruit ankyrin to points of cell-cell contact. J Biol Chem *275*, 11383-11388.

Mandler, M.D., Ku, L., and Feng, Y. (2014). A cytoplasmic quaking I isoform regulates the hnRNP F/H-dependent alternative splicing pathway in myelinating glia. Nucleic Acids Res *42*, 7319-7329.

Marta, C.B., Adamo, A.M., Soto, E.F., and Pasquini, J.M. (1998). Sustained neonatal hyperthyroidism in the rat affects myelination in the central nervous system. J Neurosci Res *53*, 251-259.

Mathey, E.K., Derfuss, T., Storch, M.K., Williams, K.R., Hales, K., Woolley, D.R., Al-Hayani, A., Davies, S.N., Rasband, M.N., Olsson, T.*, et al.* (2007). Neurofascin as a novel target for autoantibody-mediated axonal injury. J Exp Med *204*, 2363-2372.

Matter, N., Herrlich, P., and Konig, H. (2002). Signal-dependent regulation of splicing via phosphorylation of Sam68. Nature *420*, 691-695.

McCullumsmith, R.E., Gupta, D., Beneyto, M., Kreger, E., Haroutunian, V., Davis, K.L., and Meador-Woodruff, J.H. (2007). Expression of transcripts for myelination-related genes in the anterior cingulate cortex in schizophrenia. Schizophrenia research *90*, 15-27.

McInnes, L.A., and Lauriat, T.L. (2006). RNA metabolism and dysmyelination in schizophrenia. Neuroscience and biobehavioral reviews *30*, 551-561.

McKnight, G.L., Reasoner, J., Gilbert, T., Sundquist, K.O., Hokland, B., McKernan, P.A., Champagne, J., Johnson, C.J., Bailey, M.C., Holly, R.*, et al.* (1992). Cloning and expression of a cellular high density lipoprotein-binding protein that is up-regulated by cholesterol loading of cells. J Biol Chem *267*, 12131-12141.

Mei, F., Wang, H., Liu, S., Niu, J., Wang, L., He, Y., Etxeberria, A., Chan, J.R., and Xiao, L. (2013). Stage-specific deletion of Olig2 conveys opposing functions on differentiation and maturation of oligodendrocytes. J Neurosci *33*, 8454-8462.

Meister, G. (2013). Argonaute proteins: functional insights and emerging roles. Nat Rev Genet *14*, 447-459.

Meixner, A., Haverkamp, S., Wassle, H., Fuhrer, S., Thalhammer, J., Kropf, N., Bittner, R.E., Lassmann, H., Wiche, G., and Propst, F. (2000). MAP1B is required for axon guidance and Is involved in the development of the central and peripheral nervous system. J Cell Biol *151*, 1169-1178.

Menegoz, M., Gaspar, P., Le Bert, M., Galvez, T., Burgaya, F., Palfrey, C., Ezan, P., Arnos, F., and Girault, J.A. (1997). Paranodin, a glycoprotein of neuronal paranodal membranes. Neuron *19*, 319-331.

Mi, S., Lee, X., Shao, Z., Thill, G., Ji, B., Relton, J., Levesque, M., Allaire, N., Perrin, S., Sands, B.*, et al.* (2004). LINGO-1 is a component of the Nogo-66 receptor/p75 signaling complex. Nat Neurosci *7*, 221-228.

Mi, S., Miller, R.H., Lee, X., Scott, M.L., Shulag-Morskaya, S., Shao, Z., Chang, J., Thill, G., Levesque, M., Zhang, M.*, et al.* (2005). LINGO-1 negatively regulates myelination by oligodendrocytes. Nat Neurosci *8*, 745-751.

Michalski, J.P., and Kothary, R. (2015). Oligodendrocytes in a Nutshell. Front Cell Neurosci *9*, 340.

Miller, R.H., Payne, J., Milner, L., Zhang, H., and Orentas, D.M. (1997). Spinal cord oligodendrocytes develop from a limited number of migratory highly proliferative precursors. J Neurosci Res *50*, 157-168.

Mitew, S., Hay, C.M., Peckham, H., Xiao, J., Koenning, M., and Emery, B. (2014). Mechanisms regulating the development of oligodendrocytes and central nervous system myelin. Neuroscience *276*, 29-47.

Miyakawa, A., Ichimura, K., Schmidt, E.E., Varmeh-Ziaie, S., and Collins, V.P. (2000). Multiple deleted regions on the long arm of chromosome 6 in astrocytic tumours. British journal of cancer *82*, 543-549.

Miyamoto, Y., Yamauchi, J., and Tanoue, A. (2008). Cdk5 phosphorylation of WAVE2 regulates oligodendrocyte precursor cell migration through nonreceptor tyrosine kinase Fyn. J Neurosci *28*, 8326-8337.

Montag, D., Giese, K.P., Bartsch, U., Martini, R., Lang, Y., Bluthmann, H., Karthigasan, J., Kirschner, D.A., Wintergerst, E.S., Nave, K.A.*, et al.* (1994). Mice deficient for the myelin-associated glycoprotein show subtle abnormalities in myelin. Neuron *13*, 229-246.

Moore, M.J. (2000). Intron recognition comes of AGe. Nat Struct Biol *7*, 14-16.

Morikawa, T., and Manabe, T. (2010). Aberrant regulation of alternative pre-mRNA splicing in schizophrenia. Neurochemistry international *57*, 691-704.

Mulholland, P.J., Fiegler, H., Mazzanti, C., Gorman, P., Sasieni, P., Adams, J., Jones, T.A., Babbage, J.W., Vatcheva, R., Ichimura, K.*, et al.* (2006). Genomic profiling identifies discrete deletions associated with translocations in glioblastoma multiforme. Cell Cycle *5*, 783-791.

Murtie, J.C., Zhou, Y.X., Le, T.Q., Vana, A.C., and Armstrong, R.C. (2005). PDGF and FGF2 pathways regulate distinct oligodendrocyte lineage responses in experimental demyelination with spontaneous remyelination. Neurobiol Dis *19*, 171-182.

Musco, G., Stier, G., Joseph, C., Castiglione Morelli, M.A., Nilges, M., Gibson, T.J., and Pastore, A. (1996). Three-dimensional structure and stability of the KH domain: molecular insights into the fragile X syndrome. Cell *85*, 237-245.

Musunuru, K., and Darnell, R.B. (2004). Determination and augmentation of RNA sequence specificity of the Nova K-homology domains. Nucleic Acids Res *32*, 4852-4861.

Nabel-Rosen, H., Volohonsky, G., Reuveny, A., Zaidel-Bar, R., and Volk, T. (2002). Two isoforms of the Drosophila RNA binding protein, how, act in opposing directions to regulate tendon cell differentiation. Dev Cell *2*, 183-193.

Narayanan, S.P., Flores, A.I., Wang, F., and Macklin, W.B. (2009). Akt signals through the mammalian target of rapamycin pathway to regulate CNS myelination. J Neurosci *29*, 6860-6870.

Nave, K.A., and Werner, H.B. (2014). Myelination of the nervous system: mechanisms and functions. Annu Rev Cell Dev Biol *30*, 503-533.

Nigro, J.M., Cho, K.R., Fearon, E.R., Kern, S.E., Ruppert, J.M., Oliner, J.D., Kinzler, K.W., and Vogelstein, B. (1991). Scrambled exons. Cell *64*, 607-613.

Niu, J., Mei, F., Wang, L., Liu, S., Tian, Y., Mo, W., Li, H., Lu, Q.R., and Xiao, L. (2012). Phosphorylated olig1 localizes to the cytosol of oligodendrocytes and promotes membrane expansion and maturation. Glia *60*, 1427-1436.

Noble, M., Murray, K., Stroobant, P., Waterfield, M.D., and Riddle, P. (1988). Platelet-derived growth factor promotes division and motility and inhibits premature differentiation of the oligodendrocyte/type-2 astrocyte progenitor cell. Nature *333*, 560-562.

Noveroske, J.K., Hardy, R., Dapper, J.D., Vogel, H., and Justice, M.J. (2005). A new ENU-induced allele of mouse quaking causes severe CNS dysmyelination. Mamm Genome *16*, 672-682.

Novikov, L., Park, J.W., Chen, H., Klerman, H., Jalloh, A.S., and Gamble, M.J. (2011). QKI-mediated alternative splicing of the histone variant MacroH2A1 regulates cancer cell proliferation. Mol Cell Biol *31*, 4244-4255.

O'Brien, J.S., and Sampson, E.L. (1965). Lipid composition of the normal human brain: gray matter, white matter, and myelin. J Lipid Res *6*, 537-544.

O'Neill, R.C., Minuk, J., Cox, M.E., Braun, P.E., and Gravel, M. (1997). CNP2 mRNA directs synthesis of both CNP1 and CNP2 polypeptides. J Neurosci Res *50*, 248-257.

Ogawa, Y., Schafer, D.P., Horresh, I., Bar, V., Hales, K., Yang, Y., Susuki, K., Peles, E., Stankewich, M.C., and Rasband, M.N. (2006). Spectrins and ankyrinB constitute a specialized paranodal cytoskeleton. J Neurosci *26*, 5230-5239.

Ohara, R., Yamakawa, H., Nakayama, M., and Ohara, O. (2000). Type II brain 4.1 (4.1B/KIAA0987), a member of the protein 4.1 family, is localized to neuronal paranodes. Brain Res Mol Brain Res *85*, 41-52.

Ohno, G., Hagiwara, M., and Kuroyanagi, H. (2008). STAR family RNA-binding protein ASD-2 regulates developmental switching of mutually exclusive alternative splicing in vivo. Genes Dev *22*, 360-374.

Ono, K., Bansal, R., Payne, J., Rutishauser, U., and Miller, R.H. (1995). Early development and dispersal of oligodendrocyte precursors in the embryonic chick spinal cord. Development *121*, 1743-1754.

Ono, K., Yasui, Y., Rutishauser, U., and Miller, R.H. (1997). Focal ventricular origin and migration of oligodendrocyte precursors into the chick optic nerve. Neuron *19*, 283-292.

Orentas, D.M., Hayes, J.E., Dyer, K.L., and Miller, R.H. (1999). Sonic hedgehog signaling is required during the appearance of spinal cord oligodendrocyte precursors. Development *126*, 2419-2429.

Pang, Y., Zheng, B., Fan, L.W., Rhodes, P.G., and Cai, Z. (2007). IGF-1 protects oligodendrocyte progenitors against TNFalpha-induced damage by activation of PI3K/Akt and interruption of the mitochondrial apoptotic pathway. Glia *55*, 1099-1107.

Panganiban, C.H., Barth, J.L., Darbelli, L., Xing, Y., Zhang, J., Li, H., Noble, K.V., Liu, T., Brown, L.N., Schulte, B.A.*, et al.* (2018). Noise-induced dysregulation of Quaking RNA binding proteins contributes to auditory nerve demyelination and hearing loss. J Neurosci.

Paridaen, J.T., and Huttner, W.B. (2014). Neurogenesis during development of the vertebrate central nervous system. EMBO Rep *15*, 351-364.

Parkhurst, C.N., Yang, G., Ninan, I., Savas, J.N., Yates, J.R., 3rd, Lafaille, J.J., Hempstead, B.L., Littman, D.R., and Gan, W.B. (2013). Microglia promote learning-dependent synapse formation through brain-derived neurotrophic factor. Cell *155*, 1596-1609.

Paronetto, M.P., Achsel, T., Massiello, A., Chalfant, C.E., and Sette, C. (2007). The RNA-binding protein Sam68 modulates the alternative splicing of Bcl-x. J Cell Biol *176*, 929-939.

Parras, C.M., Hunt, C., Sugimori, M., Nakafuku, M., Rowitch, D., and Guillemot, F. (2007). The proneural gene Mash1 specifies an early population of telencephalic oligodendrocytes. J Neurosci *27*, 4233-4242.

Pedraza, L., Frey, A.B., Hempstead, B.L., Colman, D.R., and Salzer, J.L. (1991). Differential expression of MAG isoforms during development. J Neurosci Res *29*, 141-148.

Peles, E., Nativ, M., Lustig, M., Grumet, M., Schilling, J., Martinez, R., Plowman, G.D., and Schlessinger, J. (1997). Identification of a novel contactin-associated transmembrane receptor with multiple domains implicated in protein-protein interactions. EMBO J *16*, 978-988.

Penfield, W. (1924). Oligodendrogliaand its relation to classical neuroglia. Brain *47*, 430-452.

Penfield, W. (1932). Neuroglia: normal and pathological. In: Cytology and Cellular Pathology in the Nervous system. *2*.

Pfeiffer, S.E., Warrington, A.E., and Bansal, R. (1993). The oligodendrocyte and its many cellular processes. Trends Cell Biol *3*, 191-197.

Pillai, A.M., Thaxton, C., Pribisko, A.L., Cheng, J.G., Dupree, J.L., and Bhat, M.A. (2009). Spatiotemporal ablation of myelinating glia-specific neurofascin (Nfasc NF155) in mice reveals gradual loss of paranodal axoglial junctions and concomitant disorganization of axonal domains. J Neurosci Res *87*, 1773-1793.

Pilotte, J., Larocque, D., and Richard, S. (2001). Nuclear translocation controlled by alternatively spliced isoforms inactivates the QUAKING apoptotic inducer. Genes & Dev *15*, 845-858.

Podbielska, M., Banik, N.L., Kurowska, E., and Hogan, E.L. (2013). Myelin recovery in multiple sclerosis: the challenge of remyelination. Brain sciences *3*, 1282-1324.

Poliak, S., Gollan, L., Martinez, R., Custer, A., Einheber, S., Salzer, J.L., Trimmer, J.S., Shrager, P., and Peles, E. (1999). Caspr2, a new member of the neurexin superfamily, is localized at the juxtaparanodes of myelinated axons and associates with K+ channels. Neuron *24*, 1037-1047.

Poliak, S., and Peles, E. (2003). The local differentiation of myelinated axons at nodes of Ranvier. Nat Rev Neurosci *4*, 968-980.

Poliak, S., Salomon, D., Elhanany, H., Sabanay, H., Kiernan, B., Pevny, L., Stewart, C.L., Xu, X., Chiu, S.Y., Shrager, P.*, et al.* (2003). Juxtaparanodal clustering of Shaker-like K+ channels in myelinated axons depends on Caspr2 and TAG-1. J Cell Biol *162*, 1149-1160.

Pringle, N.P., and Richardson, W.D. (1993). A singularity of PDGF alpha-receptor expression in the dorsoventral axis of the neural tube may define the origin of the oligodendrocyte lineage. Development *117*, 525-533.

Pringle, N.P., Yu, W.P., Guthrie, S., Roelink, H., Lumsden, A., Peterson, A.C., and Richardson, W.D. (1996). Determination of neuroepithelial cell fate: induction of the oligodendrocyte lineage by ventral midline cells and sonic hedgehog. Dev Biol *177*, 30-42.

Privat, A., Jacque, C., Bourre, J.M., Dupouey, P., and Baumann, N. (1979). Absence of the major dense line in myelin of the mutant mouse "shiverer". Neurosci Lett *12*, 107-112.

Pruss, H., Schwab, J.M., Derst, C., Gortzen, A., and Veh, R.W. (2011). Neurofascin as target of autoantibodies in Guillain-Barre syndrome. Brain *134*, e173; author reply e174.

Pruss, T., Kranz, E.U., Niere, M., and Volkmer, H. (2006). A regulated switch of chick neurofascin isoforms modulates ligand recognition and neurite extension. Mol Cell Neurosci *31*, 354-365.

Pruss, T., Niere, M., Kranz, E.U., and Volkmer, H. (2004). Homophilic interactions of chick neurofascin in trans are important for neurite induction. Eur J Neurosci *20*, 3184-3188.

Qi, Y., Tan, M., Hui, C.C., and Qiu, M. (2003). Gli2 is required for normal Shh signaling and oligodendrocyte development in the spinal cord. Mol Cell Neurosci *23*, 440-450.

Qu, S., Yang, X., Li, X., Wang, J., Gao, Y., Shang, R., Sun, W., Dou, K., and Li, H. (2015). Circular RNA: A new star of noncoding RNAs. Cancer letters *365*, 141-148.

Quinlan, A.R., and Hall, I.M. (2010). BEDTools: a flexible suite of utilities for comparing genomic features. Bioinformatics *26*, 841-842.

Radomska, K.J., Halvardson, J., Reinius, B., Lindholm Carlstrom, E., Emilsson, L., Feuk, L., and Jazin, E. (2013). RNA-binding protein QKI regulates Glial fibrillary acidic protein expression in human astrocytes. Hum Mol Genet *22*, 1373-1382.

Raff, M.C., Lillien, L.E., Richardson, W.D., Burne, J.F., and Noble, M.D. (1988). Platelet-derived growth factor from astrocytes drives the clock that times oligodendrocyte development in culture. Nature *333*, 562-565.

Raine, C.S. (1984). On the association between perinodal astrocytic processes and the node of Ranvier in the C.N.S. J Neurocytol *13*, 21-27.

Raine, C.S., and Wu, E. (1993). Multiple sclerosis: remyelination in acute lesions. Journal of neuropathology and experimental neurology *52*, 199-204.

Raj, B., Irimia, M., Braunschweig, U., Sterne-Weiler, T., O'Hanlon, D., Lin, Z.Y., Chen, G.I., Easton, L.E., Ule, J., Gingras, A.C.*, et al.* (2014). A global regulatory mechanism for activating an exon network required for neurogenesis. Mol Cell *56*, 90-103.

Rajasekharan, S., Baker, K.A., Horn, K.E., Jarjour, A.A., Antel, J.P., and Kennedy, T.E. (2009). Netrin 1 and Dcc regulate oligodendrocyte process branching and membrane extension via Fyn and RhoA. Development *136*, 415-426.

Ramkissoon, L.A., Horowitz, P.M., Craig, J.M., Ramkissoon, S.H., Rich, B.E., Schumacher, S.E., McKenna, A., Lawrence, M.S., Bergthold, G., Brastianos, P.K.*, et al.* (2013). Genomic analysis of diffuse pediatric low-grade gliomas identifies recurrent oncogenic truncating rearrangements in the transcription factor MYBL1. Proc Natl Acad Sci U S A *110*, 8188-8193.

Ramon y Cajal, S. (1913). Contribucion al conocimiento de la neuroglia del cerebro humano. Trab Lab Invest Biol (Madrid) *11*, 255-315.

Rasband, M.N., Park, E.W., Vanderah, T.W., Lai, J., Porreca, F., and Trimmer, J.S. (2001). Distinct potassium channels on pain-sensing neurons. Proc Natl Acad Sci U S A *98*, 13373-13378.

Rasband, M.N., Trimmer, J.S., Peles, E., Levinson, S.R., and Shrager, P. (1999). K+ channel distribution and clustering in developing and hypomyelinated axons of the optic nerve. J Neurocytol *28*, 319-331.

Ratcliffe, C.F., Westenbroek, R.E., Curtis, R., and Catterall, W.A. (2001). Sodium channel beta1 and beta3 subunits associate with neurofascin through their extracellular immunoglobulin-like domain. J Cell Biol *154*, 427-434.

Rathjen, F.G., Wolff, J.M., Chang, S., Bonhoeffer, F., and Raper, J.A. (1987). Neurofascin: a novel chick cell-surface glycoprotein involved in neurite-neurite interactions. Cell *51*, 841-849.

Richard, S., Yu, D., Blumer, K.J., Hausladen, D., Olszowy, M.W., Connelly, P.A., and Shaw, A.S. (1995). Association of p62, a multifunctional SH2- and SH3-domain-binding protein, with src family tyrosine kinases, Grb2, and phospholipase C gamma-1. Mol Cell Biol *15*, 186-197.

Rio Hortega, D. (1921). Histogensis y evolucion normal; exodo y distribucion regional de la microglia. Memor Real Soc Esp Hist Nat *11*, 213-268.

Rio Hortega, D. (1928). Tercera aportacion al conocimiento morfologico e interpretacion functional de la oligodendroglia. Memor Real Soc Esp Hist Nat *14*, 5-122.

Rios, J.C., Melendez-Vasquez, C.V., Einheber, S., Lustig, M., Grumet, M., Hemperly, J., Peles, E., and Salzer, J.L. (2000). Contactin-associated protein (Caspr) and contactin form a complex that is targeted to the paranodal junctions during myelination. J Neurosci *20*, 8354-8364.

Robinson, S., Tani, M., Strieter, R.M., Ransohoff, R.M., and Miller, R.H. (1998). The chemokine growth-regulated oncogene-alpha promotes spinal cord oligodendrocyte precursor proliferation. J Neurosci *18*, 10457-10463.

Rodriguez-Pena, A., Ibarrola, N., Iniguez, M.A., Munoz, A., and Bernal, J. (1993). Neonatal hypothyroidism affects the timely expression of myelin-associated glycoprotein in the rat brain. J Clin Invest *91*, 812-818.

Rosenbluth, J. (1976). Intramembranous particle distribution at the node of Ranvier and adjacent axolemma in myelinated axons of the frog brain. J Neurocytol *5*, 731-745.

Rosenbluth, J., and Blakemore, W.F. (1984). Structural specializations in cat of chronically demyelinated spinal cord axons as seen in freeze-fracture replicas. Neurosci Lett *48*, 171-177.

Rosenbluth, J., and Bobrowski-Khoury, N. (2013). Structural bases for central nervous system malfunction in the quaking mouse: dysmyelination in a potential model of schizophrenia. J Neurosci Res *91*, 374-381.

Rosenbluth, J., Liang, W.L., Liu, Z., Guo, D., and Schiff, R. (1995). Paranodal structural abnormalities in rat CNS myelin developing in vivo in the presence of implanted O1 hybridoma cells. J Neurocytol *24*, 818-824.

Rosenfeld, J., and Friedrich, V.L., Jr. (1986). Oligodendrocyte production and myelin recovery in heterozygous jimpy mice: an autoradiographic study. International journal of

developmental neuroscience : the official journal of the International Society for Developmental Neuroscience *4*, 179-187.

Roth, J.J., Santi, M., Rorke-Adams, L.B., Harding, B.N., Busse, T.M., Tooke, L.S., and Biegel, J.A. (2014). Diagnostic application of high resolution single nucleotide polymorphism array analysis for children with brain tumors. Cancer genetics *207*, 111-123.

Roux, K.J., Kim, D.I., and Burke, B. (2013). BioID: a screen for protein-protein interactions. Curr Protoc Protein Sci *74*, Unit 19 23.

Rowitch, D.H., and Kriegstein, A.R. (2010). Developmental genetics of vertebrate glial-cell specification. Nature *468*, 214-222.

Rybak-Wolf, A., Stottmeister, C., Glazar, P., Jens, M., Pino, N., Giusti, S., Hanan, M., Behm, M., Bartok, O., Ashwal-Fluss, R.*, et al.* (2015). Circular RNAs in the Mammalian Brain Are Highly Abundant, Conserved, and Dynamically Expressed. Mol Cell *58*, 870-885.

Ryder, S.P., and Massi, F. (2010). Insights into the structural basis of RNA recognition by STAR domain proteins. Adv Exp Med Biol *693*, 37-53.

Ryder, S.P., and Williamson, J.R. (2004). Specificity of the STAR/GSG domain protein Qk1: implications for the regulation of myelination. RNA *10*, 1449-1458.

Saccomanno, L., Loushin, C., Jan, E., Punkay, E., Artzt, K., and Goodwin, E.B. (1999). The STAR protein QKI-6 is a translational repressor. Proc Natl Acad Sci U S A *96*, 12605-12610.

Sakers, K., Lake, A.M., Khazanchi, R., Ouwenga, R., Vasek, M.J., Dani, A., and Dougherty, J.D. (2017). Astrocytes locally translate transcripts in their peripheral processes. Proc Natl Acad Sci U S A *114*, E3830-E3838.

Salzer, J.L. (2003). Polarized domains of myelinated axons. Neuron *40*, 297-318.

Salzman, J., Chen, R.E., Olsen, M.N., Wang, P.L., and Brown, P.O. (2013). Cell-type specific features of circular RNA expression. PLoS Genet *9*, e1003777.

Samanta, J., and Kessler, J.A. (2004). Interactions between ID and OLIG proteins mediate the inhibitory effects of BMP4 on oligodendroglial differentiation. Development *131*, 4131-4142.

Savvaki, M., Panagiotaropoulos, T., Stamatakis, A., Sargiannidou, I., Karatzioula, P., Watanabe, K., Stylianopoulou, F., Karagogeos, D., and Kleopa, K.A. (2008). Impairment of learning and memory in TAG-1 deficient mice associated with shorter CNS internodes and disrupted juxtaparanodes. Mol Cell Neurosci *39*, 478-490.

Schafer, D.P., Bansal, R., Hedstrom, K.L., Pfeiffer, S.E., and Rasband, M.N. (2004). Does paranode formation and maintenance require partitioning of neurofascin 155 into lipid rafts? J Neurosci *24*, 3176-3185.

Schmitt, S., Castelvetri, L.C., and Simons, M. (2015). Metabolism and functions of lipids in myelin. Biochim Biophys Acta *1851*, 999-1005.

Schnapp, B., and Mugnaini, E. (1976). Freeze-fracture properties of central myelin in the bullfrog. Neuroscience *1*, 459-467.

Schnapp, B., Peracchia, C., and Mugnaini, E. (1976). The paranodal axo-glial junction in the central nervous system studied with thin sections and freeze-fracture. Neuroscience *1*, 181-190.

Schuller, U., Heine, V.M., Mao, J., Kho, A.T., Dillon, A.K., Han, Y.G., Huillard, E., Sun, T., Ligon, A.H., Qian, Y.*, et al.* (2008). Acquisition of granule neuron precursor identity is a critical determinant of progenitor cell competence to form Shh-induced medulloblastoma. Cancer cell *14*, 123-134.

Scolding, N.J., Frith, S., Linington, C., Morgan, B.P., Campbell, A.K., and Compston, D.A. (1989). Myelin-oligodendrocyte glycoprotein (MOG) is a surface marker of oligodendrocyte maturation. J Neuroimmunol *22*, 169-176.

Shen, S., Park, J.W., Lu, Z.X., Lin, L., Henry, M.D., Wu, Y.N., Zhou, Q., and Xing, Y. (2014). rMATS: robust and flexible detection of differential alternative splicing from replicate RNA-Seq data. Proc Natl Acad Sci U S A *111*, E5593-5601.

Sherman, D.L., and Brophy, P.J. (2005). Mechanisms of axon ensheathment and myelin growth. Nat Rev Neurosci *6*, 683-690.

Shi, Q., Saifetiarova, J., Taylor, A.M., and Bhat, M.A. (2018). mTORC1 Activation by Loss of Tsc1 in Myelinating Glia Causes Downregulation of Quaking and Neurofascin 155 Leading to Paranodal Domain Disorganization. Front Cell Neurosci *12*, 201.

Shimizu, T., Kagawa, T., Wada, T., Muroyama, Y., Takada, S., and Ikenaka, K. (2005). Wnt signaling controls the timing of oligodendrocyte development in the spinal cord. Dev Biol *282*, 397-410.

Shingu, T., Ho, A.L., Yuan, L., Zhou, X., Dai, C., Zheng, S., Wang, Q., Zhong, Y., Chang, Q., Horner, J.W.*, et al.* (2017). Qki deficiency maintains stemness of glioma stem cells in suboptimal environment by downregulating endolysosomal degradation. Nat Genet *49*, 75-86.

Shu, P., Fu, H., Zhao, X., Wu, C., Ruan, X., Zeng, Y., Liu, W., Wang, M., Hou, L., Chen, P.*, et al.* (2017). MicroRNA-214 modulates neural progenitor cell differentiation by targeting Quaking during cerebral cortex development. Sci Rep *7*, 8014.

Sidman, R.L., Dickie, M.M., and Appel, S.H. (1964). Mutant Mice (Quaking and Jimpy) with Deficient Myelination in the Central Nervous System. Science *144*, 309-311.

Simpson, A.H., Gillingwater, T.H., Anderson, H., Cottrell, D., Sherman, D.L., Ribchester, R.R., and Brophy, P.J. (2013). Effect of limb lengthening on internodal length and conduction velocity of peripheral nerve. J Neurosci *33*, 4536-4539.

Simpson, P.B., and Armstrong, R.C. (1999). Intracellular signals and cytoskeletal elements involved in oligodendrocyte progenitor migration. Glia *26*, 22-35.

Siomi, H., Choi, M., Siomi, M.C., Nussbaum, R.L., and Dreyfuss, G. (1994). Essential role for KH domains in RNA binding: impaired RNA binding by a mutation in the KH domain of FMR1 that causes fragile X syndrome. Cell *77*, 33-39.

Siomi, H., Matunis, M.J., Michael, W.M., and Dreyfuss, G. (1993a). The pre-mRNA binding K protein contains a novel evolutionarily conserved motif. Nucleic Acids Res *21*, 1193-1198.

Siomi, H., Siomi, M.C., Nussbaum, R.L., and Dreyfuss, G. (1993b). The protein product of the fragile X gene, FMR1, has characteristics of an RNA-binding protein. Cell *74*, 291-298.

Sjöstrand, F. (1949). SEM study of the retinal rods in the guinea-pig eye. J Cell Comp Physiol *33*, 383-398.

Snaidero, N., Mobius, W., Czopka, T., Hekking, L.H., Mathisen, C., Verkleij, D., Goebbels, S., Edgar, J., Merkler, D., Lyons, D.A.*, et al.* (2014). Myelin membrane wrapping of CNS axons by PI(3,4,5)P3-dependent polarized growth at the inner tongue. Cell *156*, 277-290.

Spassky, N., de Castro, F., Le Bras, B., Heydon, K., Queraud-LeSaux, F., Bloch-Gallego, E., Chedotal, A., Zalc, B., and Thomas, J.L. (2002). Directional guidance of oligodendroglial migration by class 3 semaphorins and netrin-1. J Neurosci *22*, 5992-6004.

Stokin, G.B., Lillo, C., Falzone, T.L., Brusch, R.G., Rockenstein, E., Mount, S.L., Raman, R., Davies, P., Masliah, E., Williams, D.S.*, et al.* (2005). Axonopathy and transport deficits early in the pathogenesis of Alzheimer's disease. Science *307*, 1282-1288.

Stolt, C.C., Rehberg, S., Ader, M., Lommes, P., Riethmacher, D., Schachner, M., Bartsch, U., and Wegner, M. (2002). Terminal differentiation of myelin-forming oligodendrocytes depends on the transcription factor Sox10. Genes Dev *16*, 165-170.

Stoss, O., Novoyatleva, T., Gencheva, M., Olbrich, M., Benderska, N., and Stamm, S. (2004). p59(fyn)-mediated phosphorylation regulates the activity of the tissue-specific splicing factor rSLM-1. Mol Cell Neurosci *27*, 8-21.

Suiko, T., Kobayashi, K., Aono, K., Kawashima, T., Inoue, K., Ku, L., Feng, Y., and Koike, C. (2016). Expression of Quaking RNA-Binding Protein in the Adult and Developing Mouse Retina. PLoS One *11*, e0156033.

Susuki, K., Rasband, M.N., Tohyama, K., Koibuchi, K., Okamoto, S., Funakoshi, K., Hirata, K., Baba, H., and Yuki, N. (2007). Anti-GM1 antibodies cause complement-mediated disruption of sodium channel clusters in peripheral motor nerve fibers. J Neurosci *27*, 3956-3967.

Suzuki, K., and Zagoren, J.C. (1977). Quaking mouse: an ultrastructural study of the peripheral nerves. J Neurocytol *6*, 71-84.

Suzuki, S., Ayukawa, N., Okada, C., Tanaka, M., Takekoshi, S., Iijima, Y., and Iijima, T. (2017). Spatio-temporal and dynamic regulation of neurofascin alternative splicing in mouse cerebellar neurons. Sci Rep *7*, 11405.

Tait, S., Gunn-Moore, F., Collinson, J.M., Huang, J., Lubetzki, C., Pedraza, L., Sherman, D.L., Colman, D.R., and Brophy, P.J. (2000). An oligodendrocyte cell adhesion molecule at the site of assembly of the paranodal axo-glial junction. J Cell Biol *150*, 657-666.

Takahashi, N., Roach, A., Teplow, D.B., Prusiner, S.B., and Hood, L. (1985). Cloning and characterization of the myelin basic protein gene from mouse: one gene can encode both 14 kd and 18.5 kd MBPs by alternate use of exons. Cell *42*, 139-148.

Tan, M., Hu, X., Qi, Y., Park, J., Cai, J., and Qiu, M. (2006). Gli3 mutation rescues the generation, but not the differentiation, of oligodendrocytes in Shh mutants. Brain Res *1067*, 158-163.

Taveggia, C., Thaker, P., Petrylak, A., Caporaso, G.L., Toews, A., Falls, D.L., Einheber, S., and Salzer, J.L. (2008). Type III neuregulin-1 promotes oligodendrocyte myelination. Glia *56*, 284-293.

Taylor, S.J., and Shalloway, D. (1994). An RNA-binding protein associated with Src through its SH2 and SH3 domains in mitosis. Nature *368*, 867-871.

Tekki-Kessaris, N., Woodruff, R., Hall, A.C., Gaffield, W., Kimura, S., Stiles, C.D., Rowitch, D.H., and Richardson, W.D. (2001). Hedgehog-dependent oligodendrocyte lineage specification in the telencephalon. Development *128*, 2545-2554.

Teplova, M., Hafner, M., Teplov, D., Essig, K., Tuschl, T., and Patel, D.J. (2013). Structure-function studies of STAR family Quaking proteins bound to their in vivo RNA target sites. Genes Dev *27*, 928-940.

Thangaraj, M.P., Furber, K.L., Gan, J.K., Ji, S., Sobchishin, L., Doucette, J.R., and Nazarali, A.J. (2017). RNA-binding Protein Quaking Stabilizes Sirt2 mRNA during Oligodendroglial Differentiation. J Biol Chem *292*, 5166-5182.

Thaxton, C., and Bhat, M.A. (2009). Myelination and regional domain differentiation of the axon. Results Probl Cell Differ *48*, 1-28.

Thaxton, C., Pillai, A.M., Pribisko, A.L., Dupree, J.L., and Bhat, M.A. (2011). Nodes of Ranvier act as barriers to restrict invasion of flanking paranodal domains in myelinated axons. Neuron *69*, 244-257.

Thaxton, C., Pillai, A.M., Pribisko, A.L., Labasque, M., Dupree, J.L., Faivre-Sarrailh, C., and Bhat, M.A. (2010). In vivo deletion of immunoglobulin domains 5 and 6 in neurofascin (Nfasc) reveals domain-specific requirements in myelinated axons. J Neurosci *30*, 4868-4876.

Thorvaldsdottir, H., Robinson, J.T., and Mesirov, J.P. (2013). Integrative Genomics Viewer (IGV): high-performance genomics data visualization and exploration. Brief Bioinform *14*, 178-192.

Tili, E., Chiabai, M., Palmieri, D., Brown, M., Cui, R., Fernandes, C., Richmond, T., Kim, T., Sheetz, T., Sun, H.L.*, et al.* (2015). Quaking and miR-155 interactions in inflammation and leukemogenesis. Oncotarget *6*, 24599-24610.

Traka, M., Dupree, J.L., Popko, B., and Karagogeos, D. (2002). The neuronal adhesion protein TAG-1 is expressed by Schwann cells and oligodendrocytes and is localized to the juxtaparanodal region of myelinated fibers. J Neurosci *22*, 3016-3024.

Tsai, H.H., Frost, E., To, V., Robinson, S., Ffrench-Constant, C., Geertman, R., Ransohoff, R.M., and Miller, R.H. (2002). The chemokine receptor CXCR2 controls positioning of oligodendrocyte precursors in developing spinal cord by arresting their migration. Cell *110*, 373-383.

Tsai, H.H., Macklin, W.B., and Miller, R.H. (2006). Netrin-1 is required for the normal development of spinal cord oligodendrocytes. J Neurosci *26*, 1913-1922.

Tsai, H.H., Tessier-Lavigne, M., and Miller, R.H. (2003). Netrin 1 mediates spinal cord oligodendrocyte precursor dispersal. Development *130*, 2095-2105.

Ueda, H., Levine, J.M., Miller, R.H., and Trapp, B.D. (1999). Rat optic nerve oligodendrocytes develop in the absence of viable retinal ganglion cell axons. J Cell Biol *146*, 1365-1374.

Ule, J., Stefani, G., Mele, A., Ruggiu, M., Wang, X., Taneri, B., Gaasterland, T., Blencowe, B.J., and Darnell, R.B. (2006). An RNA map predicting Nova-dependent splicing regulation. Nature *444*, 580-586.

Urbich, C., Kuehbacher, A., and Dimmeler, S. (2008). Role of microRNAs in vascular diseases, inflammation, and angiogenesis. Cardiovasc Res *79*, 581-588.

Vallstedt, A., Klos, J.M., and Ericson, J. (2005). Multiple dorsoventral origins of oligodendrocyte generation in the spinal cord and hindbrain. Neuron *45*, 55-67.

Valverde, R., Edwards, L., and Regan, L. (2008). Structure and function of KH domains. FEBS J *275*, 2712-2726.

van der Veer, E.P., de Bruin, R.G., Kraaijeveld, A.O., de Vries, M.R., Bot, I., Pera, T., Segers, F.M., Trompet, S., van Gils, J.M., Roeten, M.K.*, et al.* (2013). Quaking, an RNA-binding protein, is a critical regulator of vascular smooth muscle cell phenotype. Circulation research *113*, 1065-1075.

van Mil, A., Grundmann, S., Goumans, M.J., Lei, Z., Oerlemans, M.I., Jaksani, S., Doevendans, P.A., and Sluijter, J.P. (2012). MicroRNA-214 inhibits angiogenesis by targeting Quaking and reducing angiogenic growth factor release. Cardiovasc Res *93*, 655-665.

Venables, J.P., Klinck, R., Koh, C., Gervais-Bird, J., Bramard, A., Inkel, L., Durand, M., Couture, S., Froehlich, U., Lapointe, E.*, et al.* (2009). Cancer-associated regulation of alternative splicing. Nat Struct Mol Biol *16*, 670-676.

Venables, J.P., Vernet, C., Chew, S.L., Elliott, D.J., Cowmeadow, R.B., Wu, J., Cooke, H.J., Artzt, K., and Eperon, I.C. (1999). T-STAR/ETOILE: a novel relative of SAM68 that interacts with an RNA-binding protein implicated in spermatogenesis. Hum Mol Genet *8*, 959-969.

Vernet, C., and Artzt, K. (1997). STAR, a gene family involved in signal transduction and activation of RNA. Trends Genet *13*, 479-484.

Virchow, R. (1846). Ueber das granulirte Aussehen der Wandungen der Gehirnventrikel. Allg Z Psychiat *3*, 242-250.

Virchow, R. (1854). Ueber das ausgebreitete Vorkommen einer dem Nervenmark analogen substanz in den tierischen Geweben. Virchows Arch Pathol Anat *6*.

Volkmer, H., Hassel, B., Wolff, J.M., Frank, R., and Rathjen, F.G. (1992). Structure of the axonal surface recognition molecule neurofascin and its relationship to a neural subgroup of the immunoglobulin superfamily. J Cell Biol *118*, 149-161.

Volkmer, H., Leuschner, R., Zacharias, U., and Rathjen, F.G. (1996). Neurofascin induces neurites by heterophilic interactions with axonal NrCAM while NrCAM requires F11 on the axonal surface to extend neurites. J Cell Biol *135*, 1059-1069.

Wahl, M.C., Will, C.L., and Luhrmann, R. (2009). The spliceosome: design principles of a dynamic RNP machine. Cell *136*, 701-718.

Wang, F., Song, W., Zhao, H., Ma, Y., Li, Y., Zhai, D., Pi, J., Si, Y., Xu, J., Dong, L.*, et al.* (2017a). The RNA-binding protein QKI5 regulates primary miR-124-1 processing via a distal RNA motif during erythropoiesis. Cell Res *27*, 416-439.

Wang, F., Yuan, Y., Yang, P., and Li, X. (2017b). Extracellular vesicles-mediated transfer of miR-208a/b exaggerate hypoxia/reoxygenation injury in cardiomyocytes by reducing QKI expression. Mol Cell Biochem *431*, 187-195.

Wang, H., Kunkel, D.D., Martin, T.M., Schwartzkroin, P.A., and Tempel, B.L. (1993). Heteromultimeric K+ channels in terminal and juxtaparanodal regions of neurons. Nature *365*, 75-79.

Wang, H., Pan, J.Q., Luo, L., Ning, X.J., Ye, Z.P., Yu, Z., and Li, W.S. (2015a). NF-kappaB induces miR-148a to sustain TGF-beta/Smad signaling activation in glioblastoma. Mol Cancer *14*, 2.

Wang, K.C., Koprivica, V., Kim, J.A., Sivasankaran, R., Guo, Y., Neve, R.L., and He, Z. (2002). Oligodendrocyte-myelin glycoprotein is a Nogo receptor ligand that inhibits neurite outgrowth. Nature *417*, 941-944.

Wang, L., Zhai, D.S., Ruan, B.J., Xu, C.M., Ye, Z.C., Lu, H.Y., Jiang, Y.H., Wang, Z.Y., Xiang, A., Yang, Y.*, et al.* (2017c). Quaking Deficiency Amplifies Inflammation in Experimental Endotoxemia via the Aryl Hydrocarbon Receptor/Signal Transducer and Activator of Transcription 1-NF-kappaB Pathway. Front Immunol *8*, 1754.

Wang, S., Sdrulla, A.D., diSibio, G., Bush, G., Nofziger, D., Hicks, C., Weinmaster, G., and Barres, B.A. (1998). Notch receptor activation inhibits oligodendrocyte differentiation. Neuron *21*, 63-75.

Wang, S., Zan, J., Wu, M., Zhao, W., Li, Z., Pan, Y., Sun, Z., and Zhu, J. (2015b). miR-29a promotes scavenger receptor A expression by targeting QKI (quaking) during monocyte-macrophage differentiation. Biochem Biophys Res Commun *464*, 1-6.

Wang, Y., Vogel, G., Yu, Z., and Richard, S. (2013). The QKI-5 and QKI-6 RNA binding proteins regulate the expression of microRNA 7 in glial cells. Mol Cell Biol *33*, 1233-1243.

Watkins, T.A., Emery, B., Mulinyawe, S., and Barres, B.A. (2008). Distinct stages of myelination regulated by gamma-secretase and astrocytes in a rapidly myelinating CNS coculture system. Neuron *60*, 555-569.

Waxman, S.G., and Ritchie, J.M. (1993). Molecular dissection of the myelinated axon. Ann Neurol *33*, 121-136.

Waxman, S.G., and Sims, T.J. (1984). Specificity in central myelination: evidence for local regulation of myelin thickness. Brain Res *292*, 179-185.

Wei, Q., Miskimins, W.K., and Miskimins, R. (2005). Stage-specific expression of myelin basic protein in oligodendrocytes involves Nkx2.2-mediated repression that is relieved by the Sp1 transcription factor. J Biol Chem *280*, 16284-16294.

Wen, J., Toomer, K.H., Chen, Z., and Cai, X. (2015). Genome-wide analysis of alternative transcripts in human breast cancer. Breast cancer research and treatment *151*, 295-307.

Weng, Z., Thomas, S.M., Rickles, R.J., Taylor, J.A., Brauer, A.W., Seidel-Dugan, C., Michael, W.M., Dreyfuss, G., and Brugge, J.S. (1994). Identification of Src, Fyn, and Lyn SH3-binding proteins: implications for a function of SH3 domains. Mol Cell Biol *14*, 4509-4521.

Werner, H.B., Kramer-Albers, E.M., Strenzke, N., Saher, G., Tenzer, S., Ohno-Iwashita, Y., De Monasterio-Schrader, P., Mobius, W., Moser, T., Griffiths, I.R.*, et al.* (2013). A critical role for the cholesterol-associated proteolipids PLP and M6B in myelination of the central nervous system. Glia *61*, 567-586.

Weyn-Vanhentenryck, S.M., Mele, A., Yan, Q., Sun, S., Farny, N., Zhang, Z., Xue, C., Herre, M., Silver, P.A., Zhang, M.Q.*, et al.* (2014). HITS-CLIP and integrative modeling define the Rbfox splicing-regulatory network linked to brain development and autism. Cell Rep *6*, 1139-1152.

Wilkinson, G., Dennis, D., and Schuurmans, C. (2013). Proneural genes in neocortical development. Neuroscience *253*, 256-273.

Wilson, G.R., Wang, H.X., Egan, G.F., Robinson, P.J., Delatycki, M.B., O'Bryan, M.K., and Lockhart, P.J. (2010). Deletion of the Parkin co-regulated gene causes defects in ependymal ciliary motility and hydrocephalus in the quakingviable mutant mouse. Hum Mol Genet *19*, 1593-1602.

Wong, A.G., McBurney, K.L., Thompson, K.J., Stickney, L.M., and Mackie, G.A. (2013a). S1 and KH domains of polynucleotide phosphorylase determine the efficiency of RNA binding and autoregulation. J Bacteriol *195*, 2021-2031.

Wong, A.W., Xiao, J., Kemper, D., Kilpatrick, T.J., and Murray, S.S. (2013b). Oligodendroglial expression of TrkB independently regulates myelination and progenitor cell proliferation. J Neurosci *33*, 4947-4957.

Wong, G., Muller, O., Clark, R., Conroy, L., Moran, M.F., Polakis, P., and McCormick, F. (1992). Molecular cloning and nucleic acid binding properties of the GAP-associated tyrosine phosphoprotein p62. Cell *69*, 551-558.

Wu, H.Y., Dawson, M.R., Reynolds, R., and Hardy, R.J. (2001). Expression of QKI proteins and MAP1B identifies actively myelinating oligodendrocytes in adult rat brain. Mol Cell Neurosci *17*, 292-302.

Wu, J., Zhou, L., Tonissen, K., Tee, R., and Artzt, K. (1999). The quaking I-5 protein (QKI-5) has a novel nuclear localization signal and shuttles between the nucleus and the cytoplasm. J Biol Chem *274*, 29202-29210.

Wu, J.I., Reed, R.B., Grabowski, P.J., and Artzt, K. (2002). Function of quaking in myelination: regulation of alternative splicing. Proc Natl Acad Sci U S A *99*, 4233-4238.

Wu, J.Q., Wang, X., Beveridge, N.J., Tooney, P.A., Scott, R.J., Carr, V.J., and Cairns, M.J. (2012). Transcriptome sequencing revealed significant alteration of cortical promoter usage and splicing in schizophrenia. PLoS One *7*, e36351.

Wu, Y., Li, Z., Yang, M., Dai, B., Hu, F., Yang, F., Zhu, J., Chen, T., and Zhang, L. (2017). MicroRNA-214 regulates smooth muscle cell differentiation from stem cells by targeting RNA-binding protein QKI. Oncotarget *8*, 19866-19878.

Xi, Z., Wang, P., Xue, Y., Shang, C., Liu, X., Ma, J., Li, Z., Li, Z., Bao, M., and Liu, Y. (2017). Overexpression of miR-29a reduces the oncogenic properties of glioblastoma stem cells by downregulating Quaking gene isoform 6. Oncotarget *8*, 24949-24963.

Xiao, J., Ferner, A.H., Wong, A.W., Denham, M., Kilpatrick, T.J., and Murray, S.S. (2012). Extracellular signal-regulated kinase 1/2 signaling promotes oligodendrocyte myelination in vitro. J Neurochem *122*, 1167-1180.

Xiao, J., Wong, A.W., Willingham, M.M., van den Buuse, M., Kilpatrick, T.J., and Murray, S.S. (2010). Brain-derived neurotrophic factor promotes central nervous system myelination via a direct effect upon oligodendrocytes. Neurosignals *18*, 186-202.

Xin, M., Yue, T., Ma, Z., Wu, F.F., Gow, A., and Lu, Q.R. (2005). Myelinogenesis and axonal recognition by oligodendrocytes in brain are uncoupled in Olig1-null mice. J Neurosci *25*, 1354-1365.

Yamagishi, R., Tsusaka, T., Mitsunaga, H., Maehata, T., and Hoshino, S. (2016). The STAR protein QKI-7 recruits PAPD4 to regulate post-transcriptional polyadenylation of target mRNAs. Nucleic Acids Res *44*, 2475-2490.

Yamashita, T., Wu, Y.P., Sandhoff, R., Werth, N., Mizukami, H., Ellis, J.M., Dupree, J.L., Geyer, R., Sandhoff, K., and Proia, R.L. (2005). Interruption of ganglioside synthesis produces central nervous system degeneration and altered axon-glial interactions. Proc Natl Acad Sci U S A *102*, 2725-2730.

Yang, G., Fu, H., Zhang, J., Lu, X., Yu, F., Jin, L., Bai, L., Huang, B., Shen, L., Feng, Y.*, et al.* (2010). RNA-binding protein quaking, a critical regulator of colon epithelial differentiation and a suppressor of colon cancer. Gastroenterology *138*, 231-240 e231-235.

Yang, G., Lu, X., Wang, L., Bian, Y., Fu, H., Wei, M., Pu, J., Jin, L., Yao, L., and Lu, Z. (2011). E2F1 and RNA binding protein QKI comprise a negative feedback in the cell cycle regulation. Cell Cycle *10*, 2703-2713.

Yap, C.C., Vakulenko, M., Kruczek, K., Motamedi, B., Digilio, L., Liu, J.S., and Winckler, B. (2012). Doublecortin (DCX) mediates endocytosis of neurofascin independently of microtubule binding. J Neurosci *32*, 7439-7453.

Ye, P., Carson, J., and D'Ercole, A.J. (1995). In vivo actions of insulin-like growth factor-I (IGF-I) on brain myelination: studies of IGF-I and IGF binding protein-1 (IGFBP-1) transgenic mice. J Neurosci *15*, 7344-7356.

Ye, P., Li, L., Lund, P.K., and D'Ercole, A.J. (2002). Deficient expression of insulin receptor substrate-1 (IRS-1) fails to block insulin-like growth factor-I (IGF-I) stimulation of brain growth and myelination. Brain Res Dev Brain Res *136*, 111-121.

Yin, D., Ogawa, S., Kawamata, N., Tunici, P., Finocchiaro, G., Eoli, M., Ruckert, C., Huynh, T., Liu, G., Kato, M.*, et al.* (2009). High-resolution genomic copy number profiling of glioblastoma multiforme by single nucleotide polymorphism DNA microarray. Mol Cancer Res *7*, 665-677.

Yu, F., Jin, L., Yang, G., Ji, L., Wang, F., and Lu, Z. (2014). Post-transcriptional repression of FOXO1 by QKI results in low levels of FOXO1 expression in breast cancer cells. Oncol Rep *31*, 1459-1465.

Yu, Y., Chen, Y., Kim, B., Wang, H., Zhao, C., He, X., Liu, L., Liu, W., Wu, L.M., Mao, M., *et al.* (2013). Olig2 targets chromatin remodelers to enhancers to initiate oligodendrocyte differentiation. Cell *152*, 248-261.

Yu, Z., Chen, T., Hébert, J., Li, E., and Richard, S. (2009). A mouse PRMT1 null allele defines an essential role for arginine methylation in genome maintenance and cell proliferation. Mol Cell Biol *29*, 2982-2996.

Zaffran, S., Astier, M., Gratecos, D., and Semeriva, M. (1997). The held out wings (how) Drosophila gene encodes a putative RNA-binding protein involved in the control of muscular and cardiac activity. Development *124*, 2087-2098.

Zalc, B., Goujet, D., and Colman, D. (2008). The origin of the myelination program in vertebrates. Curr Biol *18*, R511-512.

Zearfoss, N.R., Clingman, C.C., Farley, B.M., McCoig, L.M., and Ryder, S.P. (2011). Quaking regulates Hnrnpa1 expression through its 3' UTR in oligodendrocyte precursor cells. PLoS Genet *7*, e1001269.

Zeger, M., Popken, G., Zhang, J., Xuan, S., Lu, Q.R., Schwab, M.H., Nave, K.A., Rowitch, D., D'Ercole, A.J., and Ye, P. (2007). Insulin-like growth factor type 1 receptor signaling in the cells of oligodendrocyte lineage is required for normal in vivo oligodendrocyte development and myelination. Glia *55*, 400-411.

Zhang, A., Desmazieres, A., Zonta, B., Melrose, S., Campbell, G., Mahad, D., Li, Q., Sherman, D.L., Reynolds, R., and Brophy, P.J. (2015). Neurofascin 140 is an embryonic neuronal neurofascin isoform that promotes the assembly of the node of Ranvier. J Neurosci *35*, 2246-2254.

Zhang, J., Zhao, J., Jiang, W.J., Shan, X.W., Yang, X.M., and Gao, J.G. (2012). Conditional gene manipulation: Cre-ating a new biological era. J Zhejiang Univ Sci B *13*, 511-524.

Zhang, K., Yan, F., Lei, X., Wei, D., Lu, H., Zhu, Z., Xiang, A., Ye, Z., Wang, L., Zheng, W., *et al.* (2018). Androgen receptormediated upregulation of quaking affects androgen receptorrelated prostate cancer development and antiandrogen receptor therapy. Molecular medicine reports.

Zhang, X.O., Wang, H.B., Zhang, Y., Lu, X., Chen, L.L., and Yang, L. (2014a). Complementary sequence-mediated exon circularization. Cell *159*, 134-147.

Zhang, Y., Chen, K., Sloan, S.A., Bennett, M.L., Scholze, A.R., O'Keeffe, S., Phatnani, H.P., Guarnieri, P., Caneda, C., Ruderisch, N., *et al.* (2014b). An RNA-sequencing transcriptome and splicing database of glia, neurons, and vascular cells of the cerebral cortex. J Neurosci *34*, 11929-11947.

Zhang, Y., Lu, Z., Ku, L., Chen, Y., Wang, H., and Feng, Y. (2003). Tyrosine phosphorylation of QKI mediates developmental signals to regulate mRNA metabolism. EMBO J *22*, 1801-1810.

Zhao, L., Ku, L., Chen, Y., Xia, M., LoPresti, P., and Feng, Y. (2006a). QKI binds MAP1B mRNA and enhances MAP1B expression during oligodendrocyte development. Mol Biol Cell *17*, 4179-4186.

Zhao, L., Mandler, M.D., Yi, H., and Feng, Y. (2010). Quaking I controls a unique cytoplasmic pathway that regulates alternative splicing of myelin-associated glycoprotein. Proc Natl Acad Sci U S A *107*, 19061-19066.

Zhao, L., Tian, D., Xia, M., Macklin, W.B., and Feng, Y. (2006b). Rescuing qkV dysmyelination by a single isoform of the selective RNA-binding protein QKI. J Neurosci *26*, 11278-11286.

Zhao, Y., Zhang, G., Wei, M., Lu, X., Fu, H., Feng, F., Wang, S., Lu, W., Wu, N., Lu, Z.*, et al.* (2014). The tumor suppressing effects of QKI-5 in prostate cancer: a novel diagnostic and prognostic protein. Cancer Biol Ther *15*, 108-118.

Zhou, D., Lambert, S., Malen, P.L., Carpenter, S., Boland, L.M., and Bennett, V. (1998). AnkyrinG is required for clustering of voltage-gated Na channels at axon initial segments and for normal action potential firing. J Cell Biol *143*, 1295-1304.

Zhu, H., Zhao, L., Wang, E., Dimova, N., Liu, G., Feng, Y., and Cambi, F. (2012). The QKI-PLP pathway controls SIRT2 abundance in CNS myelin. Glia *60*, 69-82.

Ziskin, J.L., Nishiyama, A., Rubio, M., Fukaya, M., and Bergles, D.E. (2007). Vesicular release of glutamate from unmyelinated axons in white matter. Nat Neurosci *10*, 321-330.

Zong, F.Y., Fu, X., Wei, W.J., Luo, Y.G., Heiner, M., Cao, L.J., Fang, Z., Fang, R., Lu, D., Ji, H.*, et al.* (2014). The RNA-binding protein QKI suppresses cancer-associated aberrant splicing. PLoS Genet *10*, e1004289.

Zonta, B., Desmazieres, A., Rinaldi, A., Tait, S., Sherman, D.L., Nolan, M.F., and Brophy, P.J. (2011). A critical role for Neurofascin in regulating action potential initiation through maintenance of the axon initial segment. Neuron *69*, 945-956.

Zonta, B., Tait, S., Melrose, S., Anderson, H., Harroch, S., Higginson, J., Sherman, D.L., and Brophy, P.J. (2008). Glial and neuronal isoforms of Neurofascin have distinct roles in the assembly of nodes of Ranvier in the central nervous system. J Cell Biol *181*, 1169-1177.

Zorn, A.M., and Krieg, P.A. (1997). The KH domain protein encoded by quaking functions as a dimer and is essential for notochord development in Xenopus embryos. Genes Dev *11*, 2176-2190.